EFFECT OF FIXTURE DYNAMICS ON THE FACE MILLING PROCESS

By

IBRAHIM MOSTAFA DEIAB, B.Sc., M.Sc.
Kuwait University, Kuwait

A Thesis
Submitted to the School of Graduate Studies
in Partial Fulfillment of the Requirements for the Degree of
Doctor of Philosophy

McMaster University

EFFECT OF FIXTURE DYNAMICS ON THE FACE MILLING PROCESS

Doctor of Philosophy (2003) McMaster University

(Mechanical Engineering) Hamilton, Ontario

Title: EFFECT OF FIXTURE DYNAMICS ON THE FACE MILLING PROCESS

Author: Ibrahim Mostafa Deiab
Master of Science, Mechanical Engineering, Kuwait University.
Bachelor of Science, Mechanical Engineering, Kuwait University.

Supervisor: Dr. Mohamed A. Elbestawi

Number of Pages: xxii, 243

ABSTRACT

Accurate prediction of dynamic machining forces is essential in order to estimate the product and process quality, tool life and stability of the machining process. To achieve such a goal, all the aspects affecting the machining process dynamics should be considered. An integrated dynamic model that takes into consideration the dynamic effects of different machining process elements on the chip load was developed. This model considers the effect of cutter geometry, cutter initial position errors, spindle tilt, workpiece geometry, machine tool dynamics, and workpiece/fixture system dynamics. The open literature has no information on the effect of fixture dynamics on the chip load and the machining process stability.

Proper modeling of the workpiece/fixture contact requires the modeling of the friction conditions because friction forces can be utilized to reduce the number of fixture components, thereby exposing more of the workpiece features to machining operations. Also, it provides a damping mechanism to dissipate input energy from machining forces out of the workpiece/fixture system. The literature lacks research on the tribological aspects of the workpiece/fixture contact. Since many factors influence the coefficient of friction, an experimental investigation was carried out to study the tribological aspects of the

workpiece/fixture contact. Based on the findings of this study a velocity limited friction model (VLFM) was incorporated in the finite element analysis of the workpiece/fixture contact.

The model utilizes NURBS curves and surfaces for the geometric modeling of the tool cutting edges and the workpiece geometry. A grid based meshing scheme for the finite element analysis was developed based on the NURBS iso curves.

An in-house finite element code was developed for the analysis of the workpiece/fixture dynamics. Simulated cutting forces showed good agreement with the experimental validation. Two case studies are presented to demonstrate the practical application of the developed methodology. The integration of all of the above in one model provides an off-line tool to simulate and optimize the machining parameters and the fixture configuration. This cuts production time and cost.

AKNOWLEDGMENTS

Thanks and gratitude is due to ALLAHA (Almighty God) for the continuous support I felt through out my life. The author would like to thank all those who supported him during the course of this work. Special thanks to my research supervisor Dr. Mohamed A. Elbestawi for his support and guidance during the course of this work. Thanks to members of the supervisory committee, Dr. Nye, Dr. Sklad and Dr. Ziada. Thanks are extended to all MMRI team for their support. Special thanks to Miky, Jim, Ed and Eugene.

I would like to thank Hossam and Marwan for their friendship and support.

I also acknowledge the help of Sarah Corthers and Juri Sakamora during the simulation runs of case study I and II respectively.

Last but certainly not the least thanks are due to my family for their continuous support.

TABLE of CONTENTS

LIST OF FIGURES

LIST OF TABLES

NOMENCLATURES

A	Nominal contact area.
A_a	Contact area contributed by deformed asperities.
A_d	Contact area contributed by wear debris.
A_i	Contact area of i^{th} individual asperity.
$A_i(\phi)$	Uncut chip area for insert i.
A_r	Real contact area.
$C\,(\theta_i(\phi))$	Nominal instantaneous chip thickness for insert i.
$C(\theta_i(\phi))_{ED}$	Effective dynamic chip thickness.
CP_j	Number of contact spots on j^{th} material.
[C]	Damping matrix.
d	Separation of two systems.
$d(\theta_i(\phi))$	Instantaneous depth of cut for insert i
DOC	Depth of Cut.
E_{dj}	Plastic deformation energy of j^{th} material.
E'	Modified Young's modulus.
$E_{Spindle}$	Spindle eccentricity.
f	Frictional work done.
f_n	Natural frequency.
f_t	Nominal feed per tooth.

$F_A(l,\phi)$	Axial cutting force component.
F_{ad}	Adhesion force.
$F_D(t)$	Damping forces.
$F_{Ext}(t)$	External forces.
$F_{Int}(t)$	Internal (nodal)forces including forces.
$F_R(l,\phi)$	Radial cutting force component.
$F_T(l,\phi)$	Tangential cutting force component.
F_{xm}	Orthogonally measured mean forces.
F_{ym}	Orthogonally measured mean forces.
$H_{1,2}$	Hardness of contacting materials.
I	Moment of inertia.
J	Number of rotational positions for one tooth period.
K_f	Specific friction cutting pressure.
K_n	Specific normal cutting pressure.
K_R	Specific radial cutting pressure.
K_T	Specific tangential cutting pressure.
[K]	Stiffness matrix.
$[K^*]$	Transformed stiffness matrix.
L	Length of the fixture element.
MRR	Metal removal rate.
[M]	Mass matrix.

N Shape functions in finite element.

$\{N_{i,p}(u)\}$ p^{th}–degree B spline basis functions for a NURBS curve.

P Applied normal load.

P_a Load supported by deformed asperities.

P_d Load supported by wear debris.

$\{P_i\}$ Control points Vector for a NURBS curve.

$\{P_{i,j}\}$ Bi-directional control net for a NURBS surface.

P_r Real applied normal load.

Q Tangential force component .

R_c Cutter radius.

R_i^* Transformed nodal point force vector.

$\{R\}$ Nodal cutting forces.

S_j Shear strength of j^{th} material.

u_m Undulations from the previous teeth(m=1,2,3).

$\{U\}$ NURBS knot vector.

Uj^* Transformed nodal point displacement vector.

v_s Velocity of the grinding wheel.

V Relative sliding velocity.

V_o Cut-off velocity in velocity limited friction model.

V_i Instantaneous cutting speed.

$\{V\}$ NURBS knot vector.

$w\,l$ Nominal depth of cut.

$\{w_{i,}\}$ Weights vector for a NURBS curve.

$\{w_{i,j}\}$ Weights for a NURBS surface.

$x_{(n-1)}$ Instantaneous X deflection in the system at time step n-1.

$y_{(n-1)}$ Instantaneous Y deflections in the system at time step n-1.

$\Delta C_j(\phi_i(\theta))$ Change in chip thickness.

$\Delta d_j(\phi_i(\theta))$ Change in depth of cut .

Δt Time interval.

β Percentage of asperity contact area under compression.

δx Virtual sliding distance.

δx_i Instantaneous X deflection of the system for the insert i at the cutter angular position, θ.

δx_{i-1} X deflection of the system for the previous insert which generated the surface.

δy_i Instantaneous Y deflection of the system for the insert i at the cutter angular position, θ.

δy_{i-1} Y deflection of the system for the previous insert which generated the surface.

δz_i Instantaneous Z deflection of the system for the insert i at the cutter angular position, θ.

δz_{i-1} Z deflection of the system for the previous insert which generated the surface.

$\varepsilon_a(i)$ Initial position error in the axial direction of the insert.

$\varepsilon_r(i)$ Initial position error in the radial direction of the insert.

ϕ Tool rotational angle.

γ_A Insert axial rake angle.

γ_L Insert lead angle.

γ_R Insert radial rake angle.

μ Coefficient of friction.

θ Insert Angular position.

θ_t Tilt angle due to the eccentricity.

σ Equivalent standard deviation of asperity height.

τ Shear stress.

τ_{aj} Shear stress within asperity adhesion area of j^{th} material.

τ_{dj} Shear stress within debris plowing area of j^{th} material.

τ_j' Ultimate shear stress of j^{th} material.

CHAPTER 1: INTRODUCTION

1.1 Preamble

The primary objective for modeling of machining processes is to develop a predictive capability for machining performance in order to facilitate effective planning of machining operations that leads to optimum performance, quality and cost. Accurate prediction of the machining force and vibration in machining processes is an important concern for manufacturing industries. Such information, if available, can lead to selection of proper machining parameters, optimal fixture design and avoidance of tool failure. The accurate prediction of the dynamic cutting forces is necessary for estimating the product and process quality, tool life and stability of the machining process.

Milling processes are dynamic in nature with feedback in the sense that, cutting forces induce vibration and vibration in return affects the cutting forces.

This dynamic interaction can cause the magnitude of cutting force or vibration amplitude to reach much higher values than the expected static values. Therefore, the dynamic responses of the structural elements, machine tool, workpiece and fixture elements must be accurately modeled and incorporated into the simulation in order to obtain accurate predictions. In the open literature, the effect of workpiece/fixture dynamics on the chip load and on machining processes stability is not investigated.

A fixture is a work holding device, which is a fundamental part of virtually every manufacturing operation from machining to assembly. The most important criteria for work holding are positioning accuracy, workpiece stability, minimal workpiece displacement/deformation, and the non-interference with the cutting tool. When a workpiece is located by a set of correctly positioned locators, a critical problem arises in where to place the clamps so that the force closure and hence workpiece stability, can be guaranteed when external dynamic cutting forces are imposed on the part. Most of the current research in the design and analysis of fixtures assumes the fixture elements to be rigid and neglect the effect of friction.

During machining, workpiece motion is generated by cutting forces and localized clamping forces along the workpiece/fixture interface, which affects the workpiece location accuracy and therefore influences the machined part quality.

Contact forces in the normal direction directly influence the workpiece deformation. Tangential (friction) force along the workpiece/fixture interface also plays an important role in fixture design. It can be utilized to reduce the number of fixture components, thereby exposing more workpiece features to machining operations. It also, provides a damping mechanism to dissipate input energy from machining forces out of the workpiece/fixture system. Therefore, modeling of the friction conditions along the workpiece/fixture interface is critical. Contact problems with friction are generally complicated by the fact that the contact surface can experience slipping, sliding, rolling or tension release depending on the magnitude of the normal and tangential forces at the contact interface. The nonlinearity of the problem arises, both from the variation of the extent of contact surfaces and also from the effect of friction.

1.2 Scope of Work

The classical approach used in industry for fixture layout and configuration is mainly a trial and error scheme in nature. It involves online examination of different combinations of fixture positions and clamping force magnitudes in the shop floor, while the machine is in production. This scheme results in many scraped parts until what is thought to be the optimum configuration is found. By the time this lengthy and resources consuming process is done, other factors would alter the process dynamics and induce changes to the fixture configuration.

The objective of this work is to investigate the effect of workpiece/fixture dynamics on the chip load and the machining process dynamics. In order to achieve this objective the following two issues were addressed: first, the tribological aspects of the workpiece/fixture contact were investigated and the effect of various factors on the contact surface such as: workpiece surface roughness, fixture element roughness and clamping force magnitude were quantified. Also, a friction model that incorporates these findings in the simulation was implemented.

The above developed models were integrated in a modular dynamic simulation system for machining processes that enables an accurate prediction of the process output and provides an off-line optimization tool for machining processes parameters as well as the fixturing configuration. This off-line optimization tool will help reduce the nonproductive machining time and cost involved in the process.

The basic framework of the simulation model is outlined in Figure 1.1. For inputs it uses workpiece geometry as defined by a 3D model of the part, cutting edge geometry, cutting conditions, machine modal information, and fixture layout for a specific workpiece configuration. The calibration constants required by the force model are also supplied as inputs. The main processing module in the simulation involves a number of computational components. The first is a geometric model, which handles part and cutting tool intersection calculations.

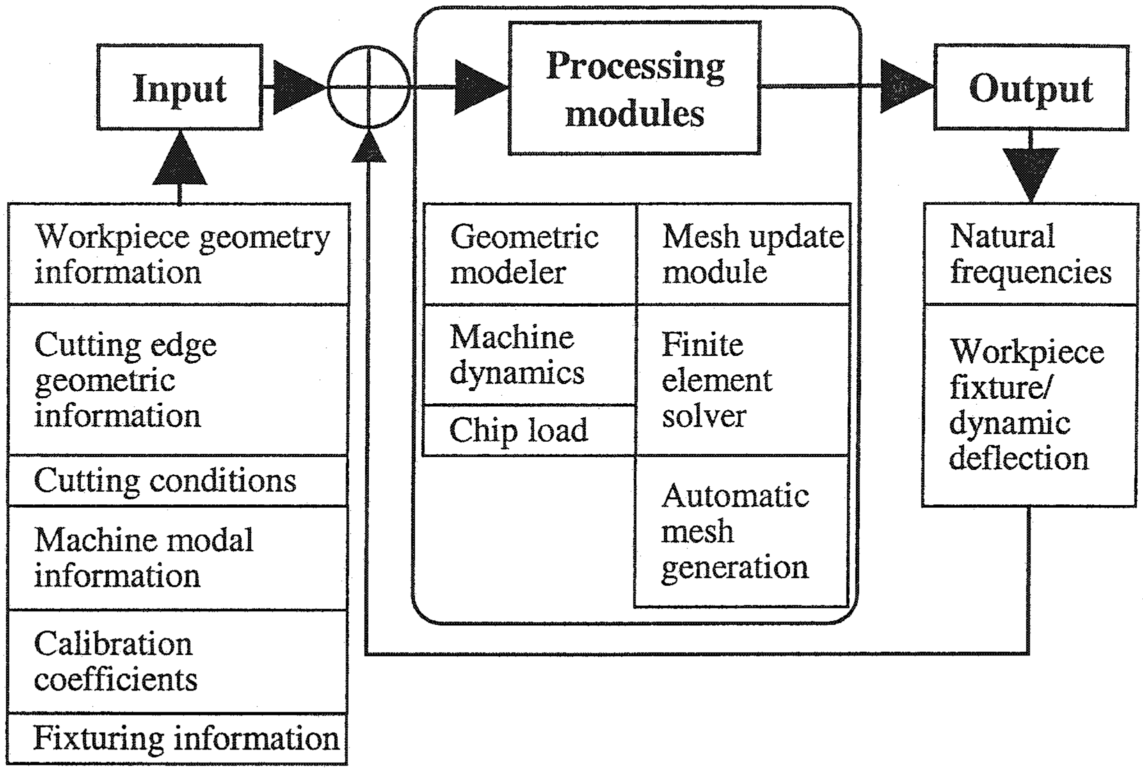

Figure 1.1 Modules of the integrated dynamic model.

This is required to establish the instantaneous chip load, which is needed by the force calculations of an arbitrarily shaped part. These forces are then applied to the dynamic model of the machine, workpiece and fixture to calculate the deflection. These deflections are then fed back so as to capture the dynamic aspect of the cutting force and the machine's response.

1.3 Thesis layout

Modeling of machining processes is an interdisciplinary subject in nature that involves many tasks such as: modeling of the workpiece and the cutting tool geometry, modeling of the cutting forces, and modeling of the process dynamics and the factors contributing to it. The approach used to achieve these tasks can be itemized as follows:

1. Development of an in-house geometric modeler for the machining process geometry (i.e. workpiece and tool cutting edges) in a manner that will enable further analysis using the finite element method. The geometric model utilizes NURBS surfaces and curves and is developed in C++ programming language.
2. Development of a mesh generating code to create all entities needed in finite element analysis. This mesh generator utilizes the workpiece boundaries and the iso curves on the NURBS surfaces to generate a finite element mesh. The code considers and updates the change in workpiece geometry during machining.

3. Development of an in-house finite element code for the dynamic analysis of workpiece/fixture contact.
4. Experimental study of the tribological aspects of the workpiece/fixture contact and the effect of workpiece surface roughness, fixture element roughness and clamping force magnitude on the contact conditions.
5. Development of a friction model to incorporate the effect of friction on the workpiece/fixture contact and consequently on the machining process dynamics.
6. Integrating all of the above into a generic simulation system for machining processes and the application to face milling and facing processes.

The methodologies behind each of these tasks are explained in the thesis chapters. Chapter two includes a literature survey of the research work in force modeling, geometric modeling of machining processes, fixture design and configuration, experimental determination of the friction coefficient and modeling of friction and contact. In chapter three, the approach used in this work for geometric modeling of milling is covered in details.

Chapter four covers the mechanistic modeling of the face milling process and the modeling of the different factors affecting the chip load; initial position errors, machine tool dynamics and workpiece fixture dynamics.

Chapter five explains the approach used to model workpiece/fixture dynamics and the formulation of the system equations using finite element analysis.

Experiments were needed at different phases of this work to calibrate the force model, to determine the friction coefficient for modular fixture applications and to validate the generalized simulation results.

The experimental investigation of the friction coefficient on the workpiece/fixture interface and the factors affecting it are presented in chapter six.

Chapter seven is dedicated to results and discussions. It includes two case studies: the analysis of fixture configuration for a flexible automotive part and a novel face machining approach for automotive industry, which is a combination of face milling and grinding. Finally, chapter eight presents the conclusions and contributions of the current research and provide suggestions for future extensions of this work.

CHAPTER 2: LITERATURE REVIEW

2.1 Introduction

The primary objective of machining processes modeling is to develop a predictive capability for process performance that will facilitate effective planning and optimization of machining parameters to achieve the required performance, quality and cost. Accurate prediction of the cutting force and vibration generated during machining is an important concern for manufacturing industries. Such information, if available, leads to selection of proper machining parameters, optimal fixture design and avoidance of tool failure. In addition, the accurate prediction of the dynamic cutting forces is needed to estimate the product and process quality, tool life and stability of the machining process.

Modeling and simulation of a machining process is an interdisciplinary topic that involves many aspects: geometric representation of the workpiece and the cutting edges, modeling of the cutting forces, accounting for the initial position errors, and modeling of the process dynamic. This also includes: machine tool dynamics and workpiece/fixture dynamics. This chapter reviews the literature on the various aspects involved in modeling and simulation of milling processes.

2.2 Mechanical Modeling of Machining Processes

In this review the modeling of the machining processes has two main categories: mechanical modeling and geometric modeling. Mechanical modeling covers the development of a force model, modeling of machining process dynamics, friction and fixture dynamics. The geometric modeling is concerned with the geometric representation of the workpiece and the tool.

2.2.1 Modeling of Cutting Forces

The milling process is dynamic in nature with feedback in the sense that, cutting forces induce vibration and vibration affects the cutting forces again. This dynamic interaction can cause the magnitude of cutting force or vibration amplitude to reach much higher values than the expected static values. Therefore, the dynamic responses of the structural elements must be accurately modeled and incorporated into the simulation in order to obtain accurate predictions.

There are several types of cutting force models that has been presented in the literature. These models can be classified into four categories, according to their sophistication and accuracy:

a- Average rigid force models,

b- Distributed rigid force models,

c- Distributed force with tool deflection feed back models and

d- Distributed force with tool dynamic models.

The first two models presented by Kline and Devor [1] rely on the relationship between metal removal rate and cutting force and do not consider the flexibility of the tool when modeling the cutting forces, i.e. static models. The third approach considers the tool flexibility and uses it as a feed back for predicting the cutting forces, which is more accurate and has been used by many researchers [2-4]. The last approach considers the dynamics of interaction between the workpiece and the tool. The dynamics are usually assumed to be a second-order damped vibration system as described by Smith and Tlusty [5] and used by Yecesan and Altintas [6].

The study of process dynamic has followed a number of diverse routes with particular emphasis on the modeling of the dynamic cutting forces. The literature includes a number of different analysis and modeling approaches for machining processes modeling. These models are classified into four major categories [7] [8]:

Analytical methods: follow either the single shear plane theory by Merchant or the parallel sided shear zone theory by Oxley. They model the physical mechanisms that take place during the cutting process in order to predict the cutting force. However, due to the complexity of some of these mechanisms most analytical models do not predict the dynamic forces accurately.

Experimental methods: focus on deriving the dynamic cutting force coefficients by using static cutting tests, dynamic cutting tests and time-series methods. The empirical nature of these methods requires re-estimation of the model for any change in the cutting conditions range.

Numerical methods: utilize finite element analysis to predict the cutting forces and chip geometry without assuming the shear zone shape and size. These methods are limited by, incomplete material models, computational burden for 3D modeling and the difficulty of incorporating the dynamic effects.

Mechanistic methods: the underlying assumption behind these methods is that the cutting forces are proportional to the uncut chip area. The constant of proportionality depends on the cutting conditions, cutting geometry and material properties.

Figure 2.1 shows the evolution of the dynamic cutting process modeling using the four categories listed above [8].

Kapoor et al. [7] presented a framework of a comprehensive dynamic cutting model based on an oblique machining process. The normal force F_n and the friction force F_f on the rake face are obtained first (Figure 2.2). Then, they are transformed to the tool–local coordinate system that consists of the tangential component, F_T, the axial component F_A and the radial component F_R.

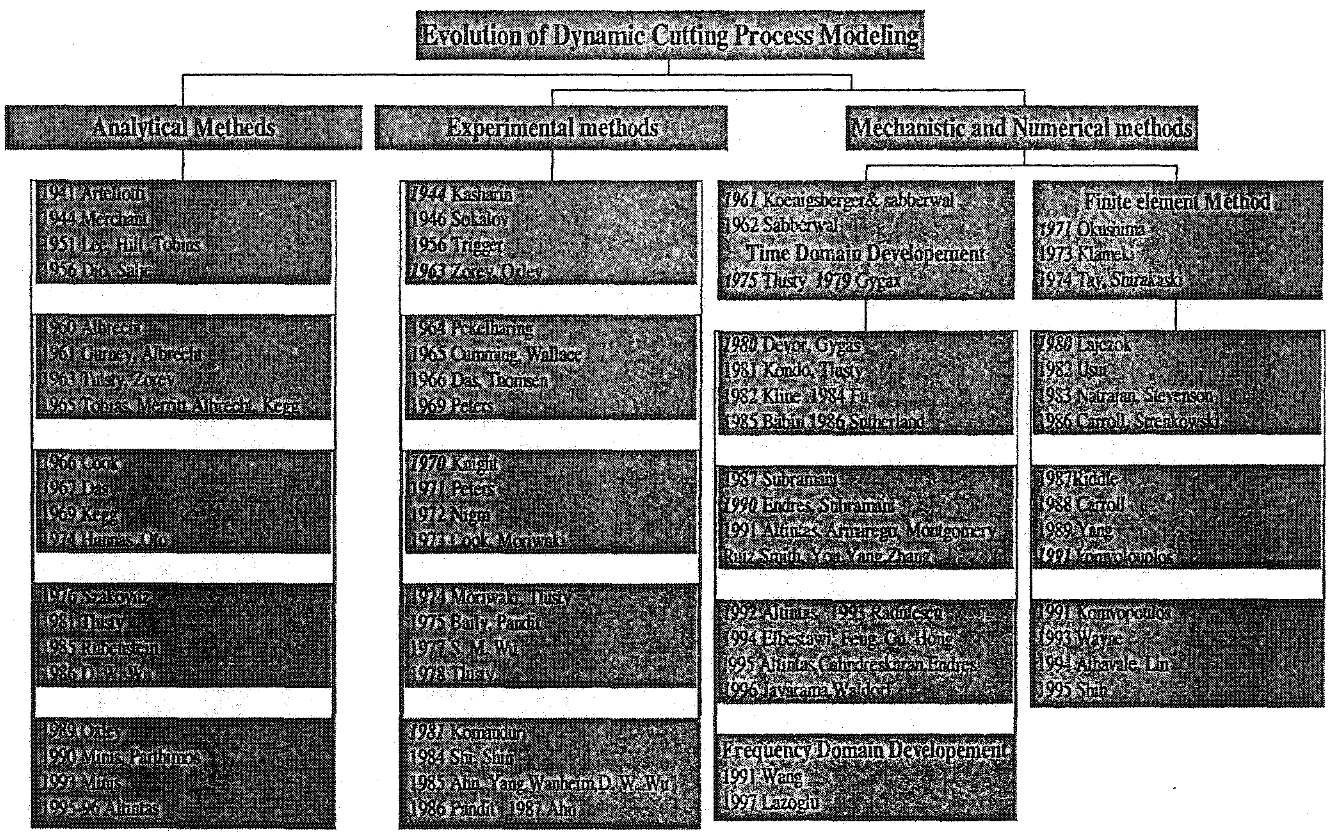

Figure 2.1. Evolution of dynamic cutting process modeling [8].

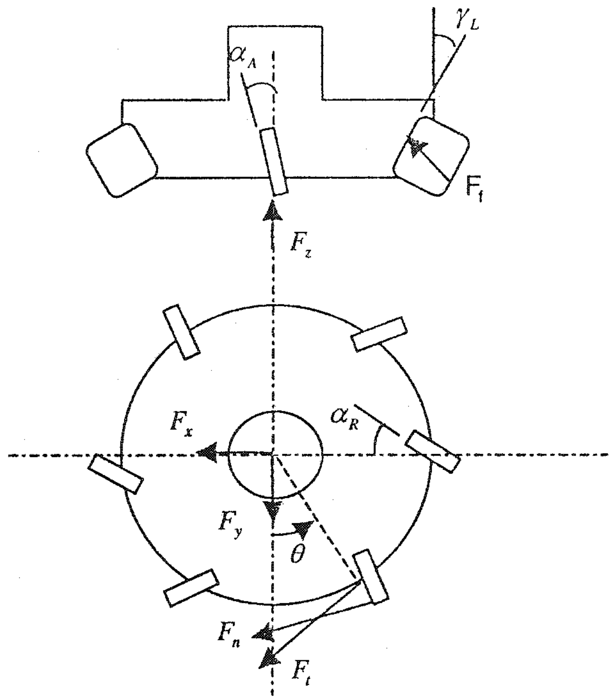

Figure 2.2. Face milling cutter geometry and force components.

The magnitude of the normal and friction forces are modeled as being proportional to the process geometry characteristics that represent the amount of material being removed at an instant in time, i.e. chip load A_c. These force relations are:

$$
\begin{aligned}
F_n &= K_n . A_c, \\
F_f &= K_f . A_c
\end{aligned}
\tag{2.1}
$$

Where K_n is the specific normal pressure and K_f is the specific friction pressure.

$$\begin{bmatrix} F_T \\ F_R \\ F_A \end{bmatrix} = [A]F_n \quad + [B]F_f \tag{2.2}$$

where A, and B are transformation matrices dependent on the process geometry.

The chip load model computes the instantaneous uncut chip thickness and chip area for given cutting conditions. The developed model allows for the incorporation of the machining process dynamics.

Gu et al. [9] presented an enhanced model for the prediction of static cutting forces in face milling. The model takes into account the effect of machine setup errors on the chip load. It is also capable of handling complex workpiece geometry and multiple pass machining. The predicted forces agreed well with experimental results.

Zheng et al. [10] presented a theoretical model of the face milling process based on Oxley's predictive machining theory [11]. The action of the milling cutter is modeled as the simultaneous actions of a number of single point cutting tools. The milling forces are predicted from the workpiece material properties, cutting parameters, cutting edge geometry and cutting conditions. The properties of the workpiece material are considered as functions of strain, strain rate and temperature in the cutting region. The model takes into consideration the effect of the intermittent contact between each milling tooth and the undeformed chip thickness on the temperature in the cutting region.

Akshay et al. [12] presented a model for the face milling process that includes the effects of cutting speed and cutting geometry, which includes the lead angle, the radial rake angle, the axial rake angle and the nose radius. An algorithm to estimate and optimize the run out is developed based on that model. The algorithm can handle workpieces with varying surface continuities.

Zheng et al. [13] presented a generalized cutting force model for milling operations. Based on the relationship between the local cutting forces and the instantaneous chipload, the analytical integration of the local cutting forces gives the resultant cutting forces in the angle domain. A unit rectangular window models the intermittent radial engagement with a variant width associated with the radial positions of the cutting edge. A Fourier transformation achieves a closed form expression of the cutting-force components at the harmonics of tooth passing frequency. The model allows for process planning, tool optimization, and on-line diagnostics. In addition, the development procedure uses a generalized cutting-edge function without involving specific cutter geometry and process configuration, thereby warranting the generalization of the model. Face and end millings were used as examples to show the applicability of the model along with experimental verification.

Young et al. [14] used the orthogonal machining theory to predict the cutting forces on face milling from knowledge of the workpiece material properties and the cutting conditions.

Kim et al. [15] presented a simulation of the static and dynamic cutting forces for face milling operations. The initial position errors of the inserts and the eccentricity of the spindle are taken into consideration as major factors affecting the variation of the chip cross-section. The structural dynamics model for the multi tooth oblique cutting operation is assumed as a multi degrees of freedom spatial system. Based on the double modulation principle and using the relative displacement of the spatial system, the dynamic cutting forces are calculated.

Bayoumi et al. [16] [17] presented an analytic force model to simulate the cutting forces in milling operations. The model starts by a representation of the cutter surface. Then chip removal kinematics, cutting force definition and determination of the integration limits from the force equation. The cutter surface is defined by ruled surfaces that are related to the cutter geometry. Cutting forces are determined by integrating the pressure and friction loads acting on these cutter surfaces. The integration limits that are functions of the rotation angle are established. The model uses process dependent parameters representing normal pressure, chip flow friction, and chip flow kinematics.

2.2.2 Modeling of Machining Processes Dynamics

The dynamic nature of milling processes greatly affects the stability of the process. The reciprocating relation between the cutting forces and vibration can cause the magnitude of cutting force components or vibration amplitude to reach much higher values than the expected static values. Therefore, the dynamic responses of the structural elements must be accurately modeled and incorporated into the simulation in order to obtain accurate predictions. Early attempts to include dynamics in the milling process were done by Sridhar et al. [18] and Optiz et al. [19] and Das and Tobais [20].

Das and Tobais [20] derived an equation for the relationship between static and dynamic cutting in the single tooth orthogonal cutting case, and applied it to the milling operations. Sridhar et al. [18] developed a comprehensive stability theory for milling that is based on the numerical integration of the milling equations for one period of cutter revolution. Optiz et al. [19] applied the stability theory of turning to the milling process by approximating the periodic coefficients of the milling equations for the periodic coefficients of the milling equations with their weighted average values over the interval between the entry and exit angles of the cutting insert. On the other hand, Jensen and Shin [21] developed an algorithm to predict stability lobes in face milling operation based on frequency domain analysis.

Tlusty and Ismail [22] proposed a dynamic approach based on a simple chip geometry relationship and a spring-mass-damper model to account for structural dynamics. The model does not consider any effect of the cutting tool geometry or cutter run out, which affect cutting forces significantly. Ismail et al. [23] presented a mechanistic model for end milling, which includes effect of the tool dynamics and wear.

Stability analysis for milling operations is much more complicated due to rotation of the cutting tool and the interrupted nature of the cutting process. The forces during milling are not only time varying but periodic as well. Time domain simulations of face milling process are capable of accounting for various non-linearities such as: variation of chip thickness, changing orientation of cutting forces, process damping, run out, complex workpiece geometry etc. Time domain simulation programs can be an effective tool in determining the onset of chatter. PTP (peak-to-peak) graphs are a way of summarizing the results of many simulation runs (Smith and Tlusty, [24]). Among the researchers involved in time domain simulations were DeVor et al. [25], Tlusty et al. [22], and Jensen and Shin [21]. Another issue is the effect of fixture positioning on the machining system stability. The machining system in the presence of contact conditions is inherently nonlinear and its dynamics are not well understood. The positioning of the fixture element can affect the dynamic characteristics of the machining system and consequently its stability. Once the dynamic characteristics of the machining system are computed, through numerical and/or experimental analysis, the fixture layout can be revised to modify these characteristics in order to avoid severe vibrations.

In all of the above, the effect of fixture dynamics on the machining process response and stability was not considered. The open literature available for fixture dynamics research does not investigate the effect of the fixture dynamics on the chipload or the stability of the machining process.

2.3 Geometric Modeling of Machining Processes

Geometric modeling of machining processes is concerned with the geometric representation of the workpiece boundaries, the tool cutting edges and most important the tool-workpiece intersection. In computer-aided design (CAD), geometric models are either characterized in terms of wire frame, surface, or solid representations [26]. Physical component models are usually developed as true solids. These might be machined objects with very regular surfaces, such as crankshafts and pistons or more often defined by complicated sculptured surfaces (connecting rod, pump impellor). The aerospace industry relies extensively on surface modeling, primarily for its use in modeling of aerodynamic surfaces such as wing sections, fuselages, rudders and so forth. The automotive industry is very interested in the application of surface models for the aesthetic design and sheet metal forming of body panels. The aerospace industry is interested in solid models for landing gear components, engine components and so forth.

Accurate shape representation is required for more than aesthetic visualization in design applications (conception, display and modification of complex forms). A precise and accurate model is required for both functional prediction (based on finite element analysis) and for manufacturing purposes (such as numerically controlled machining) [27].

One of the main issues in CAD is binary, Boolean, operations, which include intersection, union and difference. These operations are not only useful for creation and modification of geometry, but also for design purposes. One may require the intersection of a line of sight with a true solid. Collision detection can be posed as an intersection problem. The generation of a cross section is the intersection of two surfaces, which produces a curve. However, the complication for CAD systems is that the operations may not produce a geometric entity of the same type. In mathematical terminology, the set of objects is not closed under these Boolean operations. Solid objects are closed under these three operations. However, neither the set of all surfaces, nor the set of all curves, nor the set of all points is closed under these operations. For example, consider two curves. The intersection of two curves is a point (possibly a null point). The union of two curves is a curve, but the difference between two curves is two curves (end to end) with an infinitesimal gap. The operations are not guaranteed to produce a well-formed curve. Although closure is desirable, it must be sacrificed to accommodate the mixture of geometric entities required. Even if each type of geometric entity were closed under the operation we still would need to have operations that involve combinations of entities. The union of a curve and a surface produces a mixed entity, a curve, and a surface. CAD systems cannot be limited to a set of one type of entity. Points are needed to specify locations; lines are needed to specify trajectories, directions, and intersection of surfaces; surfaces are needed to specify constraints and interfaces, cross-sections, and boundary of solids, and solids are needed to specify physical objects. Different approaches have been used to model the Boolean operation between the tool and the workpiece.

Anderson [28] presented 3D-histogram algorithm based on dividing the object into squares and keeping track of the cut height above each square. Each square starts with the value of the height of the stock and each tool movement updates the height of the squares it passes over if it cuts lower than the currently stored height. In the point-vector technique presented by Chappel [29] the surface of the part is approximated by a set of points. Direction vectors are created normal to the surface at each point. A vector extends until it reaches the original stock or intersects with another surface of the part. The metal removal is simulated by calculating the envelope of intersection of each vector with each tool movement. The length of the vector is reduced if it intersects the envelope.

Drydale et al. [30] presented a method for simulating and verifying the correctness of NC programs. The method is based on approximation of the workpiece by a set of points. A vector is passed through each of the points and finding the intersections of the tool movements with these vectors simulates machining. A point selection method to minimize the error introduced by approximation is presented. The run time is inversely proportional to the allowable error and the size of the cutting tool and directly proportional to the distance the cutting tool moves.

Jerard et al. [31] presented an object–based surface discretization scheme that choose a set of points on the surface and use it as a discrete approximation of the actual surface. This scheme adapts the method used by Chappel [29] for the intersection of the tool movement with vectors passing through points on the surface of the part. This approach is assumed to improve efficiency and allow trade offs between the users selected accuracy and the CPU time.

Wang [32] [33] presented an image-space approach that uses a variation of the standard Z-buffer hidden surface algorithm. A vector normal to the plane of the screen is drawn at each pixel. Intersections of these vectors with the tool path envelopes are calculated with a scan line algorithm. For each pixel an extended Z-buffer is maintained that contains the Z-depth of all the entries and exists of the workpiece. The workpiece Z-buffer is modified by performing Boolean difference operations with the Z-buffer of the tool movement swept volume.

Van Hook [34] developed an extended Z-buffer method that differs from Wang's[32][33] in that instead of intersecting scan lines with swept volume envelope it pre computes a pixel image of the cutting tool and perform Boolean subtractions of the cutter from the workpiece as it steps along a tool path.

Another approach is the use of solid representations of both the tool and the workpiece to determine their contact face. Sagherian and Elbestawi [35] presented a simulation system for finish milling of flexible structures. The system includes an improved model for the prediction of dynamic cutting forces that takes into account the deflection of both the workpiece and the tool in the calculation of the chip load. The 3D workpiece is meshed and analyzed using a dynamic FEA package taking into account the effect of material removal.

Imani [36] presented a model-based simulation approach to accurately simulate the two and three axis milling operations of dies and molds with free form surfaces. The geometric modeling part of this technique verifies the tool paths and updates the part as the cutter removes the material, and computes the chip geometry. The physical simulation part considers the mechanics of the milling process as well as the dynamics of the tool and structure. The methodology is dependent on spatial technologies solid modeler software, ACIS.

Abrari [37] developed a simulation technique for the milling process, using solid representation of both the workpiece and the tool which is capable of predicting the cutting forces, deflections and surface error in multi- axis milling of thin Wall structures. A dynamic multi –axis force model that accounts for the tool workpiece structural interaction was presented. Finite element analysis was used to obtain the dynamic response of the workpiece under dynamic machining. The simulator presented is dependent on spatial technologies solid modeler software, ACIS.

Leu et al. [38] presented an implementation of the sweep differential equation (SDE) modeling of deformed swept volumes for NC simulation and verification. By evaluating the linear and nonlinear cutter deflections and including them in the swept volume computation result in a more accurate NC verification program useful for simulating the metal removal process. The swept volumes of the tool corresponding to cutter location, CL, data are subtracted geometrically from the workpiece to obtain the machined part. The surface error of the machined part is predicted and the portions where the error exceeds the tolerance can be identified. This method was implemented in C++ and utilized the Pro/Engineer and Pro/Manufacturing CAD/CAM packages.

NURBS curves and surfaces use in geometric representation of objects is gaining wide acceptance in industry. Most of commercial packages can provide CAD information in NURBS format.

Bailey [39] presented a mechanistic approach for simulating multi axis machining. The NURBS were utilized to represent the cutting edge profiles in a generic way allowing for different methods of manipulating the location and orientation of the cutting edge. NURBS were also used to determine the instantaneous tool-workpiece intersection during machining.

2.4 Fixture Design and Analysis

Today's fixture designers depend on heuristics such as the "3-2-1 rule", which states that a part will be immobilized when it is rigidly contacting six points[40]. Three points define a plane called the primary datum, and two additional contacts specify the secondary datum. The tertiary datum consists of a single point contact. These six locations fix the part position relative to the cutter motion (Figure 2.3).

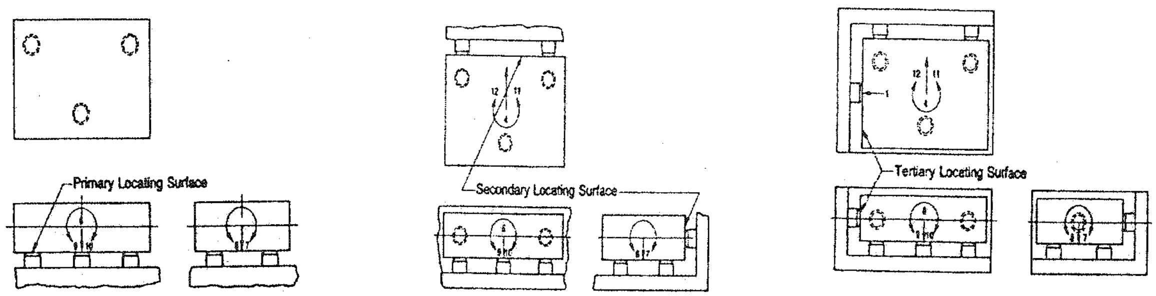

Figure 2.3. 3-2-1 method locating surfaces [41].

If friction is considered, fewer contacts can be used, as long as the applied cutting forces are not excessive. The choice of these datum points is often left up to the fixture designer. However, workpieces used in demanding applications can have their datums explicitly stated in the part drawing. These datums are also used to specify geometric relationships between part features such as perpendicularity, flatness, or concentricity. Once a suitable set of contact locations on the part has been determined, a rigid structure must be devised to hold these contacts in space. Also, the contact type must be selected. Finally, a set of clamps is chosen that apply forces to the part so that it will remain secured. The fixture is composed of active elements that apply clamping forces, and passive elements that locate or support the part (Figure 2.4)

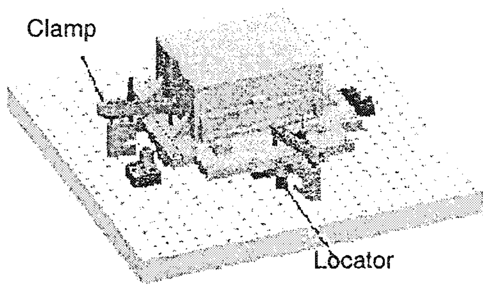

Figure 2.4. Generic modular fixture setup [42].

2.4.1 Fixturing Design Technologies

Various fixturing technologies have emerged to keep up with the ever-growing work holding technology. A number of different terms come up that are descriptive of the different fixturing hardware (Figure 2.5) are as follows [40]:

1. Modular: fixtures that are made up of standard components,
2. Intelligent: fixtures that are equipped with sensors to determine if a part is located,
3. Automatic: fixtures that are driven under computer control, and
4. Flexible: fixtures that are modular, intelligent and that can be positioned manually or automatically.

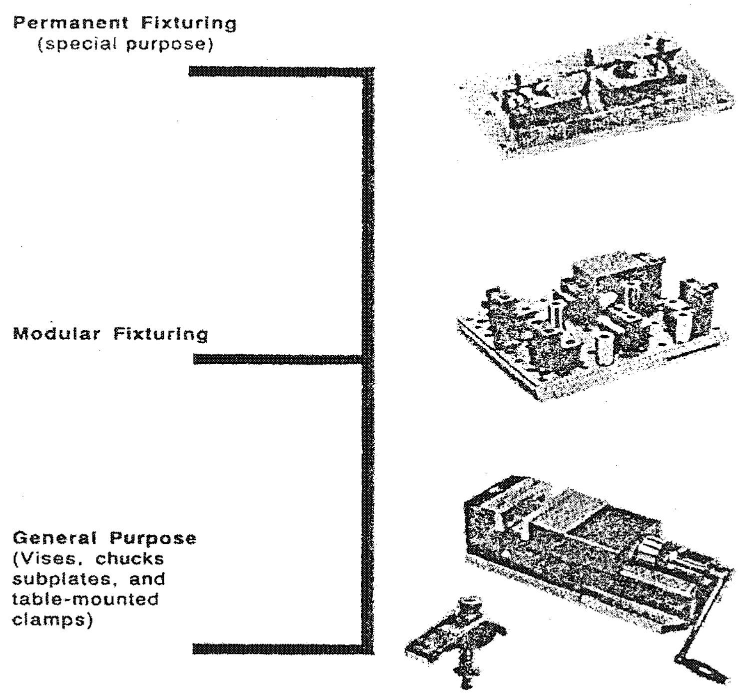

Figure 2.5. Fixture terminology [41].

2.4.2 Fixture Analysis

The open literature presents different techniques for fixture analysis. These techniques vary in their applications and capabilities. A kinematic analysis of the workpiece/fixture configuration is preformed to develop a good fixture design and eliminate the trial-and error approach in fixture implementation [40]. Such an analysis ensures that the workpiece is easily accessible and detachable, however, it does not account for its deformation or friction with fixture elements. The cutting forces are not considered in a kinematic analysis. The linear motion of the workpiece is restricted by the selection of the reference surfaces, while its rotational movement due to the cutting forces is restricted by the position of the locators. Screw theory was used to model the workpiece/fixture system, with linear programming used to determine clamping forces. Nonlinear programming has been also used to derive a quadratic model for verification of the fixture configuration. Finite element analysis has been also used for fixture design to account for the deformation of the workpiece.

Hou et al. [43] proposed a systematic architecture for fixture design by integrating: fixture layout planning, fixturing analysis, fixturing verification and fixture hardware analysis. The differential carrier of a truck is considered to demonstrate the sequence of tasks in the fixture design process. The study combines finite element analysis, using ANSYS5.2, and loading-strain experiments. The force and displacement distribution of six fixture layout plans are analyzed and compared. The hardware design is also considered to ensure that the functional requirements of the work holding are satisfied.

Melkote [44] presented a finite element- based machining fixture design modeling strategy. The spatial and temporal distributions of the reaction force system for the fixture are determined. Instantaneous machining forces are computed from a mechanistic force model. This information is used to estimate the force capacity required for fixture elements and to improve part feature surface flatness error for a face milled workpiece through improved fixture design. A three-dimensional finite element model of the workpiece and the workpiece/fixture contact is developed using ANSYS. The model assumes the fixture elements to be rigid but accounts for the presence of friction between the fixture elements and the workpiece. The fixture reactions are determined quasi–statically at discrete points by applying the corresponding machining forces in the finite element model. The initial clamping forces were not considered.

Chandra et al. [45] presented a finite element model to analyze the effect of clamping preload and machining loads, for a given clamping sequence, on the surface feature error for a face-milled structurally compliant test part.

Lee and Haynes [46] presented a method to minimize the clamping forces of the fixture elements using finite element method. The workpiece is modeled as a deformable body based on linear elasticity and coulomb friction. The problem is presented in the following equation:

$$K_{ij}^{*} \cdot U_{j}^{*} = R_{i}^{*} \quad (2.3)$$

where $[K^{*}]$ is the transformed stiffness matrix Uj^{*}, R_{i}^{*} are the transformed nodal point displacement and force vectors. At the interface between the workpiece and the fixture element, it is assumed that friction forces exits. Coulomb's law of friction was used.

Hamedi [47] conducted a structural static analysis of the workpiece/fixture system for milling operations using finite element analysis package ANSYS. The following parameters were considered: the average value of the cutting force acting on the workpiece in an end mill operation, friction between workpiece and the fixturing element in dry clean conditions and the flexibility of the fixturing elements. Contact elements were used to model the contact phenomena between the workpiece, locators and the clamps. The interaction between the workpiece and fixture element introduces a normal force which simulates the clamping force caused by the tightenness of the clamp. The initial state of contact can either be: closed and stuck (abs (f_f) < abs (μ P)), closed and sliding (abs (f_f) = abs (μ P)) or the gap is open no normal or tangential force acts across the gap element.

2.4.3 Consideration of Dynamic Machining in Fixture Design

Fixture elements designed for a workpiece experiencing dynamic machining must ensure the following [40];

1. The workpiece is restrained all the time.
2. The clamping forces are not too large or small.
3. The workpiece is deterministically positioned, accessible, and stable while under no external forces.

Chou and Barash [48], and Chou [49] used the upper bound machining conditions that are considered static to carry out fixture generation for prismatic parts using linear programming techniques. They employed the screw theory to model the forces acting on the workpiece. The fixture layout was generated on the basis of the 3-2-1 locating principle for the locators and the consideration whether or not the application of a clamp at a certain place would cause the workpiece to detach from the locators. Friction at the locators was not considered.

Lim et al [50] used an expert system to design fixtures for workpieces undergoing dynamic machining conditions. Total restrain is assured through form rather than force closures which in not a guarantee that the workpiece is constrained at all times. To prevent contact of the fixture elements with the machining tool as it makes a pass, a solid is extracted along the tool path and fixture elements that intersect it are moved. Graphical simulation is used through out to iteratively create a new fixture from a pre-existing one for a similar workpiece.

Meyer and Liou [51] presented an approach for the synthesize of the fixtures for dynamic machining conditions utilizing linear programming to solve for the minimum clamping forces and locator forces at all times.

As can be concluded from this review finite element method is the most frequently used technique for the design and analysis of fixture elements. The assumptions made for the modeling of the workpiece/fixture system varies. Most of the work done assumes the fixture elements to be rigid. Very few research papers considered the flexibility of both workpiece and fixture elements. Also the machining process was, mostly, assumed static.

2.5 Friction and Contact Modeling in Work Holding Applications

Workpiece motion arising from localized elastic deformation at the workpiece/fixture contacts due to machining and clamping forces significantly affect the workpiece location accuracy and hence the machined part quality.

Contact forces in the normal direction determine the contact pressure distribution, which directly influence the workpiece deformation. The tangential friction force also plays an important role in fixture design as it can be utilized to reduce the number of fixture components, thereby exposing more of the workpiece features to machining operations and providing a damping mechanism to dissipate input energy from machining forces out of the workpiece/fixture system. Therefore, proper modeling of the workpiece/fixture contact requires the modeling of the friction conditions. Previous researchers [52-53] used the rigid body modeling approach, which treats the workpiece and the fixture elements as perfectly rigid bodies. The overall problem was to minimize the normal clamping force at each locating point. The effect of friction was neglected.

Contact problems with friction [54] are generally complicated by the fact that the contact surface can experience slipping, sliding, rolling or tension release depending on the magnitude of the normal and tangential forces at the contact interface. The nonlinearity of the problem arises, both from the variation of the extent of contact surfaces and also from the effect of friction. Although the literature is full of research on friction and its application, it lacks research that relates to the contact found in a workpiece/fixture system.

For simple workpiece geometries, designers often rely on experience to ensure that restraint requirements are met. However, for complex workpieces, it is virtually impossible to validate total restraint without prototyping the fixture. An alternative to prototyping is total restraint analysis. If a workpiece is totally restrained by contact region geometry [54][55]. Lakshminarayana [56] provided an algebraic proof that a minimum of seven points of contact are needed to form close an object in three dimensions. Salisbury and Roth [57] extended Lakshminarayana's work to include friction. Chou et al. [58] developed a methodology for determining the locations of contact points to form close parts, which have orthogonal planar surfaces. Trappey and Liu [59] developed a nonlinear program for determining whether a set of contact points provides total restraint.

Using virtual power as a context, Ohwovoriole [60] showed that a set of contact points form close a body if there are no screws about which the body may twist without causing negative virtual power. Nguyen [61] used virtual power to examine the geometric conditions for which a set of contact points provides force closure. Kerr and Sanger [62] developed a methodology determining the locations of contact points to kinematically restrain rigid bodies through partial form closure. Assada and Kitawaga [63] developed a model based on linear programming to determine the existence of form closure

2.5.1 Friction Modeling

Models found in the literature assume the friction to obey Coulomb's friction, which make these models very sensitive to the coefficient of friction used [64]. Coefficient of friction can be found in handbooks [65]. However, the reported values are average values that where intended to be used as guidelines of the sensitivity of the coefficient of friction to the materials in contact. The fact that many factors contribute to the coefficient of friction makes experimental work a more accurate way to obtain the coefficient of friction for a particular case taking into consideration the tribological characteristics of the joint.

A great deal of progress has been made in understanding the processes involved in friction since the pioneering work of Amontons in 1699 and Coulomb in 1785[66]. The present understanding recognizes three basic elements in friction of unlubricated contact bodies [67].

1. The true area of contact between mating rough surfaces.
2. The type and strength of bond formed at the interface where contact occurs.
3. The way in which the material in and around the contacting regions is sheared and ruptured during sliding.

The importance of these three elements can be easily understood from the definition of the friction coefficient (μ) as detailed in equation (2.4):

$$\mu = \frac{Q}{F} \qquad (2.4)$$

where Q is the tangential force needed to shear the junctions between the contacting surfaces and F is the external normal force. The actual contact load P in the true area of contact differs from F by the amount of the intermolecular forces acting between the surfaces in contact as shown in equation (2.5). This force will be referred to as the adhesion, F_{ad} and, hence:

$$P = F + F_{ad} \qquad (2.5)$$

By substituting equation (2.5) into equation (2.4), we can rewrite (μ) as:

$$\mu = \frac{Q}{P - F_{ad}} \qquad (2.6)$$

where the right-hand side of equation (2.6) contains all the three elements mentioned above. The contact load P is related to the true area of contact through the general area of contacting rough surfaces. The adhesion, F_{ad} relates to the strength of the bond formed at the interface, and the tangential force, Q, to the shearing of the contact and, hence, to the friction force.

A number of mechanisms [67] of friction such as adhesion, mechanical interaction of surface asperities, plowing of one surface by asperities on the other, deformation and/or fracture of surface layers (e.g. Oxides) etc. are recognized [65]. These mechanisms will usually act simultaneously but they may occur in different proportions under different circumstances.

2.5.2 Analytical Determination of the Coefficient of Friction

In a recent paper, Melkote et al. [68] presented a new algorithm based on the contact elasticity method for determining the optimum clamping forces for a multi clamp workpiece/fixture system. The algorithm uses a contact mechanics model to determine a set of contact forces and displacements, which are then used for clamping force optimization. The frictional condition existing between any pair of contacting surfaces is determined by the relative magnitude of the normal and tangential tractions at the contacting surface. The problem is formulated as a multi-objective constrained optimization problem with one of the constraints is for the forces to satisfy Coulomb's law of friction.

Moslehy et al. [69] presented a model for the prediction of the steady state coefficient of friction. In his model the relative contribution of asperity, adhesion, asperity plowing and debris were considered. Consider two materials "1" and "2" where that designated "1" is the softer. Allowing for different average surface shear stresses at each contact area, the total plastic deformation energy is the summation of the individual contributions as suggested in Figure 2.6:

Where A_{ij} represent an individual contact area and the summation is carried over all CP_j of these for each of the two materials.

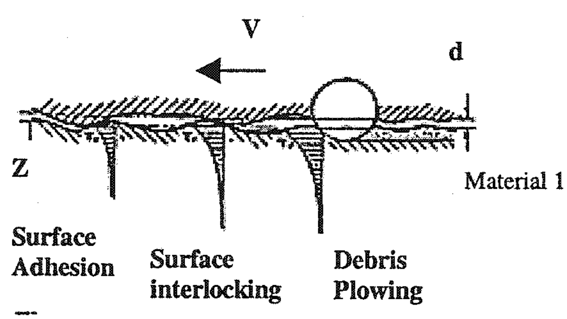

Figure2.6. Different near- surface stress contribution due to different mechanisms [69].

Now, equating the frictional work done to the plastic deformation energy stored in both materials, general equation for the coefficient of friction of a tribosystem is shown in equation (2.7):

$$\mu = \sum_{i=1}^{CP_1}\left(\frac{A_{i1}}{P}\right)\tau_1' f\left(\frac{\tau_{i1}}{\tau_1'}\right) + \sum_{i=1}^{CP_2}\left(\frac{A_{i2}}{P}\right)\tau_2' f\left(\frac{\tau_{i2}}{\tau_2'}\right) \qquad (2.7)$$

Where, the total average shear stress results from the combined effects of asperity interaction, surface adhesion and debris plowing. Equation (2.7) suggests separate analysis of the individual contributions. Figure 2.7, shows how the real contact area is comprised of both individual asperity and debris contributions A_{ai} and A_{di}, which support portions of the total normal load P_{ai} and P_{di} respectively. It follows that the resultant real area of contact and normal load can be obtained by summation as detailed in equations (2.8) and (2.9) respectively.

$$A_r = \sum A_{ai} + \sum A_{di} = A_a + A_d \qquad (2.8)$$

$$P_r = \sum P_{ai} + \sum P_{di} = P_a + P_d \qquad (2.9)$$

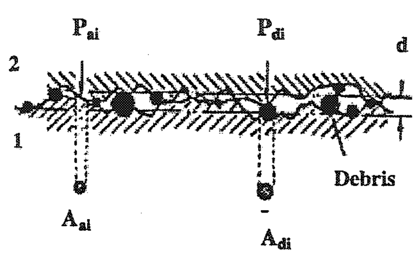

Figure 2.7. Contacts between two surfaces [69].

The expression for the coefficient of friction can be rewritten in terms of three different contributions (asperity adhesion, asperity plowing and debris), with partitioning of load and contact area between them as detailed in equation (2.10).

$$\mu = \frac{S_1}{P}\left[(1-\beta)A_a f\left(\frac{\tau_{a1}}{S_1}\right) + \beta A_a + A_{d1}\right] + \frac{S_2}{P}\left[(1-\beta)A_a f\left(\frac{\tau_{a2}}{S_2}\right) + \beta A_a f\left(\frac{S_1 H_1}{S_3 H_2}\right) + A_{d2}\right] \quad (2.10)$$

where, this equation can be used to obtain the coefficient of friction of a given tribosystem.

In another paper Moslehy et al. [70] presented the results of a parametric study conducted using the model developed in [69]. He reviewed the significance of the various parameters in the model. It is seen that the mechanical properties, surface roughness characteristics and the size of the entrapped debris are important factors while adhesion is not.

2.5.3 Experimental Determination of the Coefficient of Friction

Laboratory measurement of friction coefficients are sometimes designed to simulate particular sliding contact situations, screen materials for friction critical applications, acquire a generic friction data or learn about the fundamental nature of friction of solids or lubricated solids by carefully controlling various influences, such as normal force, velocity, surface roughness, temperature, humidity level, lubrication composition, etc. Since frictional behavior is a property of the tribosystem, and not exclusively of the materials in contact, no single test can stimulate all types of frictional situations. Rather, the method of testing must be selected to address specific needs of the investigation. Consequently, compilations of friction data should be used with care. Eight common types of tribometers [71] are shown in figure 2.8. The four geometries shown at the top of the figure are the most common and can be purchased from commercial suppliers. The reciprocating pin-on-flat is widely used, particularly in the automotive and lubricant industry, to screen materials, coatings, and oils for cylinder/piston ring friction. Commercial versions of the pin-on-flat device can be fitted for cylinder-on-flat sliding as well as piston ring segment-on-cylinder liner testing. The disk-on-disk test is a traction test in which rotating rollers (or one fixed and one rotating roller) contact each other. The pin-in-vee block test is used for screening the antiseizure properties of lubricants.

In an initial effort [72] experiments were carried out to characterize friction for commercially available fixture elements in dry contact with A356 Aluminum. This study revealed that the coefficient of friction was very sensitive to fixture element geometry and workpiece surface topography, but relatively insensitive to clamping force and fixture element size. It also revealed that even under controlled conditions, the value of the coefficient of friction vary significantly from test to test. While a good start, this work did not present evidence of the phenomena that may have resulted in variations of the friction values, nor did it address important issues such as the effects of residual cutting fluid and normal joint rigidity on friction.

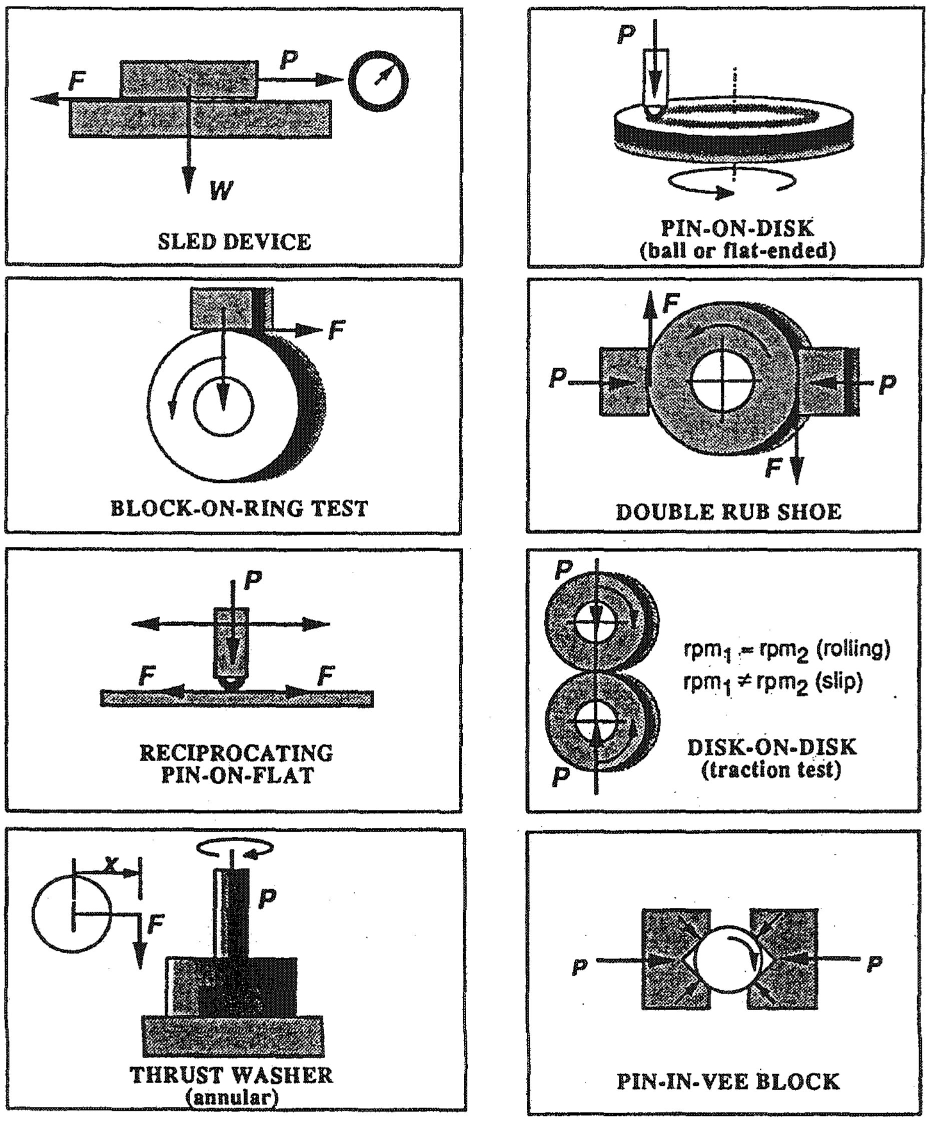

Figure2.8. Eight common types of friction testing geometries [71].

Xie et al. [64] presented a method for the experimental evaluation of the coefficient of friction for a workpiece/fixture system. The method is based on previous work done by [72] [73]. They investigated the effect of workpiece surface topography, fixture element type, fixture element size, clamping force, presence of cutting fluid at the joint and normal joint rigidity on the coefficient of friction. They assumed that friction is due to asperity interlocking and shearing at the joint interface, which is typically assumed in fixture research [73-79].

Like wise, it is generally assumed that this friction mechanism is insensitive to normal load and hence static friction coefficient (μ_s) and dynamic friction coefficient (μ_k) are constant. However, there are a variety of mechanisms that can contribute to friction. These include adhesion, micro-cold welding of asperity contact points and subterranean plowing of the contacting pair surfaces, especially in cases in which one of the contacting elements is harder than the other. In fact, any thing short of general weldment [79] of the contacting pairs can be considered a source of friction.

In general, the types of mechanisms involved are highly dependent upon the material and geometry of the contacting pairs, their surface topography and hardness, and the presence of inter-joint materials such as fluids and contaminants. In addition, environmental factors such as temperature and/or vibration are also known to affect friction.

The authors [64] gave some practical insight in the fixture tips used for automotive industry. However they did not explain the fact that coefficient of friction decreases with increased clamping load.

Other experimental procedures for the determination of the coefficient of friction exist in the literature. Worth mentioning is the ring compression test developed by Male and Cockcroft [80] and was introduced as a mean to measure the coefficient of friction in bulk metal forming. The procedure is simple; a ring is compressed between two flat platens. The internal diameter of the ring might increase or decrease based on the friction conditions at the tool-workpiece interface.

2.6 Summary

This chapter reviewed the literature available for the different disciplines involved in modeling of machining processes. As evident from this review, each of these aspects was tackled separately. The contribution of certain aspects was either neglected or considered of minor effect. For the modeling of the effect of workpiece/fixture contact on the machining processes dynamics, the open literature lacks research on this area. The research on fixture analysis and design assumed the cutting forces to be static or used the peak values in the analysis. Also, friction was neglected or coulomb's friction was assumed.

The open literature lacks a generic model for machining processes that integrates all aspects contributing and affecting the machining process dynamics and stability. Such a model would enable more accurate predictions of the cutting forces and would provide an off-line tool for design and optimization of machining process variables and fixture configuration.

CHAPTER3: GEOMETRIC MODELING OF THE MILLING PROCESS

3.1 Introduction

To accurately simulate the machining process a comprehensive geometric modeling technique is needed along with the mechanical model. Non-Uniform Rational B-Spline, commonly referred to as NURBS, have become the preferred industry standard for the representation, design and data exchange of geometric information processed by computers [81-83]. NURBS algorithms are recognized as a powerful tool for geometric design. They provide a unified mathematical basis for representing both analytic shapes and freeform entities. They are also fast, numerically stable and invariant under common geometric transformations. Most of the commercial packages can provide the parts geometric data as NURBS curves and surfaces, which would facilitate any future extension of the current work. The geometric modeling of the machining process as defined in this work has four tasks:

a) To represent the tool cutting edge,

b) To represent the local surface topology of the part,

c) To represent the workpiece-cutter intersection during machining and

d) To provide information to create/update the finite element mesh.

These were the key elements in consideration when selecting and developing the geometric modeling methodology. The special purpose geometric modeler developed in this research is based on surface modeling. It consists of a set of routines coded in C++ programming language to fulfill the four tasks listed above using surface/surface, curve/surface and curve/curve intersection routines utilizing NURBS curves and surfaces. The developed surface modeler provides enough geometric information to adopt a more comprehensive mechanistic model of the machining process and at the same time, avoids the computational burden of commercial packages. These computational burdens arise for hardware requirements for running commercial packages and software problems associated with memory handling and definition of entities intersection functions. Also, it includes an automatic mesh generation algorithm, which is capable of updating the workpiece geometry during the cutting process.

3.2 Cutting Edge Profile Representation

The type of tooling used in milling processes include ball end, flat end and face mills. The cutting edges configuration within each of these types vary and custom tooling might be required. Therefore, it is important to have a generalized modeling procedure to represent the varied cross-section of tooling. The majority of literature has dealt with simple cutting edge designs [84]. Only recently, has the literature presented work that attempts to generalize the representation of the cutting edge. Imani [36], Abrari [37] and Bailey [39] used cubic piecewise NURBS to represent the tool cutting edge profile. A p^{th} degree NURBS curve, Figure 3.2, is defined by [81]:

$$C(u) = \frac{\sum_{i=0}^{n} N_{i,p}(u) w_i P_i}{\sum_{i=0}^{n} N_{i,p}(u) w_i P} \quad 0 \leq u \leq 1 \qquad (3.1)$$

The *$\{P_i\}$* are The i control points, the *$\{w_{i,}\}$* are the weights, and the *$\{N_{i,p}(u)\}$*are the p^{th}–degree B-spline basis functions defined on the non periodic(and nonuniform) knot vector:

$$U = \left\{ \underbrace{a,\ldots\ldots,a}_{p+1}, u_{p+1}, \ldots\ldots, u_{m-p-1}, \underbrace{b,\ldots\ldots,b}_{p+1} \right\} \qquad (3.2)$$

where a=0 , b=1 and $w_i > 0$ for all i. The I^{th} B-spline basis function of degree p, denoted by $N_{i,p}(u)$, is defined as:

$$N_{i,0}(u) = \begin{cases} 1 & \text{if } u_i \leq u \leq u_{i+1} \\ 0 & \text{otherwise} \end{cases}$$

$$N_{i,p}(u) = \frac{u - u_i}{u_{i+p} - u_i} \cdot N_{i,p-1}(u) + \frac{u_{i+p+1} - u}{u_{i+p+1} - u_{i+1}} \cdot N_{i+1,p-1}(u) \qquad (3.3)$$

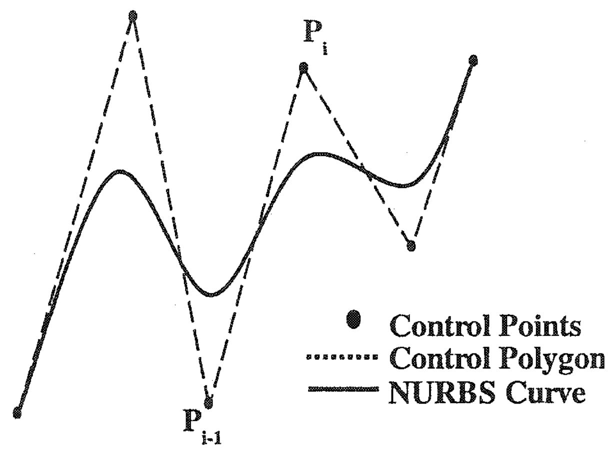

Figure 3.1. A Sample NURBS Curve

In the current work a generalized NURBS representation of an arbitrary cutting edge design is developed. The geometric representation of the cutting edge is done in two steps. First, points on the cutting edge can be measured using CMM machines, digitized from a drawing or calculated from a mathematical representation of the tool geometry. Then, these points are passed to a global interpolation/approximation algorithm that interpolates the cutting edge curve or profile. The cutting edge is interpolated as a NURBS curve. This method of representing the cutting edge is generic and allows the representation of any cutting edge profile. Figure 3.2 shows the steps involved.

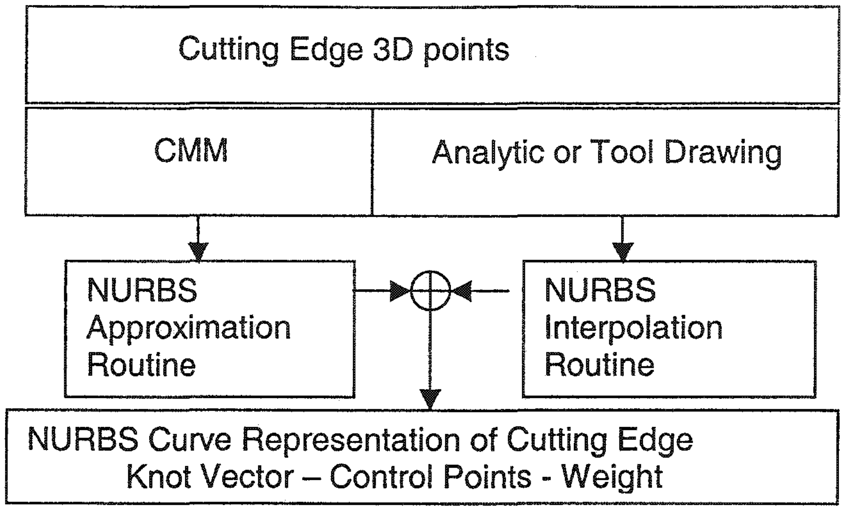

Figure 3.2. Geometric representation of the cutting edge.

3.3 Workpiece Boundary Representation

NURBS surfaces, Figure 3.3, are used to represent the bounding surfaces of the workpiece. These bounding surfaces are then used to create the mesh for the finite element analysis. Figure 3.4 shows the bounding surfaces of a freeform workpiece. A NURBS surface of degree p in the u direction and degree q in the v direction is a bivariate vector-valued piecewise rational function of the form[81]:

$$s(u,v) = \frac{\sum_{i=0}^{n}\sum_{j=0}^{m} N_{i,p}(u)N_{j,q}(v)w_{i,j}P_{i,j}}{\sum_{i=0}^{n}\sum_{j=0}^{m} N_{i,p}(u)N_{j,q}(v)w_{i,j}} \qquad 0 \le u,v \le 1 \qquad (3.4)$$

The $\{P_{i,j}\}$ form a bi-directional control net, the $\{w_{i,j}\}$ are the weights, and the $\{N_{i,p}(u)\}$ and the $\{N_{i,q}(v)\}$ are the non rational B-spline basis functions defined on the knot vectors U and V. The length of the U knot vector is r = n +p+1 and the length of the V knot vector is s =m+ q +1, where n and m, are the number of control points in u and v directions respectively. The surface equation can be written as:

$$s(u,v) = \sum_{i=0}^{n}\sum_{j=0}^{m} R_{i,j}(u,v)P_{i,j} \tag{3.5}$$

where R is the piecewise rational function

$$R(u,v) = \frac{N_{i,p}(u)N_{j,q}(v)w_{i,j}}{\sum_{k=0}^{n}\sum_{l=0}^{m} N_{k,p}(u)N_{l,q}(v)w_{k,l}} \tag{3.6}$$

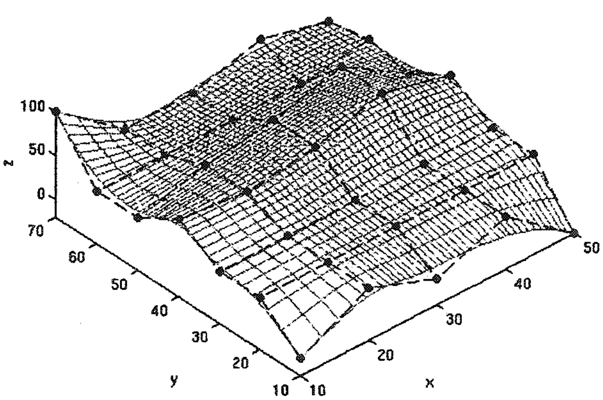

Figure 3.3. A Sample NURBS Surface

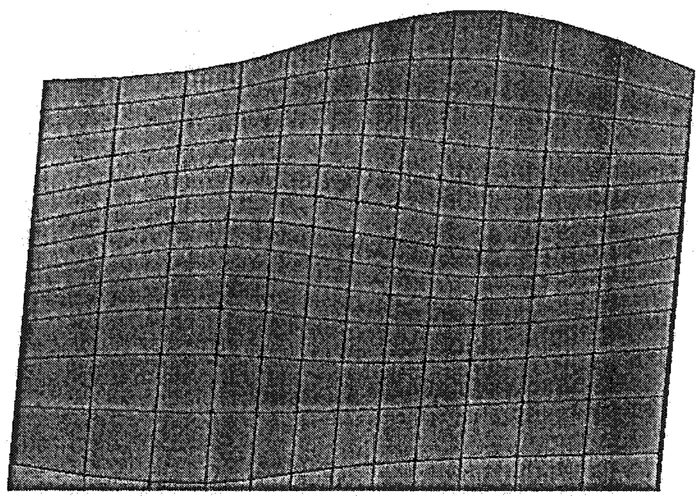

Figure 3.4. Workpiece boundary representation by the developed geometric modeler.

3.4 Part Local Surface Topology Representation

The local surface topology of the part is defined here as those surfaces generated by previous tool paths in the vicinity of the current tool position. The concept here is to offer a generalized approach to representing the local surface topology of the part without using a computationally expensive CAD system. The procedure for generating the local surface topology of the part is as follow:

The tool path information is extracted from the given cutter location (CL) data files. A data structure is generated for each tool path segment. The data structure contains the primitive surface representation and a bounding box for the given tool path segment. During simulation, a control space, Figure 3.5, is defined at the current tool position. A control space is defined as a bounding box surrounding the current tool position. The size of control space is defined by the user and is related to the geometry of the tool. Only those tool path segments, which intersect the control space, are used to create the local surface topology. A simple bounding box intersection algorithm is used to determine which tool path segments contribute to the local surface topology of the part in the vicinity of the current tool position. The advantage of the above methodology, which is an extension of the work done by Bailey[39], is that all the information required to create an accurate representation of the local surface topology of the part is contained within simple data structures for each tool path segment, Figure 3.6.

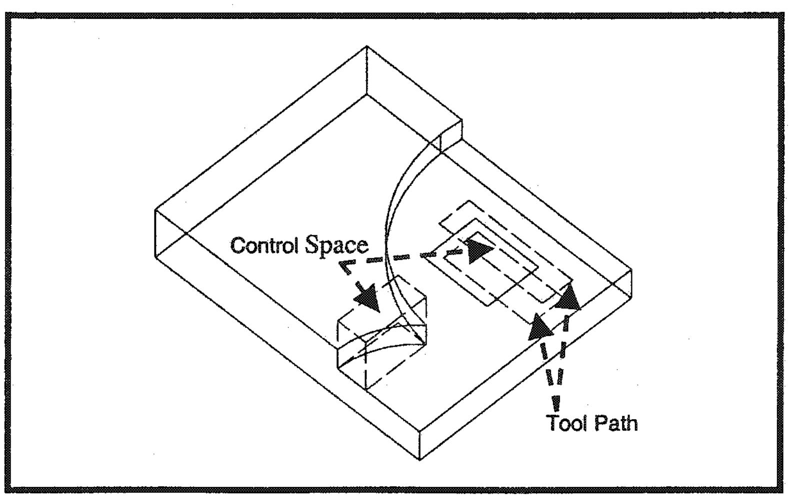

Figure 3.5. Control space definition.

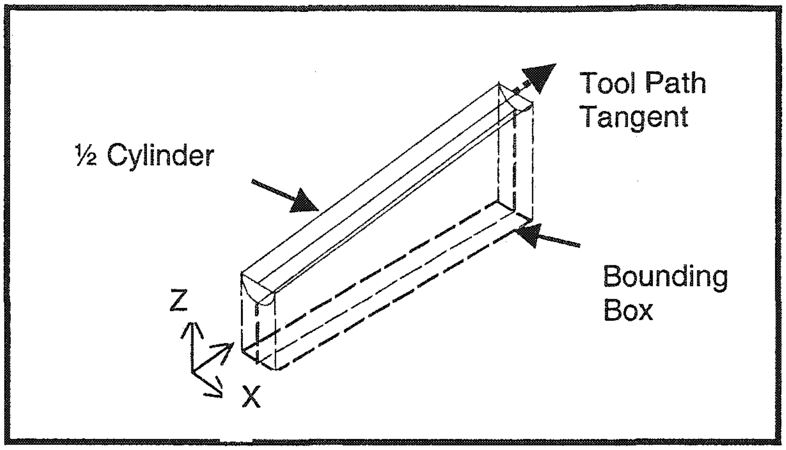

Figure 3.6. Tool path representation.

3.5 Workpiece–Cutter Intersection Model

The workpiece-cutter intersection model is used to determine if a particular insert is engaged in cut with the workpiece. If the cutting insert is engaged in cut, then the cutting forces acting on the tooth are calculated using the chip load and the cutting force model. However, if the tooth is not engaged in cut, the cutting forces are set to zero. The workpiece-tool intersection scheme developed utilizes NURBS surface/surface, curve/surface and curve/curve intersection algorithms to find the intersection surface between the workpiece and the tool. This intersection surface is intersected again with the curve representation of the cutting edge to find the incut segments. These segments are then used to compute the chip load and the cutting force (Figure 3.7). The methodology used for determining incut segments for a defined local surface topology and angular position of cutting edge is as follow:

1. Each point along the cutting edge is classified as either in/out of each tool path bounding box, which defines the local surface topology.
2. If the point on the cutting edge is contained within a tool path bounding box, determine the corresponding Z value (distance in the vertical direction) to form the primitives representing that surface ($Z_{surf,i}$).
3. Find the minimum of all $Z_{surf,i}$ (Z_{min}).
4. If the cutting edge point Z value is less than Z_{min} then the cutting edge is incut.

The above methodology is used to extract both the start and end of incut segment.

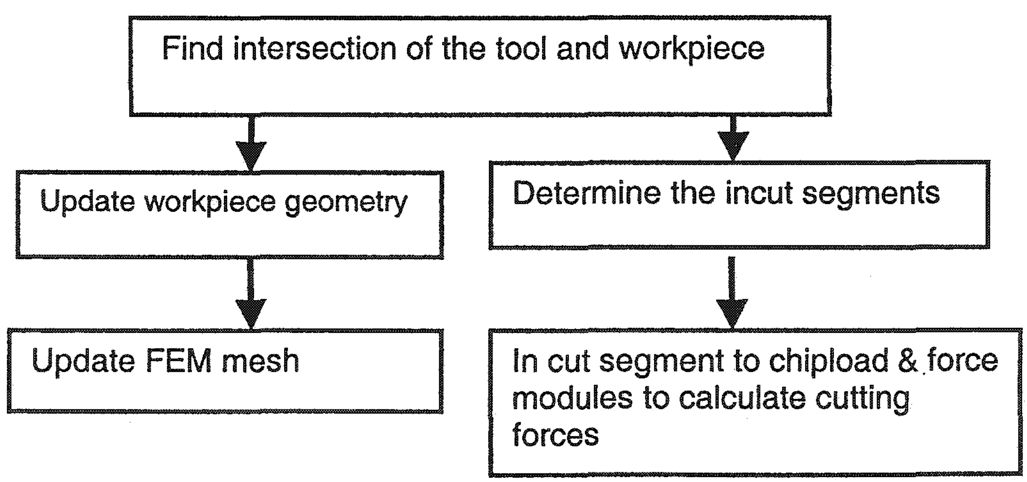

Figure 3.7. Steps involved in finding the workpiece –cutter intersection.

3.6 Automatic Mesh Generation

The finite element method is a powerful and versatile analysis tool, but its usefulness is hampered by the need to generate an elaborate mesh. This can be very time consuming and error prone if done manually. In recognition of this problem, a large number of methods have been devised to automate the mesh generation task [85]. Delaunay triangulation is considered by many researchers [86][87][88] to be the most suitable for FE analysis. Many mesh generators produce a mesh of triangles by first creating all the nodes and then consenting the nodes to form triangular elements. This triangulation maximizes the sum of smallest angles of the triangles; thus thin elements are avoided whenever possible. The Voronoi diagram of a set of N points in a plane consists of N polygons *V(i)* each centered on point *i* such that the locus of the points on the plane nearest to node i are included in *V(i).* The Delaunay triangulation is obtained by connecting the points associated with neighboring Voronoi polygons. The above definitions extend naturally to higher dimensional spaces.

There are very few published 3D-mesh generation methods compared to the 2D methods due to greatly increased complexity. While several mesh generation approaches offer the quadrilateral elements as an output in 2D, none has been extended to offer the brick element for the 3D case. The 3D mesh generation methods can be covered under the following four approaches:

1. Topology decomposition approach

This approach was developed by Wordenweber [89], it decomposes an object into a set of gross elements by connecting its vertexes to form triangles. Element sizes and shapes cannot really be considered because it is the object topology that determines how the object is decomposed. These gross elements must be refined later to satisfy the required mesh density distribution.

2. Node Connection approach

This mesh generation approach is very popular, perhaps because it is conceptually simple; there are two main phases in this approach:

2.1 Node generation: the literature presents different techniques for automatic node generation. Presented here is Cavendish random node generation technique [90]. In this technique nodes are first added to the object boundary at regular intervals. Then interior nodes are generated to satisfy mesh density requirement as follows. The object is divided into a number of zones of different desired element sizes. In zone *i* a square grid of gauge *r(i)* is superimposed. For each sub square of the grid, one interior node is randomly generated. If this node falls inside the object, and of distance greater than *r(i)* from the boundary and from previously generated nodes, it is accepted. If not, another node is generated and checked. A fixed number of attempts are made to generate an acceptable node for each sub square, if none is successful then that subsquare is not considered further.

2.2 Element generation: the previously generated nodes are connected to form elements such that no element overlap and the entire object is covered. Most methods used produce triangular elements. In addition to the Delaunay triangulation methods mentioned earlier, Lewis and Robinson [91], present a recursive algorithm that first divides the object into two halves and then keeps on dividing the halves until only triangles remain.

3. Grid-based approach

The grid-based (Iso-Parametric Mapping) approach arises from the observation that a grid looks like a mesh. It can therefore be made into a mesh provided that the grid cells along the object's boundary can be turned into elements. The surface of the structure is initially divided into triangular or quadrilateral patches. In each patch, the coordinates of the corner nodes, called key nodes, are evaluated. The number of nodes being discretized in each path is controlled by the user specified density. Once the nodal coordinates are obtained, the nodes are numbered starting from a vertex and the nodal connectivities are created. Different methods to construct the mesh exist under this approach, presented here is the method by Yerry and Shepard [92]. Their method starts with a quad tree encoding of an object. This quad tree is modified to be more suitable to mesh generation as follows:

- The object interior is subdivided into quadrants which sizes satisfy the mesh density distribution.
- Neighboring quadrants may differ by at most one length of subdivision.

- The quadrants on the boundary may have cut corners.

Each quadrant is next broken up into triangles such that the resulting mesh is conforming. The triangles, especially the boundary ones, may not be will shaped. This same method is extended to 3D. The object is octree-encoded again with some modifications. The octants are broken up into tetrahedra by using a complicated algorithm. A detailed description of this method application is found in [93].

4. Geometry decomposition approach

This approach gives some consideration to element shapes and sizes while decomposing an object. Some methods are based on recursion, others on iteration.

Cavendish et al. [86] described an interactive solid mesh generation system capable of generating valid meshes of well–proportional tetrahedral finite elements for the decomposition of multiply connected solid structures. The system uses semi-automatic node insertion procedure to locate element node points with and on the surface of a structure. An independent automatic 3D triangulator then accepts these nodes as input and connects them to from valid finite element mesh of tetrahedral elements. Sapidis and Perucchio [94] classified the different methods for mesh generation under three classes, element extraction algorithms, domain triangulation algorithms and recursive spatial decomposition algorithms.

In this research, a mesh generation scheme was developed based on the grid-based approach. The proposed scheme utilizes the iso-curves associated with the NURBS representation of the workpiece bounding surfaces to create nodes that are used to mesh the whole workpiece with brick elements. This scheme is applied to generate and update the mesh based on the updated workpiece geometry (Figure 3.8 and 3.9).

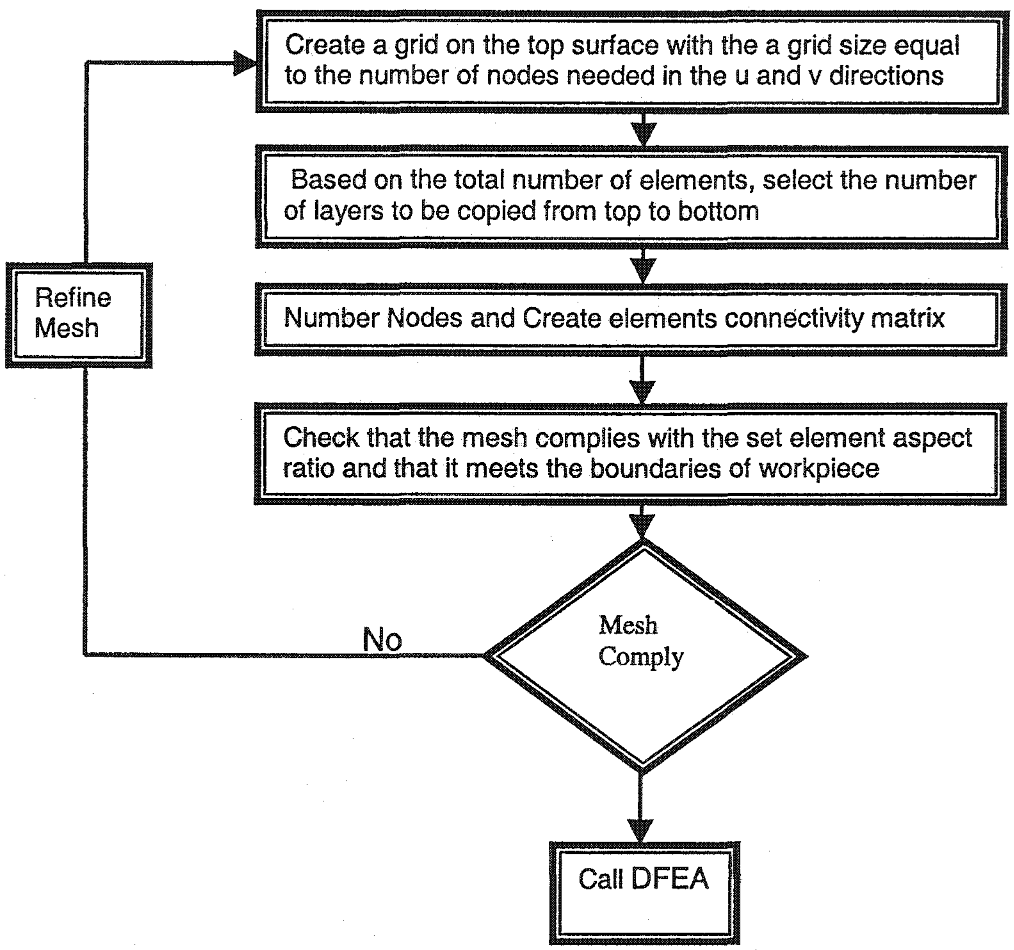

Figure 3.8. The steps involved in the mesh generation.

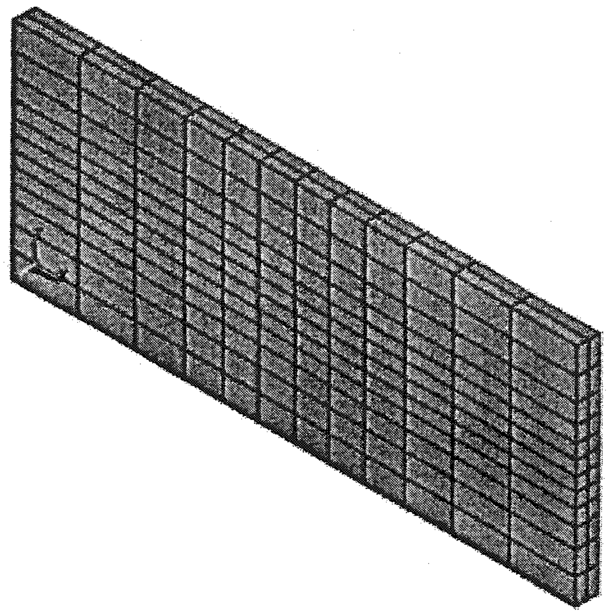

Figure 3.9. Meshed workpiece.

3.7 Summary

This chapter presents the methodology used to represent the geometric part of the simulation. The Workpiece and cutting edge representation is done using an in-house geometric modeler based on NURBS curves and surfaces. The use of the NURBS allows the interface with different commercial software packages. Figure 3.10 display a flow chart of the methodology.

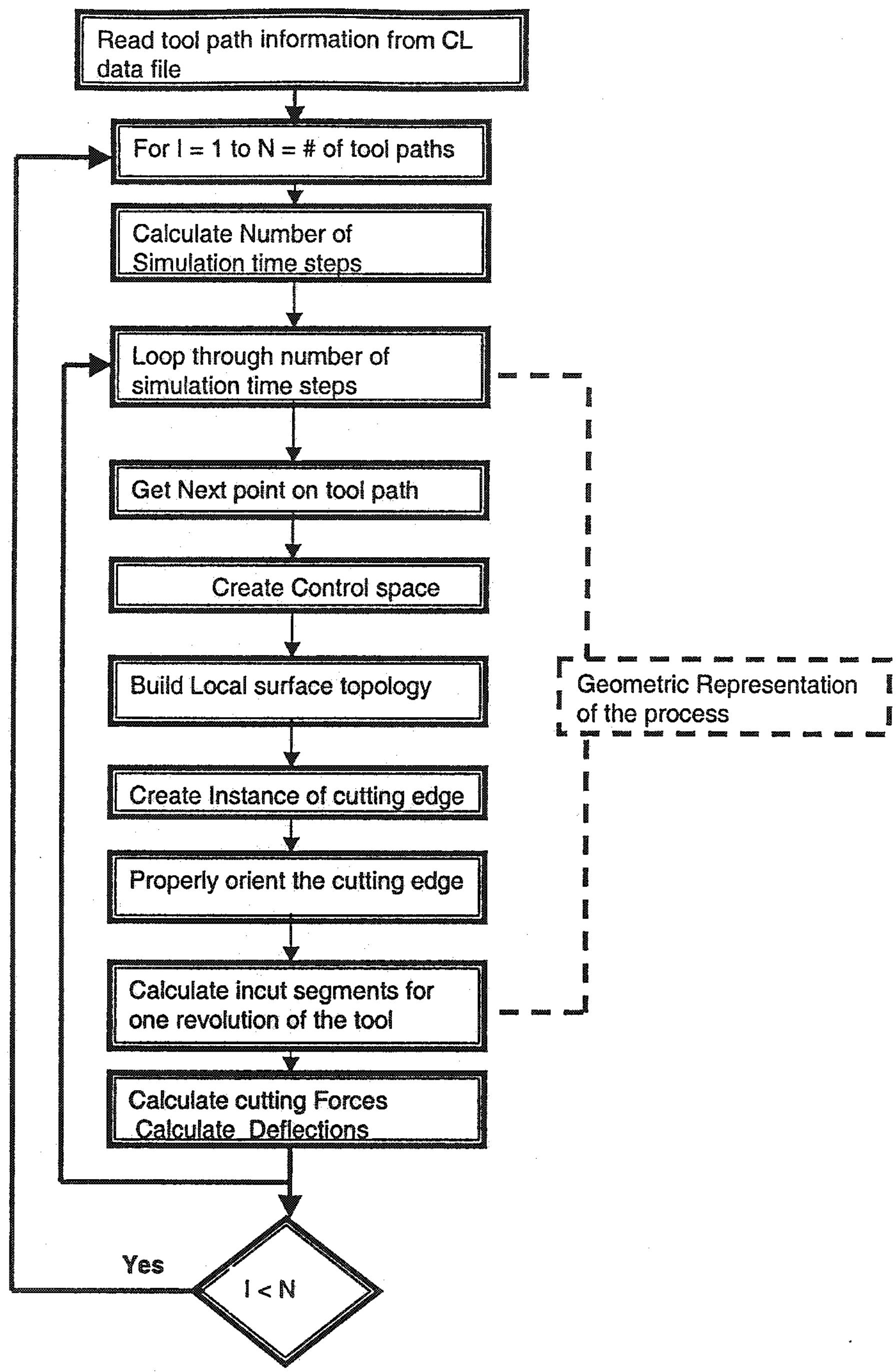

Figure 3.10. Geometric modeling flow chart.

CHAPTER 4: MECHANISITIC MODELING OF THE MILLING PROCESS

4.1 Introduction

Detailed research work has been done on modeling of machining processes. As evident from the literature the used approaches varied in its complexity and its comprehensiveness. The modeling of cutting forces either dynamic or static is a well-established topic and the literature is full of different models for different machining processes Tlusty [95], Altintas [96], Abrari [37], Jayrama [97], Gu [98], Fu [99] and Kim [15]. What is really challenging, is taking into account the factors that affects the machining process dynamic and stability. To that end the literature contains research on the effect of tool flexibility and the initial position errors on machine tool dynamics Fu [99] and Kim [15].

The open literature lacks research on the effect of the fixture element flexibility and location on the machining process dynamics. This particular topic is the motivation for this work and the objective is to capture this effect and integrate it with other factors affecting the machining process dynamics. This chapter covers the implementation of a face milling dynamic force model that integrates the effect of the tool dynamics and the initial position errors along with the workpiece/ fixture dynamics.

4.2 Development of the Cutting Force Model

The machining of complex geometries and flexible parts requires a complete consideration of the machining process dynamics (i.e. machine tool, workpiece and fixture dynamics). None of the current dynamic models available in the literature explicitly consider the effects of the machine tool and workpiece/fixture dynamics, and the workpiece/fixture contact conditions as well as the total influence of changes in cutter geometry, and the cutting conditions due to the dynamic deflections in milling. A block diagram of the various software modules for the proposed comprehensive force model is shown in figure 4.1.

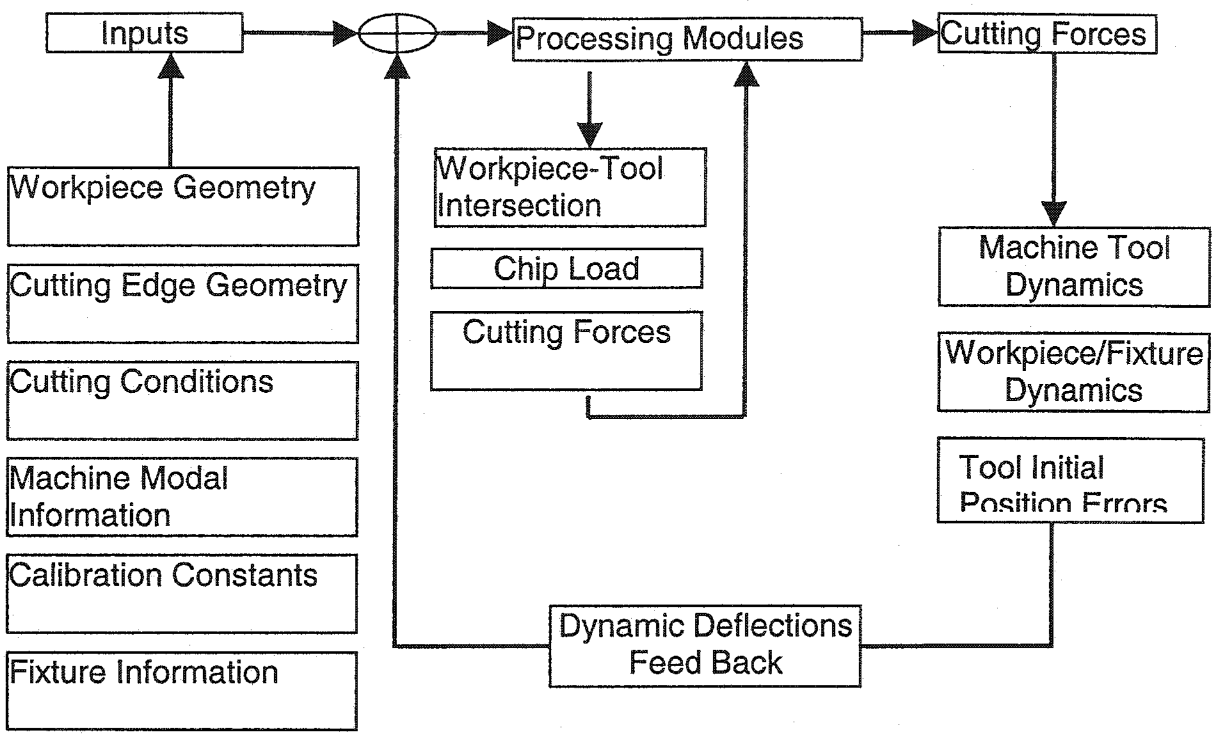

Figure 4.1. Flowchart of the proposed force model components.

It is argued here that such a model will enable an accurate prediction of the cutting process stability and the machined surface quality. The proposed dynamic model is a closed loop interaction between the workpiece-cutter intersection model, the chip load model, the cutting force model, the tool/workpiece/fixture dynamic deflection model and the deflection feed back model. It is based on previously developed models [7][15] with the following enhancements:

1. Extending the model to include the dynamic effect of both workpiece and fixturing elements. In addition to the machine tool dynamics and the cutter initial position errors.
2. Investigating and modeling of the workpiece /fixture frictional contact conditions on the dynamics of the complete machining system.

4.3 Modeling of Static Cutting Forces

The instantaneous static force components can be obtained as a resultant of all forces acting on the individual inserts engaged in cutting at a certain instant [100-103]. Figure 4.2 shows the force components as a function of the geometry of the face milling process. As can be seen from figure4.2, the nominal instantaneous chip thickness, C $(\theta_i(\phi))$, instantaneous depth of cut $D(\theta_i(\phi))$, and uncut chip area $A_i(\phi)$, on the insert i and the tool rotational angle , ϕ, are given as:

$$C\left(\theta_i(\phi)\right) = f_t \sin\left(\theta_i(\phi)\right) \qquad (4.1)$$

$$D\left(\theta_i(\phi)\right) = W \qquad (4.2)$$

$$A_i\left((\phi)\right) = C\left(\theta_i(\phi)\right) \bullet D\left(\theta_i(\phi)\right) \qquad (4.3)$$

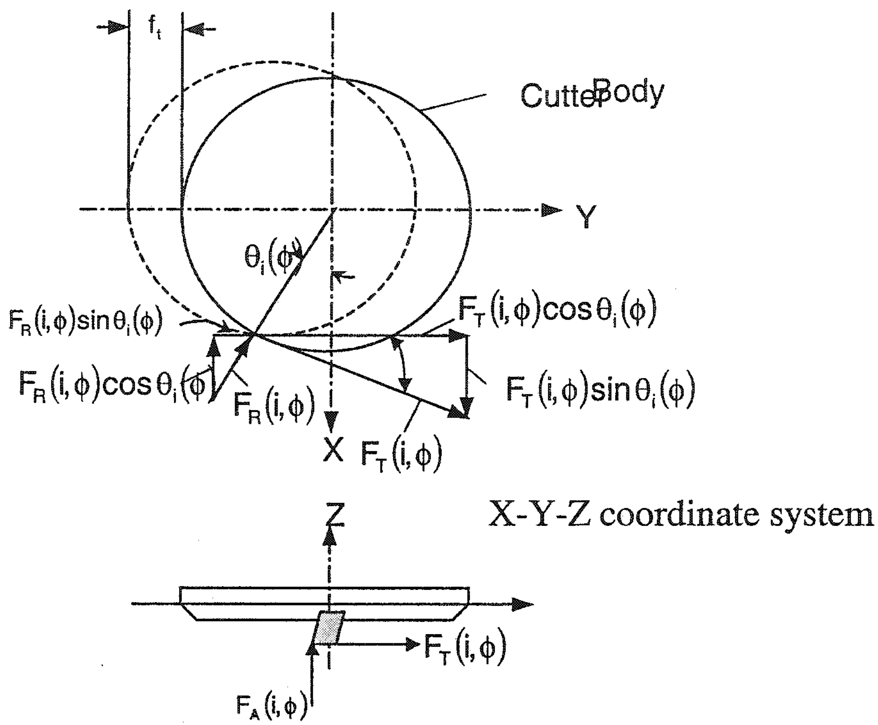

Figure 4.2. Face milling cutter geometry and force components [15].

In the milling process, the chip thickness and the instantaneous specific cutting pressure continuously change along the tooth path. Martellotti [104] and Koenigsberger and Sabberwal [105] have found that the average tangential cutting pressure, K_T and the average chip thickness may be substituted for these continuously varying quantities. The relation between the observed average cutting forces and the empirical constants in multi tooth cutting is derived from the relation between theoretical cut geometry and the mean forces. The tangential force $F_T(I,\phi)$ acting on a tooth can be expressed as the product of the cross sectional area ,$A_i(\phi)$, and of the specific cutting pressure, K_T. the radial force, $F_R(I,\phi)$ acting along the cutting edge in the radial direction of the cutter is obtained by multiplying the tangential force by an empirical constant K_R. Neglecting the effect of tool geometry, the cutting forces in the tangential and radial direction(Figure 4.3) can be expressed as:

$$F_T(I,\phi)= K_T\, A_i(\phi) \qquad (4.4)$$

$$F_R(I,\phi)= K_R\, A_i(\phi) \qquad (4.5)$$

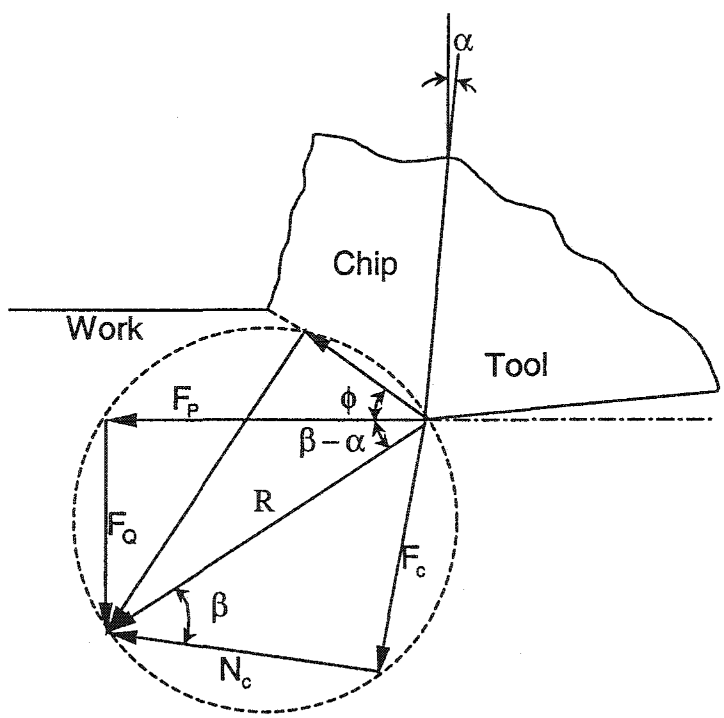

Figure 4.3. The relation between different force systems.

Since the empirical constants K_T and K_R are usually determined based on two orthogonally measured mean forces (F_{xm} and F_{ym}) the axial force F_A as shown in figure4.2 could not be predicted accurately in oblique cutting. Therefore, in three dimensional cutting an additional constant relating to the axial force is needed. In order to express the axial force more accurately, the empirical constant K_A, the ratio of the axial to tangential force is introduced below, so that the axial force F_A (l,ϕ) can be expressed as:

$$F_A(l,\phi)= K_A\, A_i(\phi) \qquad (4.6)$$

In order to consider the effect of insert geometry, the abc insert coordinate system(Figure 4. 4) is introduced: the a axis is the direction of the insert's rake face,

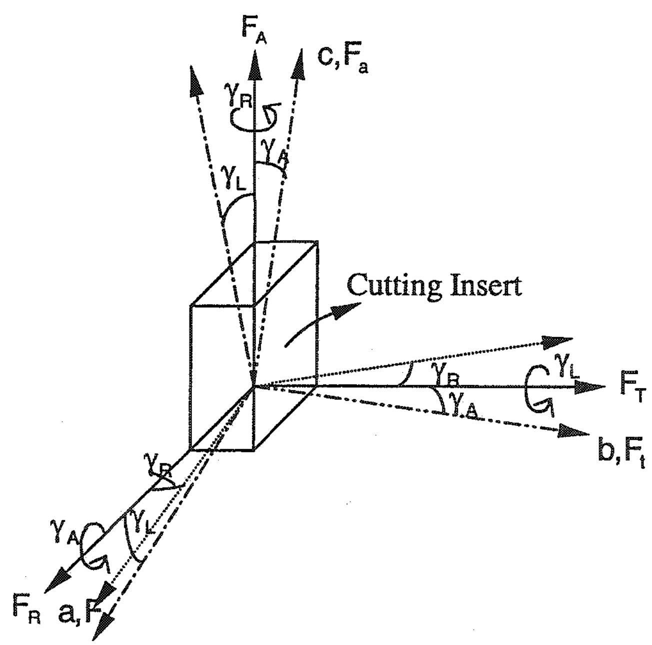

Figure 4.4. Cutting force components in insert coordinate system.

The b axis is tangential to the axial rake face; and the c axis is the direction of the insert lead face. The origin of this coordinate system is located at the edge point of the insert. The radial, axial and tangential force components in the XYZ coordinate system can be obtained by the summation of the force components decomposed in terms of the insert geometry as follows:

$$\begin{aligned}
F_T(i,\phi) &= F_t(i,\phi)\cos(\gamma_A)\cos(\gamma_R) + F_r(i,\phi)\cos(\gamma_L)\sin(\gamma_R) + F_a(i,\phi)\cos(\gamma_L)\sin(\gamma_A) \\
F_R(i,\phi) &= -F_t(i,\phi)\cos(\gamma_A)\sin(\gamma_R) + F_r(i,\phi)\cos(\gamma_L)\cos(\gamma_R) - F_a(i,\phi)\sin(\gamma_L)\cos(\gamma_A) \\
F_A(i,\phi) &= -F_t(i,\phi)\sin(\gamma_R) + F_r(i,\phi)\sin(\gamma_L) + F_a(i,\phi)\cos(\gamma_L)\cos(\gamma_A)
\end{aligned} \tag{4.7}$$

where F_t, F_r and F_a can be obtained from equations(4.4-4.6) as follows:

$$\begin{aligned}
F_t(i,\phi) &= \frac{K_T A_i(\phi)}{\cos(\gamma_R)\bullet\cos(\gamma_A)} \\
F_r(i,\phi) &= K_R * F_t(i,\phi) \\
F_a(i,\phi) &= K_A * F_t(i,\phi)
\end{aligned} \tag{4.8}$$

Substituting equation (4.8) into equation (4.7) and putting it in matrix form:

$$\begin{Bmatrix} F_T(i,\phi) \\ F_R(i,\phi) \\ F_A(i,\phi) \end{Bmatrix} = C(\theta_i(\phi)) * D(\theta_i(\phi)) \begin{bmatrix} \alpha_1 & \beta_1 & \gamma_1 \\ \alpha_2 & \beta_2 & \gamma_2 \\ \alpha_3 & \beta_3 & \gamma_3 \end{bmatrix} \begin{Bmatrix} K_T \\ K_T * K_R \\ K_T * KA \end{Bmatrix} \tag{4.9}$$

Where,

$$\alpha_1 = 1, \alpha_2 = -\tan\gamma_R, \alpha_3 = -\frac{\tan(\gamma_L)}{\cos(\gamma_R)}$$
$$\beta_1 = \frac{\cos(\gamma_L)\tan(\gamma_R)}{\cos(\gamma_R)}, \beta_2 = \frac{\cos(\gamma_L)}{\cos(\gamma_R)}, \beta_3 = \frac{\sin(\gamma_L)}{\cos(\gamma_R)\cos(\gamma_A)}$$
$$\gamma_1 = \frac{\cos(\gamma_L)\tan(\gamma_A)}{\cos(\gamma_R)}, \gamma_2 = -\frac{\sin(\gamma_L)}{\cos(\gamma_a)}, \gamma_3 = \frac{\cos(\gamma_L)}{\cos(\gamma_R)}$$

The XYZ force components acting on insert i at an angle ϕ can be obtained by resolving the radial and tangential force components:

$$\begin{aligned} F_x(i,\phi) &= F_T(i,\phi)\sin(\theta_i(\phi)) - F_R(i,\phi)\cos(\theta_i(\phi)) \\ F_y(i,\phi) &= F_T(i,\phi)\cos(\theta_i(\phi)) + F_R(i,\phi)\sin(\theta_i(\phi)) \\ F_z(i,\phi) &= F_A(i,\phi) \end{aligned} \tag{4.10}$$

The instantaneous XYZ force components at the cutter rotation angle ϕ are the sum of all simultaneously engaged inserts in cutting:

$$\begin{Bmatrix} F_X(\phi) \\ F_Y(\phi) \\ FZ(\phi) \end{Bmatrix} = \sum_{i=1}^{n} \begin{Bmatrix} F_x(i,\phi) \\ F_y(i,\phi) \\ Fz(i,\phi) \end{Bmatrix} \tag{4.11}$$

Substituting equation (4.10) into equation (4.11) we obtain:

$$\begin{Bmatrix} F_X(\phi) \\ F_Y(\phi) \\ FZ(\phi) \end{Bmatrix} = \sum_{i=1}^{n} \begin{bmatrix} \sin(\theta_i(\phi)) & -\cos(\theta_i(\phi)) & 0 \\ \cos(\theta_i(\phi)) & \sin(\theta_i(\phi)) & 0 \\ 0 & 0 & 1 \end{bmatrix} = \begin{Bmatrix} F_T(i,\phi) \\ F_R(i,\phi) \\ FA(i,\phi) \end{Bmatrix} \tag{4.12}$$

Equations (4.9) and (4.12) express the basic static force model that accounts for the cutter and insert geometry. Figures 4.5, 4.6 and 4.6a display the follow chart of the static force model and simulated cutting forces for full and half immersion ratios respectively. This same model is extended to include the machining process dynamics by considering the machine tool and workpiece/fixture system dynamics.

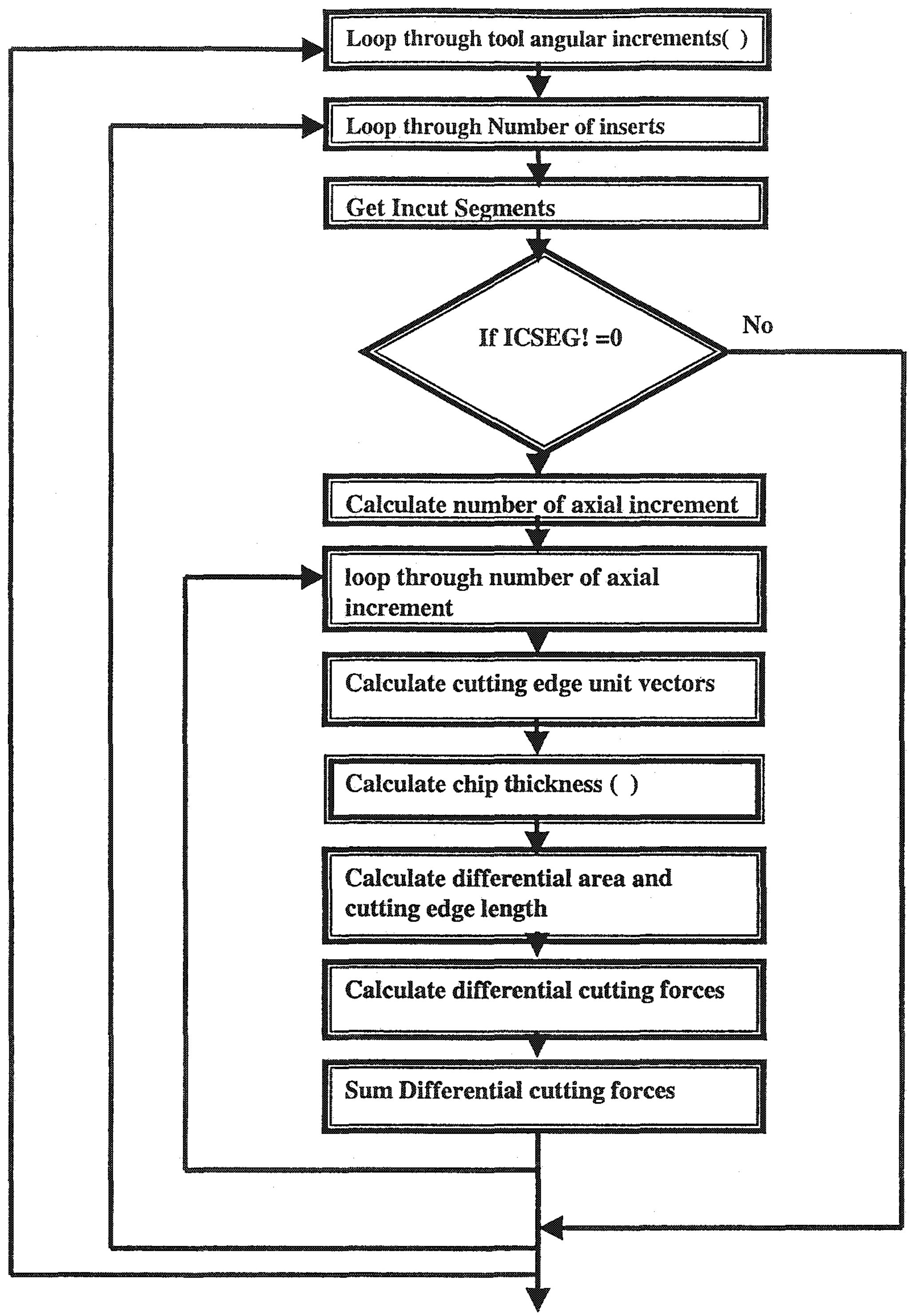

Figure 4.5. Static force model flowchart.

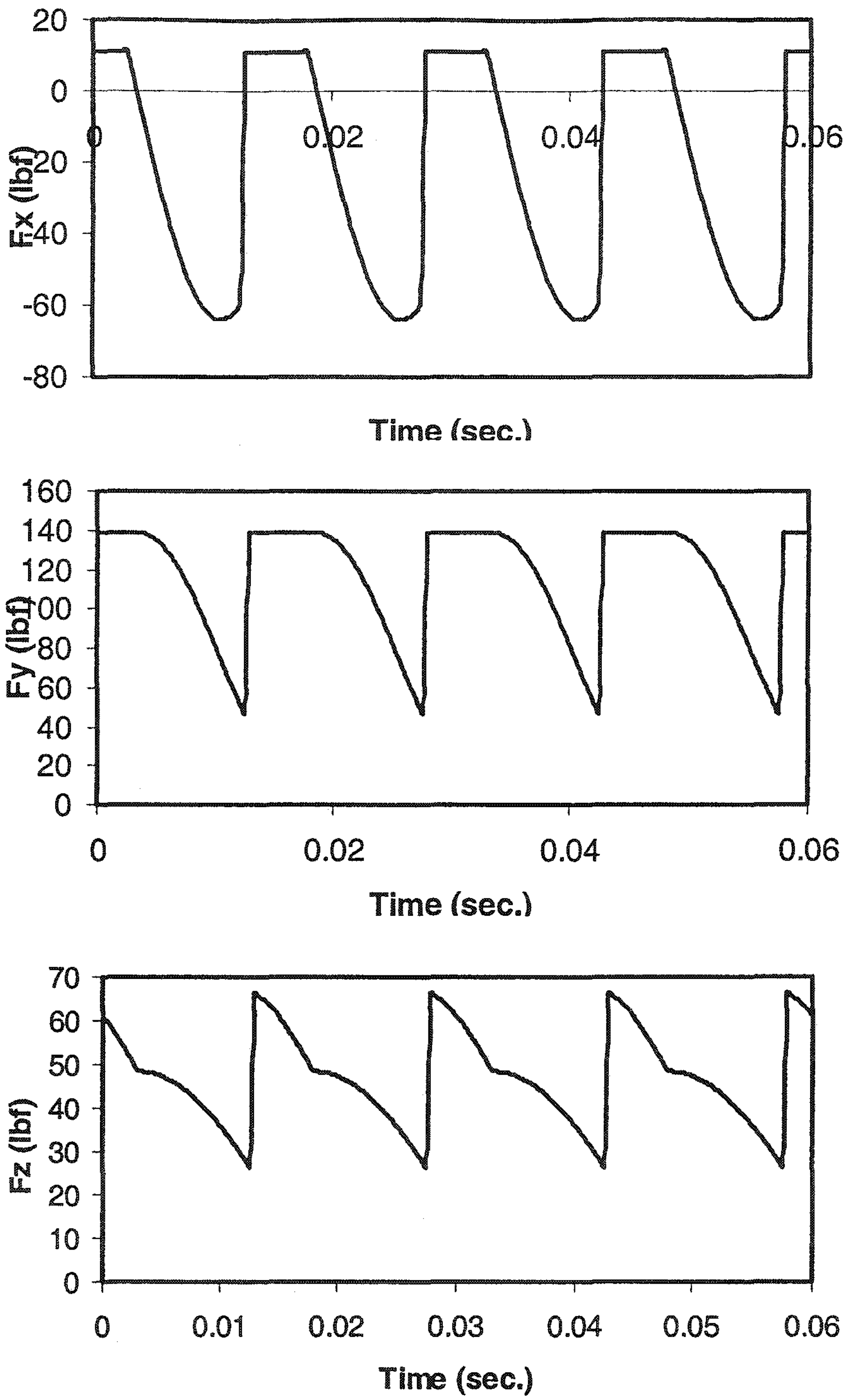

Figure 4.6. Simulated static cutting forces for face milling process (full Immersion), [depth of cut =0.150 inch, Feed rate 24 ipm and 1500 RPM.

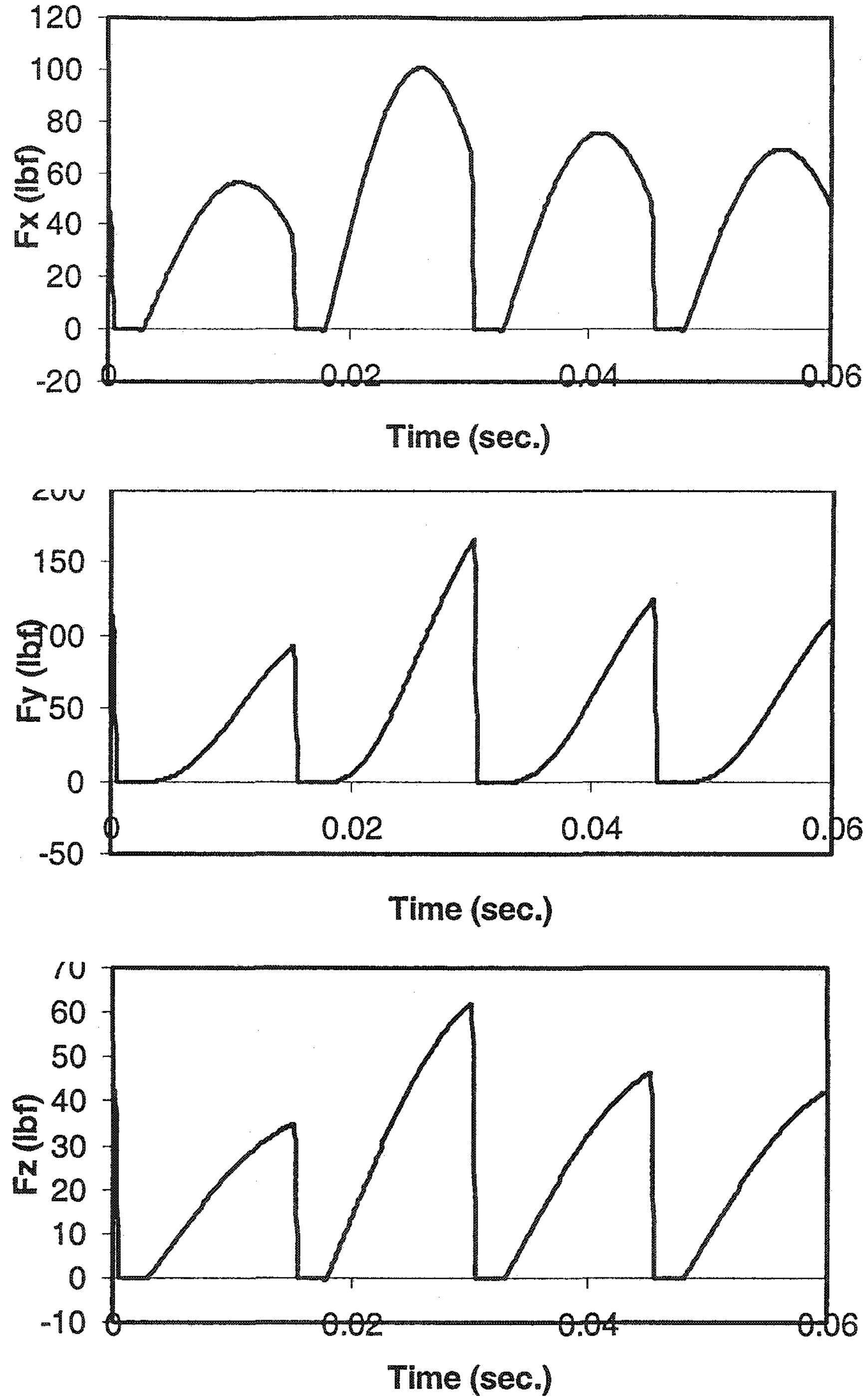

Figure 4.6a. Simulated static cutting forces for face milling process (half Immersion), [depth of cut =0.150 inch, Feed rate 24 ipm and 1500 RPM.

4.4 Time Domain Simulation of Dynamic Milling

Tobias [106] and Nigm et al.[107] reported that dynamic forces are generated by the vibration of the machine structure. In the previous sections a multi-axis rigid force model was introduced. In this section, the method of chip load regeneration first introduced in [108] is presented. The regenerative force model is based on the fact that the instantaneous cutting force on any given tooth in cut not only depends on the nominal feed per tooth (static component), but also on the current deflections of the tool/workpiece/fixture system (dynamic component), as well as the surface waviness left from the cutting operation of the previous teeth (undulation component) (Figure 4.7).

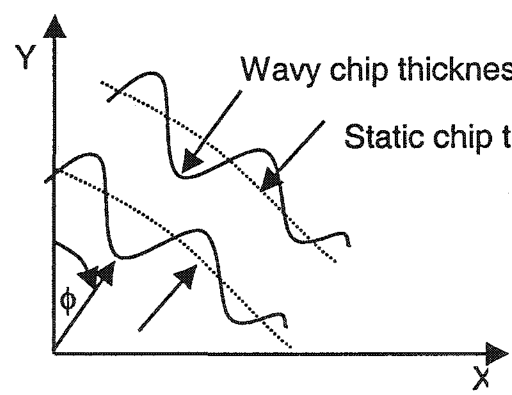

Figure 4.7. Dynamic and static chip thickness

The dynamics of the machine tool is primarily due to the dynamics of the tool, tool holder and spindle. Other parts of the machine tool, such as the machine table, can be considered to be relatively rigid compared to the spindle [15]. It is assumed that the dynamics of the spindle does not vary significantly, as the spindle moves in the workspace of the machine tool. Similar to many previous research work [24][36][37][39], the dynamic deflection of the cutter is modeled using a mass damper-spring system shown in figure 4.8. The following system of two-second order-uncoupled differential equations describes the motion of the tip of the tool in the x and the y directions.

$$M_2 \ddot{u}_2 + C_2 \dot{u}_2 + K_2 u_2 + K_1(u_2 - u_1) + C_1\left(\dot{u}_2 - \dot{u}_1\right) = 0 \qquad (4.13)$$

$$M_1 \ddot{u}_1 + K_1(u_1 - u_2) + C_1\left(\dot{u}_2 - \dot{u}_1\right) = F \qquad (4.14)$$

where u stands for both x and y directions, F is cutting force vector and M, C, and K are the mechanical parameters along the u direction. These parameters are determined experimentally at the tool tip using modal testing. If the cutting force components computed in equation (4.12) are applied to the system shown in figure 4.8, then the presence of a relative vibration between the tool and the workpiece will result in a wavy surface (Figure 4.6). As the next tooth cuts into the undulated surface of the workpiece, the static component of the chip load will be modulated by the waviness of the surface. If the variations in the modulated chip thickness result in a constant amplitude vibration, then the cutting condition is considered stable.

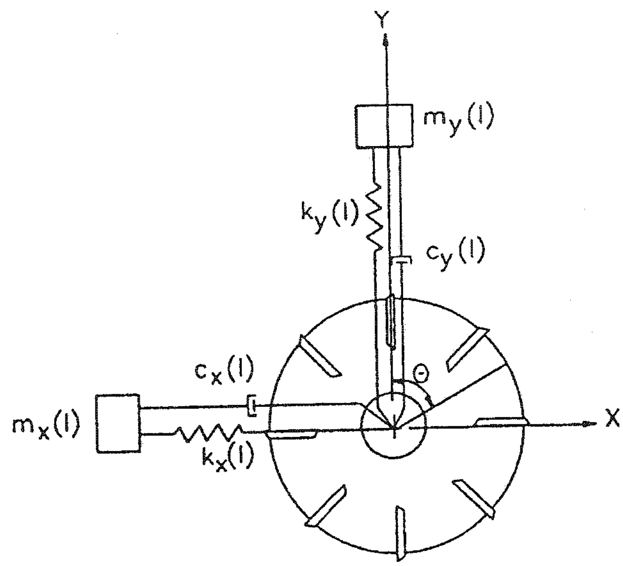

Figure 4.8. Structural model for the tool dynamic deflection [37].

On the other hand, it can result in excess energy being supplied to the system, which is totally dissipating due to damping, and then unstable self-excited vibrations (chatter) occur. Due to the nonlinear characteristic of chatter, the vibrations also stabilize at some high amplitude. For the case of static simulation, in one full rotation of the cutter, the index j varies between zero and some number J_{max}. This maximum number is selected such that a monotonic variation in the simulated force pattern is achieved. However, in the case of dynamic simulation, J_{max} should be large enough to ensure that the high-low amplitude components of the force signal are correctly simulated. Relative to the reference tooth.

From equation (4.1), it is shown that the chip thickness for a rigid force model is $C(\theta_i(\phi)) = f_t \sin(\theta_i(\phi))$ in which the quantity $f_t \sin(\theta_i(\phi))$ is the projection of the local feed per tooth in the direction of the chipload. To account for the instantaneous dynamics in the system and the surface undulations, the chip thickness can be modified as follows:

$$C(\theta_i(\phi))_{ED} = f_t \sin(\theta_i(\phi)) + x_{n-1}\cos(\theta_i(\phi)) + y_{n-1}\sin(\theta_i(\phi)) + \mathrm{Max}(u_1,u_2,u_3) \quad (4.15)$$

where $C(\theta_i(\phi))_{ED}$ is the effective dynamic chip thickness, f_t is the nominal feed per tooth, $x_{(n-1)}$, and $y_{(n-1)}$ are the instantaneous deflections in the system at time step $n-1$ and u_m ,$(m=1,2,3)$ are the possible undulations that could be left behind from the previous teeth (Figure 4.9). The first term in equation (4.15) is the static component of the chip load, the second and third terms are the effect of the current deflections on the chip thickness, and the last term accounts for the undulations left on the work surface. The relevant relation for u_m is as follows:

$$u_m = m \times f_t \sin(\theta_i(\phi)) + x_{(n-mJ)}\sin(\theta_i(\phi)) + y_{(n-mJ)}\cos(\theta_i(\phi)) \quad (4.16)$$

where index m=1,2,3 and $J=J_{max}/J_z$ is the number of rotational positions for one tooth period The basic non-linearity can be implemented by the following condition[99]: If $C(\theta_i(\phi))<0.0$, Then $C(\theta_i(\phi))=0.0$. The non-linearity condition accounts for the momentary loss of contact between the cutter and workpiece due to the high amplitude vibrations on the system.

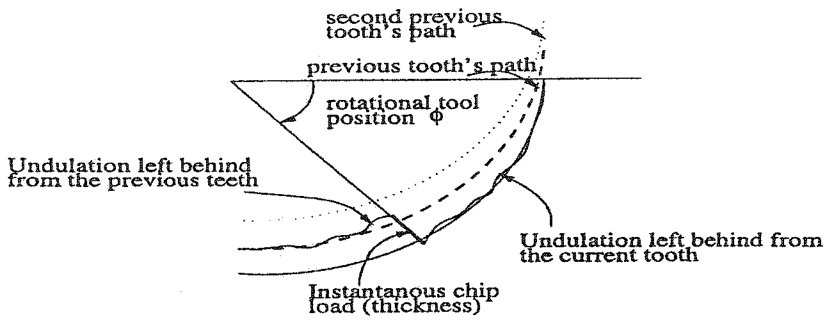

Figure 4.9. Graphical representation of the regenerative chip thickness [37].

4.4.1 Effect of Machine -Tool Dynamics on the Chip Load

The effect of the instantaneous dynamics of the system and the surface undulations, on the chip thickness and depth of cut can be expressed as:

$$\Delta C_1(\phi_i) = \left((\delta x_i - \delta x_{i-1}).\cos(\phi_i) + (\delta y_i - \delta y_{i-1}).\sin(\phi_i)\right) \tag{4.17}$$

$$\Delta d_1(\phi_i) = -\delta z_i \tag{4.18}$$

$\delta x_i, \delta y_i$, and δz_i are the instantaneous deflection of the system for the insert i at the cutter angular position, θ. $\delta x_{i-1}, \delta y_{i-1}$, and δz_{i-1} are the deflection of the system for the previous insert which generated the surface. During the simulation, the deflection history of the tool for each rotation is retained to determine the instantaneous chip thickness. To incorporate the deflection effects of previous tool path segments, the deflection along a tool path must be linked to the specific tool path segment. Figure 4.10 shows the simulated dynamic cutting forces for the same cutting parameters used in figure 4.6.

4.5 Effect of Tool Position Errors on Chip Load

The spindle eccentricity, it's tilting, and runout changes the actual feed per tooth and depth of cut. These factors should be taken into account in the face milling simulation for correct prediction of cutting forces.

In practice, the spindle in face milling may be tilted down slightly in the direction of feed to avoid the finished surface being recut by the backside of the cutter which may have deleterious effect on part surface finish. It is assumed here that the cutter is mounted perpendicular to the spindle, which rotates around the center of the cutter (and also center of the spindle) without any eccentricity. The tilting is made only on the spindle so that θ_t, the angle between spindle and the direction perpendicular to the workpiece is not zero degree (Figure 4.11).

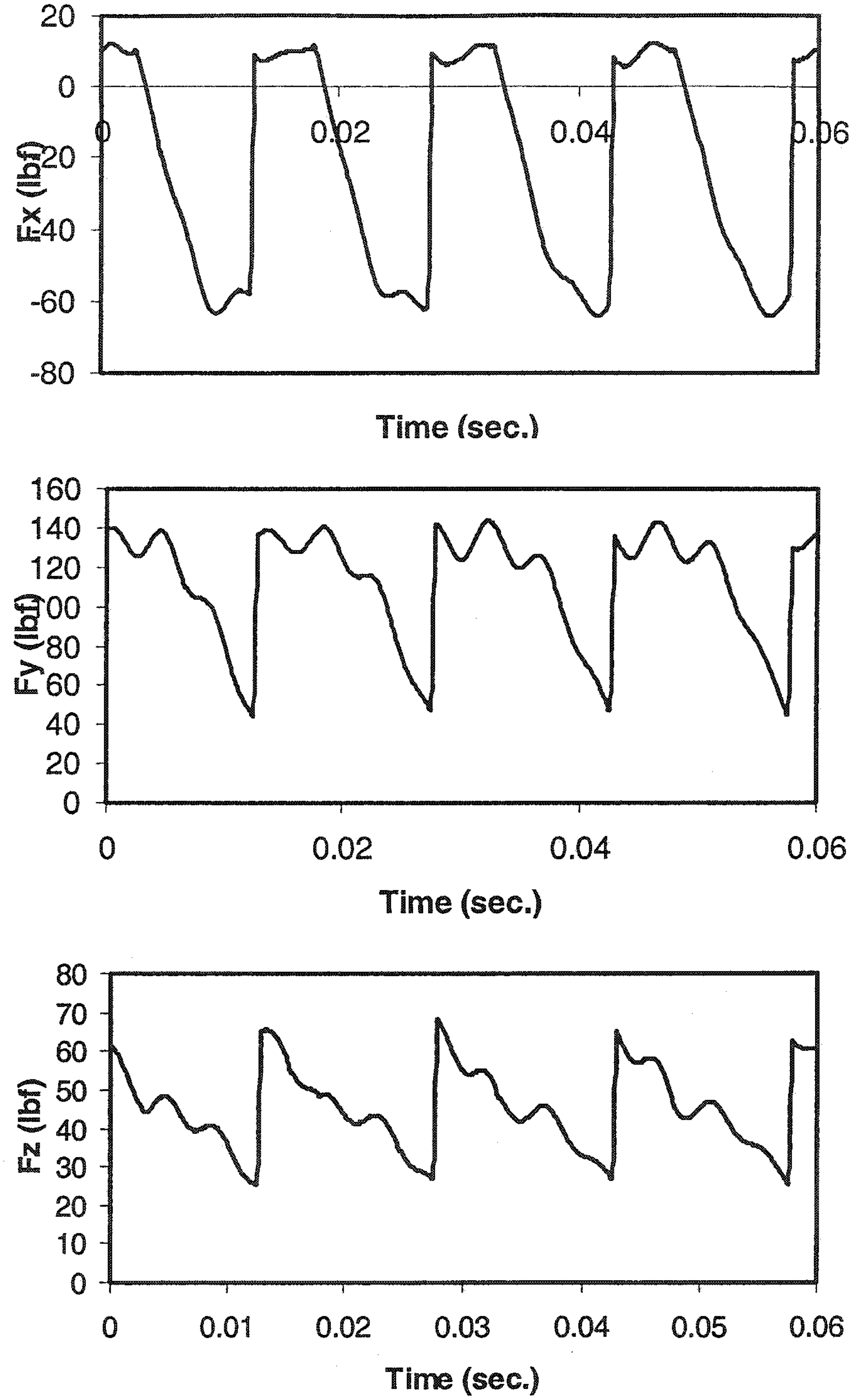

Figure 4.10. Simulated dynamic cutting forces for face milling process (full Immersion), [depth of cut =0.150 inch, Feed rate 24 ipm and 1500 RPM]

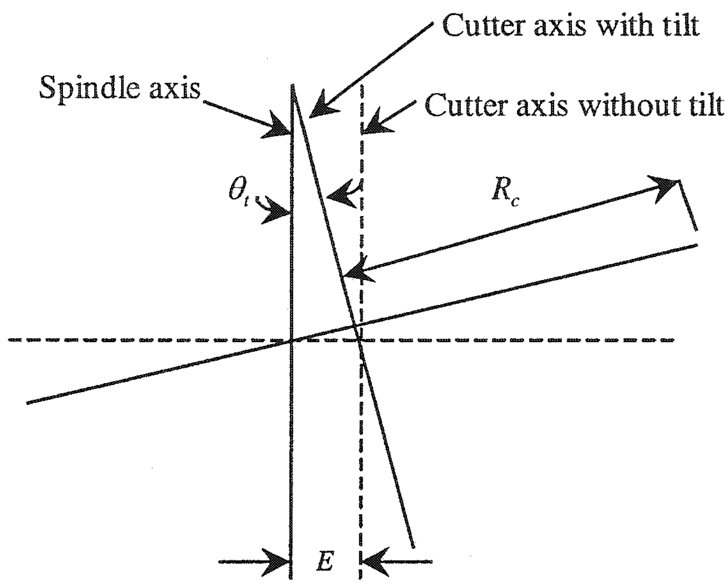

Figure 4.11. Influence of spindle tilting and eccentricity.

The insert initial position error in the radial and axial directions may change the actual feed per tooth and depth of cut. In the face milling process there are two basic types of cutter runout or throw: radial throw and axial throw. Radial throw occurs if the cutting edges of all the inserts do not lie on the surface of a cylinder whose axis is the spindle axis. Axial throw occurs if the cutting edge of all the inserts do not lie on a plane perpendicular to the spindle axis. The radial throw results in difference in the chip load of the various teeth and this could explain the well known phenomenon of reduction of tool life for the case of multi-tooth face milling versus single tooth cutting. In addition runout will produce a significant change in the instantaneous cutting forces over one cutter revolution. Peak forces may increase dramatically, as may the total peak-to-valley force variation. The combined effects of spindle eccentricity, its tilting, and axial and radial runout on the chip thickness and depth of cut are shown in Figure 4.12, and can be expressed by the following equations:

$$\Delta C_2(\phi_i) = \left(E.\sin(\phi_i) + \varepsilon_a(i)\sin(\theta_t) + [\varepsilon_r(i) - \varepsilon_r(i-1)].\cos(\theta_t).\sin(\phi_i)\right) \quad (4.20)$$

$$\Delta d_2(\phi_i) = \left(R_c.\sin(\theta_t).\sin(\phi_i) + \varepsilon_r(i)\sin(\theta_t) + [\varepsilon_a(i) - \varepsilon_a(i-1)].\sin(\theta_t)\right) \quad (4.21)$$

where R_c is the cutter radius, E is spindle eccentricity and θ_t is the tilt angle due to the eccentricity, $\varepsilon_r(i)$ is the initial position error in the radial direction of the insert, and $\varepsilon_a(i)$ is the initial position error in the axial direction.

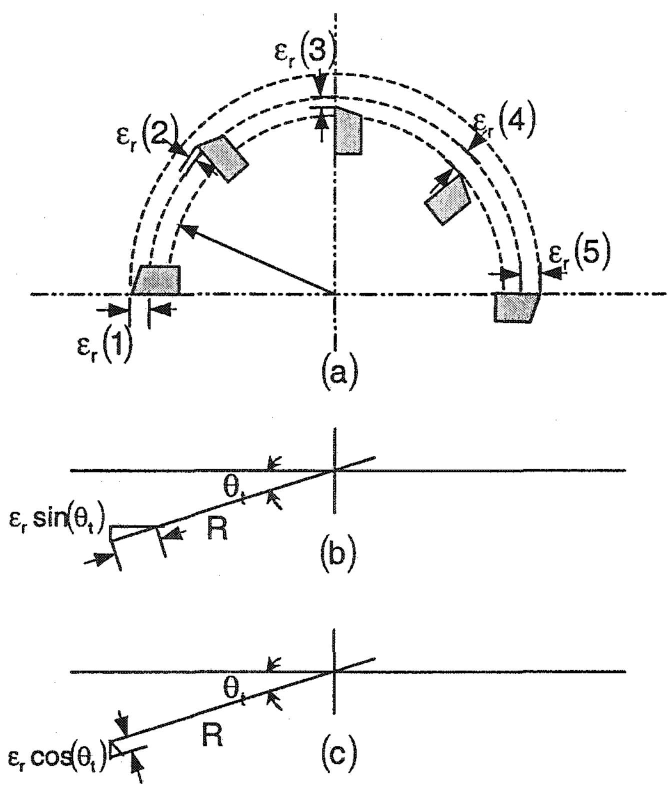

Figure4.12. Insert Radial and axial run out[15].

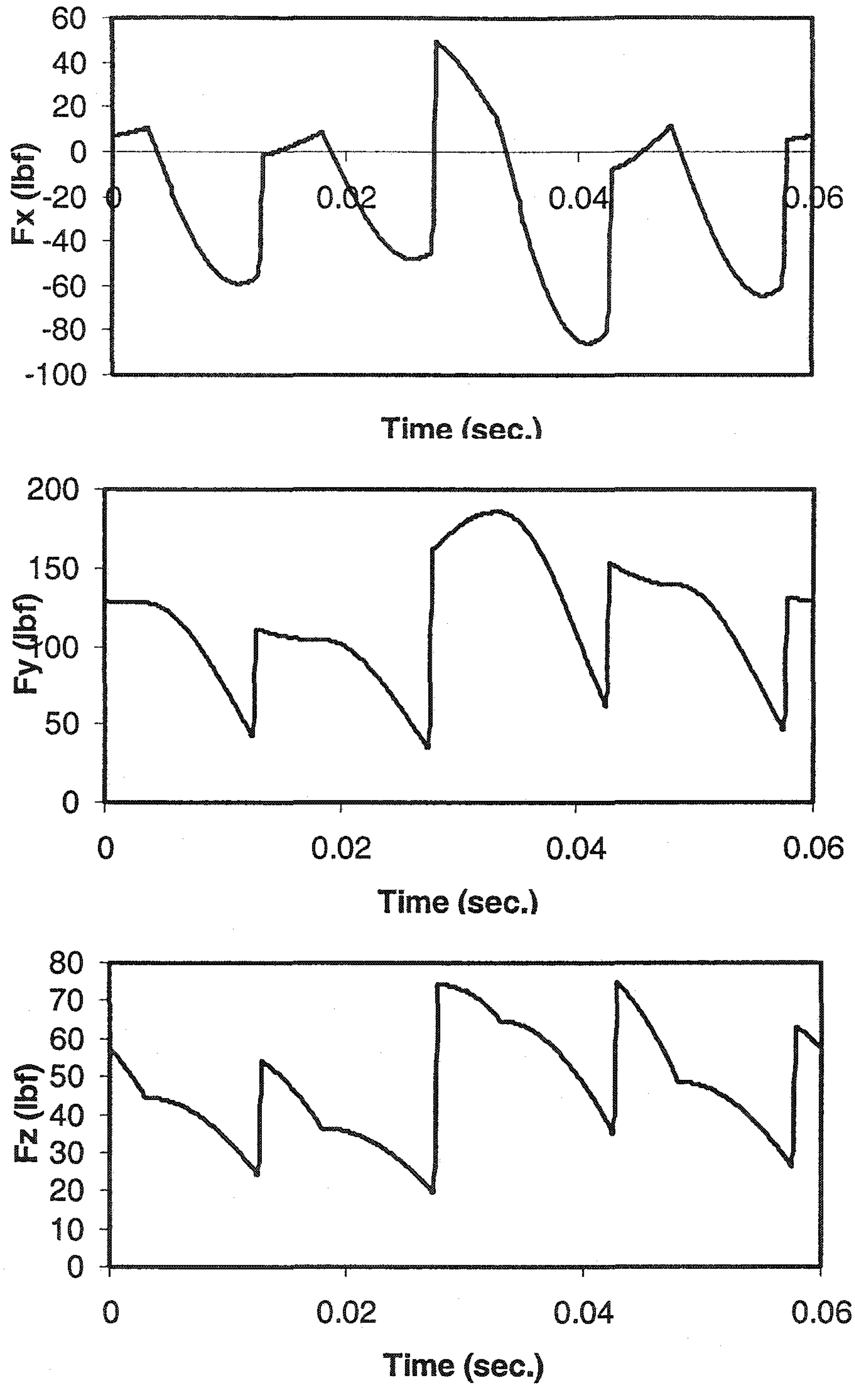

Figure 4.13. Simulated static cutting forces for face milling process with run out(full immersion), [depth of cut =0.150 inch, Feed rate 24 ipm and 1500 RPM.

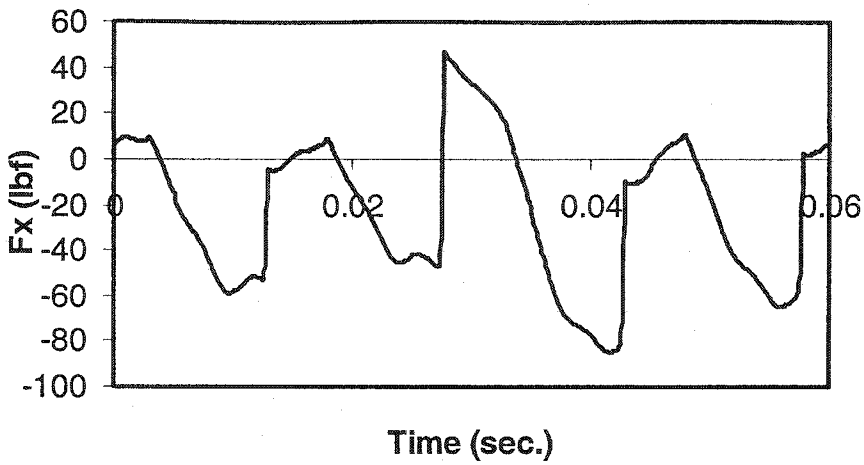

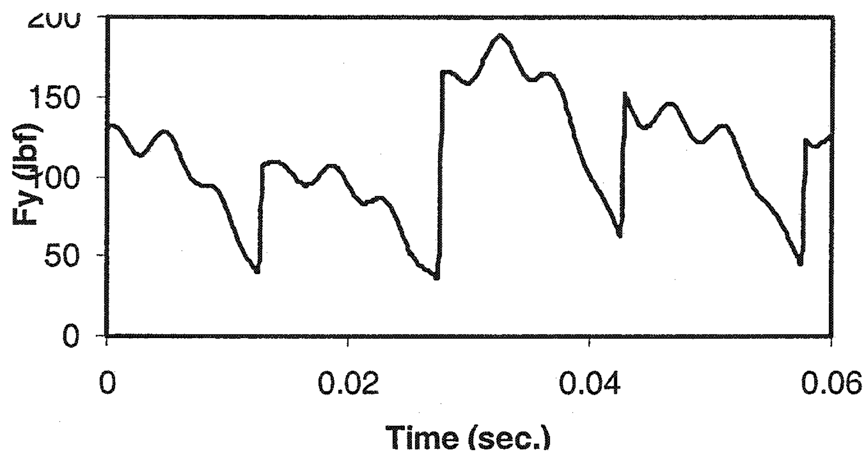

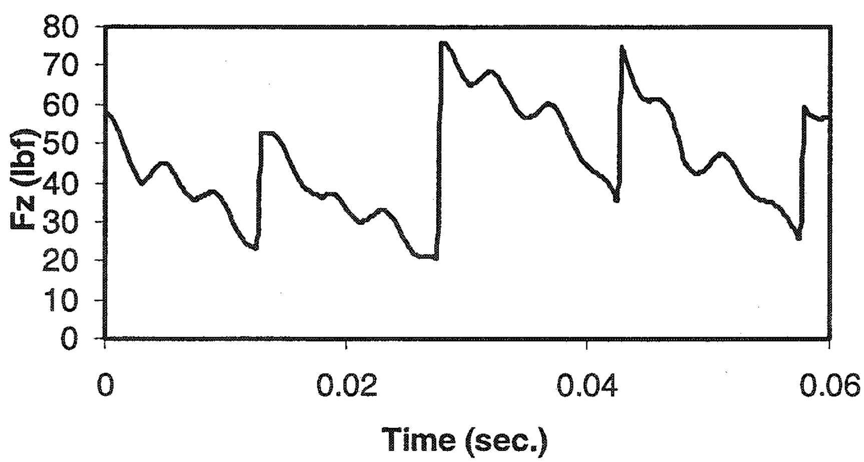

Figure 4.14. Simulated dynamic cutting forces for face milling process with run out (full immersion), [depth of cut =0.150 inch, Feed rate 24 ipm and 1500 RPM.

Figures 4.13 and 4.14 above shows the effect of both axial and radial cutter run out on the simulated static and dynamic forces respectively.

4.6 Effect of Workpiece/Fixture Dynamics on Chip Load

In contrast to the machine tool dynamics, the workpiece/fixture dynamics could change significantly, depending on the location of the cutter with respect to the workpiece, due to localized structure/geometry of the workpiece. Hence, transfer functions, which represent a fixed set of dynamics, cannot be used to model the dynamics of the workpiece/fixture system. In this case, the dynamics of this system are modeled using the finite element method, using natural frequencies and mode shapes. The mode shapes represent the spatial variation of the stiffness or the modal mass of the workpiece geometry. The FEA dynamic model of the workpiece/fixture system can be represented as:

$$[M].\{\ddot{X}\}+[C].\{\dot{X}\}+[K].\{X\}=\{R\} \qquad (4.21)$$

where: [M], [C], and [K] are the mass, damping and stiffness respectively of the finite element model, and{R} and {X} are the cutting force and the displacement at the nodes of the finite element model. The deflections of the workpiece/fixture system are computed using finite element analysis. The cutting forces, F_x, F_y, F_z, generated by each insert engaged in cut, are transformed into nodal forces, R (t), using the shape functions, N:

$$\{R\} = [N]\{F\} \tag{4.22}$$

The displacement at the nodes is transformed back to the displacement at the location of the insert inside the element using the shape functions:

$$\begin{Bmatrix} x_{w/f} \\ y_{w/f} \\ z_{w/f} \end{Bmatrix} = [N]\{X\} \tag{4.23}$$

These dynamic deflections affect both the nominal feed rate and the depth of cut. The dynamic deflections in the X and Y directions affect the nominal feed rate. In addition, due to the presence of the lead angle of the face milling cutter, the dynamic deflection in the Z direction also affects the nominal feed rate and the depth of cut. The change in the feed rate and depth of cut are given as:

$$\Delta C_3(\phi_i) = f\left((\delta x_{w/f}),(\delta y_{w/f}),(\delta z_{w/f})\right) \tag{4.17}$$

$$\Delta d_3(\phi_i) = -\delta z_{wp/f} \tag{4.18}$$

An in-house FEM code was developed in C++ language to solve for the dynamic deflections of the workpiece/fixture system. The next chapter is dedicated to the modeling of workpiece/fixture dynamics.

4.7 Integrated Dynamic Model

To include the effect of machine tool dynamics, the initial position errors of the tool, and the workpiece fixture dynamics, the instantaneous chip thickness and depth of cut are modified and expressed in the following final form:

$$C(\phi_i(\theta)) = f_t.\sin(\phi_i(\theta)) + \sum_{j=1}^{3} \Delta C_j(\phi_i(\theta)) \qquad (4.24)$$

$$d(\phi_i(\theta)) = W + \sum_{j=1}^{3} \Delta d_j(\phi_i(\theta)) \qquad (4.25)$$

where $\Delta C_j(\phi_i(\theta))$ and $\Delta d_j(\phi_i(\theta))$ are the effect of machine tool dynamics, tool position errors, and workpiece/fixture dynamics on the chip thickness and depth of cut for $j = 1,2,3$ respectively. W is the nominal depth of cut.

4.8 Summary

In this chapter the development of the dynamic force model was presented (Figure 4.15). There exists many force models for face milling in the literature. The force model developed here extend these force models a step further by incorporating the effect of workpiece/fixture dynamic deflection on the chip load. The chapter also presents some simulations for different cutting conditions to demonstrate the effect of different factors.

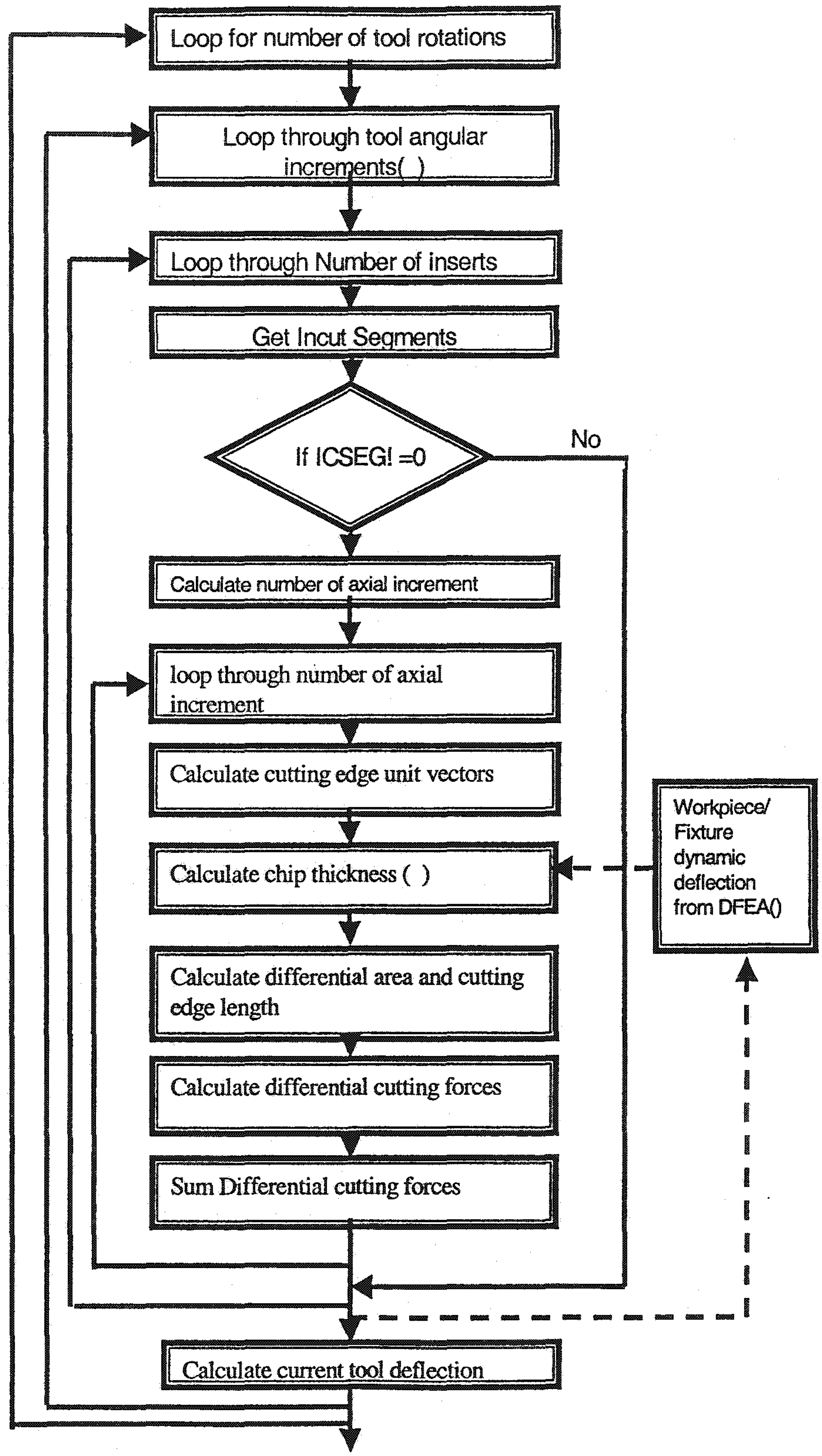

Figure 4.15. Integrated dynamic force model flowchart.

CHAPTER5: FINITE ELEMENT MODELING OF WORKPIECE/FIXTURE DYNAMICS

5.1 Introduction

In contrast to the machine tool dynamics, the workpiece/fixture dynamics could change significantly, depending on the location of the cutter with respect to the workpiece and the localized structure/geometry of the workpiece. Therefore, finite element method is the most appropriate to model the complex dynamics of this system.

5.2 Governing Equations for Structural Dynamics

To solve transient structural or continuum mechanics problems numerically, the governing hyperbolic partial differential equations are first discretized in space. This procedure is called a semi-discretization. Either finite element or finite difference methods can be used to semi-discretize the governing equations. The semi-discretization will reduce the problem to a system of ordinary differential equations in time, which in turn must be integrated to complete the solution process. In dynamic analysis the governing semi-discrete equations of motion are obtained by considering the static equilibrium at time (t). This includes the effect of acceleration–dependent inertia forces and velocity dependent damping forces, in addition to the externally applied discretized forces and the internal nodal forces of the continuum or structure, as shown in equation (5.1):

$$F_I(t) + F_D(t) + F_{Int}(t) = F_{Ext}(t) \qquad (5.1)$$

where $F_I(t)$ are the inertia forces, $F_I(t) = M\frac{dX^2}{dt^2}$, $F_D(t)$ are the damping forces, $F_D(t) = C\frac{dx}{dt}$, $F_{Int}(t)$ are the internal (nodal)forces including forces due to initial stresses in the system which may depend upon nodal displacement X, velocity $\frac{dx}{dt}$ and their histories, and $F_{Ext}(t)$ are the external forces, all of them being time dependent. M is the structural mass matrix (generally independent of time or displacement), C the damping matrix (may be a function of velocities).

The equation of static equilibrium, governing the linear dynamic response of a semi-discrete structural system,[109] and [110], at time (t) is derived from (5.1) as detailed in equation(5.2):

$$M\ddot{X} + C\dot{X} + KX = R \qquad (5.2)$$

where M is the discrete mass matrix , C is the viscous damping matrix, K is the linear stiffness matrix, R is the vector of external discrete forces which include body forces, surface forces and concentrated loads acting on the system.

The semi-discrete equations of motion for a general nonlinear structural system are:

$$M\ddot{X} + C\dot{X} + N(X) = R(t) \qquad (5.3)$$

where the resisting force vector N is the vector of nodal point(nonlinear)internal forces corresponding to the element stresses in the current configuration at time (t). Similarly R (t) refers to the externally applied nodal point forces in the configuration at time (t).

The ease of implementation of direct integration methods along with their ready usability in nonlinear studies has tended to enhance rapidly the popularity of these approaches. In direct integration, the governing ordinary second order differential equations in time, resulting from the semi-discretization of the structural system (by means of the finite element method), given by equations (5.2) and (5.3) respectively for linear and nonlinear dynamic structural response, are integrated using a numerical step-by-step procedure. In essence, direct numerical integration is based on two ideas:

1) The dynamic equilibrium equations (5.2) and (5.3) are satisfied at discrete time intervals (Δt) apart. This means that, basically, (static) equilibrium, which includes the effect of inertia and damping forces, is sought at discrete time points within the interval of solution.
2) Variation of displacements, velocities and accelerations within each time

interval Δt is assumed. Different forms of these assumed variations give rise to different direct integration schemes. Each of which, have different accuracy, stability and cost. The available direct procedures can be further subdivided into explicit and implicit methods each with distinct advantages and disadvantages. Each approach employs difference equivalents to develop recurrence relations, which may be used in a step-by-step computation of the response. The critical parameter in the use of each of these techniques is generally the largest value of the time step, which can be used to provide sufficiently accurate results, as this is directly related to the total cost of satisfactory analysis.

In the implicit methods[111][112], calculation of the displacements at the current time step involve the velocities and accelerations at the current time step itself, $(t+\Delta t)$. Hence the determination of the displacements at $(t+\Delta t)$ includes the solution of the structural matrix at every time step. Many implicit methods are unconditionally stable for linear analysis and the maximum time step length that can be employed is governed by the accuracy of the solution and not by the stability of the integration process. Although the implicit methods usually require considerably more computational effort per time step than explicit methods, the time step may be much larger since it is restricted in size only by accuracy requirements. The time step in most explicit methods, on the other hand, is restricted only by numerical stability requirements, which may result in a time step much smaller than that needed for the required accuracy, thus increasing the cost of computation. Unfortunately, both methods suffer from one major draw back. The material state during the time interval (Δt) must be estimated prior to the solution for the next time step. This may be very difficult or impossible to do, depending on the complexity of the material model and the nonlinearity which occurs during the interval (Δt). As a result equilibrium iteration is almost always necessary and convergence may not occur. This problem is not severe for well-behaved problems where the loading is monotonic, the material model is relatively simple and when the transition between elastic and plastic material behavior is gradual. However numerical failure can and often does occur even for simple problems such as elasto-plastic structures subjected to oscillatory loading. For these problems the abrupt transitions of material from elastic to plastic states can produce numerical instability problems. The problem is particularly aggravating for dynamical problems of moderate duration where changes in the stiffness and mass matrices are significant. Here material loading and unloading occurs frequently but at locations and times, which can not be predetermined.

In implicit algorithms, a matrix system is solved one or more time per step to advance the solution. Generally, implicit algorithms are most effective for structural dynamics problems. The unconditional stability of the many available implicit operators (as applied to linear systems) provides impetus to their use in structural dynamics computations. The method is implicit if the solution at time

($t+\Delta t$) requires consideration of the equilibrium condition at time ($t+\Delta t$) and the method requires the solution of a set of simultaneous equations at each time step wherein the coefficient matrix is a combination of the mass matrix, damping matrix and stiffness matrix. In large-scale problems the solution to these equations may be computationally expensive. The conventional implicit time integration procedures are Newmark, Wilson-θ and Houbolt methods [111][112]. In this work Wilson-θ method is used.

5.3 Wilson-θ Method

The Wilson-θ method is essentially an extension of the linear acceleration method [109][110] in which linear variation of acceleration from time (t)to time (t +Δt) is assumed. In the Wilson-θ method (Figure 5.1) the acceleration is assumed to be linear from time t to time ($t+\Delta t$), where $\theta \geq 1.0$. For $\theta = 1.0$, the method reduces to the linear acceleration scheme of the Newmark family of methods [111], but in this case the method is only conditionally stable. In linear problems the method is unconditionally stable for $\theta \geq 1.37$ so $\theta = 1.4$ is usually employed. The computational equations are derived as follows:

For any time τ so that $0 \leq \tau \leq \theta\Delta t$ we have, under linear acceleration assumption,

$$\ddot{X}_{t+\tau} = \ddot{X}_t + \frac{\tau}{\theta\Delta t}\left(\ddot{X}_{t+\theta\Delta t} - \ddot{X}_t\right) \tag{5.4}$$

On integrating equation (5.4) and applying the initial conditions at (t), we obtain:

$$\dot{X}_{t+\tau} = \dot{X}_t + \tau \ddot{X}_t + \frac{\tau^2}{2\theta\Delta t}\left(\ddot{X}_{t+\theta\Delta t} - \ddot{X}_t\right) \qquad (5.5)$$

On integrating (5.5) we have

$$X_{t+\tau} = X_t + \tau \dot{X}_t + \frac{\tau^2}{2}\ddot{X}_t + \frac{\tau^3}{6\theta\Delta t}\left(\ddot{X}_{t+\theta\Delta t} - \ddot{X}_t\right) \qquad (5.6)$$

At time $t+\theta\Delta t$ (i.e. $\tau=\theta\Delta t$) (5.5) and (5.6) respectively become

$$\dot{X}_{t+\theta\Delta t} = \dot{X}_t + \frac{\theta\Delta t}{2}\left(\ddot{X}_{t+\theta\Delta t} + \ddot{X}_t\right) \qquad (5.7)$$

$$X_{t+\theta\Delta t} = X_t + \theta\Delta t\,\dot{X}_t + \frac{\theta^2\Delta t^2}{6}\left(\ddot{X}_{t+\theta\Delta t} + 2\ddot{X}_t\right) \qquad (5.8)$$

From which we can solve for $\ddot{X}_{t+\theta\Delta t}$ and $\dot{X}_{t+\theta\Delta t}$ in terms of $X_{t+\theta\Delta t}$:

$$\ddot{X}_{t+\theta\Delta t} = \frac{6}{\theta^2\Delta t^2}\left(X_{t+\theta\Delta t} - X_t\right) - \frac{6}{\theta\Delta t}\dot{X}_t - 2\ddot{X}_t \qquad (5.9)$$

and

$$\dot{X}_{t+\theta\Delta t} = \frac{3}{\theta\Delta t}\left(X_{t+\theta\Delta t} - X_t\right) - 2\dot{X}_t - \frac{\theta\Delta t}{2}\ddot{X}_t \qquad (5.10)$$

To obtain the displacements, velocities and accelerations at time ($t+\theta\Delta t$), the equilibrium equations are considered at time ($t+\theta\Delta t$). This requires projection of the applied load vector to time ($t+\theta\Delta t$), which is performed linearly as:

$$R_{t+\theta\Delta t} = R_t + \theta\left(R_{t+\theta\Delta t} - R_t\right) \qquad (5.11)$$

And then the equilibrium equation at ($t+\theta\Delta t$) becomes:

$$M\ddot{X}_{t+\theta\Delta t} + C\dot{X}_{t+\theta\Delta t} + KX_{t+\theta\Delta t} = R_{t+\theta\Delta t} \qquad (5.12)$$

Substitution of equations (5.10) and (5.11) into equation (5.12) gives the following system of simultaneous equations, from which $X_{t+\theta\Delta t}$ can be obtained:

$$\left[\frac{6}{(\theta\Delta t)^2}M+\frac{3}{\theta\Delta t}C+K\right]X_{t+\theta\Delta t}=R_t+\theta(R_{t+\Delta t}-R_t)+M\left[\frac{6}{(\theta\Delta t)^2}X_t+\frac{6}{\theta\Delta t}\dot{X}_t+2\ddot{X}_t\right]+$$
$$C\left(\frac{3}{(\theta\Delta t)}X_t+2\dot{X}_t+\frac{\theta\Delta t}{2}\ddot{X}_t\right) \tag{5.13}$$

Then substituting $X_{t+\theta\Delta t}$ into equation (5.9) gives $\ddot{X}_{t+\theta\Delta t}$ which is used in equations (5.4 -5.6), all evaluated at $\tau=\Delta t$, to give:

$$\ddot{X}_{t+\Delta t}=\frac{6}{\theta^3\Delta t^3}(X_{t+\theta\Delta t}-X_t)-\frac{6}{\theta^2\Delta t}\dot{X}_t+(1-\frac{3}{\theta})\ddot{X}_t \tag{5.14}$$

$$\dot{X}_{t+\Delta t}=\dot{X}_t+\frac{\Delta t}{2}\left(\ddot{X}_{t+\Delta t}+\ddot{X}_t\right) \tag{5.15}$$

$$X_{t+\Delta t}=X_t+\Delta t\dot{X}_t+\frac{\Delta t^2}{6}\left(\ddot{X}_{t+\Delta t}+2\ddot{X}_t\right) \tag{5.16}$$

It is noted from equations (5.14-5.16) that no special starting procedure is required, since $X_{t+\theta\Delta t}, \dot{X}_{t+\theta\Delta t}$ and $\ddot{X}_{t+\Delta\theta t}$ are all expressed in terms of the same quantities at time t only. The above procedure can be extended to account for nonlinear behavior. The following two modifications are required:

1. The equivalent internal (nodal) elastic resisting forces (of the continuum or structure, for small displacement and linearly elastic problems, $F^{int} = KX$ must be replaced by its nonlinear counterpart (involving large deformations

and/or physical behavior of non linear materials), given by:

$F^{int} = \int_{V} B^{T}\sigma(\varepsilon)dV$ (5.17) at each stage of the computations.

Where σ is the nonlinear stress, B is the appropriate strain-displacement matrix; for large deformation problems, B itself is a function of the displacements, X. F^{int} will be denoted by N (X) in this section.

2. In order for the displacement and stresses to satisfy fully nonlinear conditions of the problem, it is generally necessary to perform an equilibrium iteration sequence at each time step or pre-selected time steps.

In implicit methods, equilibrium conditions are considered at the same time step for which solution is sought. If the solution is known at time (t) we wish to obtain the displacements, etc., at time (t+Δt), then the following equilibrium equations are considered at time (t+Δt) for the nonlinear case:

$$M\ddot{X}_{t+\Delta t} + C\dot{X}_{t+\Delta t} + N(X)_{t+\Delta t} = R_{t+\Delta t} \quad (5.18)$$

where the equivalent internal force vector, N(X), at time (t+Δt)is given by:

$$N(X)_{t+\Delta t} = \int_{V} [B_{t+\Delta t}]^{T} \sigma(\varepsilon)_{t+\Delta t} dV \quad (5.19)$$

N(X) is a nonlinear algebraic function of displacement, X, corresponding to the type constitutive material law defined as:

$$\sigma = f(\varepsilon) \quad (5.20)$$

Where f is a specific function.

In developing equations for the implicit integration, a formula for predicting the internal forces N(X) at time (t+Δt) in terms of the internal forces at time (t) is needed. For this purpose any of two approaches towards linearization may be used: the tangent stiffness method and the linear stiffness pseudo-force method. In the former, the internal nodal forces are predicted by:

$$N(X)_{t+\Delta t} = N(X)_t + K(X)_t \cdot \delta X \qquad (5.21)$$

Where $K(X)_t$ is the tangential stiffness matrix evaluated from conditions at time t and $\delta X = X_{t+\Delta t} - X_t$. In the pseudo-force method, the internal forces are predicted by:

$$N(X)_{\Delta t+t} = KX_{t+\Delta t} + P(X)_t \qquad (5.22)$$

where K is the linear stiffness matrix and $P(X)_t$ is the pseudo-force vector which accounts for the nonlinearities. The pseudo-force is either taken at time (t) or extrapolated to (t+Δt) from its value at t. Substituting equation (5.20) in equation (5.17) we have:

$$M\ddot{X}_{t+\Delta t} + C\dot{X}_{t+\Delta t} + K(X)_t\delta X = R_{t+\Delta t} - N(X)_t \qquad (5.23)$$

The solution of equation (5.23) yields, in general, an approximate displacement increment, δX. To improve the solution accuracy and to avoid the development of numerical instabilities it is generally necessary to employ iteration within each time step, or at selected time steps, in order to maintain equilibrium. In this case equation (5.23) can be conveniently expressed in the form:

$$M\ddot{X}^{i}_{t+\Delta t} + C\dot{X}^{i}_{t+\Delta t} + K(X)_t \Delta X^i = R_{t+\Delta t} - n(X)^{i-1}_{t+\Delta t} \qquad (5.24)$$

$$\delta X^{i}_{t+\Delta t} = \delta X^{i-1}_{t+\Delta t} + \Delta X^i ; i = 1,2,3\ .. \qquad (5.25)$$

where the superscript, i, denotes the equilibrium iteration. For the first iteration (i=1) equation (5.24) correspond to equation (5.23). In the pseudo-force formulation[112][113], the stiffness matrix K $(X)_t$ is kept at a constant initial value, with dynamic equilibrium being maintained by successive iteration by varying the pseudo-force on the right hand side of equation (5.22).

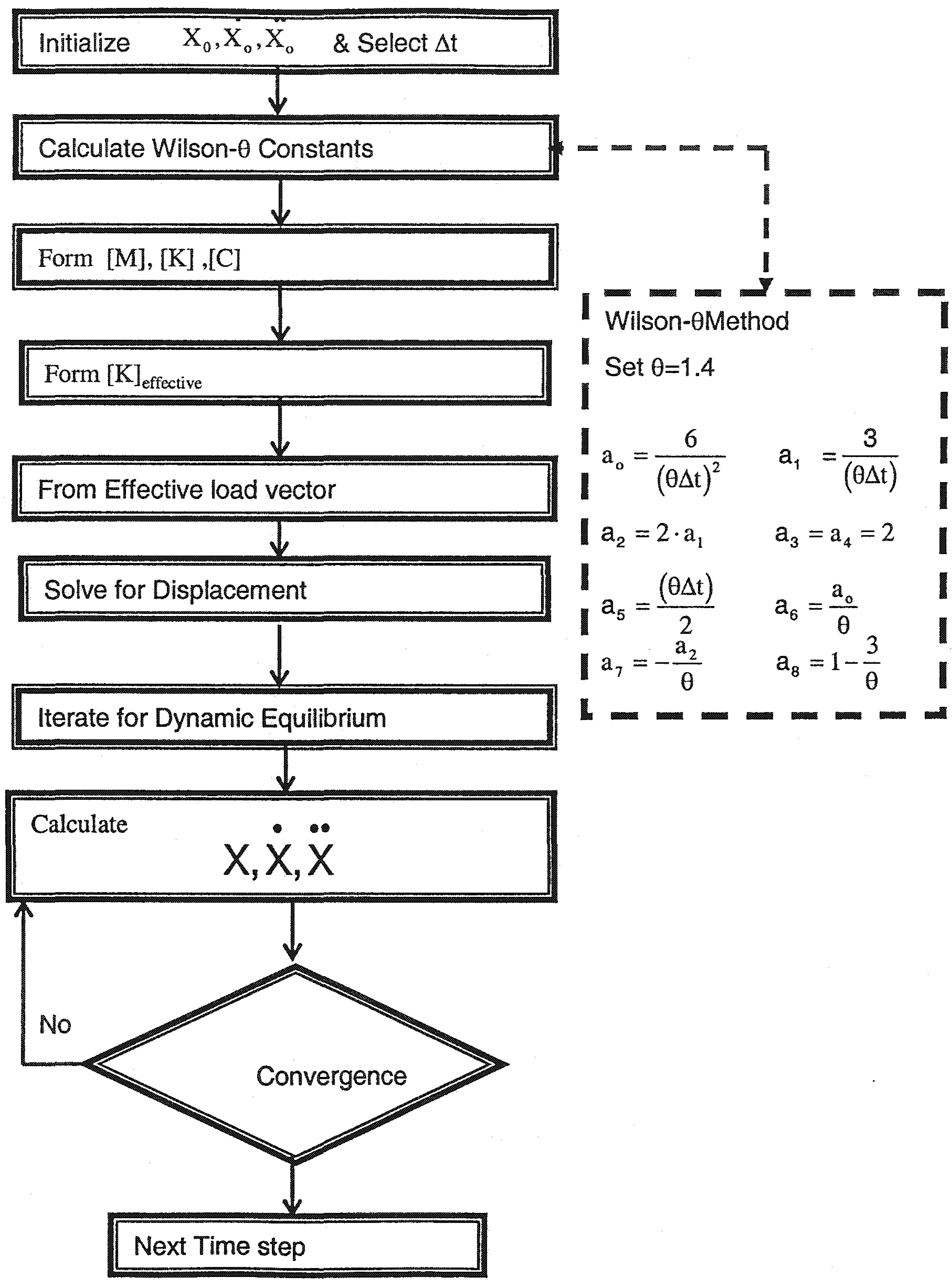

Figure 5.1. Flow chart of the Wilson-θ procedure.

5. 4 Finite Element Modeling Of Workpiece/Fixture System

An in-house finite element code was developed in C++ programming language based on the above, explained, theory to model and solve for the dynamic response of the workpiece/fixture dynamics. The code utilizes the direct integration approach to solve for the dynamic deflections of the system. Figure 5.;2 shows a general flowchart of the finite element code.

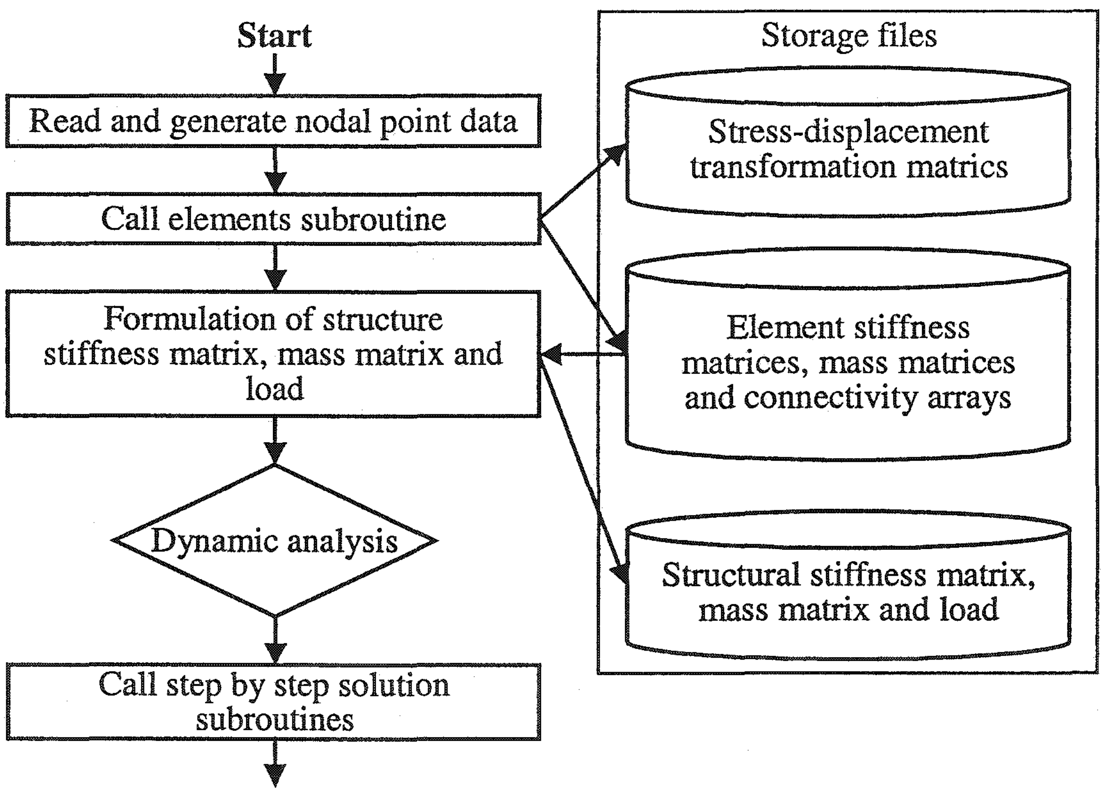

Figure 5.2. Flow chart of the developed finite element code.

5.5 Automatic Mesh Generation

In this research, a mesh generation scheme was developed based on the grid-based approach. The proposed scheme utilizes the iso-curves associated with the NURBS representation of the workpiece bounding surfaces to create nodes that are used to mesh the whole workpiece with brick elements. This scheme is applied to generate and update the mesh based on the updated workpiece geometry (Figure 5.3).

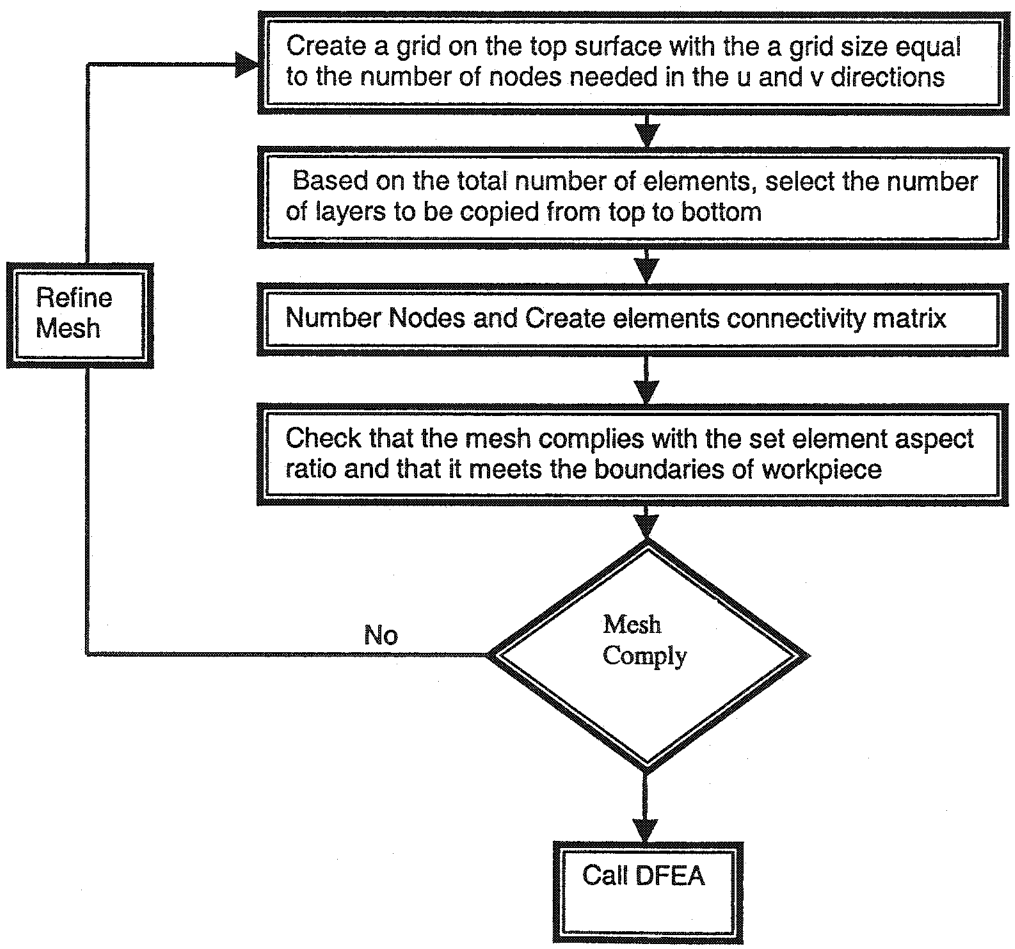

Figure 5.3. The steps involved in the mesh generation.

5.6 Finite Element Modeling of the Workpiece

The workpiece is modeled/meshed using an 8-node brick element, as shown in figure 5.4. The brick element provides a structured mesh that helps in applying the cutting forces on the specific nodes on the contact between the tool and the workpiece.

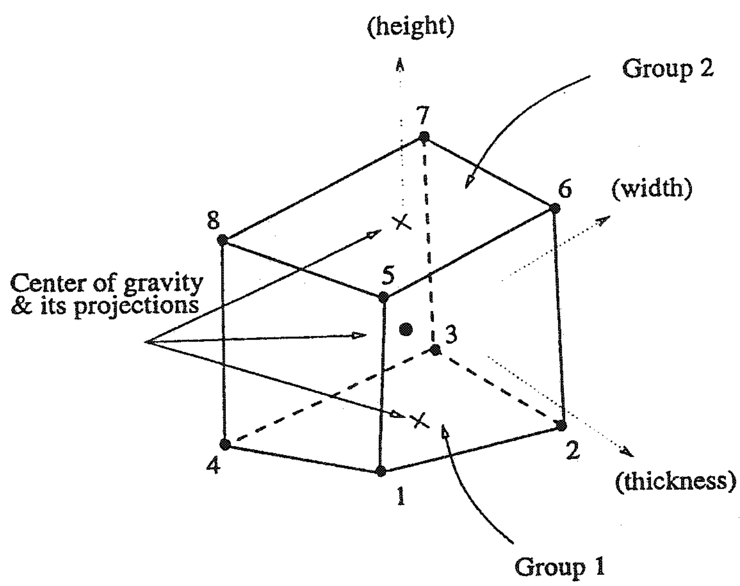

Figure 5.4. 8-node brick element .

5.7 Finite Element Modeling of Fixture Components

Two types of fixture components (Figure 5.5), namely locators and clamps, are considered in the mathematical representations of the fixture. Locators serve to accurately and uniquely position the workpiece relative to the machining coordinates, while clamps provide forces to hold the workpiece in place once it is located.

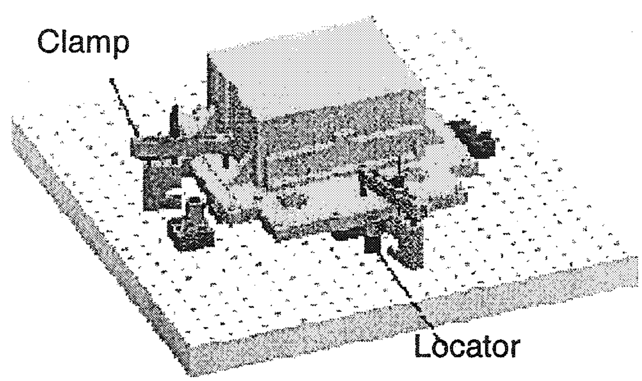

Figure 5.5. Generic modular fixture setup [42].

5.7.1 Modeling of the Fixture Elements Structural Stiffness

In modeling of fixture elements, (Figure 5.5) the fixture elements can be assumed perfectly rigid, if they are much stiffer than the workpiece.

Consequently they will not deform under clamping and/or machining force application (Figure 5.6-a). If the workpiece and fixture have comparable compliance, then the fixture elements can no longer be assumed rigid. The mating surface of the fixture element and the workpiece conforms to a surface contour, as determined by static equilibrium. In such case, the fixture element is modeled using a spring element [114] (Figure 5.6-b).

The structural stiffness of the spring element (K_s) is equivalent to the stiffness of the fixture component, k, which is determined using the geometry of the fixture component. If the fixture component is axially loaded, the stiffness (Ka) is determined using:

$$K_a = \frac{A \cdot E}{L} \qquad (5.26)$$

where: *A, L* and *E* are the cross sectional area, length and modulus of elasticity of the fixture element respectively. For transverse loading, the stiffness is calculated as:

$$K = \frac{3 \cdot E \cdot I}{L^3} \qquad (5.27)$$

where: I is the moment of inertia.

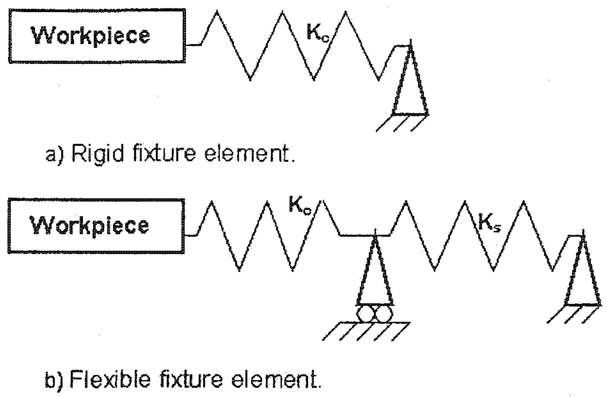

Figure 5.6. Modeling of fixture elements.

5.7.2 Modeling of the Workpiece/Fixture System Contact Stiffness

Contact forces in the normal direction determine the contact pressure distribution. This pressure directly influences the workpiece deformation. The tangential friction force also plays an important role in fixture design. It can be utilized to reduce the number of fixture elements, thereby exposing more of the workpiece features to machining operations and providing a damping mechanism to dissipate input energy from machining forces out of the workpiece/fixture system. Therefore, proper modeling of the workpiece/fixture contact requires the modeling of the friction conditions.

5.8 Enhanced Finite Element Modeling of Workpiece/Fixture Contact

Gap elements (Figure 5.7) have been used, by many researchers [46][115], to simulate the frictional contact between two nodes. It generates contact forces when two nodes approach each other (gap closed) and removing contact when the nodes move away (gap open). A gap element is defined using one node on the workpiece and the other one on the fixture component. Friction is simulated using Coulomb's law of friction, $f_f \leq \mu P$, where f_f and P are the friction and the normal forces respectively. If the friction force required to attain equilibrium is less than the maximum available friction force (μ P), then sticking conditions exist and nodes are not allowed to move along the direction of the friction force. If the required friction force exceeds the maximum available friction force, the gap elements let the nodes slip past each other, thus simulating sliding friction. The workpiece/fixture establishes contact when the normal force is compressive. If the normal force is tensile, the two nodes are decoupled. This is a limitation of the gap elements because, at each iteration, the finite element code has to check if contact is established. Although, in practice, a clamped workpiece will never lose contact with the fixturing elements, during the initial numerical iteration workpiece/fixture contact nodes may be artificially decoupled. The artificial decoupling of the nodes may result in an unconstrained rigid body motion of the workpiece and/or the fixture. The numerical solution may thus become unstable and diverge. Hence, to prevent the workpiece nodes from decoupling, a weak spring element is introduced parallel to the gap element as shown in figure 5.7. Stiffness of the weak spring is sufficiently low so that its presence does not alter the physical nature of the contact, chandra et al. [45].

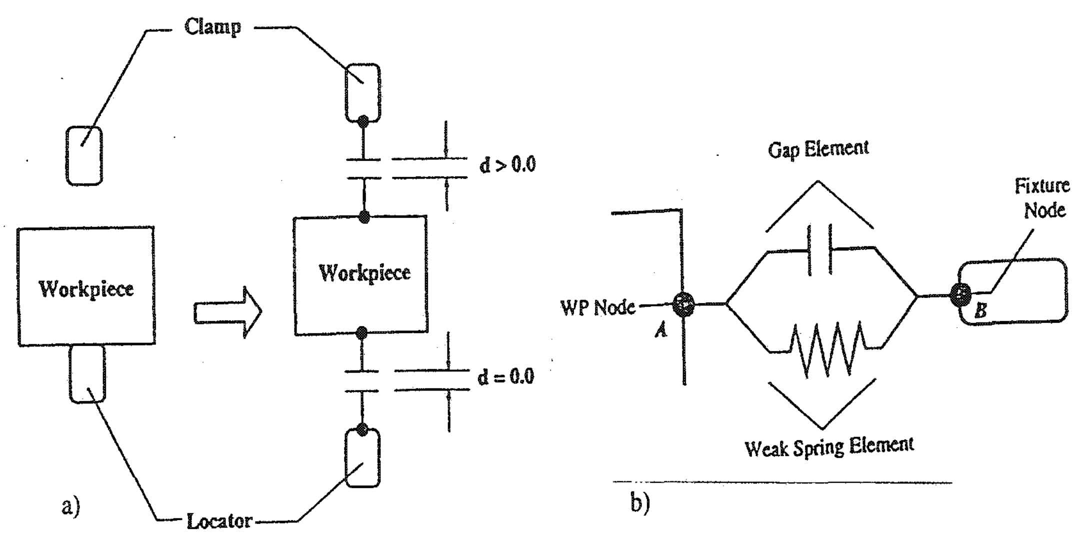

Figure 5.7. Gap element: a) classical element b) modified element [45].

The other type of element used to model the contact conditions between the workpiece and the fixture components is the virtual spring element shown in figure 5.8. The stiffness of the spring represents the rigidity of the contact conditions. The effect of surface finish, hardness of the material and the contact area should be considered when estimating the spring stiffness [114]. The stiffness is evaluated using the finite element method.

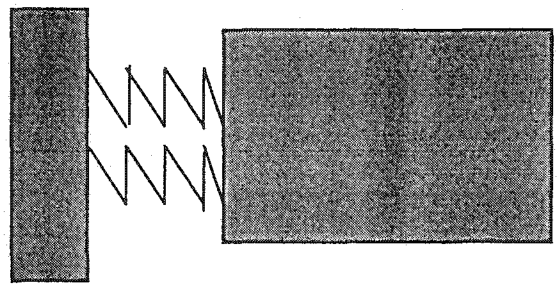

Figure5. 8. Objects connected with virtual spring element.

Recently, Fang et al. [116] proposed a finite element model to predict the friction forces at the workpiece/fixture contact. In the nonlinear friction law used, the coefficient of friction increases with the increase in the tangential displacement as was experimentally found [117]. The finite element solution incorporates the effect of the friction forces at the workpiece/fixture interfaces in the stiffness matrix.

In this research, both workpiece flexibility and fixture element flexibility are considered. An enhancement to the spring element is introduced by including the effect of friction. This is accomplished by monitoring the change in the tangential component of the global displacement at the contact area and calculating the friction forces using a modified version of Coulomb's law of friction. This modification is necessary to avoid the physical and numerical instability associated with Coulomb's law of friction. The new model provides a more realistic representation of the contact between the workpiece and the fixture element. The effect of friction, surface roughness and workpiece material is accounted for in this model.

5.9 Modeling of Friction on Workpiece/Contact Surface

Friction phenomena exist whenever contact is present. In reality, all physical boundaries are rough from a microscopic point of view [118]. The roughness of the physical boundaries contributes significantly to frictional resistance. Asperities may indent into boundary resulting in new asperities. However, frictional effects may be neglected, for simplicity, in situations where frictional forces are sufficiently small. Therefore, contact problems may be classified as frictional or frictionless.

Friction laws have received a great deal of attention in the finite element implementations of different contact algorithms. Whenever frictional contact is mentioned coulomb's law of friction is invited. Simplicity is the source of wide application of the Coulomb's law of friction in the finite element analysis of general contact problems. However, it has physical and mathematical deficiencies.

Mathematical models [118] for the quasi-static dry friction are classified as either classical model (Figure 5.9), which adopts the coulomb's friction law or non-classical models (Figure 5.10) which are suggested to cure some of the physical and mathematical deficiencies in the Coulomb's friction law. By quasi-static friction it is meant that the frictional mechanisms present when two metallic surfaces are pressed slowly together and are in static equilibrium or are slowly displaced relative to one another.

In Coulomb's law of friction, the friction force between the two bodies in contact is given as a function of the normal applied load in the form:

$$\begin{aligned} F_f &< \mu_s F_N \quad &\text{if } V_t = 0 \\ F_f &= \mu_d F_N \quad &\text{if } V_t \neq 0 \end{aligned} \qquad (5.28)$$

The friction force is proportional to the normal force F_N and is either independent of the velocity V_t, or increases slightly as the velocity diminishes. This relation becomes highly nonlinear in the vicinity of the zero sliding velocity, which causes numerical problems when simulating the sticking condition. These numerical problems become more severe in the transition between sticking and sliding or visa versa.

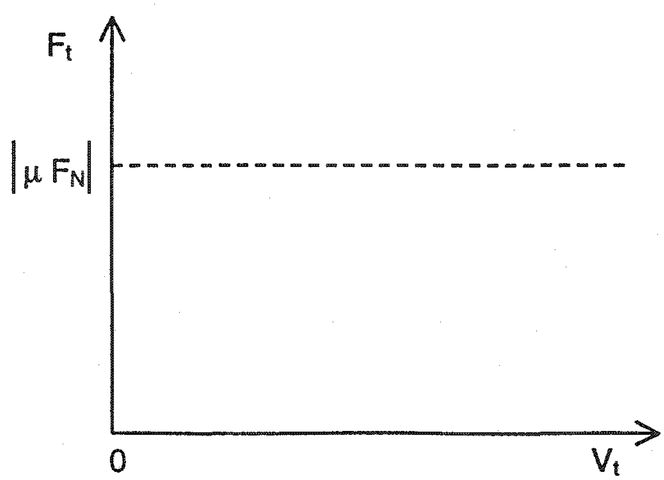

Figure5. 9. Classical friction model.

In nonlinear friction laws a frictional stiffness is used to account for the micro tangential motion on the contacting surfaces. This modification improves the numerical stability of the simulation. Coulomb's friction law can be obtained as a special case by setting this frictional stiffness to a very large value.

The Velocity limited friction law (VLFM) is given as:

$$\begin{aligned} F_f &= -\mathrm{Sign}\left(\frac{V_t}{V_0}\right)\ \mu_s\ F_N && \text{if } V_t \le V_o \\ F_f &= -\mathrm{Sign}(V_t)\ \mu_d\ F_N && \text{if } V_t > V_o \end{aligned} \tag{5.29}$$

where V_o is the cut–off velocity. Selecting the value of V_o depends on the time step, Δt, size. The smaller the value of V_o the smaller the time step, Δt. To optimize the CPU time the slope defined by V_o and $\mu_s F_N$ need to be as small as possible without affecting the solution results.

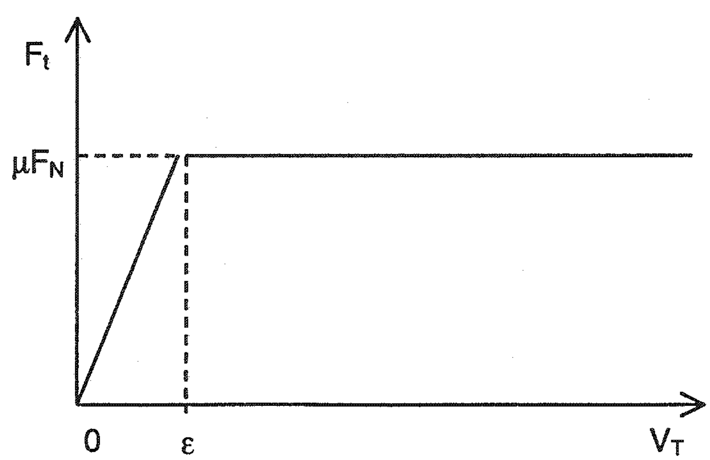

Figure 5.10. Non-Linear friction model.

5.9.1 Friction Models

Friction forces arise from the tangential motion on the contact surfaces. While friction can dissipate energy, it can cause damage as well. Therefore modeling of friction at the workpiece/fixture interface is important. However, a universal mathematical model has not yet been developed to accurately describe this phenomenon. Coulomb friction is usually applied to contact problems because of its simplicity. When using the coulomb friction model, the direction of the sliding velocity chatter occurs due to the sharp discontinuity in the friction force near the zero sliding velocity. Karnopp [119] developed a force balance friction model (FBFM) in which a zero velocity interval, $\{-V_o,+V_o\}$defines the sticking friction regime. Within this zone, the friction force is determined such that it balances the net force applied to the system. Haessig and Friedland [120] developed a 'bristle model "to capture the microscopical contact points between two surfaces. The point of contact is thought of as a bond between flexible bristles. When one surface moves relative to the other, bristle, which is formed randomly on the surface, act as springs representing the sticking friction force. As the relative displacement of a bristle exceeds a certain value, the bond snaps and a new one is formed at a certain location. The accuracy of the model depends on the number of bristles. However, the model is numerically inefficient due to its complexity.

Axisa et al. [121] developed a spring -damper friction model (SDFM), in which the sticking force is obtained by introducing adherence stiffness and an adherence damper:

$$\begin{aligned} F_f &= -\mathrm{sign}(V_t)\mu_d F_N && \text{Sliding} \\ F_f &= -\mathrm{sign}(V_t)\left(K_a\left(u_c - u_o\right) + C_a V_t\right) && \text{Adherence} \end{aligned} \qquad (5.30)$$

where K_a and C_a are the adherent stiffness and damping respectively and u_c and u_o are the current and zero velocity tangential displacements respectively. Tan and Rogers [122] extended the Karnopp model to simulate friction in multi-degree of freedom systems. They designated their model as the force balance friction model (FBFM). This sticking is tested when the absolute velocity is less than a small limiting velocity (V_o). Friction force during sticking is calculated such that it balances the net force:

$$F_f = k.\,u - F_e \qquad (5.31)$$

Where k.u represents the internal forces at the point of contact. In order for sticking to occur, this force must stratify the inequality $F_f < \mu_s F_N$, otherwise sliding occur.

In this work, a velocity limited friction model (VLFM), is implemented (Figure 5.11). It was previously used by Rogers and Pick [123], Yetisir and Weaver [124] and Hassan et al. [125]. A limiting velocity (V_o) is used to overcome the difficulties associated with the discontinuity of the classical Coulomb friction model. Depending on the value of the sliding velocity (Vt), the friction force is either an arbitrary function of the velocity (a linear function is used in the above studies) or equal to the dynamic friction capacity, F_f.

$$F_f = -\text{sign}(V_t)\mu_d F_N \qquad \text{if } V_t \rangle\, 0$$
$$F_f = -\left(\frac{V_t}{V_o}\right)\mu_s F_N \qquad \text{f } |V_t| \,\langle\, V_o \tag{5.32}$$

Where μ_d and μ_s are the coefficients of dynamic and static friction respectively and F_N is the normal force.

Hassan et al. [125] conducted simulation to evaluate three different friction models (VLFM, SDFM and FBFM) based on two aspects: accuracy and numerical efficiency. Numerical efficiency is assessed by, considering the computer processing time. A time step of 10 µsec was found to provide numerical stability when using VLFM for all the simulation cases. For the SDFM and the FBFM, a time step of 1. Accuracy wise comparison showed that the difference between the three models is negligible for small to medium contact pressures. For high contact pressures the difference is about 5%. Hence the VLFM is a fast and stable model with acceptable accuracy.

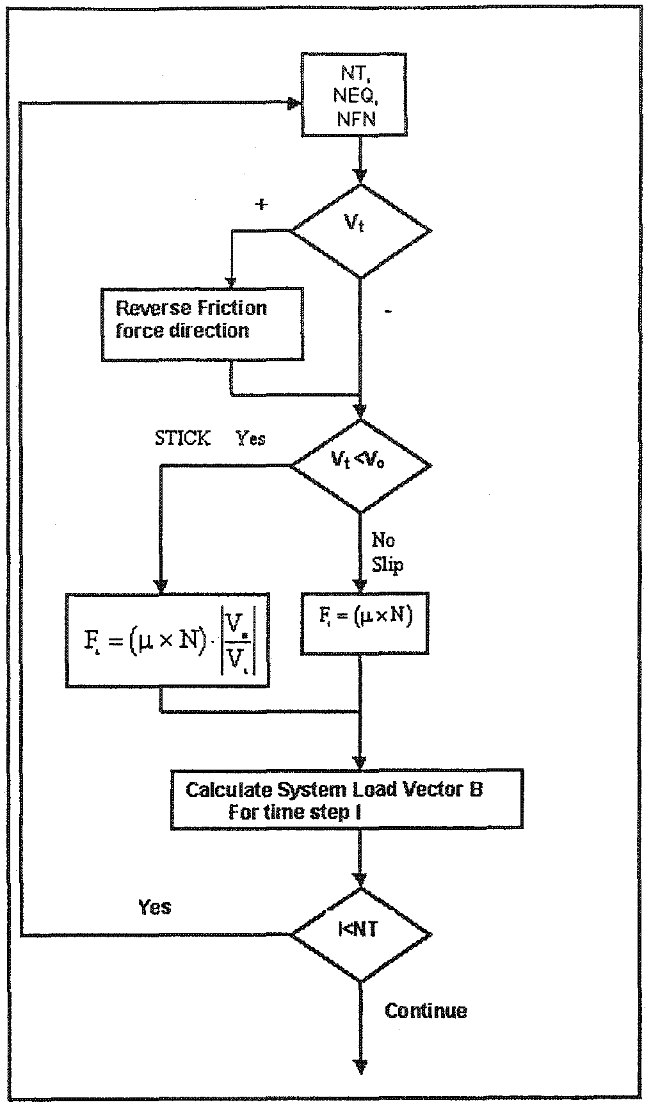

Figure 5.11. Flow chart of the VLFM friction model.

5.10 Summary

In this chapter, a review of development of the finite element modules of the simulation system for the workpiece/ fixture contact and the theory behind it was given. The meshing scheme developed was explained. The used of the pseudo-force method utilized is well suited for nonlinear localized applications and it has the advantage of reduced CPU time. The friction model adopted was explained and its use was justified compared to other friction models found in the literature based on CPU time and accuracy. The friction coefficients used in this simulation are determined experimentally as explained in the next chapter. The main steps in the simulation are shown in figure 5.12.

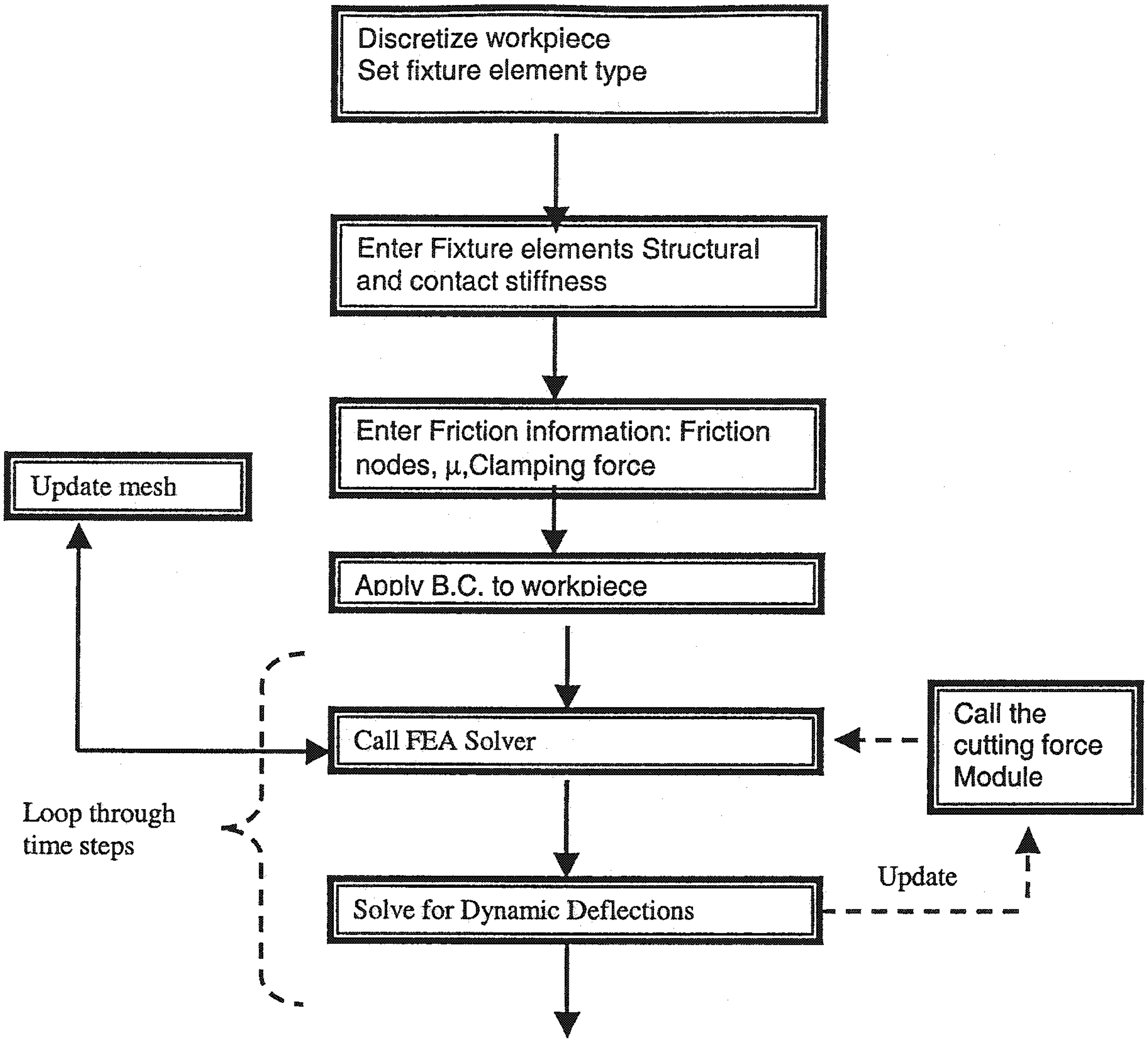

Figure 5.12. Flow chart of the simulation system.

CHAPTER 6: EXPERIMENTAL FRICTION ANALYSIS

6.1 Introduction

Experimental work was carried out at different stages of this work to calibrate the force model, to determine the friction coefficient for modular fixture applications and to validate the generalized simulation results.

For each of these tasks, proper test matrices were created to cover the factors investigated. In the first phase of experimental work, cutting tests were carried out under different feed rates, cutting speeds and depth of cuts to find the cutting pressures (K_t, K_r and K_a) that are used in the mechanistic force model. The second phase of experimental work was dedicated to investigate the factors affecting the coefficient of friction in modular fixture applications. This topic is of vital importance to the accurate modeling of the workpiece/fixture contact. Design of experiment was used in this phase and different techniques were utilized to reduce/eliminate the experimental variability associated with friction testing. The last experimental phase was carried out to validate some simulation cases.

In this chapter, experimental analysis of friction coefficient is presented.

6. 2 Experimental Determination of the Friction Coefficient

As was explained in chapter two different experimental procedures for the determination of the coefficient of friction are available in the literature. The measurement of friction involves the application of an external normal load, movement of a surface and measurement of a tangential, friction, force. Almost all friction-measuring devices involve these three essential elements [126]. However all devices do not necessarily give the same results for a given pair of surfaces even though the conditions may appear similar. This is because friction depends in greater or lesser measure, on surface cleanliness, interfacial geometry and apparatus stiffness.

6.2.1 Experimental Setup

The setup used in this work is shown in Figures 6.1 through 6.4. Figures 6.1 and 6.2 display the schematic and the actual experimental setup used in this work.

Figures 6.3 and 6.4 zoom on one of the fixture tips used in this work and on the

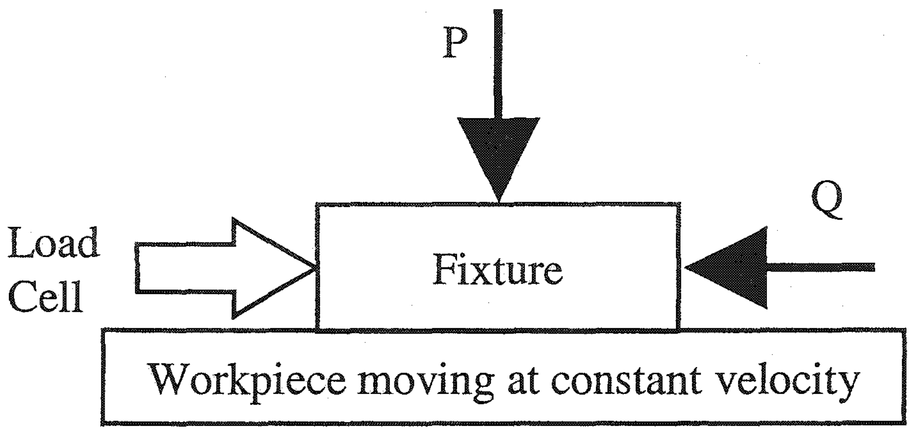

Figure 6.1 Schematic diagram of the tribometer.

hydraulic clamp used respectively. These clamps withstand pressures up to 8000psi and the clamping force magnitude is dependent on the pressure and the fixture tip contact area. It was designed based on previous designs [127] to accommodate higher applied normal load range using a hydraulic clamping system. The setup consists mainly of a hydraulic clamping system that can provide up to 55 MPa of clamping load and a ball screw feed drive. The hydraulic clamp with changeable fixture tip is fixed to an arm free to rotate in the horizontal plane. The workpiece (152.4 ×101.6 × 25.4 mm) is placed on the guided base of the ball screw motor that moves with a constant speed.

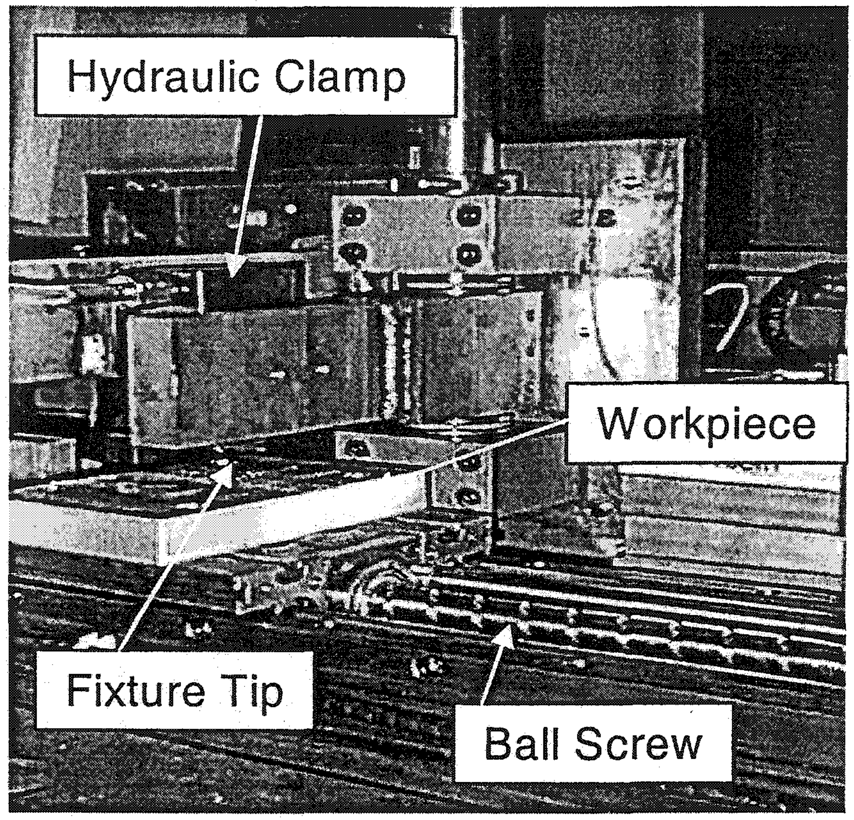

Figure 6.2 .Tribometer setup.

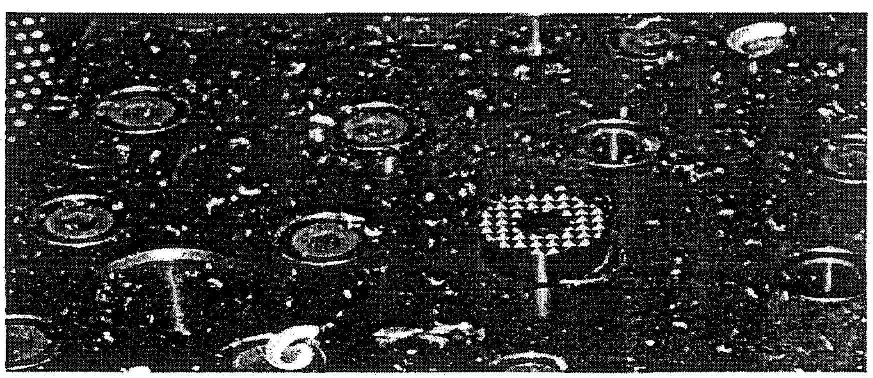

Figure 6.3 A commercial fixture tip used in the experimental work.

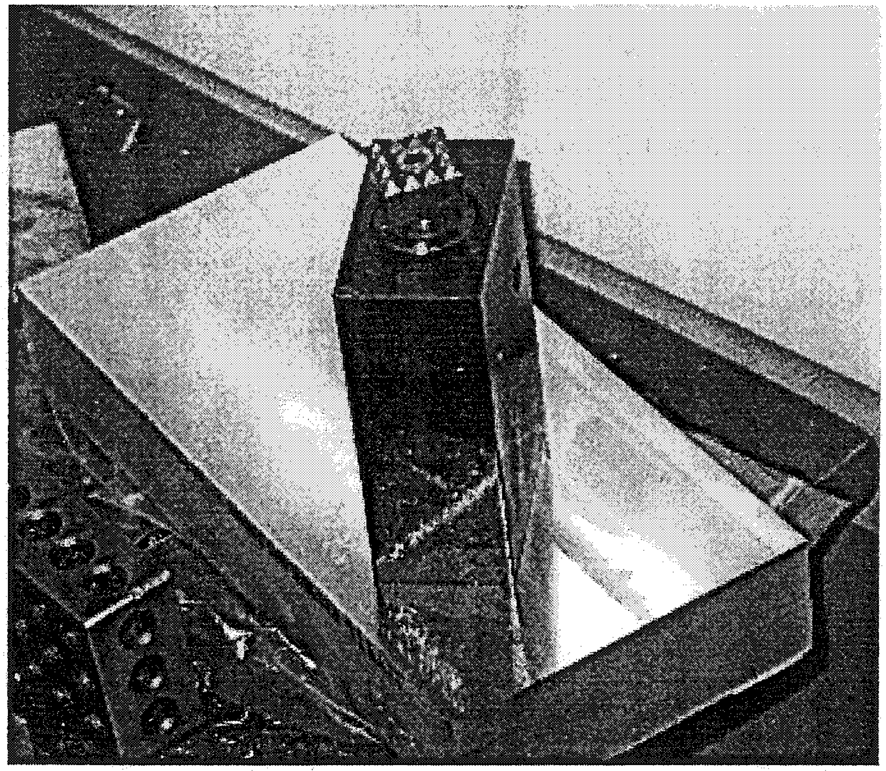

Figure 6.4 A hydraulic Clamp with changeable fixture tip.

A load cell is set to measure the friction force needed to oppose the sliding of the fixture tip. The velocity of the slide is set to 4 mm/sec, which is a typical value of the velocity range reported in literature [71]. The flexibility of the test bed setup allows for the use of variable fixture tips, workpiece samples and normal loads in order to enable the modeling of different conditions. The coefficient of friction is determined from the plot of the friction force variation with time as shown in figure 6.5. For a period of time $0\leq$ time $\leq t$, the contacting pair resists slip at the joint and the elastic strain energy builds up as the workpiece is displaced relative to the fixture tip. During this time period the friction force increases proportionally with time until it exceeds the threshold, Q_s. At this point sliding initiates at the joint and the friction force drops to an average value of Q_k.

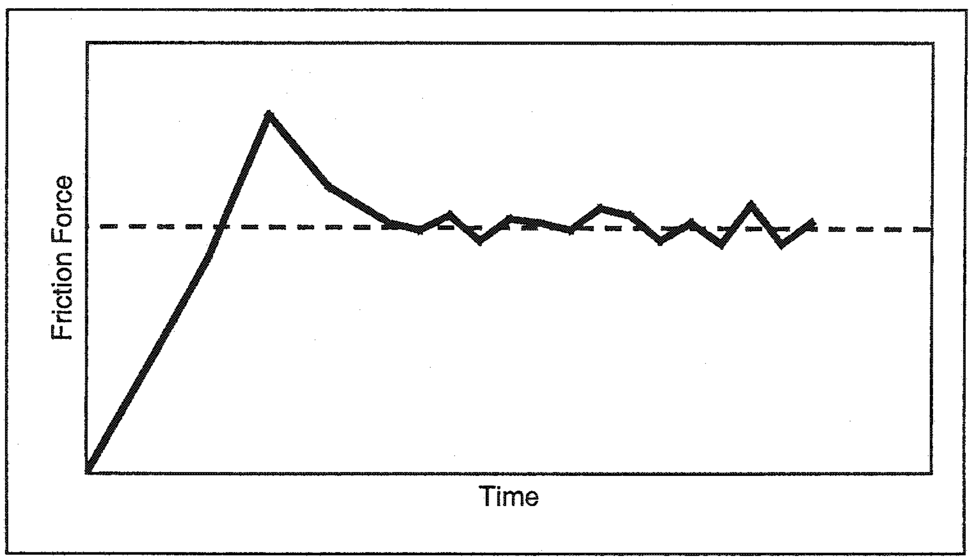

Figure 6.5. A classical friction force plot.

6.2.2 Experimental Design

A full factorial design of experiments with three factors was used for each of the two materials used in this study, Aluminum A6061 and Steel 1080. Figure 6.6 shows the factors used in this work and their levels. The levels are numbered with larger number indicating a higher level. The actual values are given in the response tables in section 6.2.3. Randomization, blocking and averaging (replication) schemes were used to reduce the process variability, the impact of noise factor and experimental error [129-130]. Randomization helps avoid any bias error by running the designed experiments at random order. Blocking divide the experiment into groups (blocks) and helps avoid bias error.

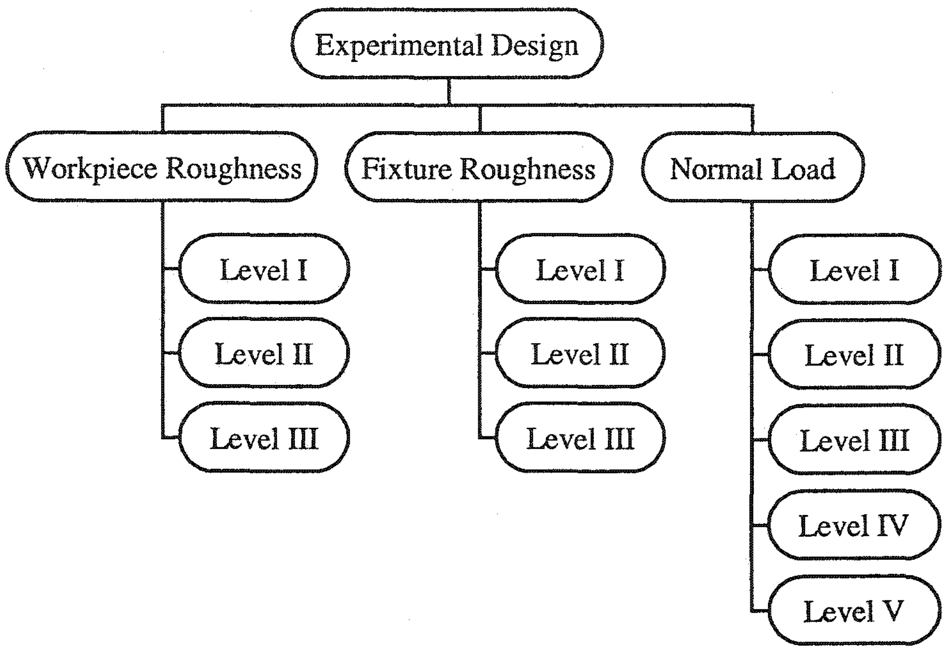

Figure 6.6 Levels of independent variables.

Replication is recommended for processes with excessive variability and helps reduce the variability by taking the average of the replicates of each trial. The experiment was repeated, for each combination of the three factors, as many times as needed for the average to converge.

Workpiece samples were machined with different feed values at a cutting speed of 1000 RPM to simulate different surface finishes. The surface roughness was measured using a portable profilometer, and the average values of the surface roughness (over 6 measurements per sample) were used in the analysis. The values are displayed in Table 6.1.

a) Sample Workpiece Material: Aluminum A6061

Machining conditions (Feed mm)	Ra	Ra	Ra	Ra	Ra	Ra	Average Ra
Cast	1.24	1.2	1.28	1.32	1.03	0.8	1.15
0.0508	1.51	0.48	2.489	0.67	0.52	0.55	1.04
0.3048	1.88	2.31	1.78	1.4	1.57	1.33	1.71
0.4572	3.34	2.08	2.89	1.7	2.89	2.68	2.60
0.6096	2.36	2.5	4.3	7.2	3	6.2	4.26

b) Sample Workpiece Material: Steel 1080

Machining conditions (Feed mm)	Ra	Ra	Ra	Ra	Ra	Ra	Average Ra
0.0254	0.96	0.76	0.85	0.71	0.75	0.65	0.78
0.127	1.67	1.62	1.63	1.43	1.25	1.65	1.54
0.1778	1.7	2.28	1.52	1.77	2.08	2.07	1.90
0.2286	2.51	2.46	2.72	2.66	2.82	2.9	2.68
0.2794	2.7	2.73	2.32	2.23	2.48	2.25	2.45

Table 6.1. Workpiece samples surface Roughness R_a (μm).

The fixture tips used are manufactured from M2 high-speed steel, hardened to 60 ±1 HRC with black oxide finish. They have a diamond serration pattern where the tooth pitch indicates their surface roughness. A higher tooth pitch indicates a coarser surface.

The effect of a factor on a response variable is the change in the response when the factor goes from its low level to its high level. Using the concept of response table [131], the effect of each factor can be estimated by finding the average value for the response variable at both its high and low levels. Then calculating the arithmetic difference between these two average values. Since the columns for the factors in the response table (Tables 6.2and 6.3) are orthogonal, the other factors do not distort the estimate of the effect of any particular factor.

6.2.3 Experimental Results

In this section the experimental data obtained is presented in tabular and graphical forms. The data show the relation between the friction coefficient (dependent variable) and the workpiece roughness, fixture tip roughness and clamping force magnitude (independent variables). The response tables (6.2 and 6.3) display the average value of the friction coefficient (both static and dynamic) for each of the designed experiments. The effect of the levels variation of the experiment factors on both the static and dynamic friction coefficients is evident from the friction coefficient values displayed.

	Average		Workpiece Roughness (Ra μm)			Fixture(tooth pitch *90 deg)			Normal Load(lbf)			
	μ stat	μ dyn	L	M	H	L	M	H	L	1	M	2
1	0.407	0.376	1.15			0.094			936			
2	0.080	0.070	1.15			0.094				1123.2		
3	0.298	0.275	1.15			0.094					1248	
4	0.075	0.070	1.15			0.094						1435.2
5	0.242	0.226	1.15			0.094						
6	0.434	0.386	1.15				0.094		936			
7	0.293	0.284	1.15				0.094			1123.2		
8	0.271	0.250	1.15				0.094				1248	
9	0.246	0.242	1.15				0.094					1435.2
10	0.269	0.237	1.15				0.094					
11	0.439	0.398	1.15					0.188	936			
12	0.368	0.362	1.15					0.188		1123.2		
13	0.357	0.318	1.15					0.188			1248	
14	0.239	0.239	1.15					0.188				1435.2
15	0.243	0.225	1.15					0.188				
16	0.483	0.412		1.71		0.094			936			
17	0.087	0.081		1.71		0.094				1123.2		
18	0.261	0.247		1.71		0.094					1248	
19	0.226	0.226		1.71		0.094						1435.2
20	0.255	0.229		1.71		0.094						
21	0.510	0.433		1.71			0.094		936			
22	0.300	0.280		1.71			0.094			1123.2		
23	0.335	0.304		1.71			0.094				1248	
24	0.244	0.240		1.71			0.094					1435.2
25	0.245	0.226		1.71			0.094					
26	0.461	0.413		1.71				0.188	936			
27	0.276	0.260		1.71				0.188		1123.2		
28	0.342	0.300		1.71				0.188			1248	
29	0.228	0.215		1.71				0.188				1435.2
30	0.239	0.218		1.71				0.188				
31	0.435	0.386			4.26	0.094			936			
32	0.106	0.101			4.26	0.094				1123.2		
33	0.314	0.295			4.26	0.094					1248	
34	0.096	0.096			4.26	0.094						1435.2
35	0.229	0.215			4.26	0.094						
36	0.402	0.369			4.26		0.094		936			
37	0.326	0.324			4.26		0.094			1123.2		
38	0.314	0.293			4.26		0.094				1248	
39	0.249	0.247			4.26		0.094					1435.2
40	0.230	0.216			4.26		0.094					
41	0.503	0.448			4.26			0.188	936			
42	0.330	0.324			4.26			0.188		1123.2		
43	0.320	0.285			4.26			0.188			1248	
44	0.255	0.252			4.26			0.188				1435.2
45	0.212	0.198			4.26			0.188				
	13.073	12.093	17.250	25.650	63.900	1.410	1.410	2.820	8424.000	10108.8	11232.0	12916.8

Table 6.2. Full factorial experimental data and results for Aluminum 6061

	Average		Workpiece Roughness (Ra μm			Fixture(tooth pitch *90 deg)			Normal Load(lbf)				
	μ stat	μ dyn	L	M	H	L	M	H	L	1	M	2	H
1	0.06	0.057	0.076			0.094			936				
2	0.086	0.057	0.076			0.094				1123.2			
3	0.065	0.059	0.076			0.094					1248		
4	0.065	0.062	0.076			0.094						1435.2	
5	0.194	0.186	0.076			0.094							1560
6	0.357	0.354	0.076				0.094		936				
7	0.347	0.342	0.076				0.094			1123.2			
8	0.265	0.245	0.076				0.094				1248		
9	0.218	0.205	0.076				0.094					1435.2	
10	0.188	0.18	0.076				0.094						1560
11	0.31	0.298	0.076					0.188	936				
12	0.301	0.289	0.076					0.188		1123.2			
13	0.263	0.253	0.076					0.188			1248		
14	0.24	0.235	0.076					0.188				1435.2	
15	0.215	0.206	0.076					0.188					1560
16	0.072	0.064		0.154		0.094			936				
17	0.072	0.062		0.154		0.094				1123.2			
18	0.063	0.059		0.154		0.094					1248		
19	0.055	0.055		0.154		0.094						1435.2	
20	0.069	0.066		0.154		0.094							1560
21	0.34	0.326		0.154			0.094		936				
22	0.33	0.324		0.154			0.094			1123.2			
23	0.27	0.259		0.154			0.094				1248		
24	0.26	0.251		0.154			0.094					1435.2	
25	0.213	0.205		0.154			0.094						1560
26	0.323	0.311		0.154				0.188	936				
27	0.33	0.305		0.154				0.188		1123.2			
28	0.284	0.273		0.154				0.188			1248		
29	0.25	0.241		0.154				0.188				1435.2	
30	0.257	0.234		0.154				0.188					1560
31	0.101	0.07125			2.68	0.094			936				
32	0.09	0.068			2.68	0.094				1123.2			
33	0.086	0.043			2.68	0.094					1248		
34	0.048	0.0385			2.68	0.094						1435.2	
35	0.041	0.03525			2.68	0.094							1560
36	0.35	0.175			2.68		0.094		936				
37	0.32	0.18			2.68		0.094			1123.2			
38	0.254	0.127			2.68		0.094				1248		
39	0.25	0.11			2.68		0.094					1435.2	
40	0.1935	0.09675			2.68		0.094						1560
41	0.412	0.206			2.68			0.188	936				
42	0.3	0.195			2.68			0.188		1123.2			
43	0.2965	0.14825			2.68			0.188			1248		
44	0.2	0.135			2.68			0.188				1435.2	
45	0.234	0.117			2.68			0.188					1560
Sum	9.538	7.809	1.140	2.310	40.200	1.410	1.410	2.820	8424.000	10108.8	11232.0	12916.8	14040.0
# of Exp.	45.000	45.000	45	45	45	45	45	45	45	45	45	45	45
Average	0.212	0.174	0.076	0.154	2.680	0.094	0.094	0.188	936	1123	1248	1435	1560
Range			2.89			0.094			624				

Table 6.3. Full factorial experimental data and results for Steel1080

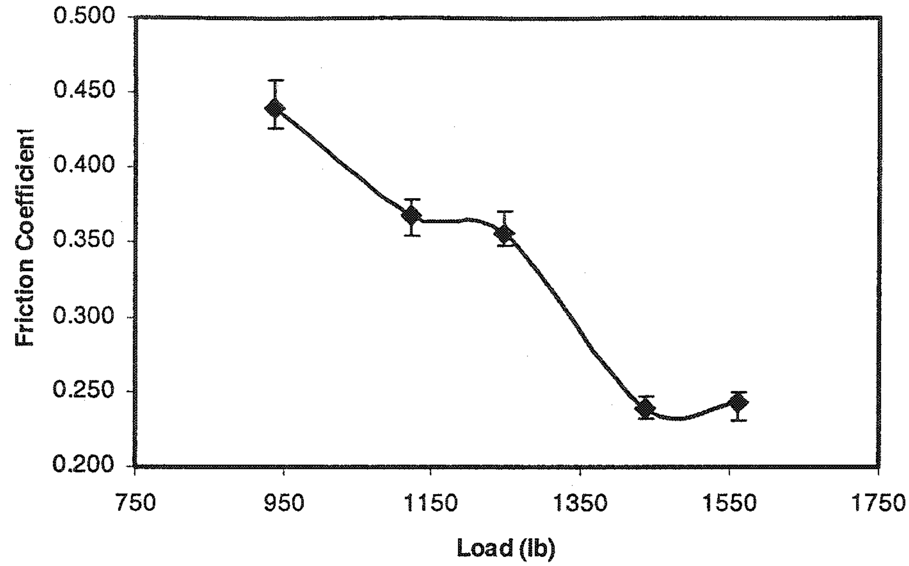

Figure6.7 . Static Friction Coefficient versus clamping Load (Aluminum Workpiece Ra=, 1.15 μm, coarse fixture tip)

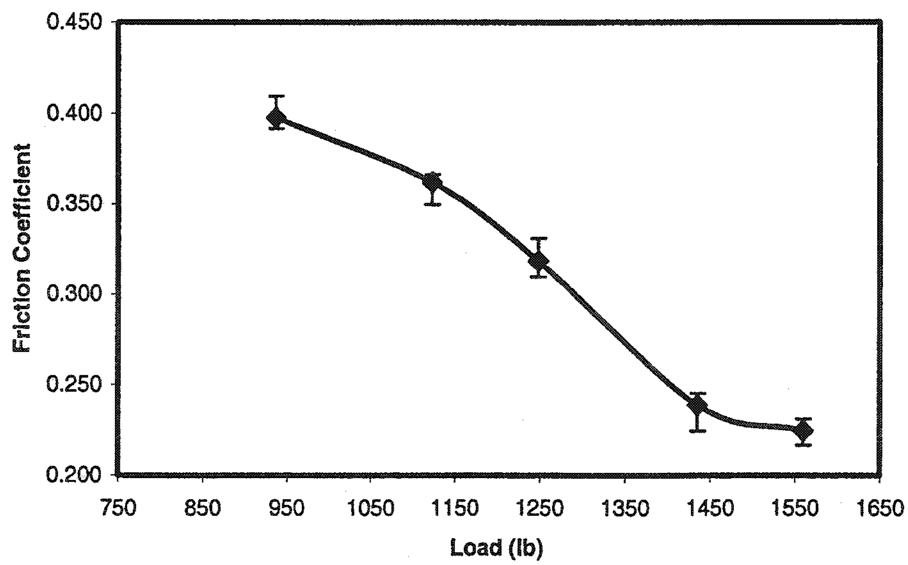

Figure6.8. Dynamic Friction Coefficient versus clamping Load (Aluminum Workpiece Ra=, 1.15 μm, coarse fixture tip).

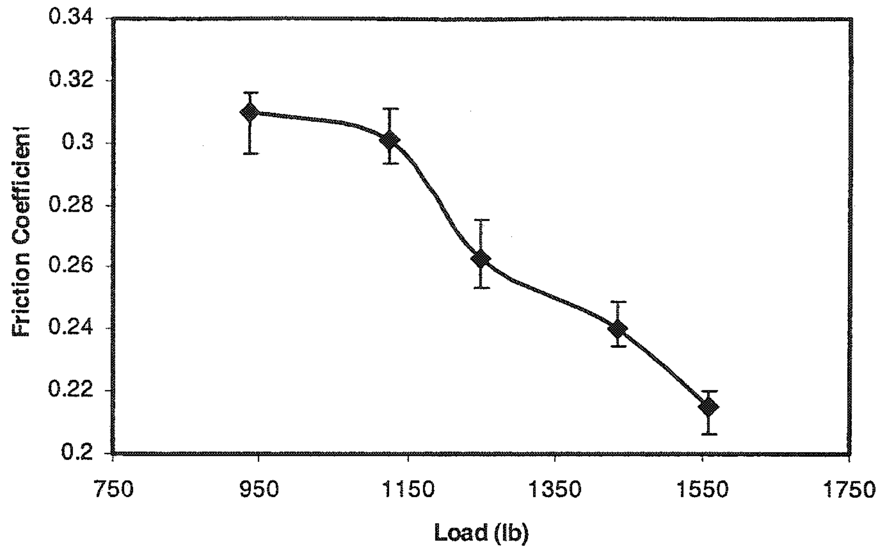

Figure 6.9. Static Friction Coefficient versus clamping Load (Steel Workpiece Ra=, 3. μm, coarse fixture tip)

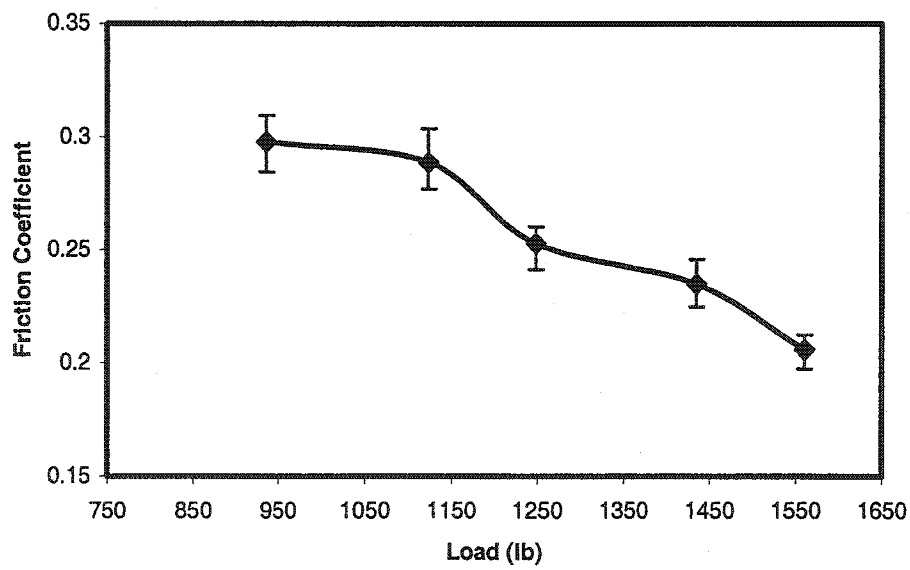

Figure 6.10. Dynamic Friction Coefficient versus clamping Load (Steel Workpiece Ra=, 3.0 μm, coarse fixture tip)

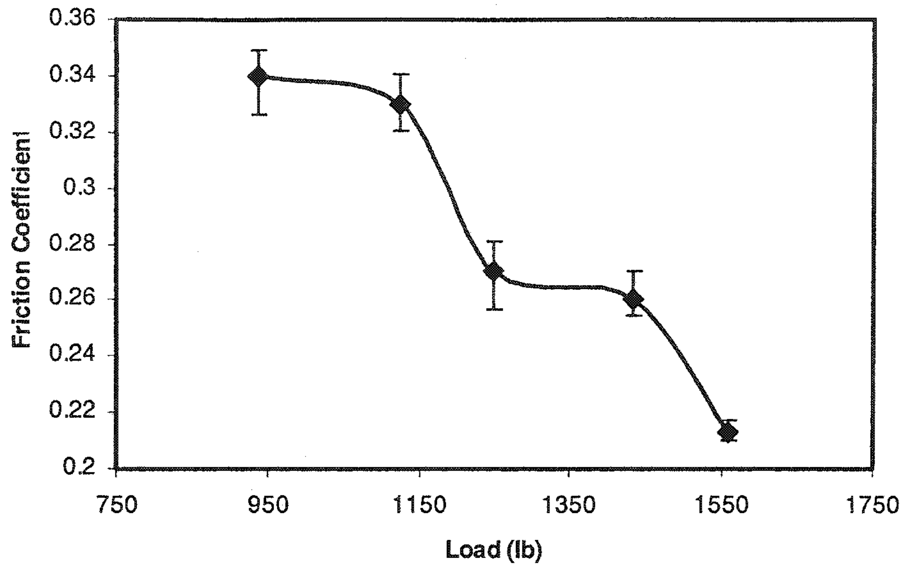

Figure 6.11. Static Friction Coefficient versus clamping Load (Steel Workpiece Ra=, 5.0 μm, medium fixture tip)

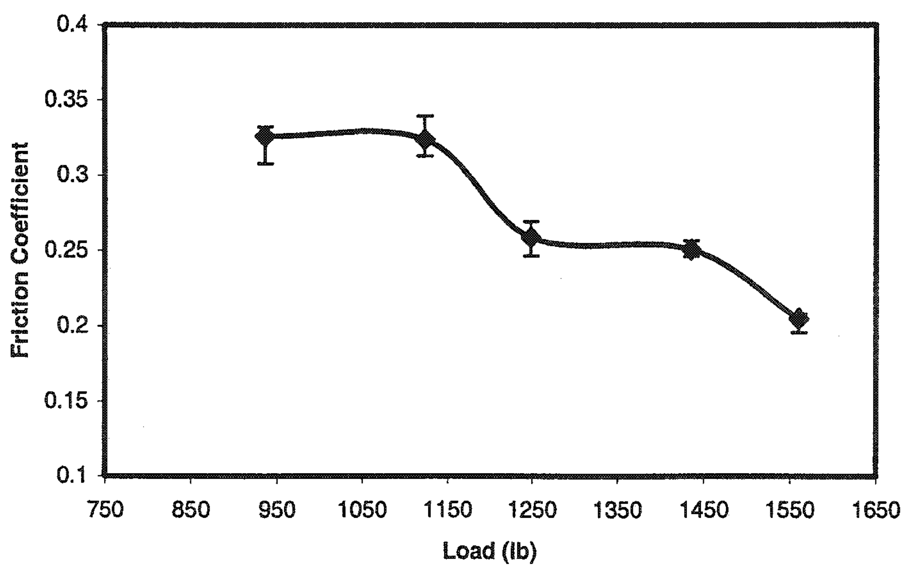

Figure 6.12. Dynamic Friction Coefficient versus clamping Load (Steel Workpiece Ra=, 5.0 μm, medium fixture tip)

Figures 6.7 to 6.12 show the relation between the friction coefficient, μ_s and μ_k, and the normal load, P, for different conditions. It can be seen that μ decreases as P increases which is opposed to the assumption that friction force changes according to the normal load since, by definition, μ represents the proportionality between these two quantities. This relation is very important in fixturing application, especially for flexible parts when optimum (minimal) clamping forces are required to maintain the machined part geometric integrity. The same trend of decreasing μ with increasing P was reported before by [64][72], however it was not explained. Two different perspectives could be used to explain this phenomenon:

A) Based on the quasi-static friction model given by [69]. The coefficient of friction for a quasi-steady static system can be given as:

$$\mu = \frac{A_a}{P} \cdot \begin{bmatrix} (1-\beta) \cdot S_1 \cdot f \cdot \left(\dfrac{\tau_{a1}}{S_1}\right) + \\ \beta \cdot S_1 + (1-\beta) \cdot S_2 \cdot f\left(\dfrac{\tau_{a2}}{S_2}\right) \\ + \beta \cdot S_2 \cdot f \cdot \left(\dfrac{S_1 \cdot H_1}{S_2 \cdot H_2}\right) \end{bmatrix} \tag{6.1}$$

Note that the term in square brackets depends only on the shear strengths and adhesive properties of the contacting materials and does not change with P or A_o. Therefore, a variation in nominal contact pressure can affect μ only through changes of the A_a/P term as shown in equation (6.2):

$$\left(\frac{A_a}{P}\right) = \left(\frac{3 \cdot \pi \cdot R^{1/2}}{4 \cdot E' \cdot \sigma^{1/2}}\right) \frac{F_1 \cdot (d/\sigma)}{F_{3/2} \cdot (d/\sigma)} \tag{6.2}$$

where the factor in large parentheses is a constant as long as the asperity geometry remains fixed. When the nominal pressure P/A_0 increases, the separation d decreases. In turn, μ varies in accordance with the ratio $F_1(d/\sigma)/F_{3/2}(d/\sigma)$. Calculations show that this ratio decreased from 1.5 to 0.93 as d/σ decreases from 3.5 to 0.09. Thus, μ is affected by the nominal pressure.

B) Considering elastic and plastic conditions on the contact surface between two objects, different dependencies of friction force on normal force can be demonstrated. If we accept that $Q = \tau \cdot A$ then for μ to be independent of the normal force, the shear stress τ must be independent of shear force and the true contact area A must be proportional to P.

In contrast to this linear dependency of friction force on P, the elastic contact equations of Hertz [71] show that for a sphere pressed against a flat body, the area of contact is proportional to $P^{2/3}$. In that case, the friction coefficient is expected to decrease as a function of contact pressure.

Figures 6.13 to 6.15 show the effects of the fixture tip roughness and workpiece roughness on the coefficient of friction when all the other variables are constant, for the workpiece materials used. Often, a direct relationship can be established between the friction forces generated in a system and the initial surface texture, which includes roughness and waviness. However, in some cases, wear processes destroy the initial surface texture and it is inappropriate to try to correlate frictional behavior with the initial surface finish. However, if contact pressure is low, or if the contacting materials are hard, the initial surface features may be preserved for an extended period of sliding, therefore playing a role in determining the coefficient of friction (figure 6.14). On the other hand, if the contact pressures are high, or if one or both contacting materials are relatively soft, the initial surface finishes will be quickly damaged and will have minimal effect on the sliding friction. In this situation, the surface finish of the material will be determined by the wear properties of the materials and other factors like transfer and debris layer formation.

In non-lubricated sliding, the surface roughness does not generally have a marked effect on friction. With extremely smooth surfaces, it may be possible to obtain elastic rather than plastic deformation when the surfaces are first placed in contact. However, if there is appreciable adhesion between the surfaces the friction force will probably produce plastic deformation around the contact regions. The sliding process itself will thus roughen the surface. Surface and plastic flow will occur in subsequent traversals of the surface. If, however the interfacial adhesion is very small the deformation may remain primarily elastic even during sliding. In this case the sliding process may produce a steady smoothing of the surface. Surface roughness may, to some extent, determine whether for a given load the deformation will be primarily elastic or plastic. This will necessarily affect the friction.

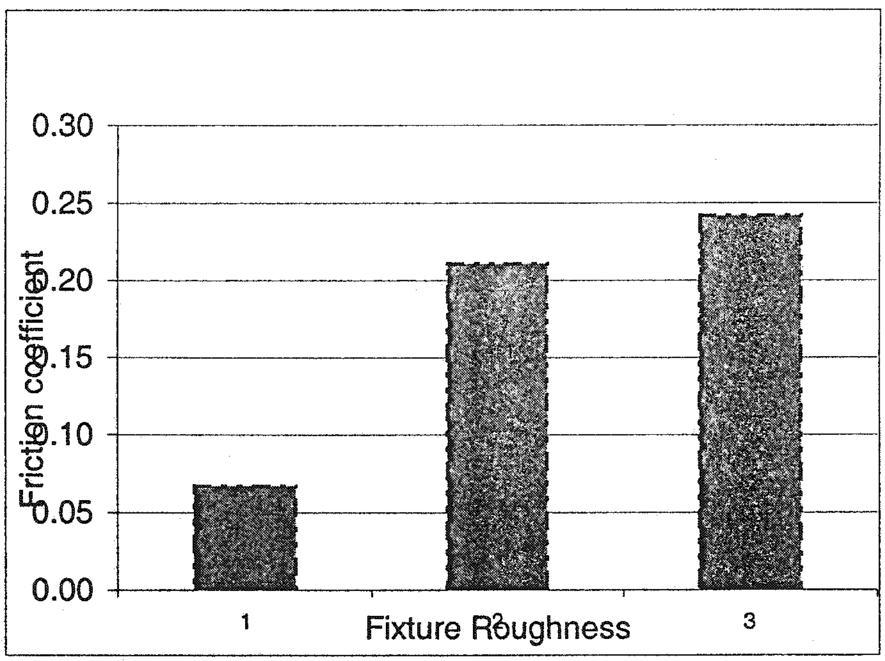

Figure 6.13: Coefficient of friction versus fixture tip roughness levels (1 = Low, 2 = Medium, 3 = High), P=6942N, workpiece material: steel 1080, Ra = 1.54).

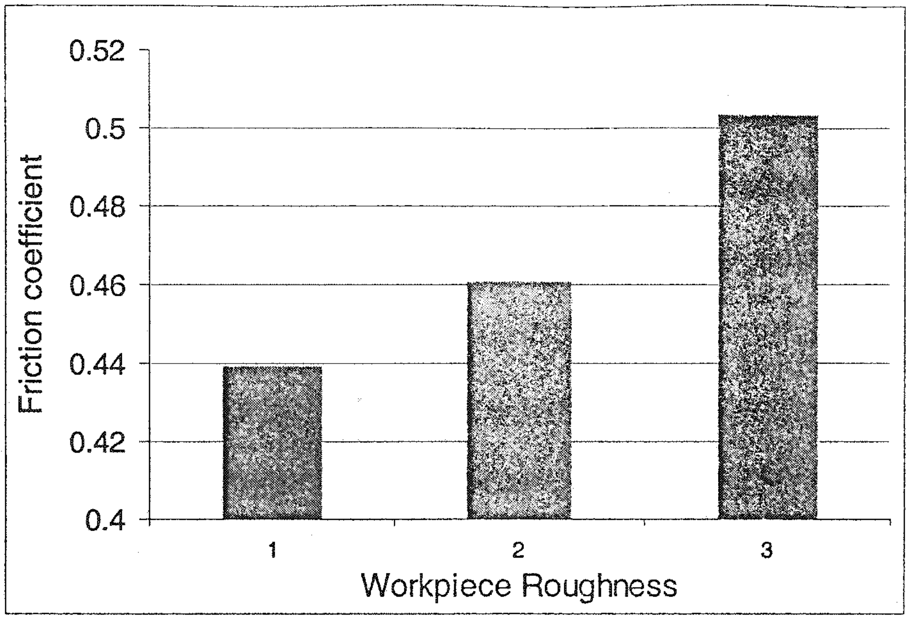

Figure 6.14: Coefficient of friction versus steel workpiece roughness (1- Ra = 0.78, 2– 1.54, 3- 2.68), P = 6942N, medium roughness fixture tip.

Figure 6.15: Coefficient of friction versus Al 6061 workpiece roughness (1- Ra = 1.15,2– 1.71, 3-4.26), P = 4165N, coarse fixture tip.

This experimental data constitutes a nucleus of a database for fixture application that can either be extended or interpolated/extrapolated to obtain realistic values for the friction coefficient for fixture applications. A sub set of the experimental data for Aluminum workpiece presented in table 6.2 was used to run a regression analysis with the friction coefficient as the dependent variable and the workpiece roughness, fixture tip roughness and normal load magnitude as the independent variables. Figure 6.16 shows the good agreement between the experimental and the predicted values.

The regression statistics are displayed in table 6.4. ANOVA results are shown in table 6.5 and the regression coefficients and standard error are shown in table 6.6.

Regression Statistics	
Multiple R	0.938596596
R Square	0.880963569
Adjusted R Square	0.865437079
Standard Error	0.034678824
Observations	27

Table 6.4 Summary of the regression statistics for the Al6061 workpiece.

	Coefficients	*Standard Error*
Intercept	0.743302097	0.040085117
Workpiece roughness	-0.002327662	0.004930797
Fixture roughness	0.175137904	0.150612453
LOAD	-0.000340218	2.61983E-05

Table 6.5 ANOVA result for Al6061 workpiece..

ANOVA			
	df	*SS*	*MS*
Regression	3	0.204707903	0.068235968
Residual	23	0.027660279	0.001202621
Total	26	0.232368182	
		F	*Significance F*
Regression	3	56.73938645	8.7437E-11
Residual	23		
Total	26		

Table 6.6. Regression coefficients for Al6061 workpiece test.

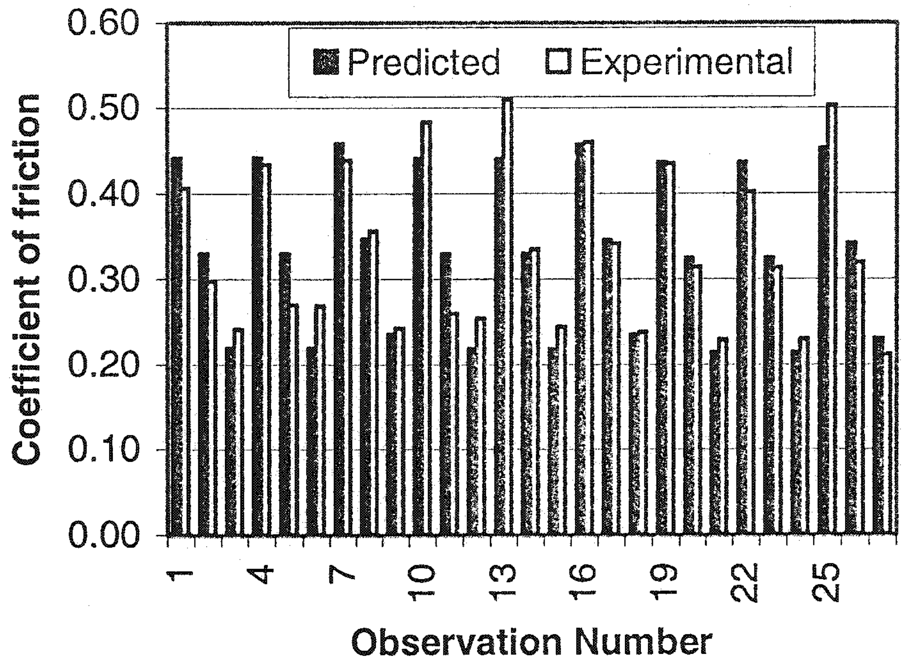

Figure 6.16 Predicted and experimental values of the coefficient of friction for AL6061 workpiece.

CHAPTER 7: RESULTS AND DISCUSSION

7.1 INTRODUCTION

In this chapter simulation results and discussion are presented. In the first part the mechanistic force model calibration and validation results are presented and discussed. Simulation runs are presented to show the effect of contact stiffness, fixture location and friction coefficient on the cutting forces. Then some simulation cases are validated. At the end of the chapter, two case studies are presented and discussed to demonstrate the real application of the current research.

7.2 Mechanistic Force Model Calibration

The basic underlying assumption behind any mechanistic force model is that the cutting forces are proportional to the uncut chip area. The actual function which relates the constant of proportionality, called the specific cutting energy, to the cutting geometry and conditions under the given tool-workpiece materials combination is determined by fitting experimental data in a process called calibration. Calibration tests are used to determine the tangential, radial and axial cutting force coefficients. It has been demonstrated by many investigators that the representative pressure values tend to depend significantly on the uncut chip thickness (t_c), cutting velocity (V), and normal rake angle (α_n)[7]. It is proposed here that these coefficients are functions of cutting edge geometry, cutting speed and feed per tooth. The functional form of the equations representing the variations of these coefficients is detailed in equation (7.1),

$$K_i = e^{(a_1 + a_2 \cdot V_i + a_3 \cdot B_i)} \qquad (7.1)$$

where K_i is the instantaneous cutting coefficient, V_i and B_i are the instantaneous cutting speed and geometric constants respectively. The coefficients a_1, a_2, and a_3 are functions of the instantaneous feed per tooth. The functional form of equation was formulated similar to Kapoor et al. [7] and Jayaram [131]. Kapoor expressed the cutting force coefficient as an exponential function of chip thickness and cutting speed.

The first step in the calibration procedure is to reformulate the force model presented in chapter 4 into a form that separates the cutting force coefficients and the geometric factors. The cutting forces can be written as:

$$\begin{aligned} F_x &= A_t.K_1 + A_r.K_2 + A_a.K_3 \\ F_y &= B_t.K_1 + B_r.K_2 + B_a.K_3 \\ F_z &= C_t.K_1 + C_r.K_2 + C_a.K_3 \end{aligned} \qquad (7.2)$$

Equation 7.2 is in the form of multiple parameters linear regression model and the full derivation can be found in appendix I. For each cutting test the average cutting force coefficients [K_1, K_2 and K_3] can be determined using linear regression analysis. It is assumed that for constant feed rate, each k_i can be represented in the power law form (equation 7.1), which is shown in equation (7.3),

$$\ln(K_i) = a_1 + a_2.V_j + a_3.\beta_j \quad (7.3)$$

Grouping test that have constant feed rate and using log-linear regression, the parameters a_i can be determined for each K_i.

Milling operations with a single insert were carried out on an "OKUMA Cadet V4020" machining center (Figure 7.1) for a wide range of cutting conditions. The workpiece material was aluminum A6061. The insert material was uncoated carbide 'H10'. Both axial and radial rake angles are equal to 18^0. The range of cutter rotational speed was 500 to 3000 RPM. The feed per tooth range was 0.002 to 0.008 inch and the depth of cut range was 0.040 to 0.250 inch. The three components of the cutting force were measured using a Kistler dynamometer type 9225A.

The experimental data was preprocessed before used in the calibration program to reduce variability of the data and consequently improve the simulation prediction accuracy. Averaging of more than one revolution was used to reduce variability. Figure 7.2 shows the averaging of the cutting force components over five cutter revolutions to reduce the experiment variability.

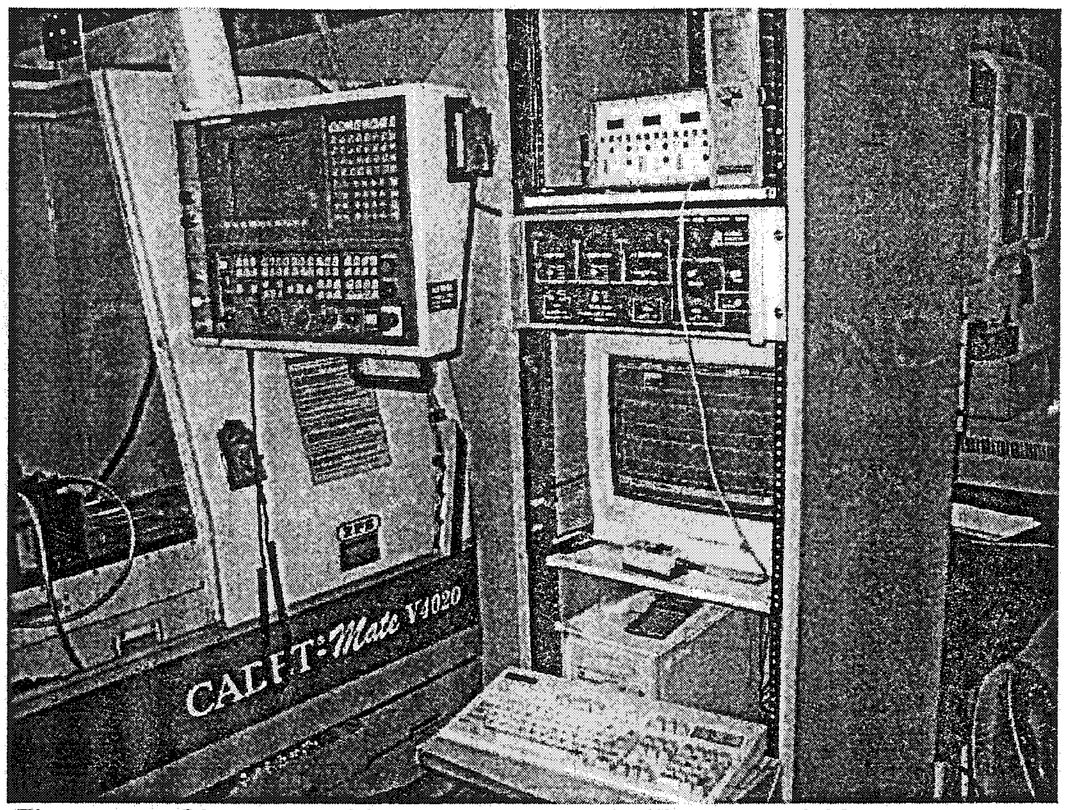

Figure 7.1. Okuma machining center and the Data acquisition system.

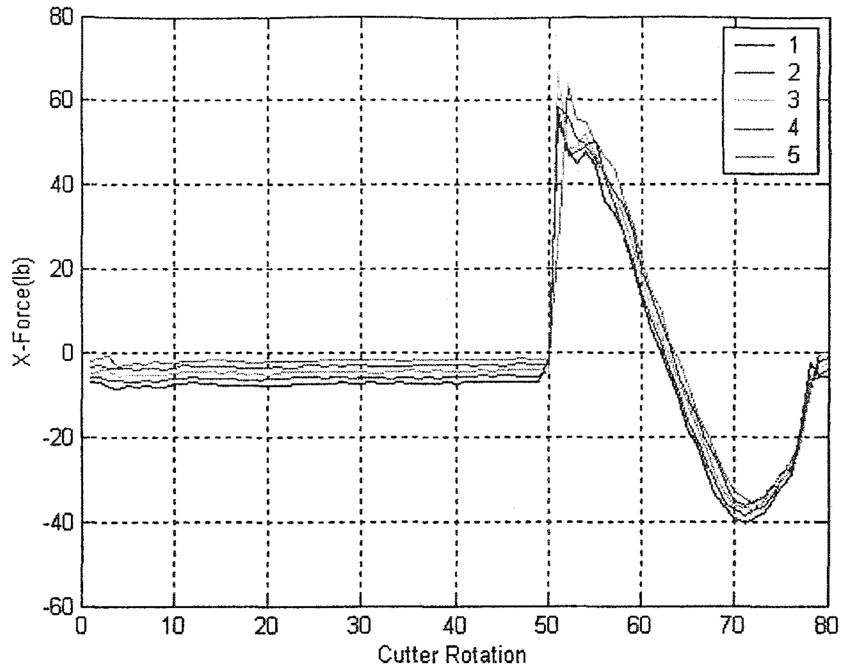

Figure 7.2 a Preprocessing of experimental data (5 revolutions).

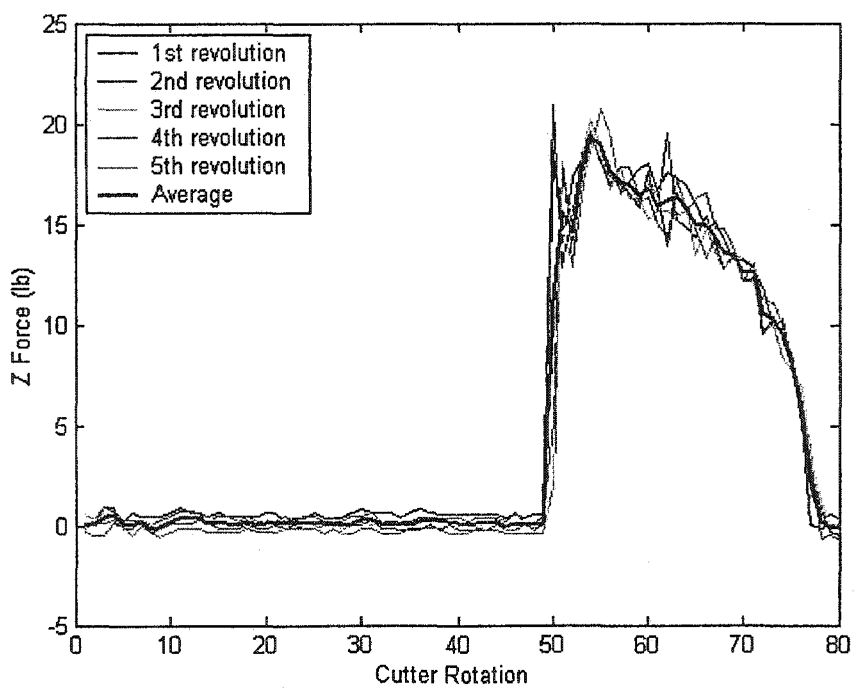

Figure 7.2b Preprocessing of experimental data.

7.3 Mechanistic Force Model Validation

The following figures (7.3-7.5) show the measured and predicted cutting forces for different cutting parameters. The simulated three force components and resultant force are shown in solid line for single insert cuts at different cutting parameters values. The dotted line represents the measured data. The difference between the measured and predicted value, particularly in the axial direction, can be attributed to the fact that single insert cutting in face milling causes the cutter to tilt which is avoided in the normal practice by introducing spindle tilt in the opposite direction to avoid back cut. The force exerted by this single insert is also a function of the cutter rotation angle, which will create different cutter tilt at different cutter angular locations, which will change the effective axial depth of cut cutting causing this variation in the force signature. The shift between the measured and predicted data that noticed in some of the figures is due to the selection of the begin angle, which is a control variable in the simulation that can be tuned to eliminated this shift. The difference between the measured and predicted forces is acceptable and falls with in the norms.

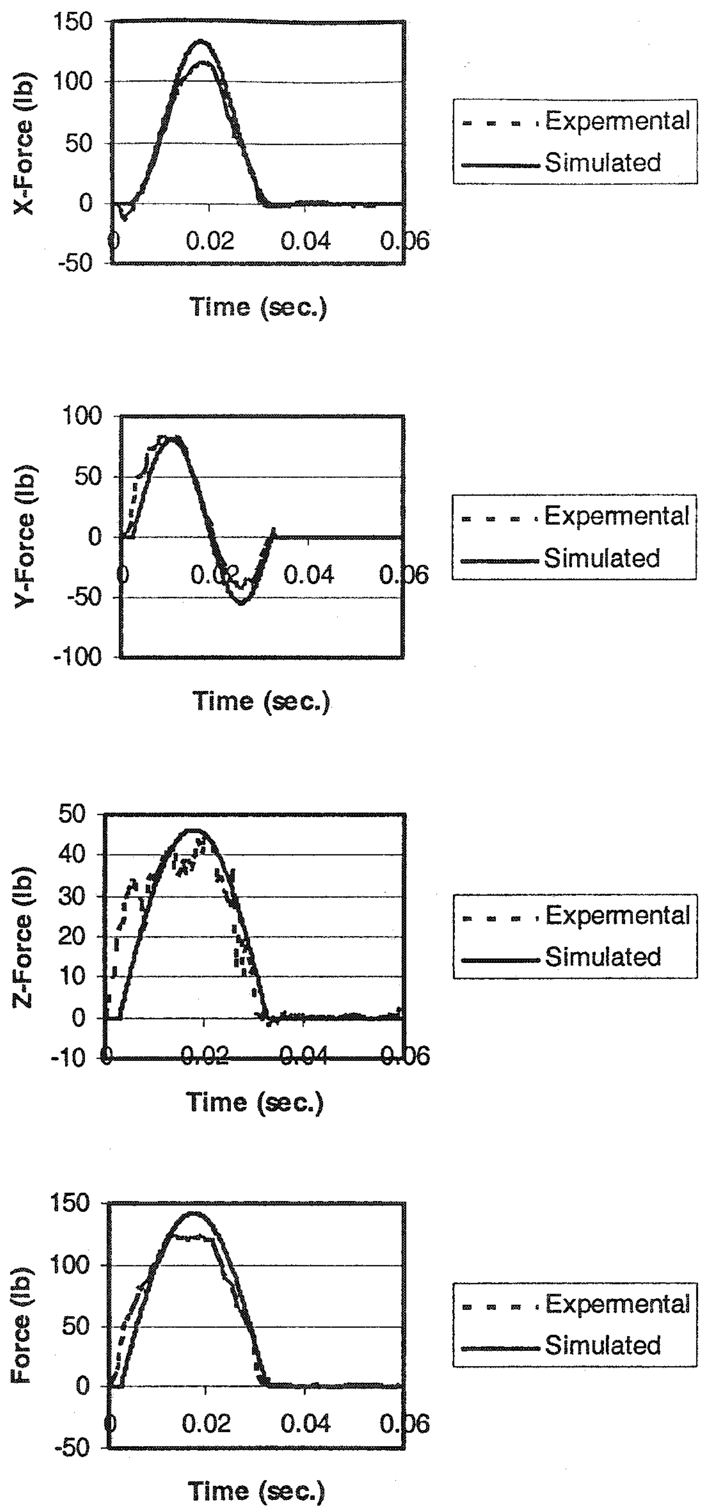

Figure 7.3. Measured and predicted force components and resultant for Aluminum 6061, 1000RPM, and 0.15 inch DOC 6 IPM feed rate.

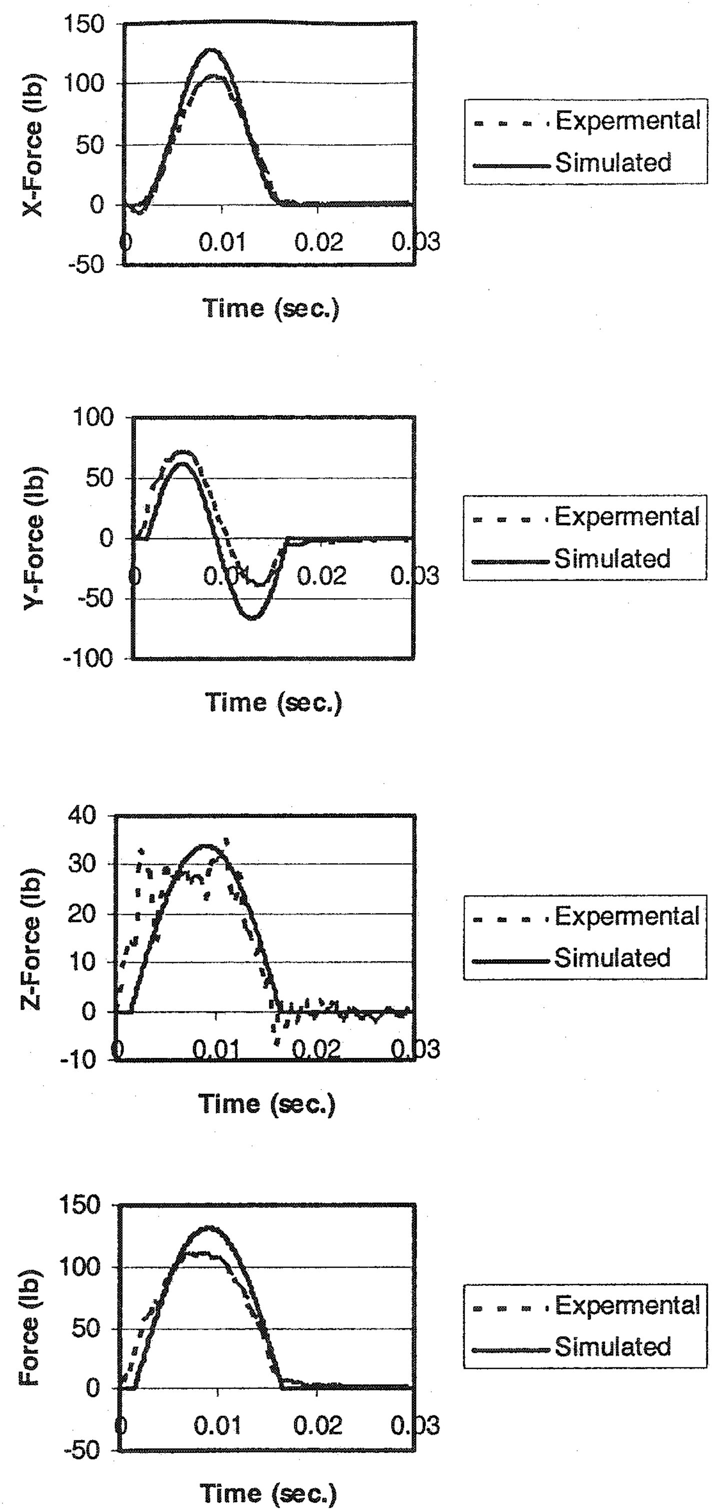

Figure 7.4 Measured and predicted force components and resultant for 2000RPM, 0.150 inch DOC, 12 IPM feed rate.

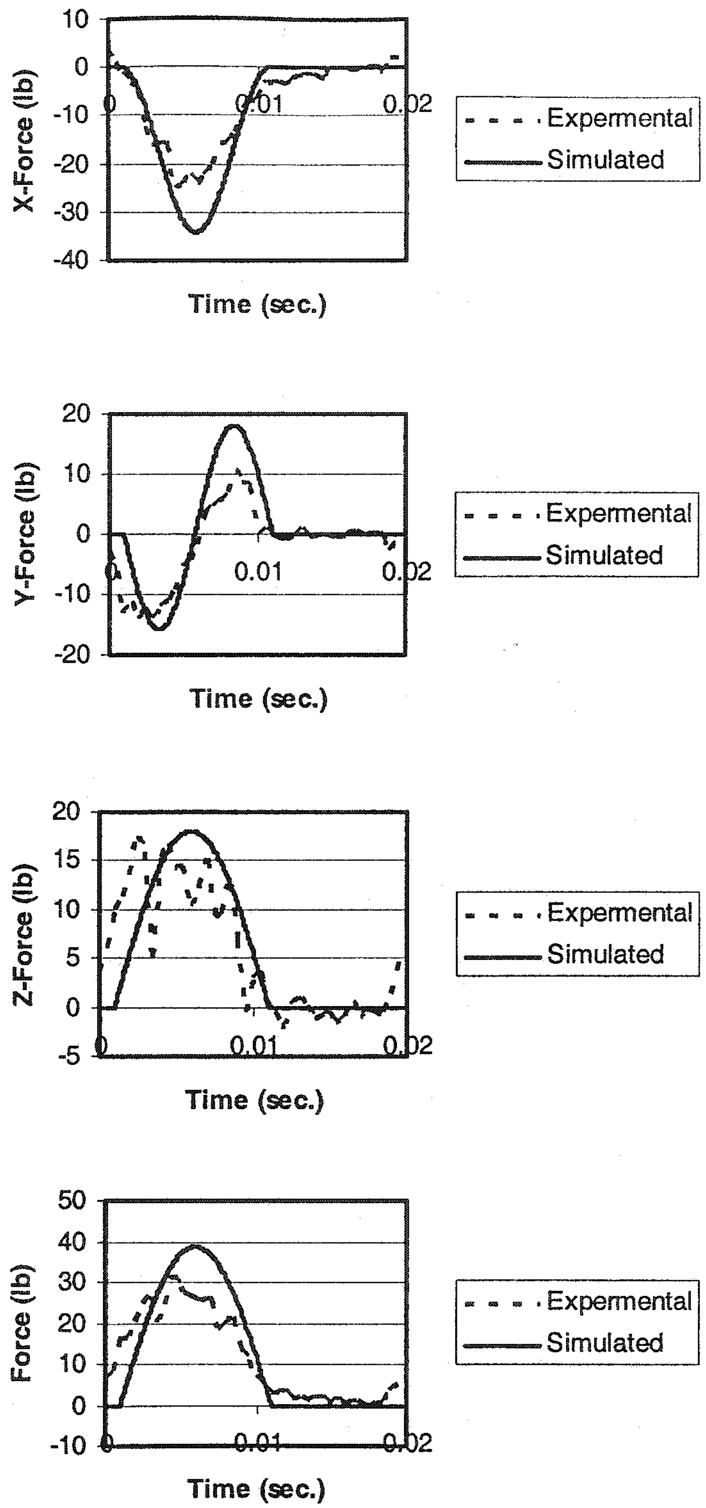

Figure 7.5. Measured and predicted force components and resultant for 3000 RPM, 0.040 Inch DOC and 12 IPM feed rate.

7.4 Effect of Fixture Configuration and Contact stiffness on the Machining System Dynamics

The proper modeling of the fixture elements becomes increasingly important when machining flexible parts as fixture dynamics and positioning will affect the natural frequencies of the machining system and consequently, can play a role in chatter control. The machining system in the presence of contact conditions is inherently nonlinear and its dynamics are not well understood. Once the dynamic characteristics of the machining system are computed through numerical and /or experimental analysis, the fixture layout can be revised to modify the dynamic characteristics of the machining system in order to avoid severe vibrations and part deflection as demonstrated in case study I. Figure 7.6 shows how the location (position) of the clamping elements affects the dynamic characteristics of the system. The clamps are located symmetrically from the centre of the aluminum workpiece, 8 inches in length. The X-axis represents the distance between the clamp and the fixture. The simulation is repeated for different workpiece thickness (1/2, 3/2, 5/2 and 4 inch) as shown in figure 7.6 respectively, to demonstrate the effect of the workpiece flexibility on the system dynamics. Such simulations can be used as an aid in determining when it is feasible to consider the fixture element to be flexible/ rigid compared to the workpiece flexibility. This control can be further extended by using non-symmetrical fixture configurations to stiffen certain features of the part being machined as demonstrated in case study I.

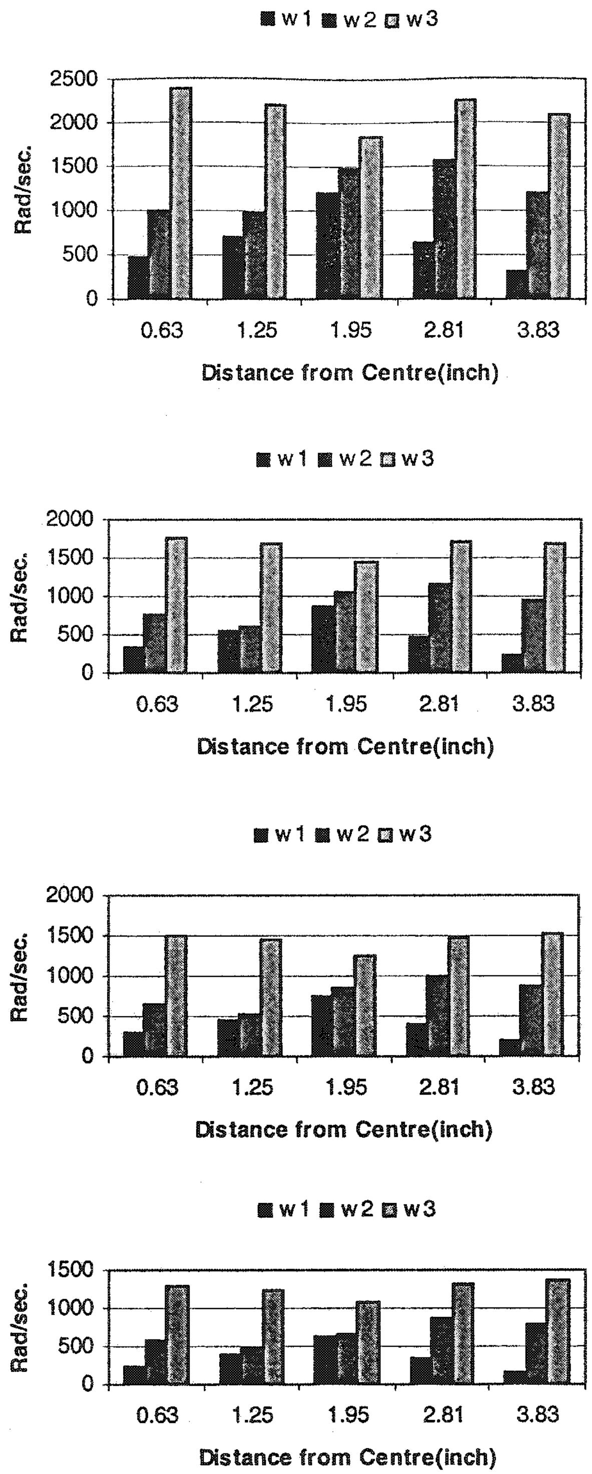

Figure 7.6 Effect of Fixture element location and workpiece dimensions on the system natural frequency.

Figure 7.7 shows the effect of contact stiffness on the natural frequency of the process. The contact stiffness clearly affects the natural frequency by increasing the stiffness while the system mass is constant. it can be seen that there is a critical value of the contact stiffness after which the system is insensitive to the increase in contact stiffness. This trend was reported before by Hassan et al.[126].

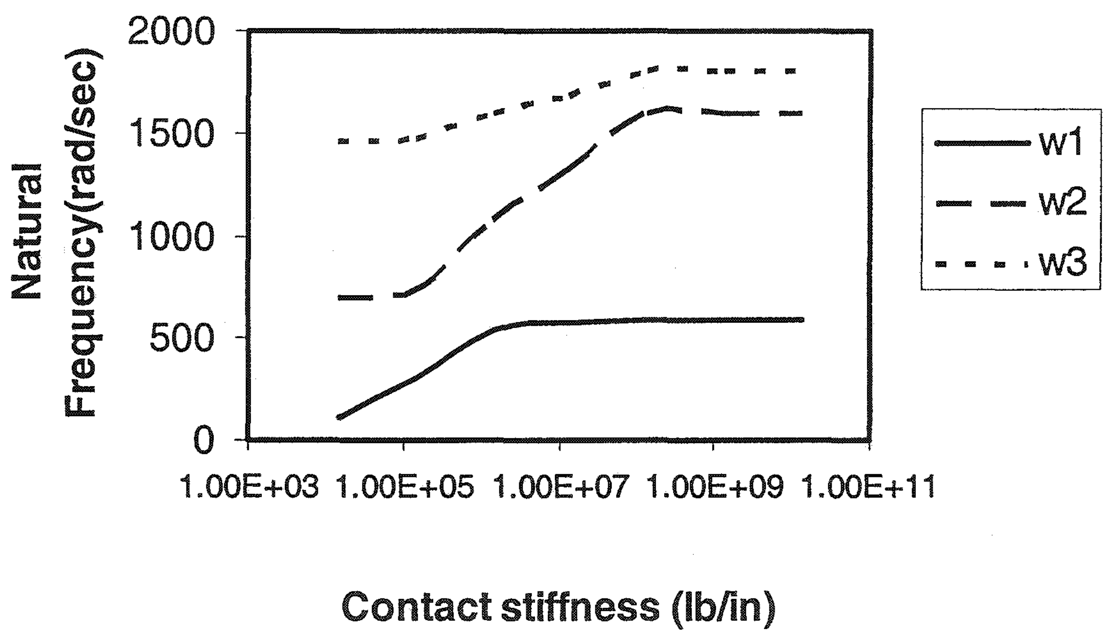

Figure 7.7. Effect of contact stiffness on the workpiece/fixture dynamic Characteristics (Aluminum workpiece, 6/8×4×8 inch)

7.5 Simulation Runs

Accuracy in the prediction of static cutting forces is critical to the development of the dynamic simulation program since the pattern of cutting forces affects the pattern of vibration, which in turn will determine dynamic cutting forces. Static and dynamic cutting force profiles with and without run out were presented in chapter 4. Using the developed integrated model, multiple runs of the simulation were executed to explore the effect of contact stiffness, the coefficient of friction and the fixture elements locations on the dynamic cutting forces.

Figure 7.8 illustrates the noticeable effect of contact stiffness on the cutting forces. Although the contact stiffness is used to restrain the system and it is a direct function of the clamping force, excessive clamping force could have a negative effect of the system and workpiece geometric integrity by introducing pre-machining deformation to the part. Figure 7.9 shows the negative effect of using excessive contact stiffness (1.4e9 lb/in). It can be seen here the increase in the force magnitude which can be contributed to the preload deformation associated with the excessive stiffness and to the complex dynamics of the machining system. This is dependent on the part geometry and on the fixture configuration in place.

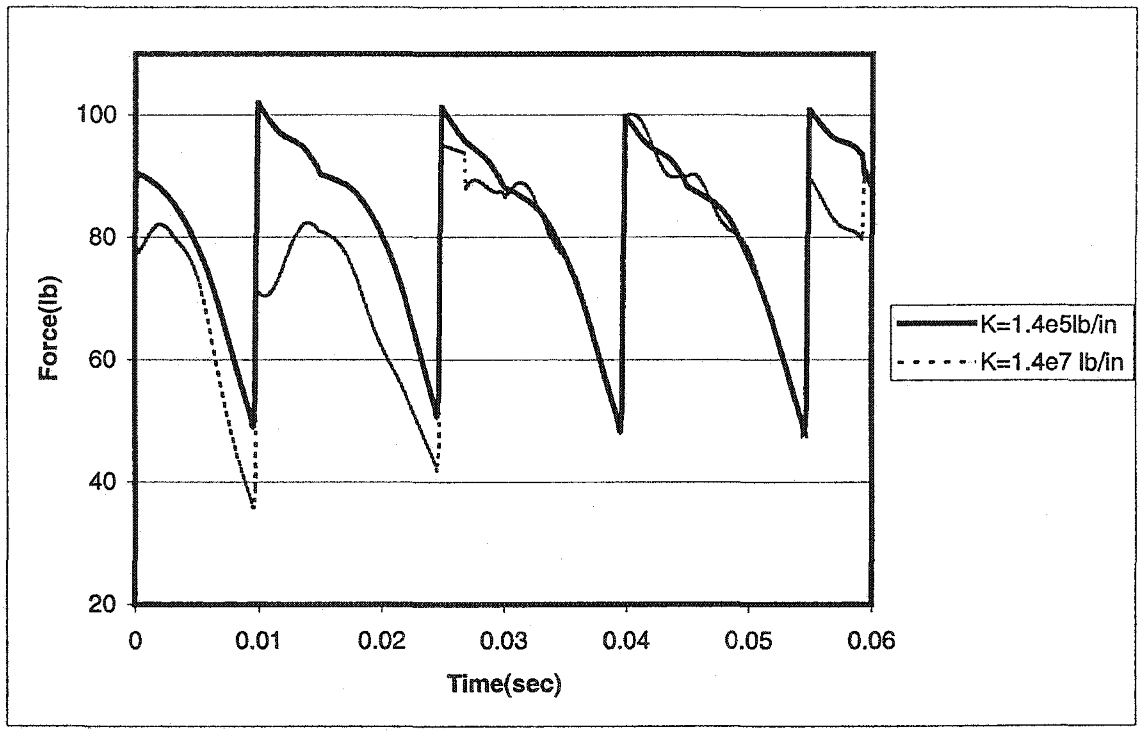

Figure 7.8 Effect of contact stiffness on the resultant cutting force for Aluminum workpiece.

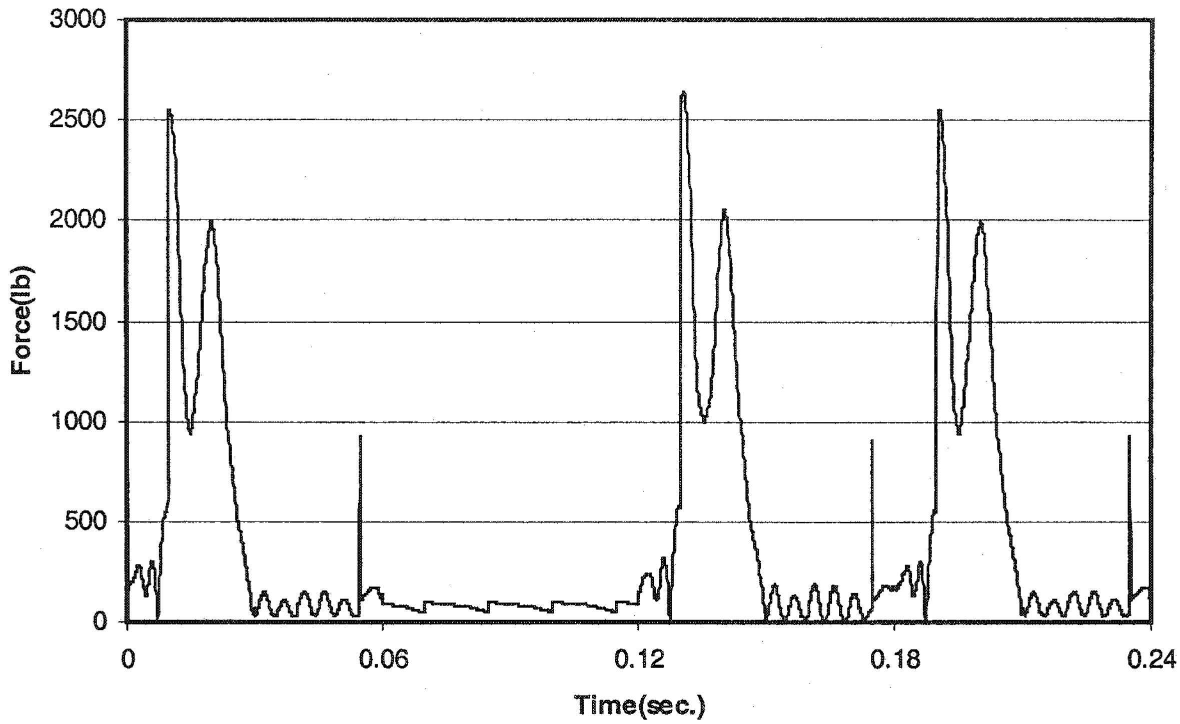

Figure 7.9 Effect of excessive contact stiffness on the resultant cutting forces.

Fixture elements location was shown to have an effect on the dynamics of the system as it can stabilize the system or otherwise. Figure 7.10 shows the effect of the fixture location on the cutting forces where the fixtures were placed symmetrically from the center of the workpiece perpendicular to the cutting direction. In series 1 the distance from center was 1.95 inch and for series 2 the distance was 2.5 inch from the center of the 8 inch workpiece. Figure 7.11 shows the effect of fixture location on the cutting forces when using a poor fixture configuration, where the fixture elements are located toward the end of the workpiece (3.8 inch from center) providing no support to the mid span. The above discussion is totally case dependent and the workpiece geometry has a major influence on the fixture configuration. Case study I presents a typical example of the importance of selecting the fixture element position.

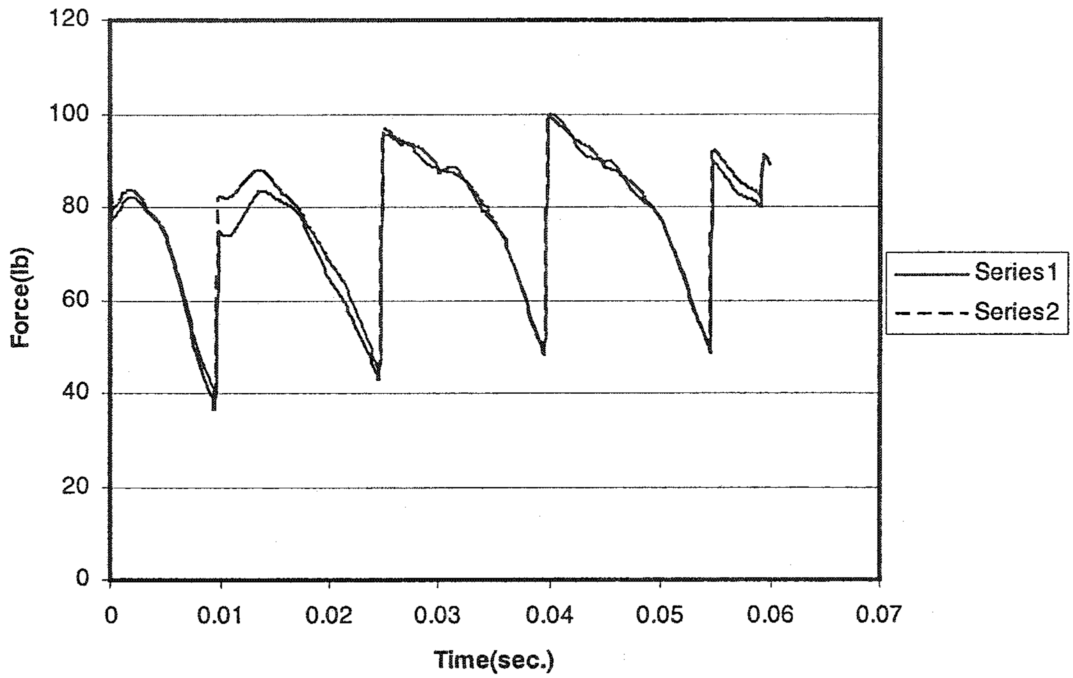

Figure 7.10 Effect of Fixture locations on the resultant cutting force.

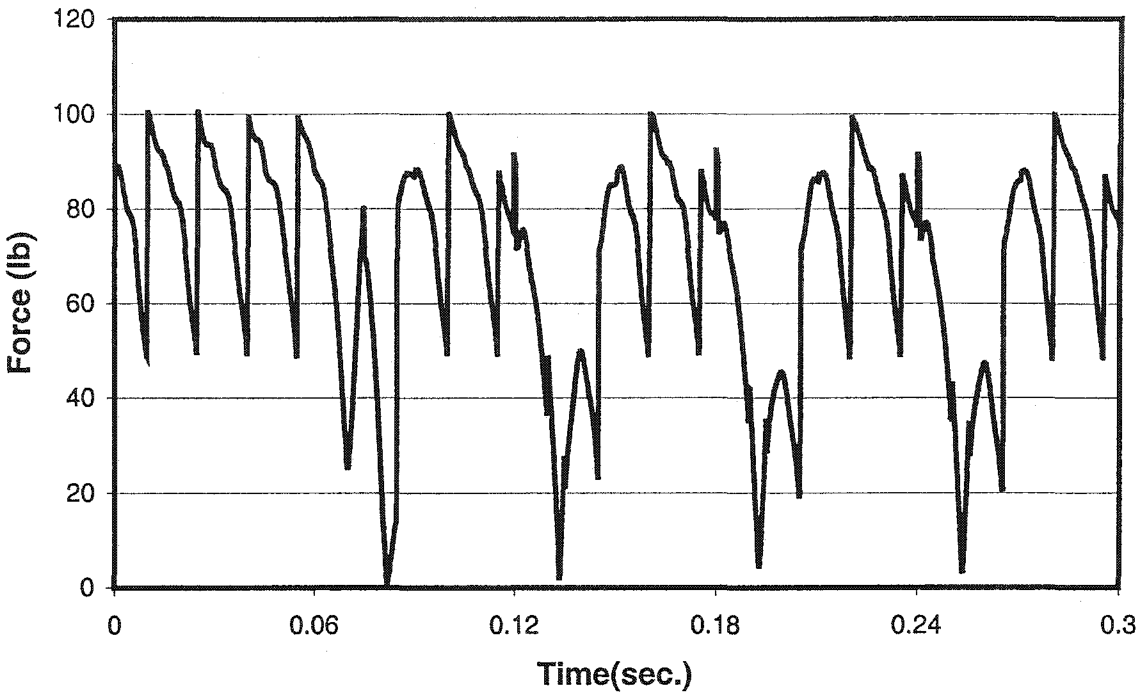

Figure 7.11 Effect of fixture location of the resultant cutting force, a poor fixture scenario, Kc= 1.4e7lb/in.

Figure 7.12 shows the effect of the coefficient of friction on the dynamic cutting force. The friction can play a significant role in reducing the process deflection and providing more restraints to the workpiece in situations where the number of clamps need to be reduced and also when the clamping force need to be kept under a certain limit. However, scenarios like the one in figure 7.13 seldom happen in practice. Where, the norms safety precautions would not allow the total dependence on friction to restrain the workpiece. The role of friction can be seen implicitly through the contact stiffness, clamping load and fixture tip roughness where is has been correlated experimentally.

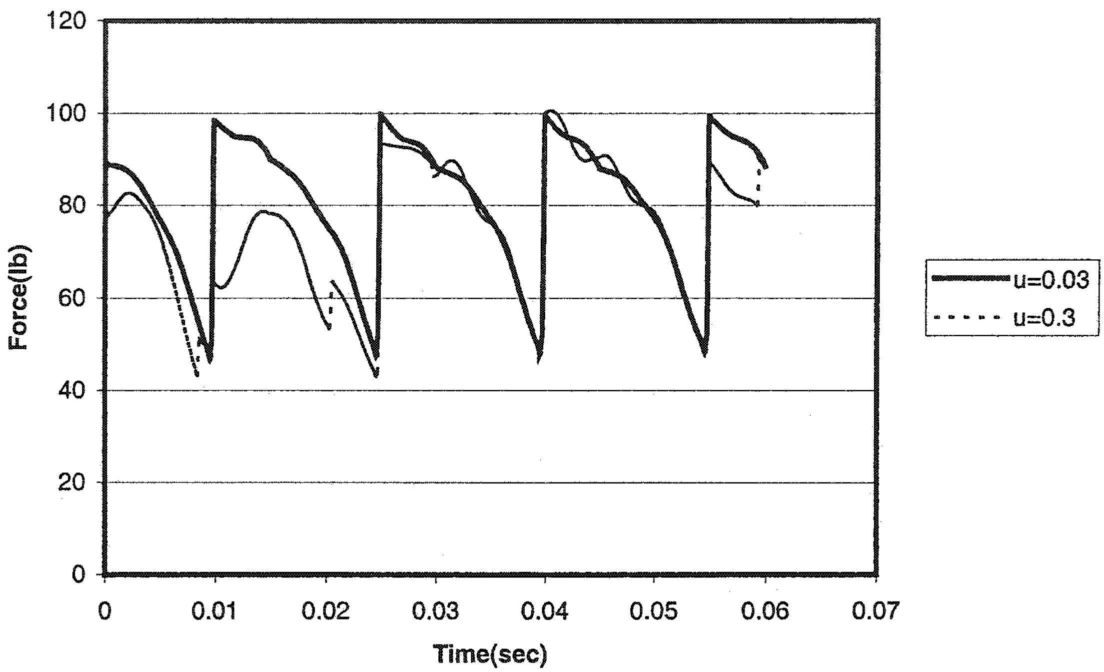

Figure 7.12 Effect of friction coefficient on the resultant cutting force.

7.6 Validation of the Simulation System

At this stage, experiments were needed to validate the simulation results and see how they compare to real cutting conditions and scenarios. Using the previously obtained calibration coefficients and friction data, simulation cases were conducted at different cutting conditions and the same cases were ran on an OKUMA machining center (figure 7.13). Cutting forces were measured using a Kistler dynamometer, and a data acquisition system. The data was collected at sampling frequency of 2000 Hz per channel. Cutting tool radial and axial run out was measured and the values are shown in table 7.1.

Insert	Axial Run out (inch)	Radial Run out (inch)
1	0.0	0.0
2	0.0075	0.002
3	0.001	0.002
4	0.001	0.0015

Table7.1. Radial and axial run out values for the 4 insert cutter.

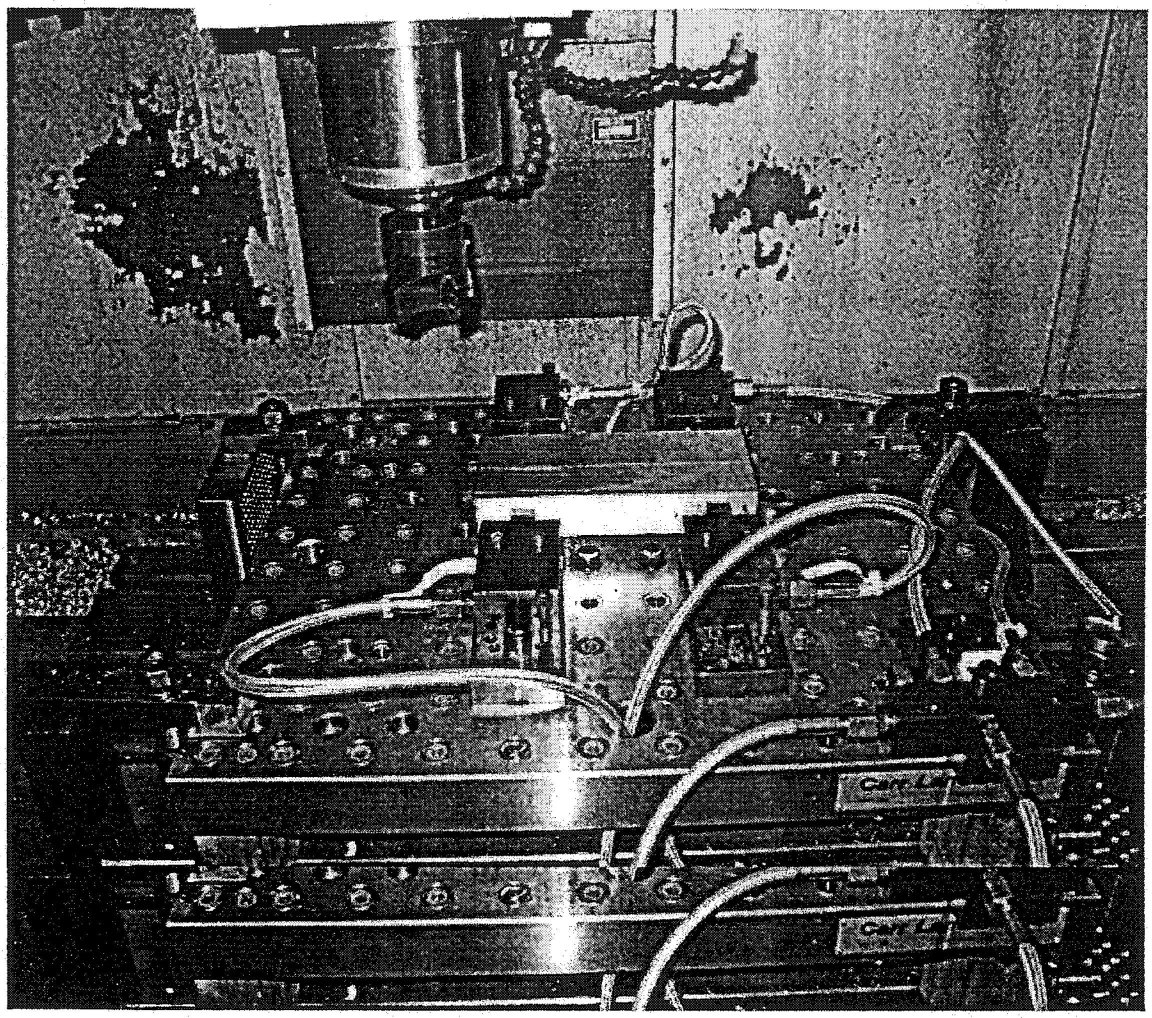

Figure 7.13 Experimental setup for simulation validation.

Figures 7.14 and 7.15 show the comparison between the measured and predicted force components and the resultant force for two different cutting parameters sets. The high frequency variation that appears can be attributed to the change in the system dynamics due to the interrupted nature of cutting in the milling process. The difference between the predicted and measured force magnitudes falls within 10% to 15%.

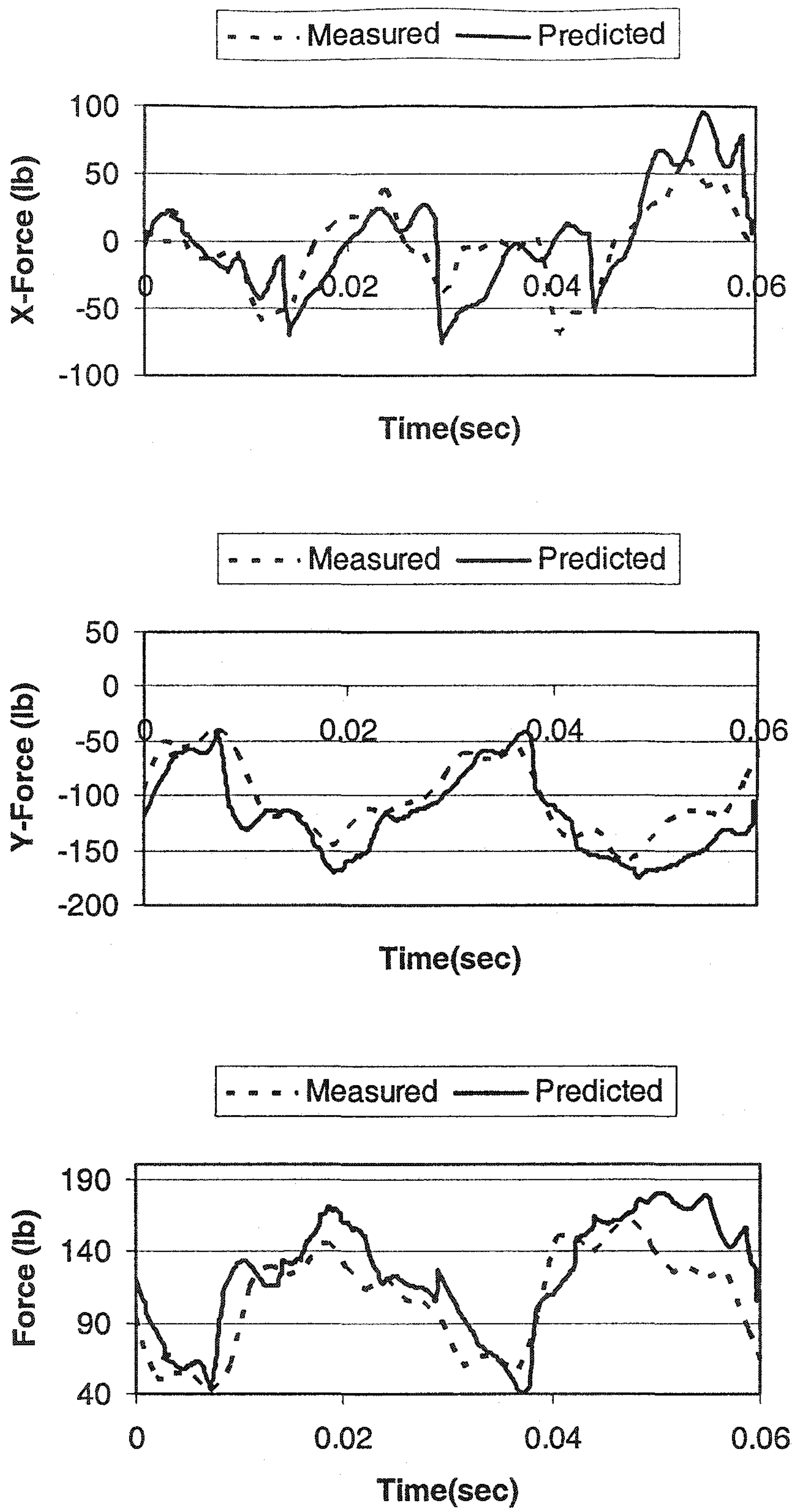

Figure 7.14 Predicted and measured cutting forces(X,Y and resultant) for (μ - =0.375, Al Workpiece, clamping force =1248 lb, 24 IPM,0.15 in DOC, 1000RPM).

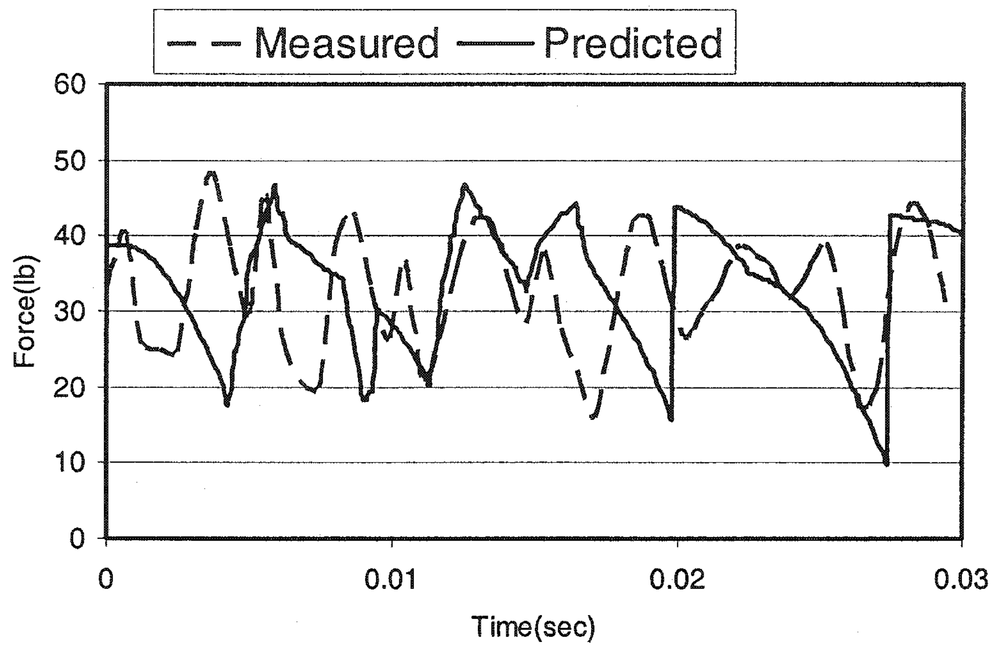

Figure 7.15 Predicted and measured resultant cutting forces for (μ =0.375, Al - Workpiece, clamping force =1248 lb, 48 IPM, 0.04 in DOC, 2000RPM).

7.7 Case study I: Evaluation and Design of Part Support Fixture Layout for Post-Cast Machining of an Automotive Engine Casing Cover

7.7.1 Introduction to case study I

This case study presents the typical practice in industry with a part that has been sent to the shop floor with a fixture configuration that has not been verified. The problem here is further complicated due to the inherent flexibility of the automotive engine casing cover component, the part is susceptible to geometric deformation during post-cast machining operations. Deflection during machining can potentially introduce inaccuracies into the part geometry ultimately reducing part functionality during application. This component provides mounting/support facilities for a series of engine accessories, as well as forms a partial reservoir for the containment of pressurized lubricant. Manufactured parts have demonstrated geometric inaccuracies, which have resulted in a loss of seal integrity, as well as misalignment of locating and supporting features. The part is scheduled for manufacturing using an 8-station indexing machine designed and constructed by Manufacturer. Figure 7.16 illustrates the proposed part fixture arrangement and it's orientation as originally suggested.

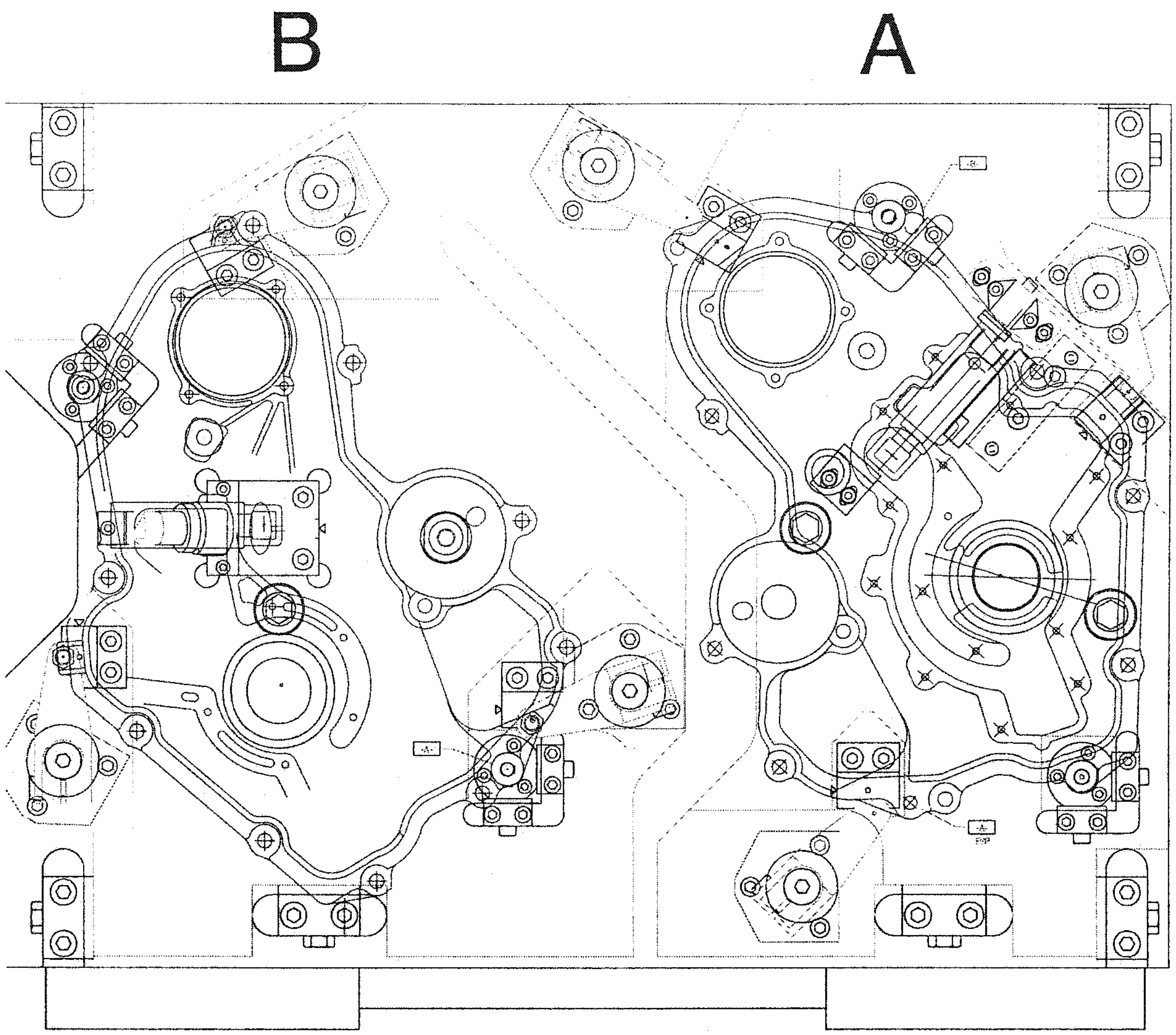

Figure 7.16 Configurations A & B fixture set-up (original configuration).

7.7.2 Modeling and Analysis

7.7.2.1 Approach

In order to minimize part deflection in the vicinity of the component's critical features, the original fixture configuration was evaluated using the previously developed methodology to identify potential improvements with respect to individual part supporting element layout.

The critical features for analysis of set-up configuration A were identified as; (1) the internal pump chamber, (2) outer peripheral seal land and (3) assembly datum stations (A) and (B), (4) relief hole on the underside of the valve body housing. These features are clearly indicated in Figure 7.17. Set-up configuration B supports machining operations for the following features; the tensioner mounting surface, the access cover mounting surface, the valve body housing and the crank bore seal housing. These features are depicted in Figure 7.18.

To better understand the part response, modal analysis was performed on the part under the influence of the proposed clamping configuration. The first three mode shapes revealed expected bending patterns describing areas of significant deflection, and thus identifying locations for placement of part support elements. Alternate fixture configurations were designed and investigated for set-up configurations A and B, and are described in the following sections.

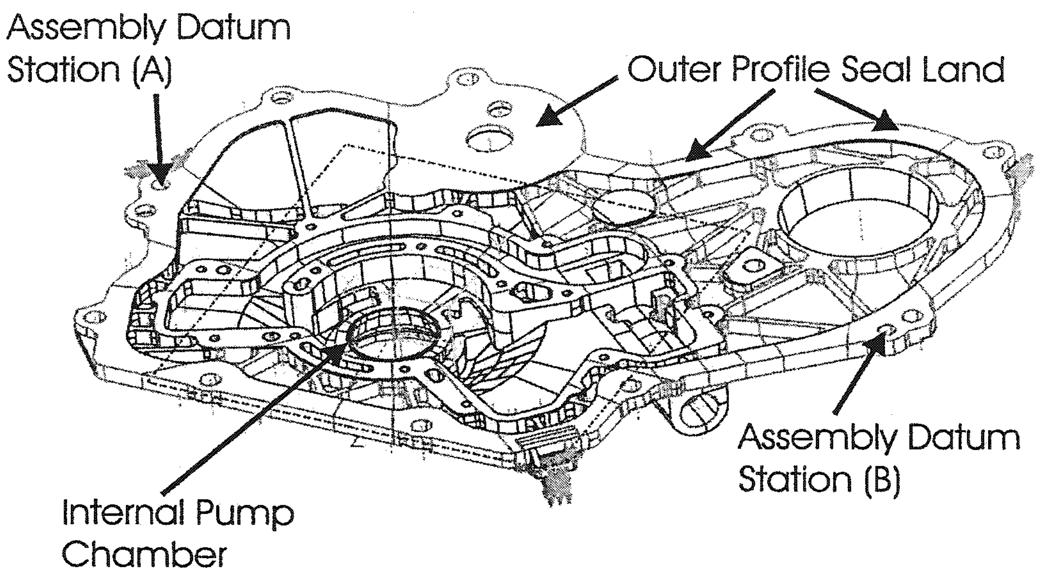

Figure 7.17 Configuration A critical features.

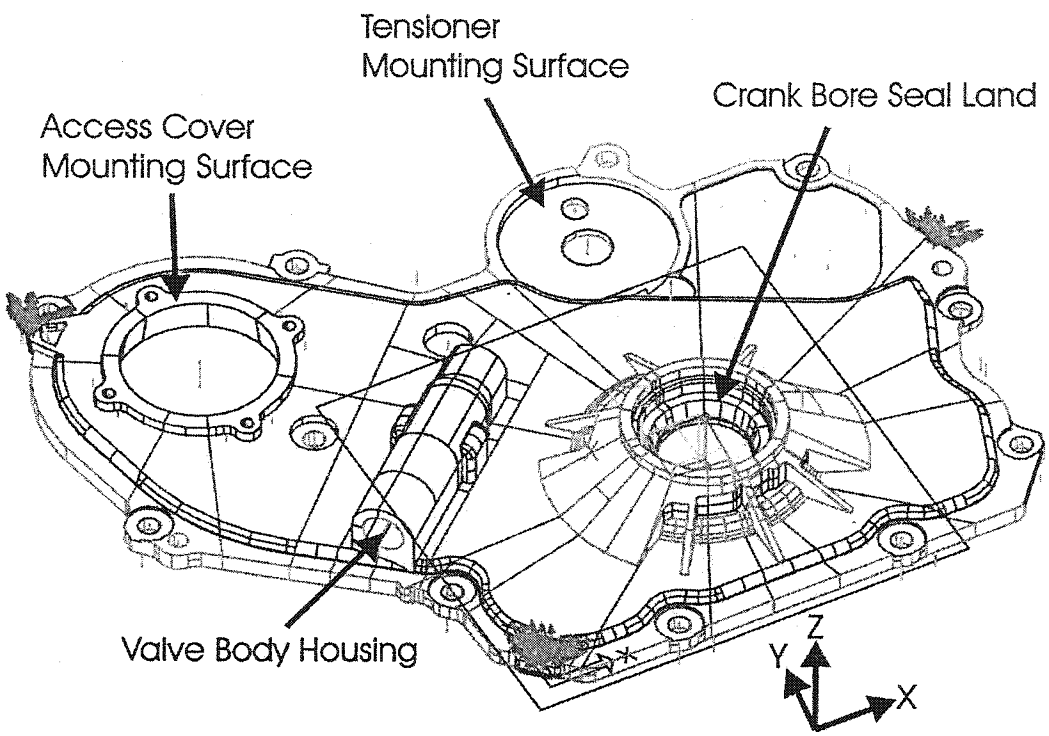

Figure 7.18 Configuration B critical features

The main machining process was face milling in addition to grinding, boring, chamfering and drilling. Face milling forces were calculated based on the mechanistic force model provided earlier in chapter 4.

7.7.2.2 Geometric modeling

Due to the geometric complexity of the part the simulation system was interfaced with SDRC Ideas software package to utilize the CAD model provided. A finite element mesh was generated using the detailed solid model of the part. The finite element mesh consisted of 134328 nodes and 77161 tetrahedral elements. After optimization, solutions could be generated in approximately 30 minutes on a 350 MHz Pentium computer. Material properties for cast aluminum were incorporated into the finite element model. The material (mechanical) properties are shown in table 7.2:

PROPERTY	***VALUE***
Density	2710 kg/m^3
Modulus of Elasticity	69 Gpa
Tensile Strength	250 Mpa
Yield Strength (shear)	165 Mpa

Table 7.2. Material properties used for finite element analysis.

7.7.2.3 Modeling of Fixture Elements

Hydraulic clamps were used on the 8-Station dial machine to secure the part. These clamps are hydraulic and pinch the part between the surface of the actuated clamp and a rigid back support. The surface area of contact is approximately 125 mm^2 (0.2 in^2), developing a clamping pressure of 100 bar (1500 psi). This corresponds to an approximate clamping force of 1300 N (300lb$_f$). The clamping force behaves similar to a pre-load, i.e. the clamp points are essentially rigid until the reaction force at the clamp exceeds the pre-load developed by the clamping pressure. When the reaction force at the clamp exceeds the pre-load, the clamp deflects. Over the course of this investigation, reaction forces were verified to be less than the prescribed 300lb_f, and therefore the clamps were modeled as rigid restraints in which all translation and rotation at each contact points is zero.

For both the original A and B set-up configurations, it was proposed to provide additional support primarily in the direction normal to the plane of the part. The B configuration also includes a work support at the base of the valve body inclined at 45° to the plane of the part. The support is advanced to the part and locked in place, restricting translation in the direction of the support. The contact surface is provided by a button type support. Fixture elements have been modeled at their point of contact by restraining the part at a single node in the direction of the support pin motion. The stiffness of the collar locking mechanism was deemed to be sufficiently larger than that of the part, thus permitting the support to be modeled as a rigid fixture. Work supports should not induce significant force on the part at the point of contact. For the purpose of this analysis, contact forces were assumed to be negligible. However, due to the flexibility of this part, relatively small contact forces will cause the part to deflect, irrespective of cutting load at the tool/workpiece interface. Figure 7.19 illustrates the sensitivity (stiffness) of the part for the original work support configuration, A.

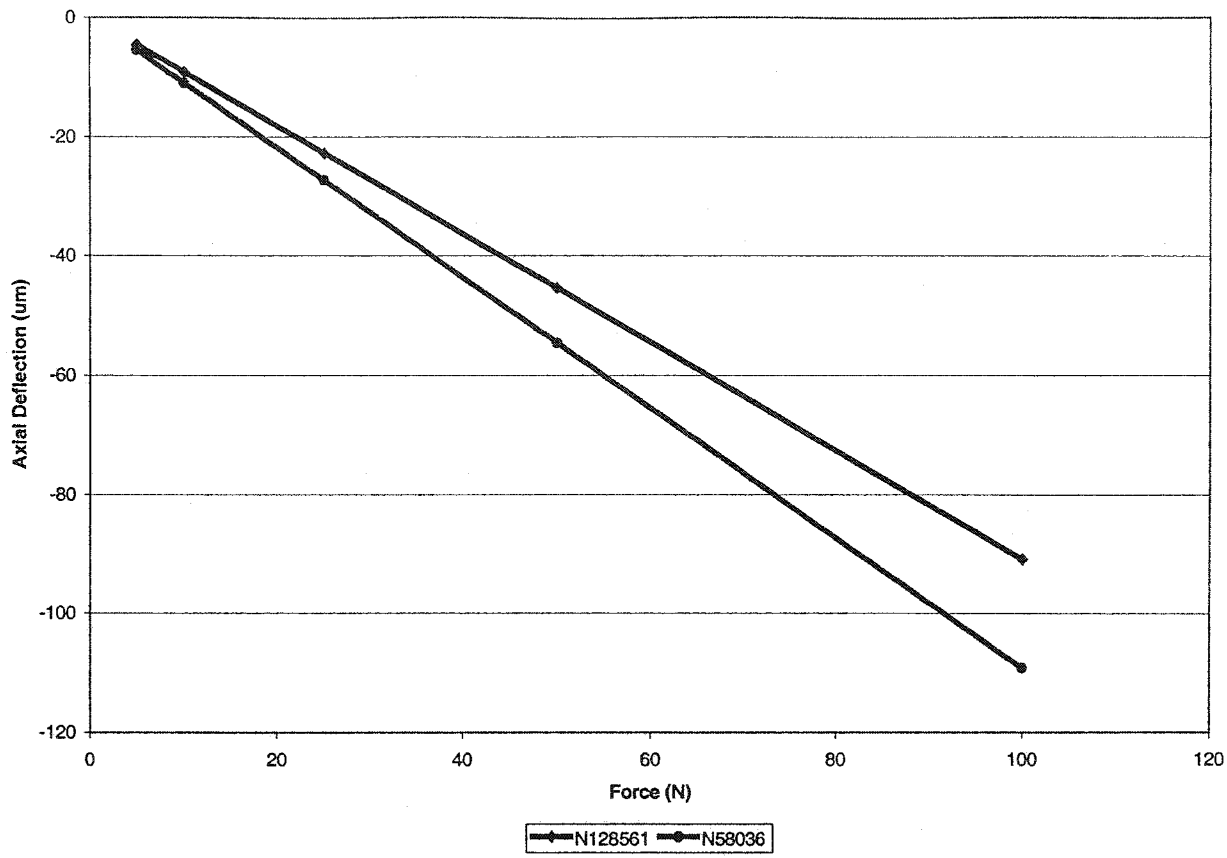

Figure 7.19 Deflection caused by work support pre-load.

These results indicate that relatively small pre-loads may potentially cause the part to deflect.

7.7.3 Finite Element Analysis

Finite element analysis was carries out to identify potential part deformation as a function of cutting forces developed at the tool/workpiece interface, and use this information to optimize placement of individual fixture elements. Due to the qualitative nature of finite element analysis, results obtained for the original set-up configuration were utilized as a baseline for performance evaluation of each alternate set-up, which was developed over the course of this investigation.

7.7.3.1 Modal Analysis

The first three mode shapes and natural frequencies estimated using finite element analysis are demonstrated in Figures 7.20 to 7.22. The first mode shape corresponds with a natural frequency of 247 Hz, and demonstrates significant bending in the immediate vicinity of the tensioner-mounting surface (Figure 7.20). The second mode shape corresponds with a natural frequency of 302 Hz, and demonstrates deformation (bending), at the part extremities. (Figure 7.21). The third mode shape corresponds with a natural frequency of 445 Hz and demonstrates significant deformation (bending), over the entire part profile (Figure 7.22). The demonstrated modes of vibration provide insight into how the component will deform structurally if vibration is introduced during machining. Vibration can be initiated by an instantaneous displacement of the component at the tool/workpiece interface.

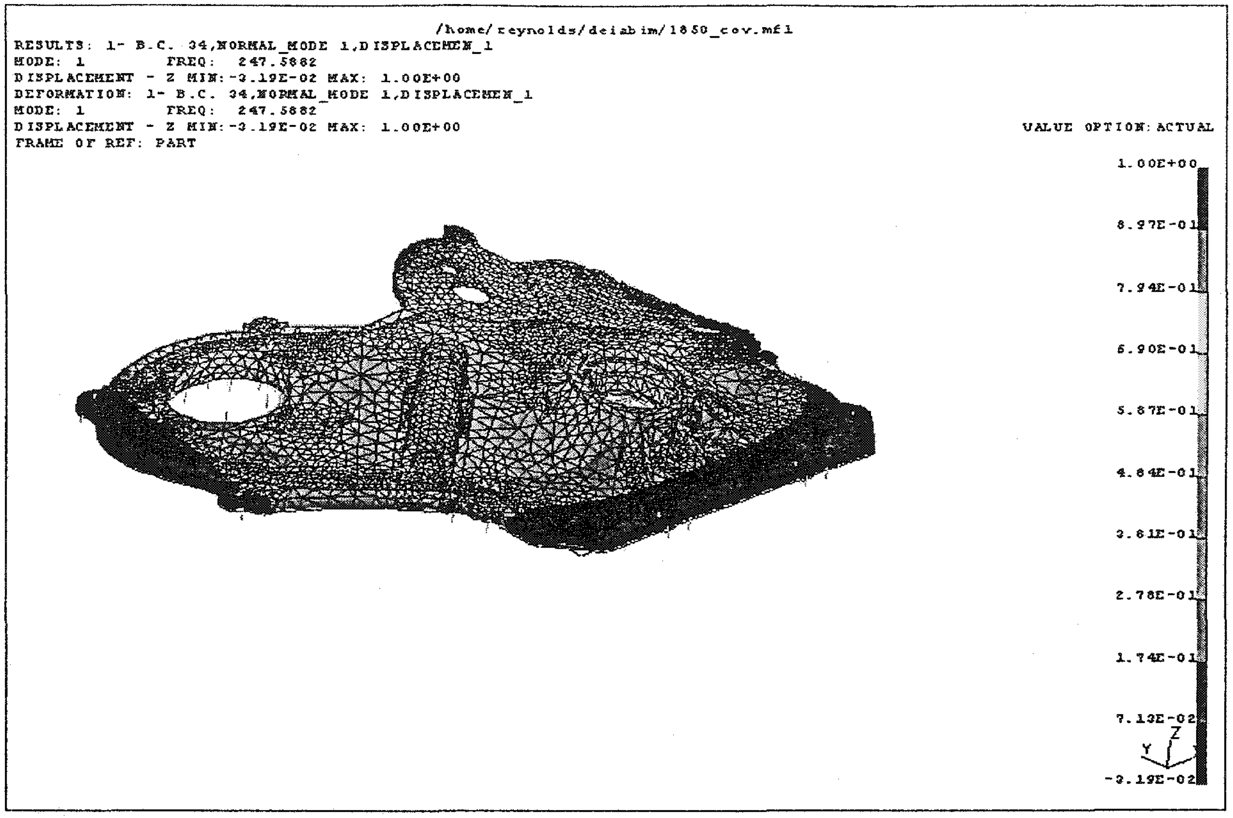

Figure 7.20 Fundamental mode shape: original clamping arrangement.

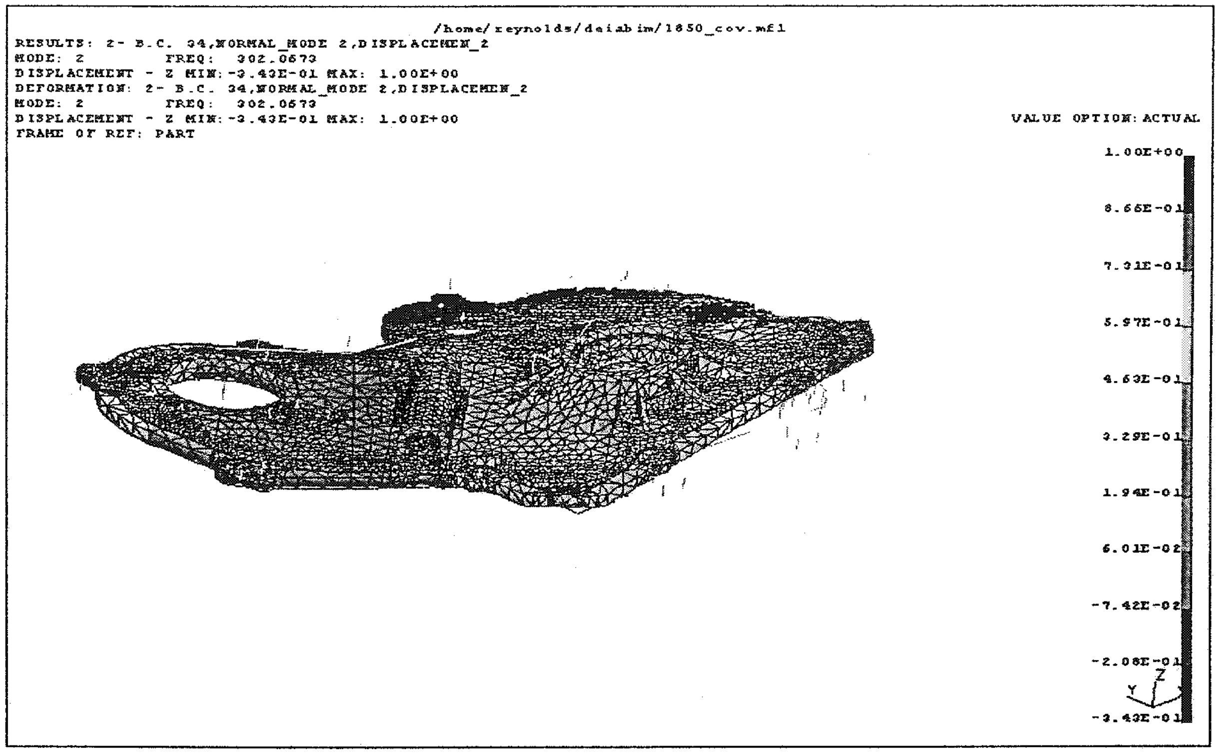

Figure 7.21 Second mode shape: original clamp arrangement.

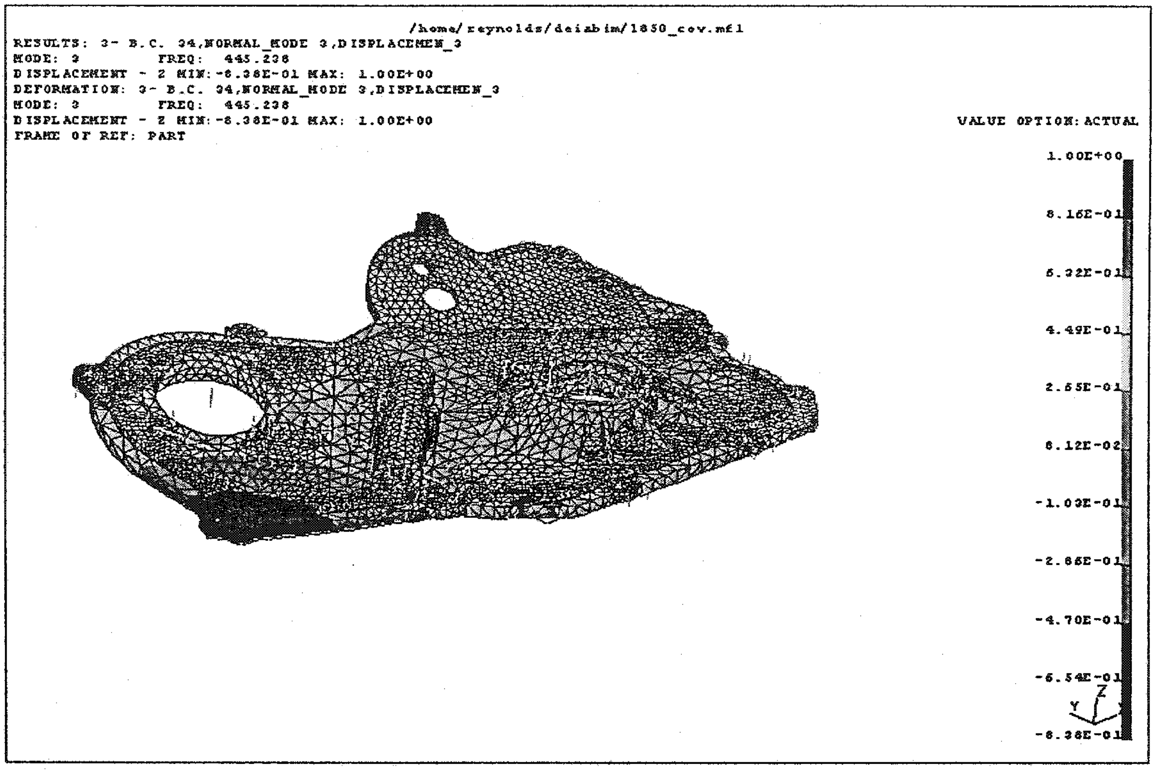

Figure 7.22. Third mode shape: original clamping configuration, no work supports.

If the part is not adequately supported, the localized displacement may be propagated throughout the part compromising the geometry of the profile created by the metal removal process. The amplitude and frequency of the induced vibration is dependant on; cutting frequency, structural rigidity of the part, as well as the part's material characteristics.

To verify the dynamic results reported by finite element analysis, experimental modal tests were performed to obtain natural frequencies from the actual part. Part response was measured at different locations along the peripheral seal land. The measured results indicated part natural frequency values of 246 Hz, 283 Hz and 462Hz, respectively. Frequency values reported by finite element analysis were consistently within 15% of the corresponding experimentally determined natural frequency values.

7.7.3.2 Analysis of Fixture Configuration A

The original set-up of configuration A, proposed by Manufacturer, consists of 3 clamps located around the periphery of the part supplemented by 2 work supports. Figure 7.23 depicts work support locations, relative to the part geometry, for configuration A. Individual work support addition/relocation was based on the deformation demonstrated by the part when subjected to simulated machining forces. The designed alternative set-up configurations have been denoted A-1 and A-2, and are demonstrated in Figures 7.24 and 7.25.

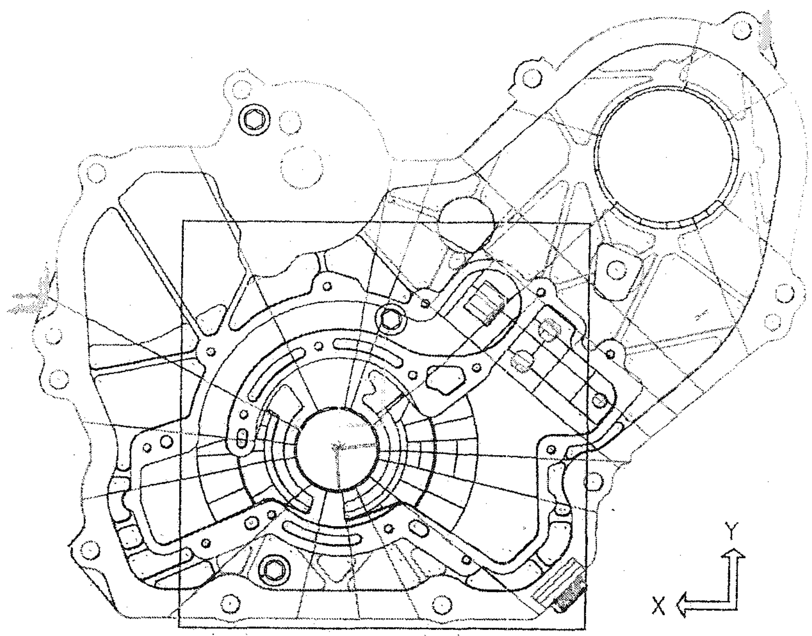

Figure 7.23 Original support layout set-up configuration A.

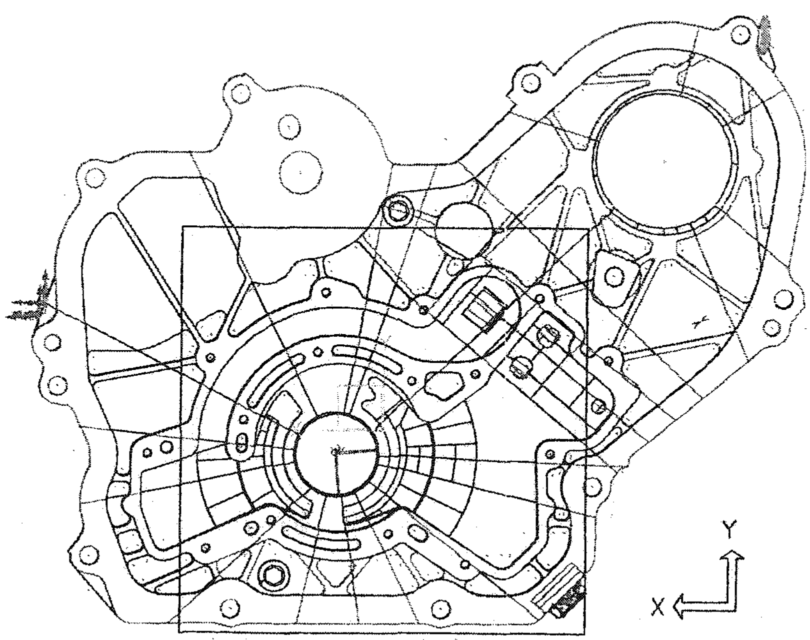

Figure 7.24 Alternate support layout set-up configuration A-1.

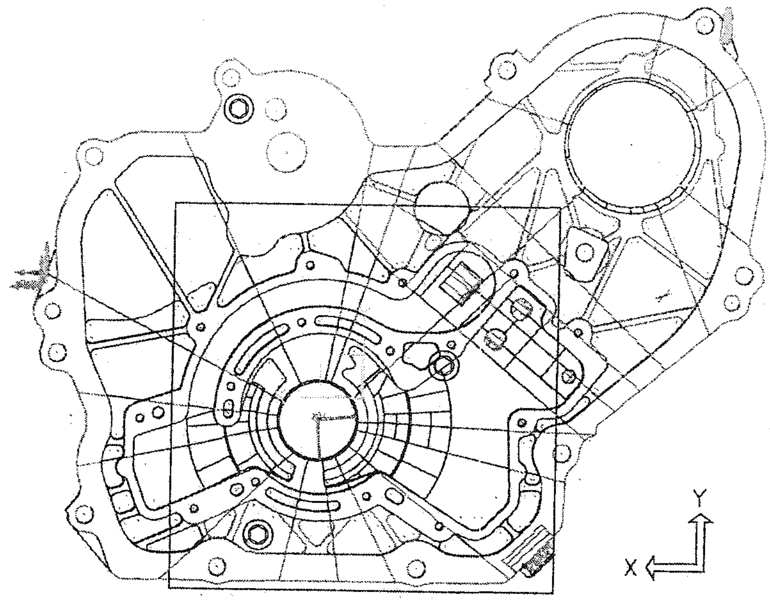

Figure 7.25 Alternate support layout set-up configuration A-2.

The alternate set-up configurations demonstrated in Figures 7.24 and 7.25, differ only in the location of the work support near the valve body. The mode shapes reported by finite element analysis indicate a tendency of the part to bend in this central area.

All cutting forces were modeled as three-dimensional point loads applied at each tool/workpiece intersection. Six milling scenarios (mill_1 – mill_6) were selected for analysis and comparison of configurations A, and the two proposed modifications A-1, and A-2. Each load set designator (mill_x) denotes the instantaneous tool-workpiece intersection at a given tool position (feed increment). The six milling scenarios investigated are depicted in Figure 7.26.

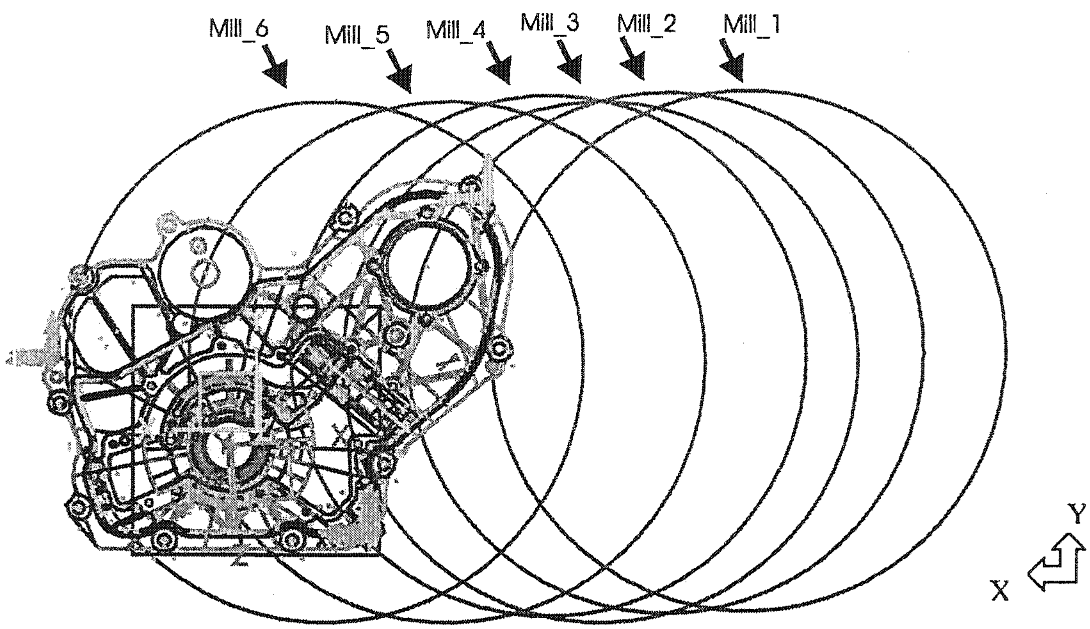

Figure 7.26 Progressive cutter locations on outer peripheral seal land.

For each milling scenario, instantaneous deflection induced at the tool/workpiece interface introduced inconsistencies into the machined surface profile. Figures 7.27-7.31 demonstrate the spatial response of the part as a function of the simulated cutting forces applied at each identified tool/workpiece intersection. The profile generated under the translating cutting edge will be a function of the differential in deflection over the entire machined surface of the part. For instance, in the case of mill_1, the part appears to bow in the middle under the cutter. For this particular case, depicted in Figure 7.27, tool engagement with the part only occurs at a single central location relative to the workpiece, therefore part deflection is most likely to be developed at this interface.

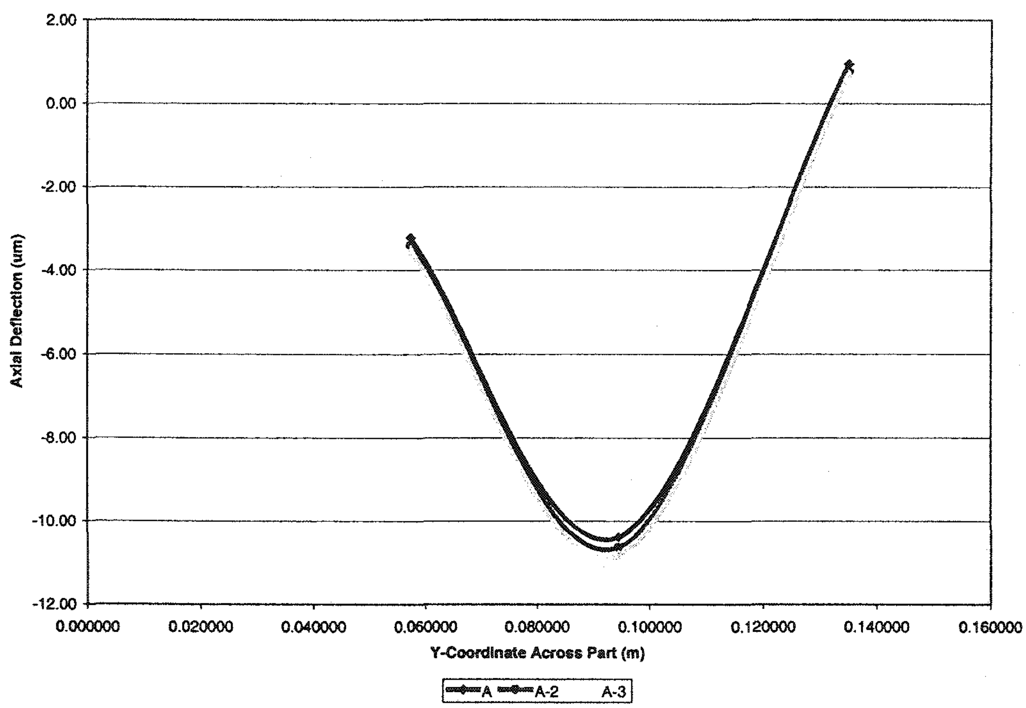

Figure 7.27 Deflection across the part under the cutter for load set 'mill_1.'

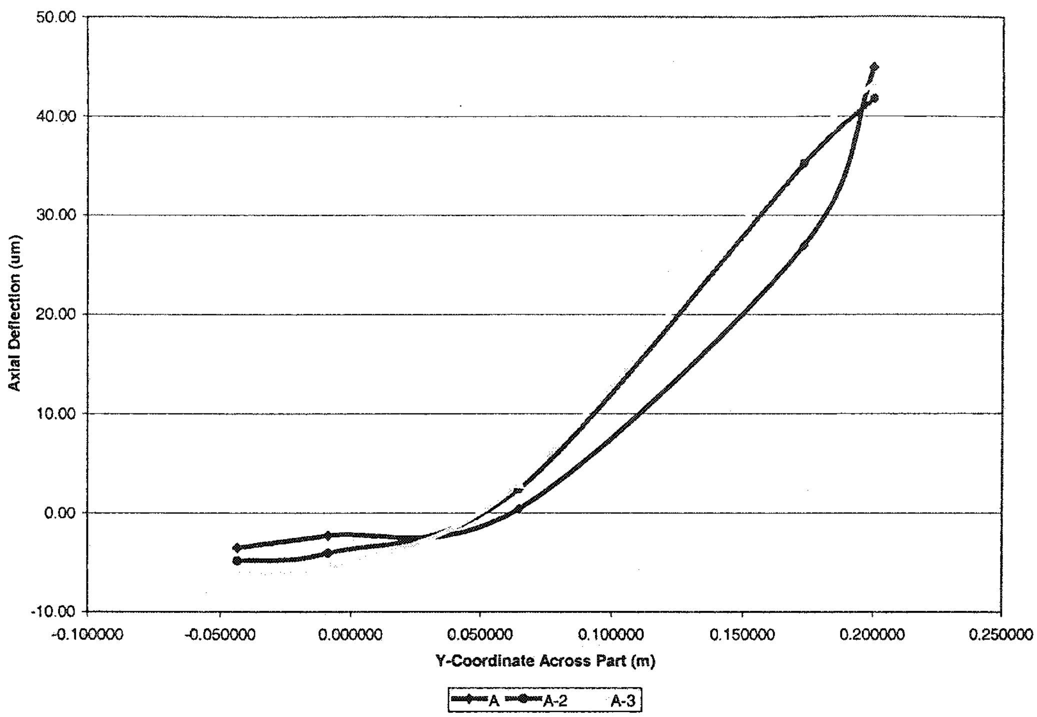

Figure 7.28 Deflection at tool/workpiece interface, load set 'mill_3.'

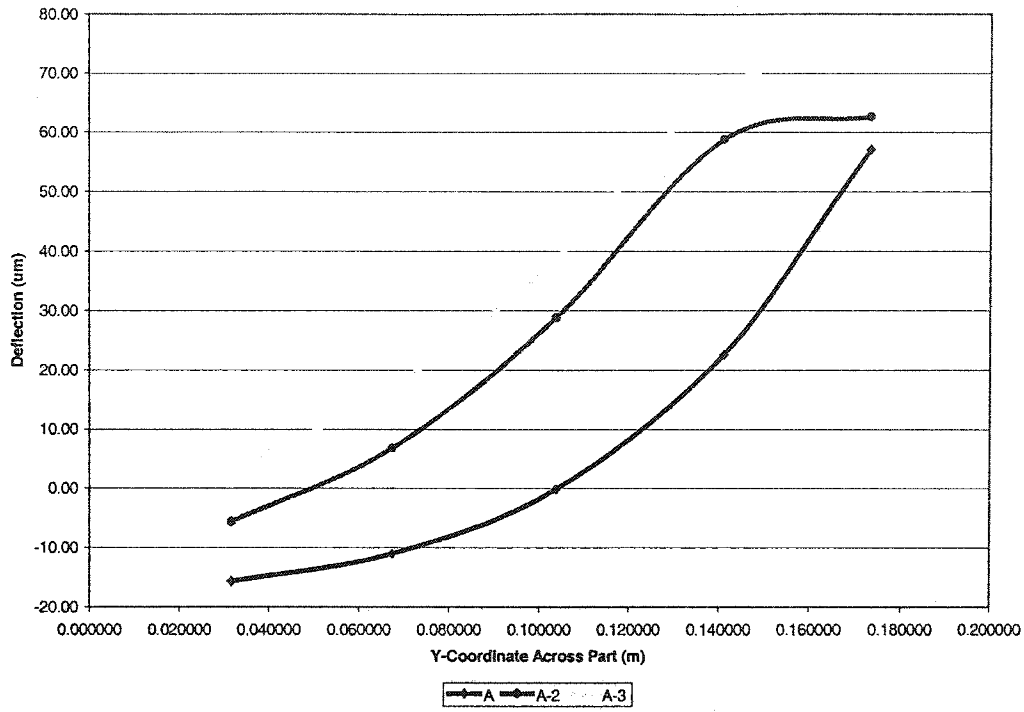

Figure 7.29 Deflection at tool/workpiece interface, load set 'mill_4.'

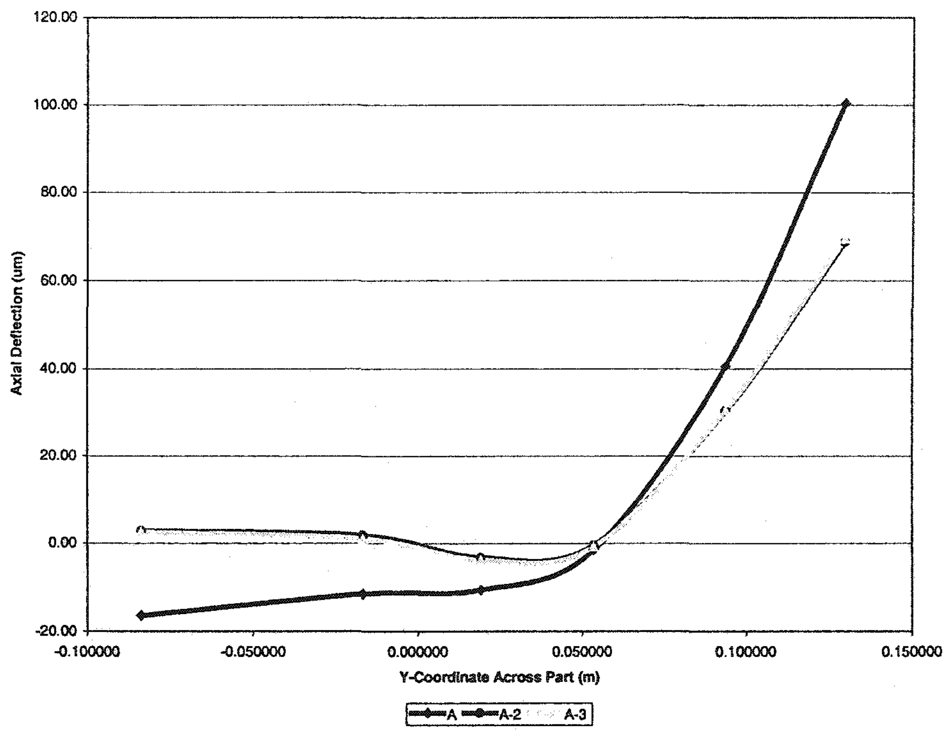

Figure 7.30 Deflection at tool/workpiece interface, load set 'mill_5.'

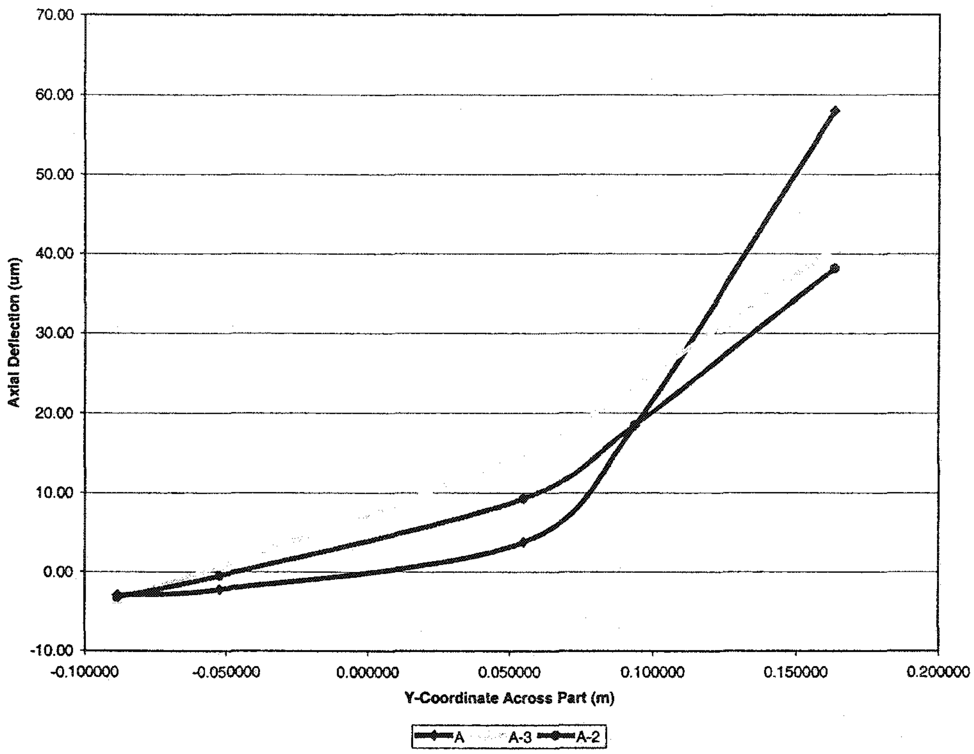

Figure 7.31 Deflection at tool/workpiece interface, load set 'mill_6.'

Load Set	mill_1	mill_2	mill_3	mill_4	mill_5	mill_6
A	4.16	-16.68	48.412	72.73	116.8	60.92
A-1	4.1675	-16.079	46.6	68.254	65.99	41.37
A-2	4.2014	-15.79	49.43	67.936	67.01	44.15

Table 7.3 Summary of differential deflection (μm) across part at tool/workpiece interface.

Table 7.3 summarizes the differential deflection across the part transverse to the direction of feed, for tool position denoted in Figure 7.26. Since the absolute value of deflection at various locations is not indicative of surface profile variation spatially across, or along the part, differential values have been reported to describe the magnitude of potential profile inaccuracies. The greatest deviation of surface profile is observed for the deflection results of 'mill_5' (Figure 7.30). Both alternate arrangements, A-1 and A-2 show significant improvement over the original set-up configuration A. A similar trend is observed for the less critical load case 'mill_6' (Figure 7.31). Load case 'mill_3' (Figure 7.28) shows a very slight advantage of A-1 over either A-2 or A, although it is most significant in comparison with A. Load case 'mill_4' shows a slight benefit of A-1 and A-2 over A.

7.7.3.3 Analysis of Fixture Configuration B

The Manufacturer designed the original set-up configuration B to support machining operations for each of the aforementioned features. The original set-up was analyzed initially using finite element analysis to establish a baseline for performance evaluation. The original set-up of configuration B, proposed by the manufacturer is depicted in Figure 7.32. This set-up is comprised of three clamps located around the periphery of the part, and includes two individual work supports. Initial finite element analysis results for the original configuration B demonstrated significant deformation of the tensioner face geometry. These results were utilized as design criteria for the development of alternative work support configurations B-1, and B-2. Configurations B-1, and B-2 are depicted in Figures 7.33 and 7.34 respectively.

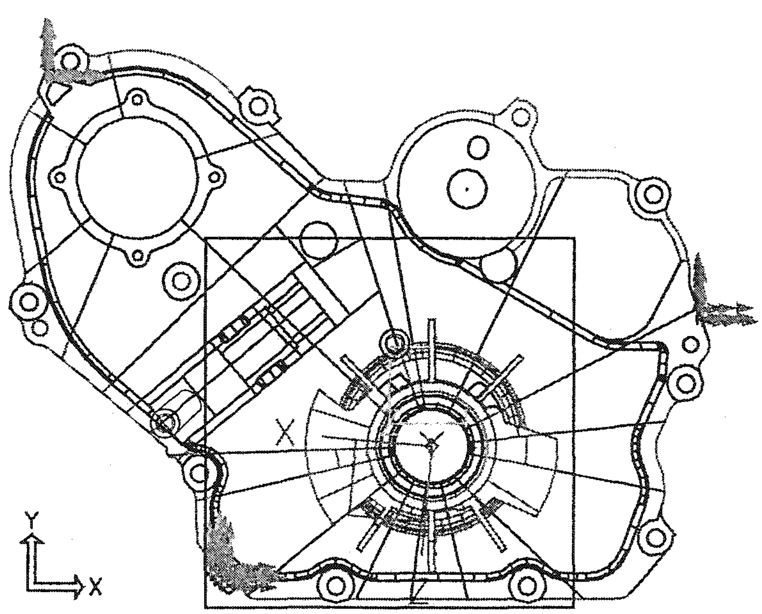

Figure 7.32 Original work support configuration B.

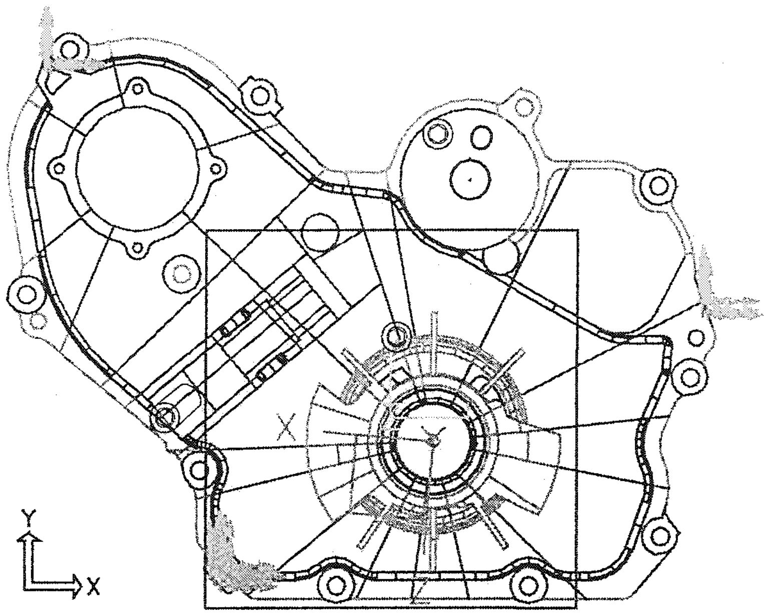

Figure 7.33 Developed work support configuration B-1.

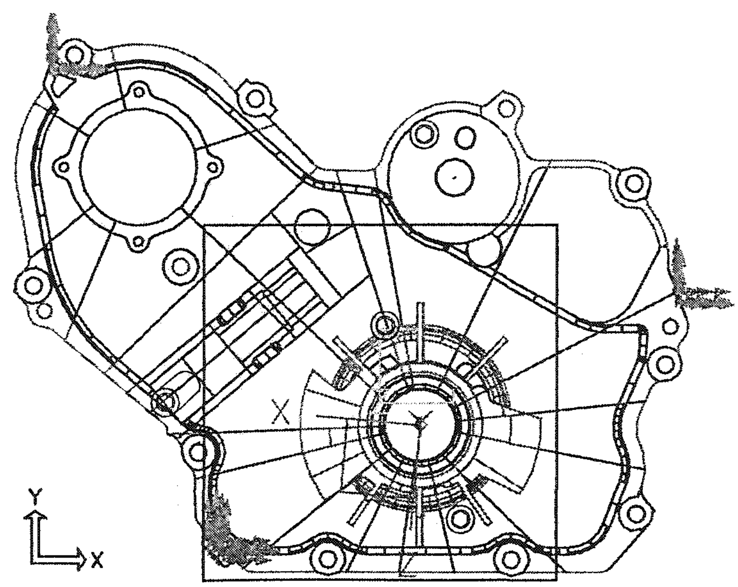

Figure 7.34 Developed work support configuration B-2.

Production of the valve body housing demonstrates two different machining operations. The first operation is a drilling process, while the second operation combines boring, chamfering and surface machining processes.

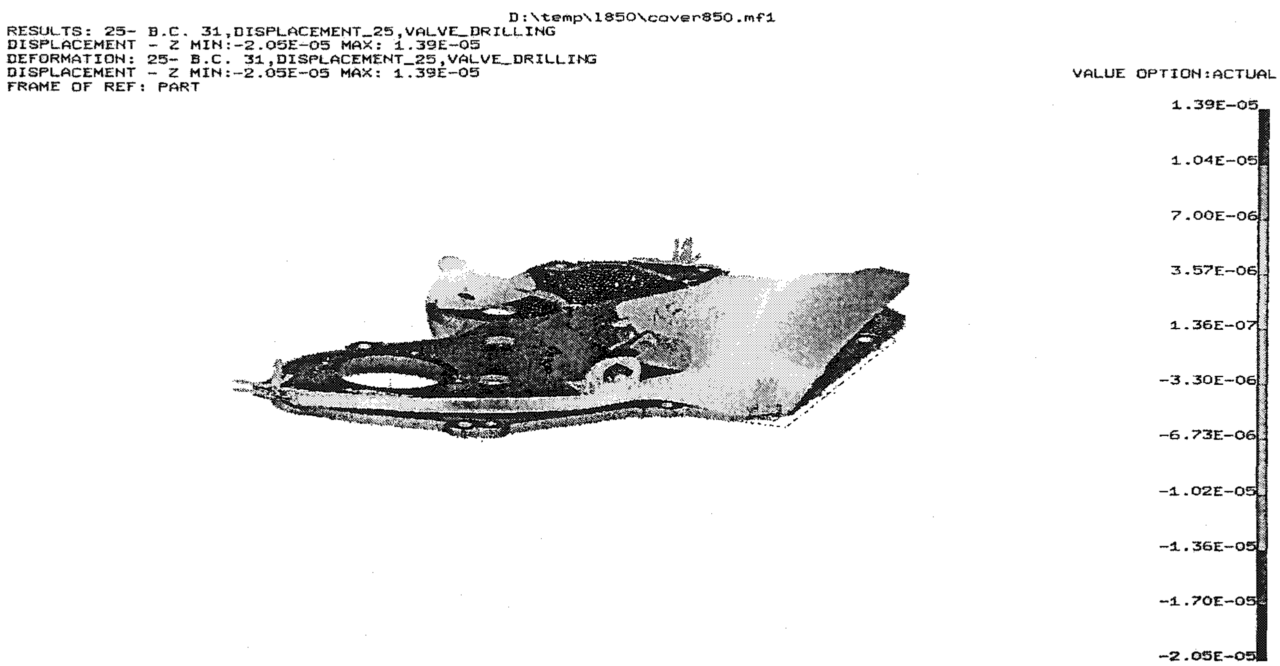

Figure 7.35 Part response: drilling, configuration B.

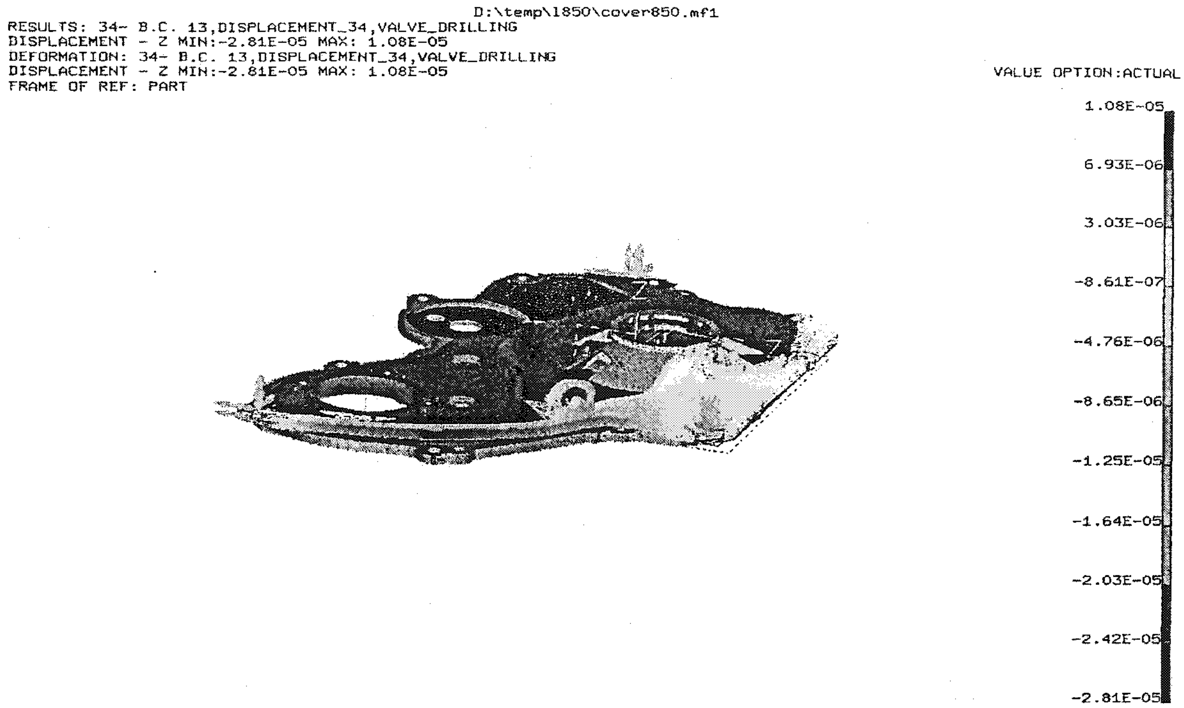

Figure 7.36 Part response: drilling, configuration B-1.

The part response to applied drilling forces for configuration B, and B-1, is depicted in Figures 7.35 and 7.36 respectively. Part deflection values reported at the tool/workpiece interface for configuration B-1 were reduced by 40% relative to the reported values for configuration B. Maximum deflection values for configuration B-1 were reduced by 30% relative to configuration B.

In machining the Crank Bore Seal housing facing, chamfering and boring machining operations are performed simultaneously using a single tool.

Configuration B-2 demonstrated the most favorable performance in terms of minimizing workpiece deformation under load application for this particular machining operation. Deflection values in the Z-direction - (normal to the plane of the part) - relative to those reported for configuration B, were reduced up to 30% at points of load application,(tool/workpiece intersection points). A 30% relative reduction in maximum part deflection was also reported. Deflection values reported in the X and Y directions were negligible for all cases considered. The physical response of the model under load, as determined through finite element analysis, is demonstrated in Figures 7.37-7.39 for set-up configurations B, B-1, and B-2 respectively.

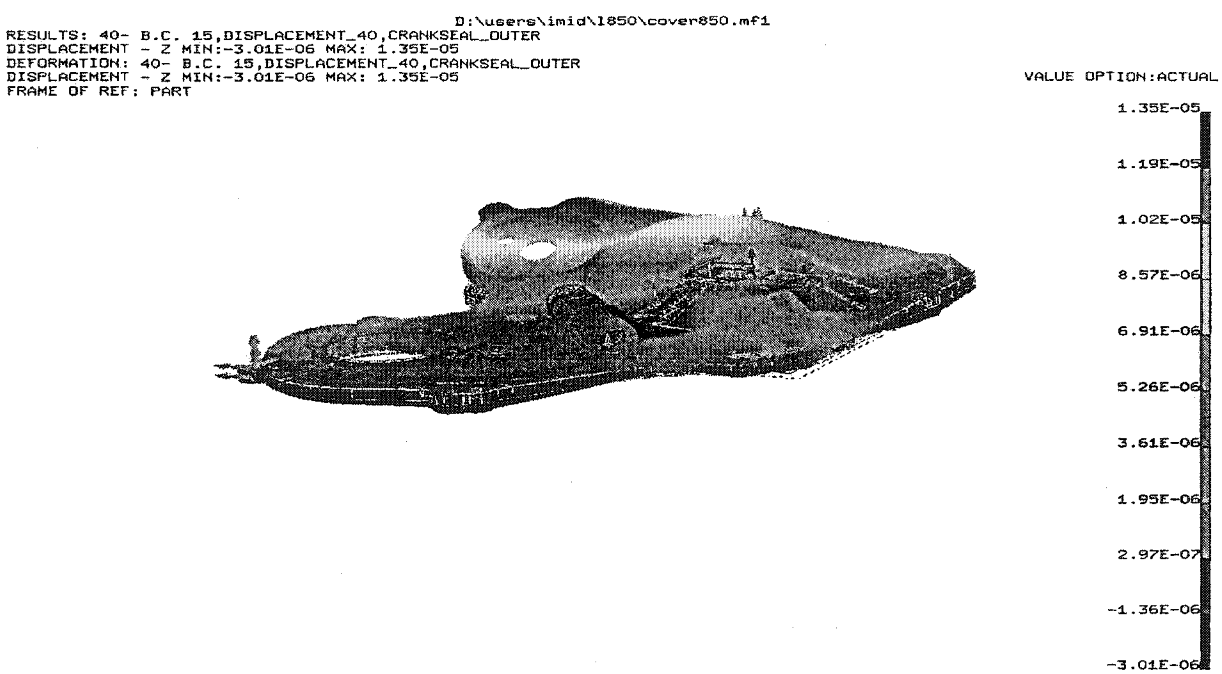

Figure 7.37 Part response: facing/chamfering/boring/, configuration B

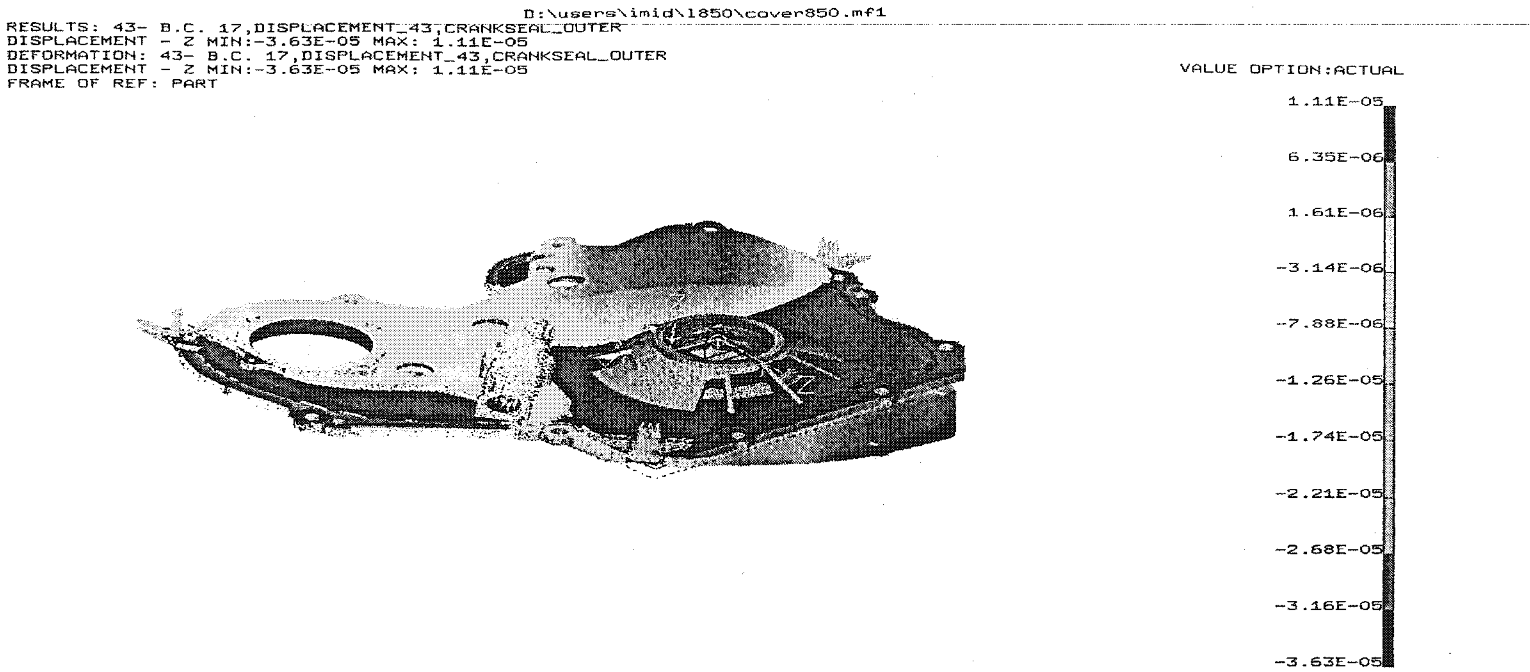

Figure 7.38 Part response: facing/chamfering/boring, configuration B-1.

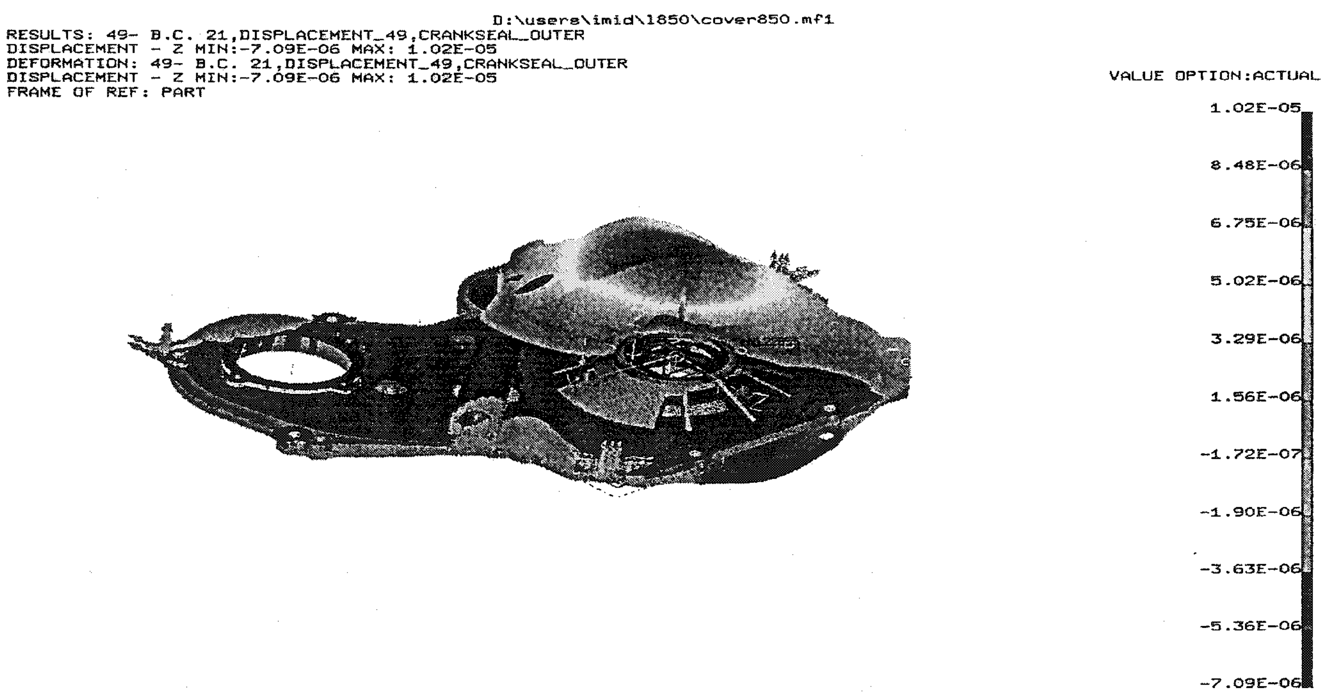

Figure 7.39 Part response: facing/chamfering/boring, configuration B-2.

In machining the tensioner mounting surface and the access cover-mounting surface face milling and boring operations are required. Configuration B-1 demonstrated the most favorable performance in terms of minimum workpiece deformation. Figures 7.40 and 7.41 demonstrate part response to the applied machining forces for configurations B, and B-1 respectively.

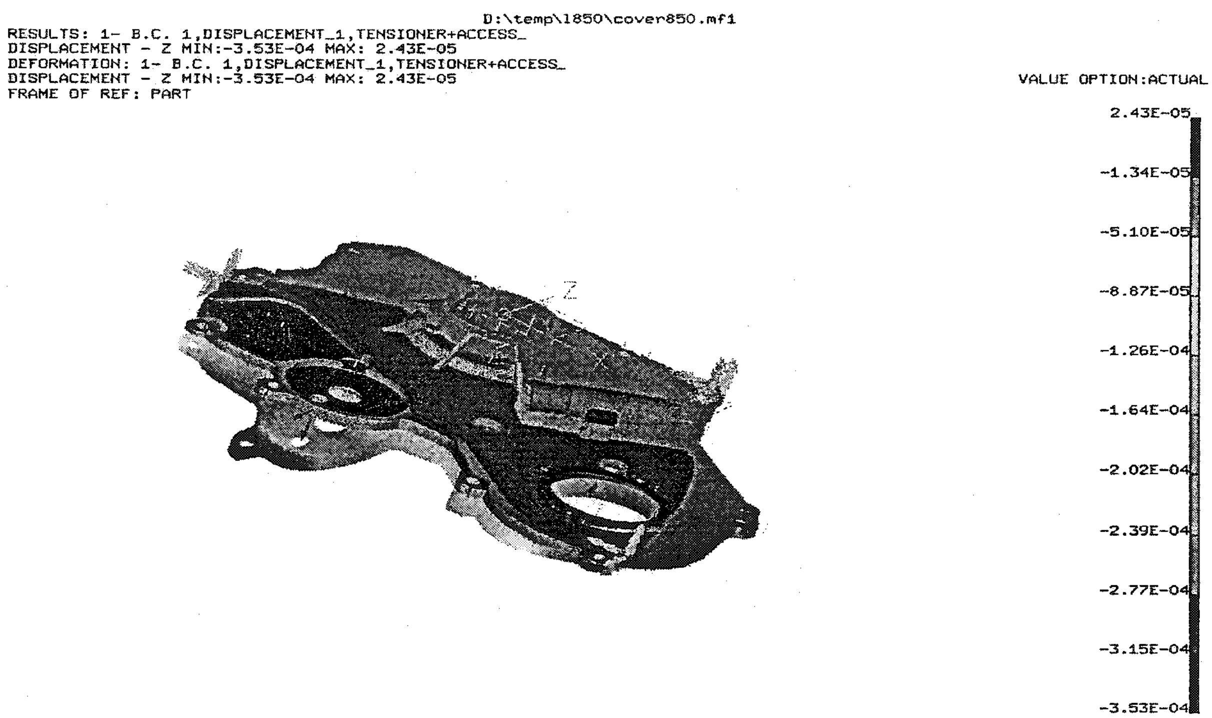

Figure 7.40 Part response: face milling/boring, configuration B

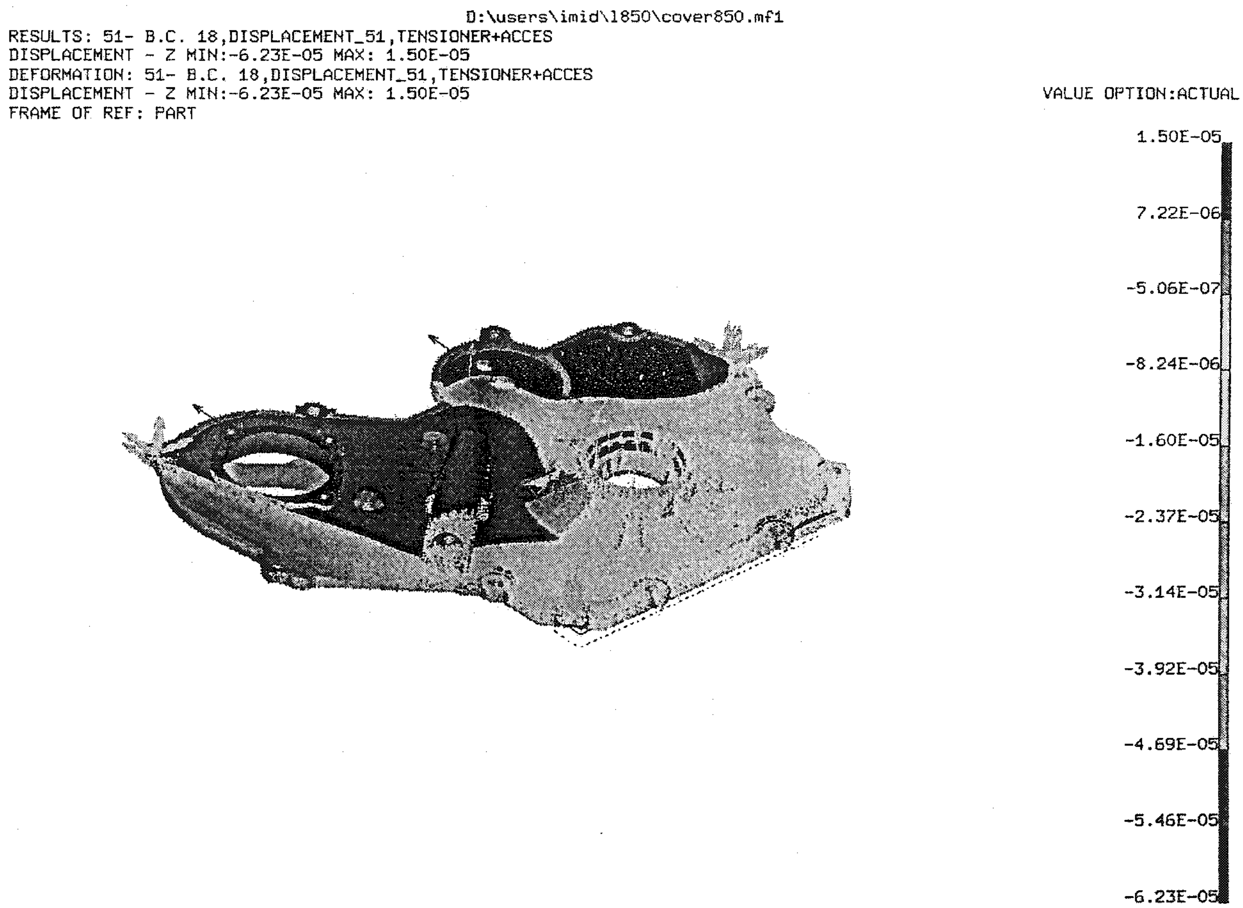

Figure 7.41 Part response: face milling/boring, configuration B-1

7.7.4 Case Study I Summary and Conclusions

The results of this case study demonstrate the vitality of fixture configuration to the process stability and geometric integrity of the machined part. It illustrates how by only modifying individual fixture element location the system response can be altered and driven to the stable zone and the part deflection can be minimized. Which conform to previous results. The results also demonstrated the local effect of the cutting force and how the response varies with the change of the cutter position. The results also demonstrated a very important point, that is the consideration of the part flexibility, fixture element flexibility or both is totally dependent on the application and that for very flexible parts, as in this case study, it might be reasonable to neglect the fixture element flexibility. It is unfortunate that such analysis was carried out after the part has been already in production and so many parts have to be scraped. The current methodology can be integrated into the design process and provide a concurrent environment a result of which would be to develop an optimum or at least near optimum fixture configuration prior to part production which definitely will reduce production cost and time.

7.8 Case Study II Development of a Novel Modular and Agile Face Machining Technology

7.8.1 Case Study II Introduction

The automotive industry has been under considerable pressure to reduce vehicle emissions. This has put increased demands on face machining operations in terms of flatness and micro surface finish characteristics. Improperly sealed joints and surfaces dissipate energy and leak fluids. Given cost and productivity realities of the industry, process improvements must be achieved without significant cost or cycle time increases. To address these issues a novel machining technology has been developed that combines milling and grinding into one face machining operation [132].

Face machining is a process required by a wide family of parts that come in different shapes and sizes. These parts are typically made from a variety of different materials or a combination of materials. In the automotive industry for example, parts range from heavy cylinder blocks made of cast iron, or aluminum with cast iron inserts, to light cover plates and thin oil pans. To successfully deal with this product variety, while meeting production constraints, an agile process is required [133].

A prototype machine tool, based on this face machining technology, has been designed and constructed to test its performance on high volume automotive components. The expectation is that if specific performance criteria can be met on this prototype machine then this technology will be applied across a wide family of face machined parts. Rather than redesign the machine for each new part, the designers decided to use modular components in the design.

The use of modular components aids the development of detailed and accurate simulation models. The results of these simulations can be used to predict performance and thus allow for detailed process development activity [7]. Physics based simulations of these different machine configurations must include the dynamics of the machine, fixture and part, as well as, the unique excitation and interaction that comes from the combination of the milling and grinding processes [42].

7.8.2 Novel Agile Face Machining Concept

This face machining concept involves the combination of a cutting operation performed using geometrically defined cutting edges, namely milling, with a grinding operation that is based on non-defined cutting edges. Figure 7.42 illustrates the relative position of the face mill inserts and the grinding wheel. The milling inserts provide the process with the high metal removal rate capability, while the grinding surface generates the high micro surface finish and part flatness. Thus a significant productivity improvement can be achieved as the feed rate of the face mill is usually limited by the surface finish requirements of the part.

In some applications face mills have been used with large flat wipers. The wiper is often capable of generating the surface finish required, however the large contact area associated with the wiper results in high cutting forces and excessive part deflections when applied to thin parts with minimal support.

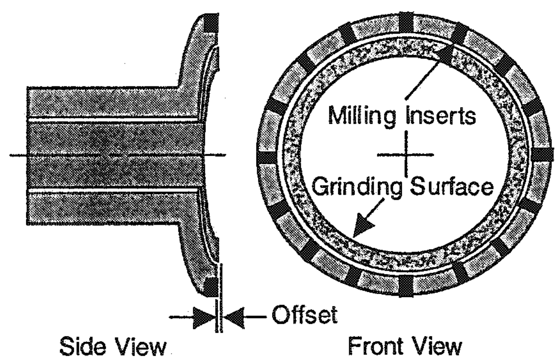

Figure 7.42 Face mill with concentric grinding wheel.

To facilitate process setup each spindle is powered independently and the grinding wheel can be moved with respect to the milling inserts. Thus separate speeds and directions of rotation can be commanded, as well as different depths of cut.

Traditionally separate processes and hence machine tools have been specified for each process. Combining these processes in this manner provides a number of benefits. Table 7.4 summarizes some of these benefits. Economic savings include the use of one machine versus two. This means reduced floor space requirements, less overall maintenance and lower operating costs. Furthermore, less part handling is required and the cutting load on the grinding operation is minimized, as no allowance needs to be made for fixturing errors between processes. This results in significantly reduced tooling costs for the grinding operation. A general machine layout of one possible configuration is shown in Figure 7.43 without guarding.

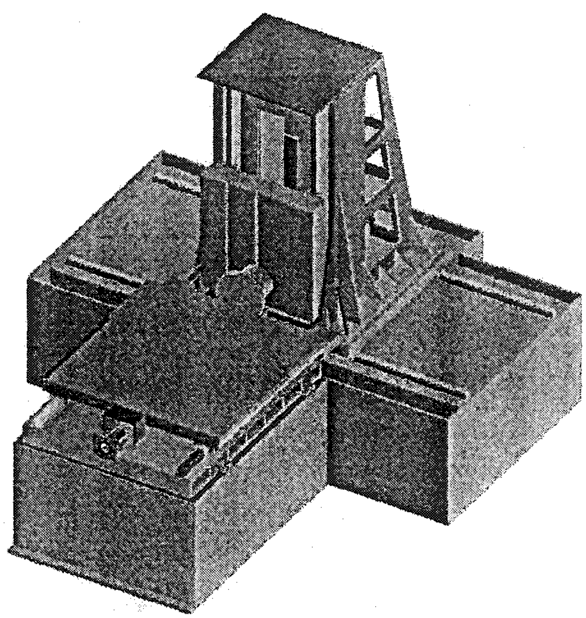

Figure 7.43 General layout of machine without guarding.

Consideration	Milling Alone	Grinding Alone	Combined Process
Metal Removal Rate (MRR)	High MRR possible Limited by machine rigidity Limited by cutting edge strength and chip clearing	Lower MRR Limited by rigidity Limited by workpiece burn and wheel clogging	High MRR Additional process damping from grinding improves the stability of the process thus allowing higher depths of cut and feed rate
Surface finish characteristics	Reduce feed rate to improve surface finish reduces MRR Larger nose radius inserts increase cutting force	Excellent surface finish capability High degree of control over surface properties by altering grit properties	Excellent surface finish capability High degree of control over surface properties by altering grit properties
Burr formation	Large burrs possible	Greatly reduced burring	Burrs small enough to be removed consistently with wire brushing operation
Fixturing requirements	Extra rigidity required to stabilize part	Refixturing errors for grinding requires large material allowance	No refixturing required between processes
Machine requirements	Single machine	Requires two machines to get the same MRR and surface	Both processes incorporated into one machine Lower maintenance costs Less floor space required
Spindle requirements	Single axis of rotation	Single axis of rotation	Two concentric axes of rotation
Part handling	Single transfer into and out of process	Extra transfer required between mill and grinder if utilizing both	Traditional transfer

Table 7.4: Individual and combined process considerations.

7.8.3 Dynamic Model of Machine and Process

7.8.3.1 Framework of the Model

The basic framework of the simulation model [42] is outlined in Figure 7.44. For inputs it uses workpiece geometry as defined by a 3D model of the part, cutting edge geometry, cutting conditions, machine modal information, and fixture layout for a specific workpiece configuration. The calibration constants required by the force models are also supplied as inputs. These values are established using cutting tests for each process individually. The main processing module in the simulation involves a number of computational components. The first is a geometric model, which handles part and cutting tool intersection calculations. This is required to establish the instantaneous chip load, which is needed by the force calculations for both the milling and grinding of an arbitrarily shaped part. These forces are then applied to the dynamic model of the machine, workpiece and fixture to calculate the deflection. These deflections are then fed back so as to capture the dynamic aspect of the cutting force and the machine's response.

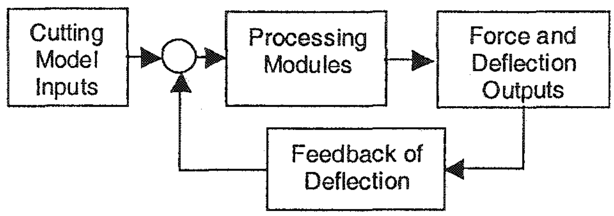

Figure 7.44 Framework for the integrated dynamic model.

7.8.3.2 Dynamics

The dynamics of the machine are established by considering the characteristics of the individual components. Supplier information for the standard components such as linear rails and ball screws were used to establish the stiffness of these components. An example of the data available for the Y-axis linear rail is shown in Figure 7.45. Detailed three-dimensional CAD models of the machine's components were used to establish the weights of critical components. These CAD models were also used for the Finite Element Analysis (FEA) of the structural components to establish modes and natural frequencies of vibration. The first two modes of vibration for the column are shown in Figure 7.46.

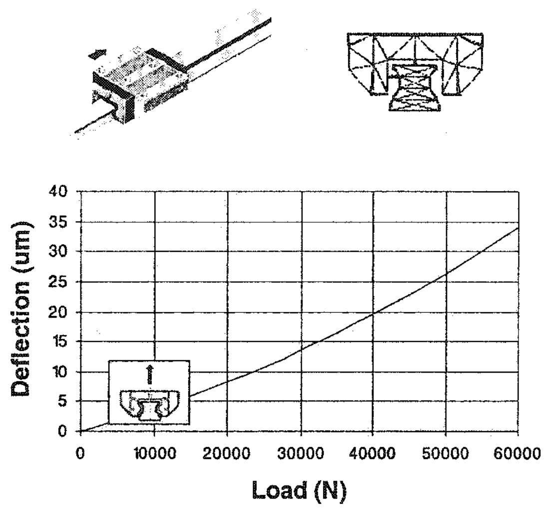

Figure 7.45 Lift-off stiffness of the axis rail module.

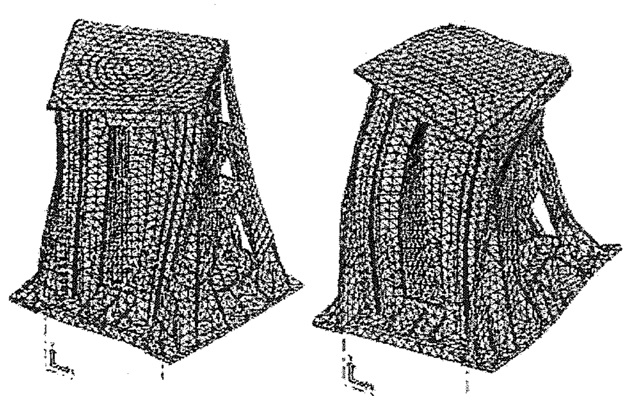

First Mode f_n= 206 Hz   Second Mode f_n = 352 Hz

Figure 7.46 Dynamic characteristics of column module.

The damping in the main structure was estimated based on logarithmic decrement accelerometer measurements made on the prototype machine. The model of the machine's dynamics was then tuned to bring the results of the modal analysis inline with the results of the actual modal testing on the prototype machine. This involved altering the distribution of mass and stiffness properties of the joints to account for manufacturing deviations and actual performance characteristics of the machine components.

7.8.3.3 Milling Force Model

The force model developed in chapter 4 was used for this case study. Equations (7.4) and (7.5) are used to include the effects of the dynamics of the machine tool, fixture and workpiece, as well as the tool's initial position errors. w is the nominal Depth of Cut (DOC), d_m the instantaneous DOC, and $\Delta d_m(\phi_i(\theta))$ the change in DOC due to the dynamics of the milling and grinding processes.

$$C(\phi_i(\theta)) = f_t . \sin(\phi_i(\theta)) + \sum_{j=1}^{3} \Delta C_j(\phi_i(\theta)) \tag{7.4}$$

$$d_m(\phi_i(\theta)) = w + \sum_{j=1}^{3} \Delta d_{mj}(\phi_i(\theta)) \tag{7.5}$$

7.8.3.4 Grinding Force Model

The relationships used to find the tangential F_t' and normal F_n' grinding forces [134], and [135] are outlined in equations (7.6), (7.7) and (7.8).

$$F_t' = F_1\left(\frac{v_w d_g}{v_s}\right)^f \qquad (7.6)$$

$$F_n' = F_2\left(\frac{v_w d_g}{v_s}\right)^f \qquad (7.7)$$

$$d_g = w_g + \sum_{j=1}^{3} \Delta d_g \qquad (7.8)$$

Where F_1 , F_2 and f are calibration constants. v_w is the workpiece speed, which in this case is the feed rate of the spindle. v_s is the cutting velocity of the wheel and w_g is the nominal DOC, d_g the instantaneous DOC and Δd_g the change in DOC due to dynamics experienced by milling and grinding and the influence of the surface created by milling. The values for the calibration constants F_1, F_2 and f were selected based on similar grinding processes reported in the literature [135] and preliminary testing on the prototype machine.

7.8.4 Case Study II Simulation Results

Simulation results are shown for a milling speed of 790m/min, a grinding speed of 6075m/min, a Feed rate of 2400mm/min with 4 milling inserts and a 1mm nominal DOC for milling, and 0.09mm nominal DOC for grinding.

Figure 7.47 compares the Z direction cutting forces for the milling operation alone to the combined process. The forces from grinding are small since the grinding DOC is selected to be only large enough to remove the feed marks created by the milling operation. This is done to minimize the work done by the grinding process.

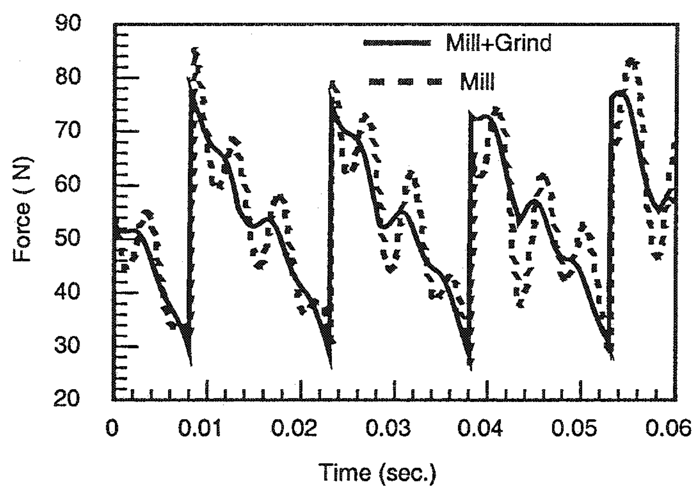

Figure 7.47 Simulation of cutting forces.

The benefits of the additional process damping introduced by the grinding operation can be seen through the reduction in the magnitude of the force oscillations. Figure 7.48 shows the corresponding reduction in the dynamic deflections under the cutting inserts in the Z direction associated with the combined process.

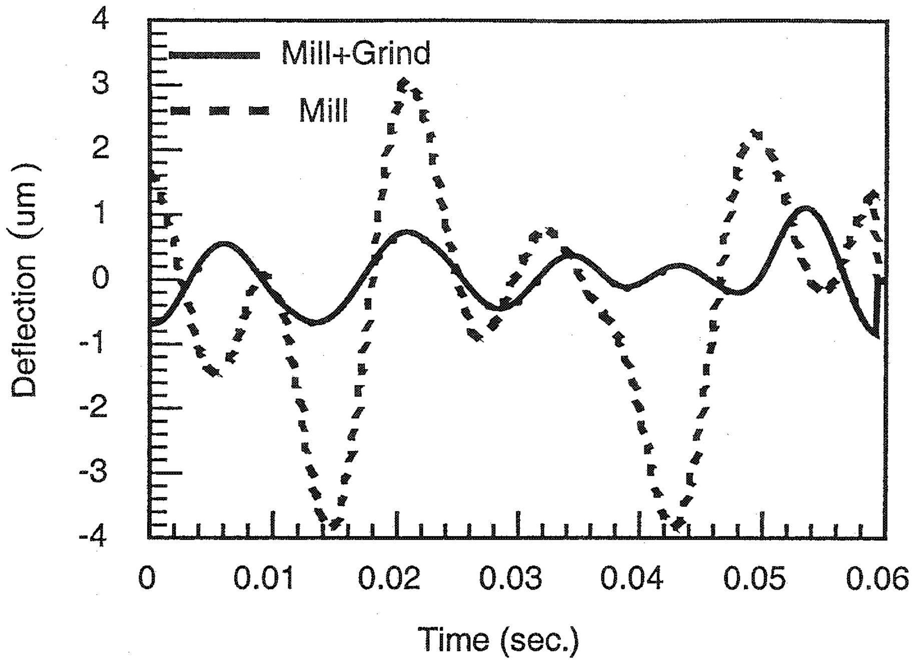

Figure 7.48 Simulation of deflection.

Keeping all other variables constant, the milling DOC was increased to 3.8 mm, the grinding DOC was doubled and the simulated Z force is shown in Figure 7.49 In the case with only milling the cutting forces exhibit exponential growth. When the grinding wheel is added the increase in process damping serves to stabilize the machining action.

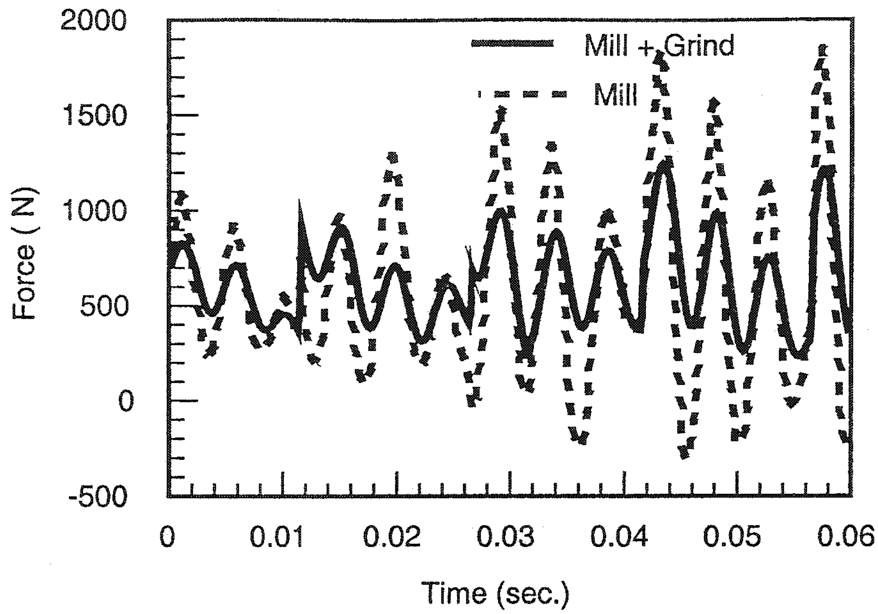

Figure 7.49 Simulation of cutting forces.

7.8.4.1 Selected Prototype Machine Results

Figure 7.50 shows a close up of the surfaces and Ra values achieved using a face mill alone and with the combined process. When working with a joint using a gasket, there are specific surface properties required to optimize the seal. By changing the grit properties, and process parameters the surface characteristics can be controlled.

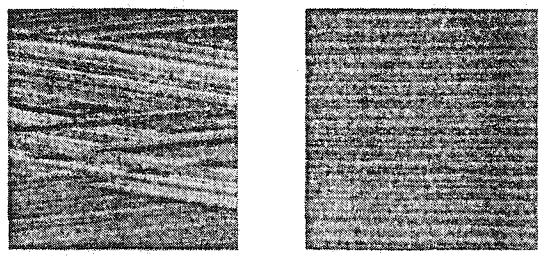

Milling Only Ra=2.41μm Milling + Grinding Ra=0.74μm

Figure 7.50 Comparison of Surface Finishes

Improvements in flatness have also been observed when combining the two processes. Consistently on one part a flatness value of 35 micrometers was measured on a traditional face milling operation versus 20 micrometers for the combined process of milling and grinding.

7.8.5 Case Study II Summary and Conclusions

A novel process involving the combination of milling and grinding into a single operation has been investigated. Process improvements in terms of higher MRR and improved micro surface finishes have been measured using the prototype machine. A detailed simulation model capturing elements of the physics of the operation have been presented. The additive nature of the forces and the benefits of adding the grinding to the operation in terms of additional process damping can be seen in the simulation results and from the preliminary results of the prototype machine.

CHAPTER 8: CONCLUSIONS AND RECOMMENDATIONS FOR FUTURE WORK

8.1 Conclusions

The objective of this work was to provide a tool to help in improving the fixture configuration selection process. The methodology developed in this work helped achieving this goal by integrating the different factors affecting the process dynamics in the same simulation. The developed model predicts the static and dynamic cutting forces at any instant during the cut. Findings of this study demonstrate the important effect of fixture dynamics on the machining process dynamics and the vitality of the fixture configuration selection to the machining process stability. The Friction coefficient was determined experimentally for modular fixture applications and its relation to the clamping force magnitude, workpiece roughness and fixture tip roughness was quantified.

The results of the first case study demonstrate the vitality of fixture configuration to the process stability and geometric integrity of the machined part.

It illustrates how by only modifying individual fixture element location the system response can be altered and driven to the stable zone and the part deflection can be minimized. The results also demonstrated the local effect of the cutting force and how the response varies with the change of the cutter position. The results also demonstrated a very important point, that is the consideration of the part flexibility, fixture element flexibility or both is totally dependent on the application and that for very flexible parts, as in this case study, it might be reasonable to neglect the fixture element flexibility. It is unfortunate that such analysis was carried out after the part has been already in production and so many parts have to be scraped. If the current methodology was integrated into the design process it would provide a concurrent environment a result of which would be to develop an optimum or at least near optimum fixture configuration prior to part production which definitely will reduce production cost and time.

The second case study presents a novel process involving the combination of milling and grinding into a single operation has been investigated. Process improvements in terms of higher MRR and improved micro surface finishes have been measured using the prototype machine. A detailed simulation model capturing elements of the physics of the operation has been presented. The additive nature of the forces and the benefits of adding the grinding to the operation in terms of additional process damping can be seen in the simulation results and from the preliminary results of the prototype machine.

In summary the main contribution of this work is quantifying the effect of workpiece/fixture dynamics interaction on the machining process and integrating this effect with all the other dynamic effects in a generic simulation. In lieu of this, an experimental procedure was developed to determine the friction coefficient for modular hydraulic work holding systems. An in house simulation package was developed based on the presented model to simulate different machining processes. The modularity of the present approach allows for further development and for the use of different commercial packages and at the same time avoids the computational burden associated with commercial solid modelers. The main contributions of this research work are:

- Presentation of an integrated model to simulate machining processes dynamics.
- Quantifying the effect of fixture dynamics on the chip load.
- Developing an experimental setup to determine the friction coefficient for hydraulic work holding systems.
- Defining the relation between clamping force and friction coefficient and using it to take into account the frictional contact when modeling workpiece/fixture dynamics.
- Modularity of the model allow for simulating different/combined machining process.
- Presenting a tool for off-line optimization of fixture layout and machining process parameters.

8.2 Recommendations for Future Work

Machined surface quality and dimensional accuracy are of crucial importance in several industries, e.g. automotive and aerospace. Achieving the design tolerances poses a challenging problem especially when machining thin-walled or flexible parts, e.g. fuselages and turbine blades.

One way of assuring the optimum machined surface quality is to improve the simulation accuracy of the process at hand, taking into account all factors that affect its dynamics and stability. One of these factors is the fixturing scheme. The dynamics of fixture elements plays a major role in the machining process dynamics. Parameters such as clamping force magnitude, position of the fixture element and the surface roughness of the fixture tip, i.e. friction coefficient, can adversely affect the geometric integrity of the machined part. These same parameters can be used to manipulate the dynamic characteristics of the machine tool and consequently reduce or damp undesired vibrations. Fixture elements dynamics are highly nonlinear and require experimental investigation and numerical modeling of the dynamic frictional contact between the workpiece and the fixture element. This work need to be extended to include models for different machining processes and different cutting tools geometry.

A novel and tangible methodology to improve the machined surface quality is grind-mill machining, which is a combination of face milling and grinding processes. Grinding is known to provide the best surface finish among machining processes while face milling improves metal removal rate. By combining these two processes together, the stiffness and stability of the machine tool is enhanced due to the weight of the grinding wheel and the machined part surface finish is improved due to grinding process.

To realize this methodology, the following topics needs in depth investigation:

1. Development of an accurate grinding dynamic force model.
2. Experimental and numerical modal analysis of the new machine dynamics.
3. Modeling of the interaction of the milling and grinding processes dynamics.
4. Implementation of an integrated simulation of the two processes dynamic models.
5. Development of an optimum fixture configuration to accommodate the settings of the hybrid process.
6. Experimental validation of the developed methodology.

This new hybrid machining methodology along with a comprehensive model of the machining process dynamics provides a feasible optimization tool that can be used in a concurrent engineering environment to reduce both machining cost and time. This approach would greatly help in improving the machined surface quality of flexible parts.

APPENDIX I: FORCE MODEL CALIBRATION

This appendix gives the mathematical details for performing the multiple parameter linear regression analysis (LSE) to determine the cutting pressures $\{K_1, K_2, K_3\}$. The general form is:

$$Y = X\psi + \varepsilon \tag{I.1}$$

Where Y is the vector of responses, ψ is the vector of model parameters, ε is the vector of random error and X is the model specification matrix. The errors, ε are assumed to be uncorrelated having zero means and the same variance.

The normal equation of the general linear model [39][132] is:

$$\left(X' \cdot X\right) \cdot \psi = X' \cdot Y \tag{I.2}$$

The solution of the normal equation is given as:

$$\psi = \left(X' \cdot X\right)^{-1} \cdot X' \cdot Y \tag{I.3}$$

The sum of squares at the minimum is given as:

$$S(\psi) = Y'Y - \psi' X' X \psi \tag{I.4}$$

An estimation of the residual variance [130][132] ,σ^2 , is written as:

$$s^2 = \frac{S(\psi)}{n-k} \tag{I.5}$$

where n is the number of observations and k is the number of model parameters. A (1-ε) confidence region for ψ [132] can be written as:

$$S = S(\psi)\left[1 + \frac{k}{n-k} F_{\alpha}(k, n-k)\right] \tag{I.6}$$

where $F_{\alpha}(k, n\text{-}k)$ is the significance point of the F distribution with k and n-k degree of freedom. From chapter 4,the force model is written in the following form:

$$\begin{aligned} F_x &= K_t(A_t + K_r \cdot A_r + K_a \cdot A_a) \\ F_y &= K_t(B_t + K_r \cdot B_r + K_a \cdot B_a) \\ F_z &= K_t(C_t + K_r \cdot C_r + K_a \cdot C_a) \end{aligned} \tag{I.7}$$

Defining K_1=K_t, K_2=$K_t.K_r$ and K_3=$K_t.K_a$ equation (I.7) can be rewritten in matrix form as:

$$\begin{Bmatrix} F_x \\ F_y \\ F_z \end{Bmatrix} = \begin{bmatrix} A_t & A_r & A_a \\ B_t & B_r & B_a \\ C_t & C_r & C_a \end{bmatrix} \cdot \begin{Bmatrix} K_1 \\ K_2 \\ K_3 \end{Bmatrix} \tag{I.8}$$

Least Square model takes the form:

$$\begin{aligned} F_{mx} &= K \cdot A + E_x \\ F_{my} &= K \cdot B + E_y \\ F_{mz} &= K \cdot C + E_z \end{aligned} \tag{I.9}$$

The sum squared error (SSE) is taken as:

$$
\begin{aligned}
SSE &= \sum_i^n e_i^2 \\
&= \sum_i^n \left(e_{xi}^2 + e_{yi}^2 + e_{zi}^2\right) \\
&= \sum_i^n \left(e_{xi}^2\right) + \sum_i^n \left(e_{yi}^2\right) + \sum_i^n \left(e_{zi}^2\right) \\
&= \sum_i^n \left[F_{mxi} - \left(K_1 \cdot A_{ti} + K_2 \cdot A_{ri} + K_3 \cdot A_{ai}\right)\right]^2 + \\
&\sum_i^n \left[F_{myi} - \left(K_1 \cdot B_{ti} + K_2 \cdot B_{ri} + K_3 \cdot B_{ai}\right)\right]^2 + \\
&\sum_i^n \left[F_{mzi} - \left(K_1 \cdot C_{ti} + K_2 \cdot C_{ri} + K_3 \cdot C_{ai}\right)\right]^2
\end{aligned}
\tag{I.10}
$$

The sum of square errors is minimized:

$$
\frac{\delta SSE}{\delta K_i} = 0 \quad ,i = 1,2,3 \tag{I.11}
$$

The partial derivatives are given as:

$$
\begin{aligned}
\frac{\delta SSE}{\delta K_1} = &-2 \cdot \sum_i^n \left[F_{mxi} - \left(K_1 \cdot A_{ti} + K_2 \cdot A_{ri} + K_3 \cdot A_{ai}\right)\right] \cdot A_{ti} \\
&-2 \cdot \sum_i^n \left[F_{myi} - \left(K_1 \cdot B_{ti} + K_2 \cdot B_{ri} + K_3 \cdot B_{ai}\right)\right] \cdot B_{ti} \\
&-2 \cdot \sum_i^n \left[F_{mzi} - \left(K_1 \cdot C_{ti} + K_2 \cdot C_{ri} + K_3 \cdot C_{ai}\right)\right] \cdot C_{ti}
\end{aligned}
\tag{I.11a}
$$

$$
\begin{aligned}
\frac{\delta SSE}{\delta K_2} = &-2 \cdot \sum_i^n \left[F_{mxi} - \left(K_1 \cdot A_{ti} + K_2 \cdot A_{ri} + K_3 \cdot A_{ai}\right)\right] \cdot A_{ri} \\
&-2 \cdot \sum_i^n \left[F_{myi} - \left(K_1 \cdot B_{ti} + K_2 \cdot B_{ri} + K_3 \cdot B_{ai}\right)\right] \cdot B_{ri} \\
&-2 \cdot \sum_i^n \left[F_{mzi} - \left(K_1 \cdot C_{ti} + K_2 \cdot C_{ri} + K_3 \cdot C_{ai}\right)\right] \cdot C_{ri}
\end{aligned}
\tag{I.11b}
$$

$$\frac{\delta SSE}{\delta K_3} = -2 \cdot \sum_i^n \left[F_{mxi} - \left(K_1 \cdot A_{ti} + K_2 \cdot A_{ri} + K_3 \cdot A_{ai}\right)\right] \cdot A_{ai}$$
$$-2 \cdot \sum_i^n \left[F_{myi} - \left(K_1 \cdot B_{ti} + K_2 \cdot B_{ri} + K_3 \cdot B_{ai}\right)\right] \cdot B_{ai} \quad \text{(I.11c)}$$
$$-2 \cdot \sum_i^n \left[F_{mzi} - \left(K_1 \cdot C_{ti} + K_2 \cdot C_{ri} + K_3 \cdot C_{ai}\right)\right] \cdot C_{ai}$$

Rearranging Equation (I.11) gives equations (I.12),(I.14)and (I.16):

$$\begin{aligned}
&\sum_i^n \left(F_{mxi} \cdot A_{ti} + F_{myi} \cdot B_{ti} + F_{mzi} \cdot C_{ti}\right) = \\
&\quad K_1 \cdot \sum_i^n \left(A^2{}_{ti} + B^2{}_{ti} + C^2{}_{ti}\right) + \\
&\quad K_2 \cdot \sum_i^n \left(A_{ti} \cdot A_{ri} + B_{ti} \cdot B_{ri} + C_{ti} \cdot C_{ri}\right) + \\
&\quad K_3 \cdot \sum_i^n \left(A_{ti} \cdot A_{ai} + B_{ti} \cdot B_{ai} + C_{ti} \cdot C_{ai}\right)
\end{aligned} \quad \text{(I.12)}$$

Simplifying equation (I.12) we get:

$$Y_1 = K_1 \cdot X_{1,1} + K_2 \cdot X_{1,2} + K_3 \cdot X_{1,3}$$

where,

$$\begin{aligned}
Y_1 &= \sum_i^n \left(F_{mxi} \cdot A_{ti} + F_{myi} \cdot B_{ti} + F_{mzi} \cdot C_{ti}\right) \\
X_{1,1} &= K_1 \cdot \sum_i^n \left(A^2{}_{ti} + B^2{}_{ti} + C^2{}_{ti}\right) \\
X_{1,2} &= K_2 \cdot \sum_i^n \left(A_{ti} \cdot A_{ri} + B_{ti} \cdot B_{ri} + C_{ti} \cdot C_{ri}\right) \\
X_{1,3} &= K_3 \cdot \sum_i^n \left(A_{ti} \cdot A_{ai} + B_{ti} \cdot B_{ai} + C_{ti} \cdot C_{ai}\right)
\end{aligned} \quad \text{(I.13)}$$

$$\begin{aligned}
&\sum_i^n \left(F_{mxi} \cdot A_{ri} + F_{myi} \cdot B_{ri} + F_{mzi} \cdot C_{ri}\right) = \\
&\quad K_1 \cdot \sum_i^n \left(A_{ti} \cdot A_{ri} + B_{ti} \cdot B_{ri} + C_{ti} \cdot C_{ri}\right) + \\
&\quad K_2 \cdot \sum_i^n \left(A^2{}_{ri} + B^2{}_{ri} + C^2{}_{ri}\right) + \\
&\quad K_3 \cdot \sum_i^n \left(A_{ri} \cdot A_{ai} + B_{ri} \cdot B_{ai} + C_{ri} \cdot C_{ai}\right)
\end{aligned} \quad \text{(I.14)}$$

Simplifying equation (I.14) we get:

$$Y_2 = K_1 \cdot X_{2,1} + K_2 \cdot X_{2,2} + K_3 \cdot X_{2,3}$$

where,

$$\begin{aligned}
Y_2 &= \sum_i^n \left(F_{mxi} \cdot A_{ri} + F_{myi} \cdot B_{ri} + F_{mzi} \cdot C_{ri}\right) \\
X_{2,1} &= K_2 \cdot \sum_i^n \left(A_{ti} \cdot A_{ri} + B_{ti} \cdot B_{ri} + C_{ti} \cdot C_{ri}\right) \\
X_{2,2} &= K_1 \cdot \sum_i^n \left(A^2{}_{ri} + B^2{}_{ri} + C^2{}_{ri}\right) \\
X_{2,3} &= K_3 \cdot \sum_i^n \left(A_{ri} \cdot A_{ai} + B_{ri} \cdot B_{ai} + C_{ri} \cdot C_{ai}\right)
\end{aligned} \tag{I.15}$$

$$\begin{aligned}
&\sum_i^n \left(F_{mxi} \cdot A_{ai} + F_{myi} \cdot B_{ai} + F_{mzi} \cdot C_{ai}\right) = \\
&K_1 \cdot \sum_i^n \left(A_{ti} \cdot A_{ai} + B_{ti} \cdot B_{ai} + C_{ti} \cdot C_{ai}\right) + \\
&K_2 \cdot \sum_i^n \left(A_{ri} \cdot A_{ai} + B_{ri} \cdot B_{ai} + C_{ri} \cdot C_{ai}\right) + \\
&K_3 \cdot \sum_i^n \left(A^2{}_{ai} + B^2{}_{ai} + C^2{}_{ai}\right)
\end{aligned} \tag{I.16}$$

Simplifying equation (I.16) we get:

$$Y_3 = K_1 \cdot X_{3,1} + K_2 \cdot X_{3,2} + K_3 \cdot X_{3,3}$$

where,

$$\begin{aligned}
Y_3 &= \sum_i^n \left(F_{mxi} \cdot A_{ai} + F_{myi} \cdot B_{ai} + F_{mzi} \cdot C_{ai}\right) \\
X_{3,1} &= K_2 \cdot \sum_i^n \left(A_{ti} \cdot A_{ai} + B_{ti} \cdot B_{ai} + C_{ti} \cdot C_{ai}\right) \\
X_{3,2} &= K_3 \cdot \sum_i^n \left(A_{ri} \cdot A_{ai} + B_{ri} \cdot B_{ai} + C_{ri} \cdot C_{ai}\right) \\
X_{3,3} &= K_1 \cdot \sum_i^n \left(A^2{}_{ai} + B^2{}_{ai} + C^2{}_{ai}\right)
\end{aligned} \tag{I.17}$$

Rearranging equations (I.13), (I.15) and (I.17) in matrix form:

$$\begin{bmatrix} X_{1,1} & X_{1,2} & X_{1,3} \\ X_{2,1} & X_{2,2} & X_{2,3} \\ X_{3,1} & X_{3,2} & X_{3,3} \end{bmatrix} \cdot \begin{Bmatrix} K_1 \\ K_2 \\ K_3 \end{Bmatrix} = \begin{Bmatrix} Y_1 \\ Y_2 \\ Y_3 \end{Bmatrix} \tag{I.18}$$

The solution of equation (I.18) takes the form:

$$\{K\} = [X]^{-1} \cdot \{Y\} \tag{I.19}$$

REFERENCES

1. Kline W. A., and Devor R. E, 1982, " Prediction Of Surface Accuracy In End Milling", ASME Journal Of Engineering For Industry, Vol. 113, n. 3, pp. 272-278.

2. Sutherland J. W. and Devor R. E., 1986," Improved Method For Cutting Force And Surface Error Prediction In Flexible End Milling Systems", ASME Journal Of Engineering For Industry, vol. 108, n. 4, pp. 269-279.

3. Armarego E. J. and Deshpande N. P., 1991,"Computerized End Milling Force Prediction With Cutting Model Allowing Eccentricity And Cutter Deflections", Annals of CIRP, Vol. 40,n. 1, pp. 25-29.

4. Feng H-Y and Menq C-H, 1996, "A Flexible Ball-End Milling System Model For Cutting Force And Machining Error Prediction", ASME Journal Of Manufacturing Science And Engineering, Vol. 118, n. 4, pp. 461-469.

5. Smith S., and Tlusty J.,1991, "An Overview Of Modeling And Simulation Of The Milling Process", ASME Journal Of Engineering For Industry, Vol. 113,n.2, pp.169-175.

6. Yucesan G. and Altintas Y., 1993, "Prediction Of Ball End Milling Forces", ASME Journal Of Engineering For Industry, Vol. 118,n.1, pp.95-103.

7. Kapoor S. G., Devor R. E., Zhu R., Gajjela R., Parakkal G. and Smithey D.,1998, "Development Of Mechanistic Models For The Prediction Of Machining Performance: Model-Building Methodology", Machining Science And Technology, Vol. 2 , n. 2, pp. 213-238.

8. Ehmann K. F., Kapoor S.G., Devor R. E., Lazoglu I., 1997, "Machining Process Modeling: A Review", Journal of Manufacturing Science and Engineering, Vol. 119,n. 4(b) ,pp. 655-663.

9. Gu F., Kapoor S. G., Devor R. E. and Bandyopadhyay,1997, "An Enhanced Cutting Force Model For Face Milling With Variable Cutter Feed Motion And Complex Workpiece Geometry", Journal of Manufacturing Science and Engineering, Vol.119, pp.467-475.

10. Zheng H.Q., Li X. P., Wong Y. S. and Nee A. Y. C., 1999, "Theoretical Modeling And Simulation Of Cutting Forces In Face Milling With Cutter Run out", International Journal Of Machine Tool And Manufacture, Vol. 39,pp. 2003-2018.

11. Oxley P. L. B., 1989, "The Mechanics Of Machining: An Analytical Approach For Assessing Machinability", Ellis Horwood Ltd.

12. Akshay, Kapoor S. G. and Devor R. E., 1998, "A Model-Based Approach For Radial Run-Out Estimation In The Face Milling Process", Transactions of North American Manufacturing Research Institute, Vol. 26, pp. 261-266.

13. Zheng Li, Li Yawei and Liang S. Y., 1997, "A Generalized Model Of Milling Forces", International Journal of Advanced Manufacturing Technology Vol. 14,n. 3, pp.160-171.

14. Young Hong-Tsu, Mathew P. and Oxley P.L.B., 1994,"Predicting Cutting Forces In Face Milling", International Journal Of Machine Tool And Manufacture, Vol. 34, pp. 771-783.

15. Kim H. S. and Ehmann K. F., 1993, "A cutting Force Model for Face Milling Operations", International Journal of Machine Tool and Manufacture, Vol. 33, n. 5, pp.651-673.

16. Bayoumi A.E., Yucesan G. and Kendall L. A., 1994," An Analytic Mechanistic Cutting Force Model for Milling: A Theory and Methodology", ASME Journal of Engineering For Industry Vol. 116, n. 3, pp. 324-330.

17. Bayoumi A.E., Yucesan G. and Kendall L. A., 1994," An Analytic Mechanistic Cutting Force Model for Milling: A Case Study of Helical Milling Operation", ASME Journal of Engineering for Industry Vol. 116, n. 3, pp. 331-339.

18. Optiz, H.E. and Werntze, G., 1972," Application of a Process Control Computer for Measurement of Dynamic Cutting Coefficients" Annals of the CIRP, Vol.21, n.1, pp.99-103.

19. Sridhar R., Hon R. E. and Long R. E., 1968, "Stability Algorithm For The General Milling Process", ASME Journal of Engineering for Industry, Vol.90,pp. 330-334

20. Das M. K. And Tobias S. A., 1967," The Relation between the Static and the Dynamic Cutting of Metals", International Journal of Machine Tools Design and Research, Vol.7, pp.63-89.

21. Jensen, S. A. and Shin, Y. C., 1999,"Stability Analysis in Face Milling Operations, Part 1: Theory of Stability Lobe Prediction", ASME Journal of Manufacturing Science and Engineering, Vol.121, p.600-613.

22. Tlusty, J. and Ismail, F., 1983,"Special Aspects of Chatter in Milling", ASME Journal of Vibration, Acoustics, Stress and Reliability in Design, Vol.105, n. 1,pp. 4-32.

23. Ismail F., Elbestawi, M. A., Du R., and Urbasik K., 1993, "Generation Of Milled Surfaces Including Tool Dynamics And Wear", ASME Journal of Engineering for Industry, Vol.115, n. 3,pp.245-252.

24. Smith, S., and Tlusty, J., 1993,"Efficient Simulation Programs for Chatter in Milling", Annals of the CIRP, Vol.42, pp.463-466.

25. Devor, R. E., Kline, W. A., and Zdeblick, W. J., 1980, "A Mechanistic Model For The Force System In The End Milling With Application To Machining Airframe Structures", Proceedings of the 8th North American Manufacturing Research Conference, pp.297-303.

26. Taylor D. L., 1992,"Computer Aided Design", Addison-Wesley.

27. Zeid, I., 1991,"CAD/CAM Theory and Practice", McGraw-Hill.

28. Anderson R. O., 1978,"Detecting and Eliminating Collisions In NC Machining", Computer Aided Design, Vol. 10, n. 4, pp.231-238.

29. Chappel I. T., 1983,"The Use of Vectors to Simulate Material Removed by Numerically Controlled Milling ", Computer Aided Design, Vol. 15, n. 4, pp156-158.

30. Drysdal R. L., Jerard R. B., Schaudt B. and Hauk K., 1989,"Discrete Simulation Of The NC Machining", Algorithmica, Vol. 4, pp.33-60.

31. Jerard R. B., Drydale R. L., Huack K., Schuadt B. and Majewick J.,1989," Methods For Detecting Errors In Numerically Controlled Machining Of Sculptured Surfaces", Computer Graphics And Applications, Vol. ,pp.26-39.

32. Wang W.P and Wang K. K., 1986,"Real.-Time Verification of Multi-Axis NC Programs with Raster Graphics", IEEE proceedings of International Conference on Robotics and Automation, California, USA.

33. Wang W.P and Wang K. K., 1986,"Geometric Modeling of Swept Volume of Moving Solids", Computer Graphics And Applications, Vol. 6, n.12 pp.8-17.

34.Van Hook Tim, 1986,"Real-Time Shaded NC Milling Display", Computer Graphics, Vol.20, n. 4, pp.15-20.

35. Sagherian R. and Elbestawi M.A., 1990,"A Simulation System For Improving Machining Accuracy In Milling", Computers In Industry, Vol. 14, n. 4,pp.293-305.

36. Moetakef-Imani B., 1997, "Model Based Die Cavity Machining Simulation Methodology", Ph.D. Thesis, McMaster University, Ontario, Canada.

37. Abrari F., 1998,"Multi-Axis Milling Of Flexible Parts", Ph.D. Thesis, McMaster University, Ontario, Canada.

38. Leu M.C., Lu F. and Blackmore D., 1998,"Simulation Of NC Machining With Cutter Deflection By Modeling Deformed Swept Volumes", Annals of the CIRP, Vol. 47, n. 1, pp.441-446.

39. Bailey T., 2001," Generic Mechanistic Modeling For Multi-Axis Machining ", Ph.D. Thesis, McMaster University, Ontario, Canada.

40. Menassa R. J, 1989,"Synthesis, Analysis and Optimization of Fixtures for Prismatic Parts", PhD Thesis, Rensselaer Polytechnic Institute.

41. Care Lane Manufacturing, 1991, "Modular Fixturing Handbook", 2nd edition, St. Louis, Missouri, USA.

42. Deiab I. M., Veldhuis S. C. and Dumitrescu M., 2002,"Dynamic Modeling of Face Milling Process Including the Effect of Fixture Dynamics", Transactions of the North American Manufacturing Research Conference, pp.461-468, Purdue University, USA.

43. Hou Jian Liang and Trappey Amy J.C., 1997,"A System Approach Fixture Design and Analysis: A Work holding Illustration of Truck Differential Carrier" ASME Journal of Manufacturing Science and Technology Vol.2, pp.229-236.

44. Melkote S. N., S. M. Devor R,. Kapoor S and. Burkey J, 1995, "Prediction of Reaction Force System For Machining Fixtures Based on Machining Process Simulation" Transactions of the North American Manufacturing Research Conference Vol. 23, pp. 207-214.

45. Chandra P., Thavale S. M., Kapoor S. G, and Devor R. E.,1997, "Finite Element Based Fixture Analysis Model for Surface Error Predictions due to Clamping and Machining Forces", ASME Journal of Manufacturing Science and Technology Vol.6,n.2, pp. 245-252.

46. Lee J.D. and Haynes L.S, 1987, "Finite-Element Analysis of Flexible Fixturing System", ASME Journal of engineering for industry, Vol. 109, N.2, pp. 134-139

47. Hamedi M., Rogers R. J, Nadkarni G. R. and Bonham D. J., 1999, " On Realistic Modeling of Workpiece- Fixture Interaction", Proceedings of the 31st MATADOR Conference, Manchester, U.K., pp.. 557-562.

48. Chou, Y-C and Barash M.M, 1989, "Automatic Configuration of Machining Fixtures: a Methodology", Proceedings of the Integrated Systems Conference & Society For Integrated Manufacturing Conference, pp. 390-397.

49. Chou, Y-C. , 1990, "A Methodology For Automatic Layout Of Fixtures Elements Based On Machining Forces Considerations" Advances In Product Design and Manufacturing, ASME Winter Annual Meeting, Dallas Texas, pp. 181-189.

50. Lim B.S, Imao, Yoshida, Goto, K.; Koh, S.L.; Lim, D.; Chin, L.; Gan, S.C., 1992,"Integrated Module Fixture Design, Pricing And Inventory Control Expert System" International Journal of Production Research, Vol.30,n. 9,pp. 2019-2044.

51. Meyer R. T., Liou F. W. , 1997, "Fixture Analysis under Dynamic Machining", International Journal of Production Research, Vol. 35, N. 5, pp.1471-1489.

52. Jeng S., Chen L. and Chieng W, 1995, "Analysis Of Minimum Clamping Forces", International Journal Of Machine Tools And Manufacture, Vol. 35, N. 9, pp.1213-1224.

53. Shawki G. S. A and Abdel-Aal M. M., 1966," Rigidity Considerations in Fixture Design -Contact Rigidity at Locating Elements", International journal of machine tool design and research, Vol. 6, pp. 207-220.

54. Demeter E. C., 1994,"Restraint Analysis Of Fixtures Which Rely On Surface Contact", JASME Journal of Engineering for Industry, Vol. 116, pp. 207-215.

55. Hinkle, R. Th., 1958, "Kinematics of Machines", Prentice-Hall.

56. Lakshminarayana, K., 1978, "Mechanics of Form Closure", Transactions of ASME, Vol32, n. 78, pp. 1-8.

57. Salisbury J. K. and Roth, B., 1983, " Kinematic and Force Analysis Of Articulated Mechanical Hands", ASME Journal of Mechanisms, Transmissions and Automation In Design, Vol. 105, pp. 35-41.

58. Chou, V. C., Chandra V and Barash, M., 1989, "A Mathematical Approach To

Automatic Configuration Or Machining Fixtures, Analysis And Synthesis", ASME Journal of Engineering For Industry, Vol.111, pp. 299-306.

59. Trappey, A. J., and Liu, C. R., 1992, "An Automatic Workholding Verification System", Journal of Robotics and Computer Integrated Manufacturing, Vol.9, n. 4/5, pp.321-326.

60. Ohwovoriole, B. N., 1987, "Kinematics and Friction in Grasping by Robotic Hands," ASME Journal Of Mechanisms, Transmission and Automation In Design, Vol.109, pp. 398-404.

61. Nguyen, V., 1988, "Constructing Force-Closure Grasps", International Journal of Robotics Research, Vol. 7, n. 3, pp. 3-16.

62. Kerr, D. R., and Sanger D. J., 1983,"Analysis of Kinematic Restraint", Proceeding of the Sixth World Congress for the Theory of Mechanisms and Machines, India, pp. 299- 303.

63. Assada H and Kitagawa, M, 1989, "Kinematic Analysis and Planning for Form Closure Grasps by Robotic Hands", Journal of Robotics and Computer Integrated Manufacturing, Vol. 5, n.4, pp. 293-299.

64. Xie W., Demeter E. C. and Trethewey M. W., 2000,"An Experimental Evaluation of the Coefficient of Friction of Common Workpiece-Fixture Element Pairs", International Journal Of Machine Tools And Manufacture, Vol. 40, pp. 467-488.

65. ASM Metals handbook-Friction,1990, "Lubrication and Wear Technology", Vol. 18, Metals park, Ohio.

66. Chang W. R., Etsion I., and Bogy D. B., 1988," Adhesion Model for Metallic Rough Surfaces", Journal of Tribology, Vol. 110, pp. 50-56.

67. Tabor D., 1981, "Friction-The Present State of Our Understanding", ASME Journal of Lubrication Technology, Vol. 103, pp.169-179.

68. Li B. and Melkote N., 2001,"Fixture Clamping Force Optimization And Its Impact On Workpiece Location Accuracy", International Journal Of Advanced Manufacturing Technology, Vol. 17, pp. 104-113.

69. Zhang J., Moslehy F. A and Rice S. L., 1991,"A Model For Friction In Quasi-Steady-State Sliding Part I: Derivation", Wear, Vol. 149, pp. 1-12.

70. Zhang J., Moslehy F. A. and Rice S. L., 1991,"A Model for Friction in Quasi-Steady-State Sliding Part II. Numerical Results and Discussion", Wear, Vol. 149, pp.13-25.

71. Blau, Peter, J, 1996, " Friction Science and Technology", Marcel Dekker.

72. Xie W., Demeter, E.C. and Trethewey M. W., 1999, "An Experimental Evaluation Of The Coefficient Of Friction Of Workpiece-Fixture Element Pairs", Transactions of the North American research Conference, pp. 197-203.

73. Nivatvongs K., Cheng H. S., Ovaert T. C. and Wilson W. R. D., 1991,"Influence Of Surface Topography On Low-Speed Asperity Lubrication Breakdown And Scuffing", Wear, Vol. 143, pp. 137-148.

74. Hurtado J .E. and Melkote S. N., 1998, "A Model For The Prediction Of Reaction Forces In A 3-2-L Machining Fixture", Transactions of the North American Manufacturing Research Conference, pp. 335-340.

75. Liao Y. J., Hu S. J., and Stephenson D. A., 1998,"Fixture Layout Optimization Considering Workpiece-Fixture Contact Interaction: Simulation Results" Transactions of the North American Manufacturing Research Conference, pp. 341–346.

76. Hochenberger M. J., and Demeter E. C., 1996, “The Application of Meta Functions To the Quasi-Static Analysis of Workpiece Displacement Within A Machining Fixture”, ASME Journal of Manufacturing Science and Engineering, Vol. 118, pp. 325-331.

77. Reams M. and Melkote S. N., 1996, ”Quick Estimation Of Reaction Forces For Prediction Of Machining Fixture Quality”, Proceedings of the Second SME Symposium on Manufacturing Science, Detroit, MI, USA, pp. 154-l59.

78. Sayeed Q. A. and Demeter E. C.,1994, “Machining Fixture Design And Analysis Software”, International Journal of Production Research, Vol. 32, n. 7, pp 1655-1674, .

79. Lee, S. G. and Cutkowsky M. R., 1991, “Fixture Planning With Friction”, ASME, Journal of Engineering For Industry, Vol. 113, pp. 320-327.

80. Male A. T. and Cockcroft M. G., 1964,”A Method for The Determination Of The Coefficient Of Friction Under Conditions Of Bulk Plastic Deformation”, Journal of the Institute of Metals, Vol.93, pp. 38-47.

81. Piegle L. and Tiller W., 1997,”The NURBS Book”, 2nd edition, Spinger.

82. ElKott D. F., 2001," Automatic Sampling for CMM Inspection Planning of Free Form Surfaces", M. A. Sc. Thesis, University of Windsor, Canada.

83. ElKott D. F., ElMaraghy H., and ElMaraghy W., 2002, "Automatic Sampling for CMM Inspection Planning of Free Form Surfaces", International Journal of Production Research, Vol. 40, n. 11, pp.2653-2676.

84. Smith S. and Tlusty J., 1991,"An Overview of Modeling and Simulation of the Milling Process", ASME Journal of Engineering for Industry, Vol.113, n.1, pp.169-175.

85. K. Ho-Le, 1988, "Finite Element Mesh Generation Methods: Review And Classification", Computer Aided Design, Vol. 20 n. 1, pp. 27-38.

86. Cavendish J. C., D., Field A., and Frey W.H., 1985," An Approach to Automatic Three-Dimensional Finite Element Mesh Generation", International Journal for Numerical Methods In Engineering, Vol. 21,n.2, pp. 329-347.

87. Buell W. R. and Bush B. A., 1973," Mesh Generation: A Survey", ASME Journal of Engineering for Industry, pp. 332-339.

88. Thacker W. C., 1980, "Brief Review Of Techniques For Generating Irregular Computational Grids", International Journal Of Numerical Methods In Engineering, Vol. 15, n. 6, pp. 438-444.

89. Wordenweber B, 1984," Finite Element Mesh Generation", Computer Aided Design, Vol. 16 n. 5, pp.285-291.

90. Cavendish J.C, 1974, "Automatic Triangulation Of Arbitrary Planar Domains For The Finite Element Methods", International Journal of Numerical Methods in Engineering. Vol. 8, n 4, pp. 679-696

91. Lewis, B. A. and Robinson, J. S., 1978," Triangulation Of Planar Regions With Applications", Computer Graphics, Vol. 21,n. 4,pp. 324-332

92. Yerry .M. A. and Shepard M.S., 1985," Automatic Mesh Generator for Three-Dimensional solids", Computers and Structures, Vol. 20,pp. 31-39.

93. Yerry, M. A. and Shepard, M.S., 1984,"Automatic Three-Dimensional Mesh Generation by the Modified–Octree Technique", International Journal of Numerical Methods in Engineering, Vol. 20, n.11, pp.1965-1990.

94. Sapidis N. and Perucchio R, 1989," Advanced Techniques for Automatic Finite Element Meshing from Solid Models", Computer Aided Design, Vol. 24, n. 4, pp.248-253.

95. Tlusty J., 1984,"Dynamics of High Speed Machining", ASME Journal of Engineering for Industry. Vol. 12, pp. 101-126.

96. Altintas Y. and Chan P. K., 1992," In Process Detection and Suppression of Chatter in Milling", International Journal of Machine Tools and Manufacture, Vol.32, n. 3, pp. 329-347.

97. Jayrama S., 1997," Stability and Vibration Analysis of Turning and Face Milling Processes", Ph.D. Thesis, University of Illinois at Urbana Champaign.

98. Gu F.,1993," Prediction of Cutting Forces and Surface Errors In Face Milling With Generalized Cutter and Workpiece Geometry", Ph.D. Thesis , University of Illinois at Urbana Champaign.

99. Fu H. J. , Devor R. E. and Kapoor S. G.,1984," A Mechanistic Model For Prediction Of The Force System In Face Milling Operations", ASME Journal Of Engineering In Industry, Vol. 106,n. 1,pp.81-88.

100. GyGax P.E.1979,"Dynamics of Single Tooth Milling, Annals of the CIRP, Vol. 28, n. 1, pp.65-70.

101. GyGax P. E., 1980,"Experimental Full Cut Milling Dynamics", Annals of the CIRP, Vol. 29, pp.61-66.

102. Ruzhong Z. and Wang K. K.,1983," Modeling Of The Cutting Force Pulsations In Face Milling", Annals of the CIRP, Vol. 32, pp.21-26.

103. Kline W. A., and Devor R. E.,1983," The Effect Of Run Out On Cutting Geometry And Forces In Milling", International Journal Of Machine Tool Design And Research, Vol. 23,n.2,pp.123-140.

104. Martellotti M. E., 1941," An Analysis of the Milling Process", Transactions of ASME, Vol.63, pp. 667- 700.

105. Koenigsberger F. and Sabberwal J. P., 1961," An Investigation into the Cutting Force Pulsations during Milling Operations", International Journal of Machine Tool Design and Research, Vol.1.

106. Tobias S. A., 1965, "Machine tool vibration", Wiley, New York, USA.

107. Nigm M. M. and Sadek M. M. and Tobias S. A., 1977," Determination Of Dynamic Cutting Coefficients From Steady State Cutting Data", International Journal of Machine Tool Design and Research, Vol.17,n.1,pp.19-37.

108. Tlusty J. and Ismail F., 1981, "The Basic Nonlinearity In Machining Chatter", Annals of the CIRP, Vol. 30, pp. 299-304.

109. Bathe, 1982, "Finite Element Procedures In Engineering Analysis", Prentice-

110. Robert D. C., David S. M. and Michael P., 1989, "Concepts and Applications of Finite Element Analysis", John Wiley & Sons 3rd edition.

111. Dokainish M. A. and. Subbaraj K, 1989, "A Survey of Direct Time-Integration Methods in Computational Structural Dynamics-I. Explicit Methods", Computers and Structures. Vol. 32, n. 6, pp. 1371-1386.

112. Subbaraj K and Dokainish M.A., 1989, "A Survey of Direct Time-Integration Methods in Computational Structural Dynamics-II. Explicit Methods", Computers and structures. Vol. 32, n. 6, pp. 1387-1401.

113. Hassan, M, 2000," Dynamics of Loosely Supported Heat Exchanger Tubes", McMaster University, Canada.

114. Yeh, H. and Loiu, F. W.,1999," Contact Condition Modeling for Machining Fixture Setup Processes", International Journal of Machine Tools and Manufacture, Vol. 39, n.5, pp. 787-803.

115. Chandra P, Athavale S. M., Devor R. E., and. Kapoor S. G,1996," Effect of Preloads on the Surface Flatness during Fixturing of Flexible Workpieces", Proceeding on the Second S. M. Symposium on Manufacturing Science, pp. 146-152.

116. Fang, B., Devor, R. E. and. Kapoor, S. G, 2000, "On The Prediction of Friction Force at Workpiece-Fixture Interface", Transaction of North American Manufacturing Research Institute, Vol. 28, pp. 209-214.

117. Courtney-Pratt, J. S and Eisner, E., 1957," The Effect of Tangential Force on the Contact of Metallic Bodies", Proceedings of the Royal Society of London: Series A. Vol. 238, pp. 529- 550.

118. AbdelSalam Usama, 1995, "A Finite Element Contact Algorithm applied to the Analysis of Expanded Tube Joints", Ph.D. Thesis, McMaster University, Canada.

119. Karnopp D., 1985, "Computer Simulation of Stick-Slip Friction in Mechanical Dynamic Systems", ASME Journal of Dynamic Systems, Measurements and Control, Vol.107, pp.100-103.

120. Haessig D. and Friedland B., 1991," On The Modeling and Simulation of Friction", Journal of Dynamic Systems, Measurements and Control, Vol. 113,pp. 354 362.

121. Axisa, F., Antunes, J. and Villard B., 1988,"Overview of Numerical Methods for Predicting Flow-Induced Vibrations", ASME Journal of Pressure Vessel Technology, Vol.100, pp.6-14.

122. Tan, X. and Rogers, R., 1996, "Dynamic Friction Modeling in Heat Exchanger Tube Simulations", Flow Induced Vibration, Vol.328, pp. 347-358.

123. Rogers, R. and Pick R., 1977,"Factors associated with support plate forces Due to Heat Exchanger Tube vibratory Contact", Nuclear Engineering and Design, Vol. 44, n.2, pp. 247-253.

124. Yetisir M. and Weaver D.,1986, "The Dynamics of Heat Exchanger U-Bend Tubes with Flat-Bar Supports", ASME Journal of Pressure Vessel Technology, Vol. 108, pp. 406-412.

125. Hassan M. A., Weaver D.S. and Dokainish M. A., 2002, "Parametric Studies of the Turbulence Response of Heat Exchanger Tubes in Loose Supports', ASME International Mechanical Engineering Congress and Exhibition. New Orleans, USA.

126. Childs T.H.C. and Tabor D., 1967, "Basic principles of dry friction testing", Proceedings of the Institute of Mechanical Engineers, Vol. 182, pp. 7-15.

127. Deiab I.M. and Elbestawi M. A., 2002," Tribological Aspects of Workpiece/Fixture Contact in Machining Processes", Proceedings of ASME International Mechanical Engineering Congress and Exhibition, New Orleans, USA.

128. Montgomery D. C., 1997, "Design and Analysis of Experiments" 4th edition, John Wiley and Sons.

129. Ross P. J., 1988," Taguchi Techniques for Quality Engineering", McGraw-Hill.

130. Lochner Robert H. and Matar Joseph E., 1990," Designing for Quality", Quality resources.

131. Jayaram S., Kapoor S.G. and Devor R.E., 2001," Estimation of the Specific Cutting pressures for Mechanistic Force Models", International Journal of Machine Tool and Manufacture, Vol.41, pp. 265-281.

132. Elbestawi M. A., Veldhuis S.C., Deiab I. M., Habel M. and Roberts C., 2002," Development of a Novel Modular and Agile Face Machining Technology", Annals of the CIRP, Vol.51, pp.307-310.

133. Koren, Y., Pasek, Z.J., Szuba, P., 1999, "Design of a Precision, Agile Line Boring Station", Annals of the CIRP, Vol. 48, no. 1, pp. 313-316.

134. Tönshoff, H.K., Peters, J., Inasaki, I., Paul, T., 1992, "Modeling and Simulation of Grinding Processes", Annals of the CIRP, Vol. 41,no. 2, pp.677-688.

135. Malkin, S., 1989, "Grinding Technology Theory and Applications of Machining with Abrasives", Society of Manufacturing Engineers, Dearborn, MI, USA.